5-2012

TAZ AS A REGULATOR OF MESENCHYMAL TRANSFORMATION AND CLINICAL AGGRESSIVENESS IN GLIOMAS

Katrina Salazar

TAZ AS A REGULATOR OF MESENCHYMAL TRANSFORMATION AND CLINICAL AGGRESSIVENESS IN GLIOMAS

by

Katrina Lumen Salazar, B.S.

APPROVED:

_____
Kenneth Aldape, M.D.
Supervisory Professor

_____
Russell Broaddus, M.D./Ph.D.

_____
Daniel Cahill, M.D./Ph.D.

_____
Pierre McCrea, Ph.D.

_____
Erik Sulman, M.D/Ph.D.

APPROVED:

_____
Dean, The University of Texas
Graduate School of Biomedical Sciences at Houston

TAZ AS A REGULATOR OF MESENCHYMAL TRANSFORMATION AND CLINICAL AGGRESSIVENESS IN GLIOMAS

A

DISSERTATION

Presented to the Faculty of The University of Texas Health Science Center at Houston

and The University of Texas M. D. Anderson Cancer Center

Graduate School of Biomedical Sciences

in Partial Fulfillment

of the Requirements

for the Degree of

DOCTOR OF PHILOSOPHY

by

Katrina Lumen Salazar, B.S.

Houston, Texas

May 2012

COPYRIGHT

DEDICATION

This dissertation is dedicated to my mother, Sonia Lumen Salazar (1946-2006), to whom I owe my ambition, my independent nature, and my interest in medicine.

TAZ AS A REGULATOR OF MESENCHYMAL TRANSFORMATION AND CLINICAL AGGRESSIVENESS IN GLIOMAS

Publication No._____

Katrina Lumen Salazar, B.S.

Supervisory Professor: Kenneth Aldape, M.D.

Glioblastoma multiforme (GBM) is an aggressive, high grade brain tumor. Microarray studies have shown a subset of GBMs with a mesenchymal gene signature. This subset is associated with poor clinical outcome and resistance to treatment. To establish the molecular drivers of this mesenchymal transition, we correlated transcription factor expression to the mesenchymal signature and identified transcriptional co-activator with PDZ-binding motif (TAZ) to be highly associated with the mesenchymal shift. High TAZ expression correlated with worse clinical outcome and higher grade. These data led to the **hypothesis** that TAZ is critical to the mesenchymal transition and aggressive clinical behavior seen in GBM.

We investigated the expression of TAZ, its binding partner TEAD, and the mesenchymal marker FN1 in human gliomas. Western analyses demonstrated increased expression of TAZ, TEAD4, and FN1 in GBM relative to lower grade gliomas. We also identified CpG islands in the TAZ promoter that are methylated in most lower grade gliomas, but not in GBMs. TAZ-methylated glioma stem cell (GSC) lines treated with a demethylation agent showed an increase in mRNA and protein TAZ expression; therefore, methylation may be another novel way TAZ is regulated since TAZ is epigenetically silenced in tumors with a better clinical outcome.

To further characterize the role of TAZ in gliomagenesis, we stably silenced or over-expressed TAZ in GSCs. Silencing of TAZ decreased invasion, self-renewal, mesenchymal protein expression, and tumor-initiating capacity. Over-expression of TAZ led to an increase in invasion, mesenchymal protein expression, mesenchymal differentiation, and tumor-initiating ability. These actions are dependent on TAZ interacting with TEAD since all these effects were abrogated with TAZ could not bind to TEAD. We also show that TAZ and TEAD directly bind to mesenchymal gene promoters. Thus, TAZ-TEAD interaction is critically important in the mesenchymal shift and in the aggressive clinical behavior of GBM.

We identified TAZ as a regulator of the mesenchymal transition in gliomas. TAZ could be used as a biomarker to both estimate prognosis and stratify patients into clinically relevant subgroups. Since mesenchymal transition is correlated to tumor aggressiveness, strategies to target and inhibit TAZ-TEAD and the downstream gene targets may be warranted in alternative treatment.

TABLE OF CONTENTS

LIST OF ILLUSTRATIONS

LIST OF TABLES

CHAPTER 1: INTRODUCTION

Glioblastoma multiforme (GBM)

Glioblastoma multiforme (GBM) is the most aggressive and highest grade glioma (World Health Organization grade IV), responsible for approximately 12-15% of intracranial neoplasms and 60-75% of astrocytic tumors [1]. The incidence is 3-4 cases per 100,000 population per year [1]. GBM is often separated into two subtypes, primary and secondary, based on molecular, genetic, and clinical presentation [1]. Primary GBMs often present at 50 years of age or older and patients usually have a clinical history of less than 3 months [1]. Genetic alterations in primary GBM include loss of heterozygosity (LOH) 10q (70%), epidermal growth factor receptor (EGFR) amplification (36%), $p16^{INK4a}$ deletion (31%), TP53 mutation (28%), and phosphatase and tensin homologue on chromosome 10 (PTEN) mutation (25%) [1]. Secondary GBMs arise from lower grade gliomas, including anaplastic astrocytomas. The median time to progression to GBM from low-grade astrocytoma (WHO grade II) is 5.1 years and from anaplastic astrocytoma (WHO grade III) is 1.9 years [1]. Genetic alterations are similar as those seen in primary GBM, but the differences in the type and frequency are identified. For secondary GBM, the frequency of genetic alterations are LOH 10q (63%), EGFR amplification (8%), $p16^{INK4a}$ deletion (19%), TP53 mutation (65%), and PTEN mutation (4%) [1]. In addition, mutations in IDH1 and IDH2 (discussed below) are unique to secondary GBM, and can serve as the principal genetic marker of these tumors. The Cancer Genome Atlas (TCGA) analyzed the molecular characteristics of a large set of GBM and confirmed the following characteristics: mutations in neurofibromatosis 1 (NF1); amplification of EGFR, including a variant III deletion of the extracellular domain; phosphatidylinositol-3-OH kinase (PI(3)K) pathway activation; and methylguanine methyltransferase (*MGMT*) promoter methylation. Using a multidimensional profiling technique, TCGA data analysis indicated that the three major pathways involved in GBM

pathogenesis include receptor tyrosine kinase (RTK) signaling, p53 and retinoblastoma (RB) tumor suppressor pathways [2].

Mutations of critical genes and alterations of specific pathways have been shown to play a role in gliomagenesis. Mutations/deletions in the PTEN, TP53, and RB1 pathways are well-known in the pathogenesis of GBMs and groups have shown the significance of these mutations using mouse models to induce astrocytomas *in vivo* [3,4,5,6]. In addition to EGFR amplification, a mutation that results in a tandem kinase domain duplication (TKD-EGFR) escapes known mechanisms of receptor down-regulation (i.e.—phosphorylation and competitive inhibition of ligand binding) and confers tumorigenicity [7]. A novel exon 27 deletion in the carboxyl-terminal domain of EGFR was shown to induce cellular transformation in the absence of ligands [8]. Newly identified mutations in gliomas include mutations of the isocitrate dehydrogenase (IDH) metabolic enzymes IDH1 and IDH2, where the majority of the mutations change a single amino acid located in the isocitrate binding site (R132 of IDH1 and R172 of IDH2). These IDH1 and -2 mutations are early genetic modifications that occur early and frequently in astrocytomas and oligodendrogliomas. The resulting neomorphic enzyme was shown to acquire novel properties that result in the accumulation of 2-hydroxyglutarate [9]. Patients whose tumors exhibit IDH mutations tend to have a better prognosis compared to those who lack the mutation. In addition, since IDH mutations are specific among CNS neoplasms to the diffuse gliomas, this marker has diagnostic utility [10]. Additional genes and proteins implicated in GBM formation include connective tissue growth factor (CTGF) [11], integrin b8 [12], homeobox A9 (HOXA9) [13], and the forkhead box M1 (FoxM1)—β-catenin interaction [14]. It is likely that further research will discover new gene mutations and proteins involved in GBM pathogenesis.

The cell of origin of GBM is unknown, but several lines of investigation have led to specific insights on this topic. One group has shown that mutant p53 proteins are first detectable in neural stem cells (NSCs) in the subventricular zone (SVZ) and that progenitor-like cells in the SVZ-associated areas initiate gliomagenesis [15]. This suggests that the cell of origin may be NSCs located within the SVZ; however, other groups have shown that NSCs gave rise to gliomas regardless of their location [16]. These studies suggest that NSCs play a vital step in gliomagenesis and that the location of these NSCs is less important. NSCs and gliomas have a few common intrinsic characteristics including the ability to invade and proliferate, diverse lineage possibilities, association with white-matter tracts and blood vessels, and immature expression profiles of nestin, EGFR, PTEN, hedgehog, telomerase and Wnt [17]. Another group suggests that the oligodendrocyte precursor cell (OPCs) is the cell of origin even if the initial mutations occur in NSCs [18]. Overall, these studies show that the cell of origin for glioma is still elusive.

Clinically, patients present with varied symptoms, including signs of raised intracranial pressure, such as headaches, papilledema, and nausea/vomiting [1]. A ring-enhancing lesion seen on contrast-enhanced magnetic resonance imaging (MRI) or computed tomography (CT) suggests a diagnosis of GBM; however, definitive diagnosis depends on pathology. Histologic features of GBM include increased cellularity, nuclear atypia, microvascular proliferation, and pseudopalisading necrosis (the last two being pathognomonic for GBM) [1]. Primary and secondary GBMs are pathologically indistinguishable despite the molecular and genetic differences between the two classifications.

Currently, the standard of care for GBM is maximal surgical resection combined with adjuvant radiotherapy and chemotherapy with temozolomide (TMZ) [1]. Patients with GBM

containing a methylated *MGMT* promoter benefited from TMZ, whereas those who did not have a methylated *MGMT* promoter lacked such a benefit [19]. Other alternatives include targeting EGFR in a subset of GBM patients [20]. At least some of the pathways driving GBM formation could be directly responsible for the therapy resistance of this tumor type. Possible therapeutic approaches exist that may either overcome or take advantage of these GBM genetic alterations to improve the response of these tumors to DNA-damaging therapy [21].

Unfortunately, despite this aggressive therapeutic regimen, the median survival for patient remains 12-15 months and local recurrence remains a leading cause of mortality. Because of this, more needs to be understood about molecular genetic abnormalities that drive its biologic and clinical behavior. Histology provides little to predict patient survival time, but genetic profiling has consistently identified clinical subgroups that correlate with prognosis [22,23,24,25,26]. Analyzing both the DNA and mRNA-based tumor profiles together allows for a more robust method of clinical classification and can better identify genes vital to gliomagenesis [27].

The mesenchymal signature and GBM

To identify molecular abnormalities that drive the clinical behavior of GBM, our laboratory performed extensive microarray studies on GBM and found distinct gene signatures, proneural, mesenchymal, and proliferative that associate with clinical behavior [24]. After further analysis, the proliferative gene signature was found to be less robust than the other two groups. The proneural gene signature, characterized by over-expression of genes associated with neural development, is associated with a less aggressive, better clinical course while the

mesenchymal gene signature, characterized by over-expression of genes associated with mesenchyme, extracellular matrix (ECM), cell motility, wound healing, and angiogenesis, is associated with exceptionally aggressive clinical behavior, poor outcome and resistance to treatment in GBM [24,25]. In addition, pre- and post-treatment samples from the same patients indicate that the expression of some of these mesenchymal genes is increased during recurrence, suggesting a shift to the mesenchymal subtype over time [24]. This shift from proneural to mesenchymal transition (PMT) in GBM may drive its aggressive behavior. Currently, it is unknown what drives this PMT in GBM.

A mesenchymal phenotype is the hallmark of tumor aggressiveness in human malignant glioma, but the regulatory programs responsible for the mesenchymal signature are largely unknown. One group showed that the two transcription factors, CCAAT/enhancer binding protein-beta (C/EBP-β) and STAT3, are synergistic initiators and regulators of the mesenchymal transformation in human gliomas that predicts poor clinical outcome [28]. We speculated that more transcription factors, besides STAT3 and C/EBP-β, may be involved in PMT. We performed correlation analyses to identify the molecular mechanisms by which the mesenchymal shift occurs, asking which transcription factors were most highly correlated with the mesenchymal gene expression signature in the array data and identified a number of transcription factors (**Table 1**). Analysis of correlations to this signature showed that transcriptional co-activator with PDZ-binding motif (TAZ; also known as WW domain containing transcription regulator 1, WWTR1) was one of the transcription regulators with the highest positive correlation with the mesenchymal signature (i.e.—high TAZ expression is positively associated with higher expression of key mesenchymal genes and is tightly associated with the mesenchymal change). High expression of TAZ also correlated with higher grade gliomas as well as poorer patient outcome. TAZ is regulated by the Hippo pathway,

Table 1: Transcription factors associated with the mesenchymal signature

Gene Symbol	Gene Name
C/EBP-δ	CCAAT/enhancer binding protein delta
C/EBP-β	CCAAT/enhancer binding protein beta
CSDA	Cold shock domain protein A
RCAN1	Regulator of calcineurin 1
WWTR1	WW domain containing transcription regulator 1
PTRF	Polymerase 1 and transcript release factor
RBMS1	RNA binding motif, single stranded interacting protein 1
XBP1	X-box binding protein 1
KLF10	Kruppel-like factor 10
TGIF1	TGF-β-induced factor homeobox 1
ELK3	ETS-domain protein (SRF accessory protein 2)
ATF3	Activating transcription factor 3
SP100	SP100 nuclear antigen
RBMS1	RNA binding motif, single stranded interacting protein 1

is the paralog of Yes-associated protein (YAP), and binds to many transcription factors, the most well-characterized being transcriptional enhancer activator domain (TEAD)/transcriptional enhancer factor (TEF).

The Hippo Pathway

The Hippo pathway was originally described in *Drosophila* and Hippo (Hpo) was found to regulate cell death as well as cell proliferation via Cyclin E and *Drosophila* inhibitor of apoptosis protein (diap) [29]. The pathway is composed of three units: first, the upstream cell surface regulators (i.e.—cell adhesion molecules and cell polarity complexes); second, a serine-threonine kinase cascade; and third, a downstream transcription co-activator target [30]. Recently, it was discovered that the Hippo pathway is conserved in unicellular organisms, indicating the pathway predates Metazoa origins [31]. The pathway is interconnected with the BMP [32], transforming growth factor β (TGF-β) [33], and Wnt/β-catenin [34,35] signaling pathways (**Fig. 1**).

Numerous upstream proteins have been described to regulate the Hippo pathway. Examples include Ataxia telangiectasia mutated (ATM) that regulates Ras association family 1A (RASSF1A) [36]; Lethal giant larvae (Lgl) that regulates RASSF localization [37]; RASSF1A and RASSF6 that inhibit mammalian sterile20 kinases 2 (MST2), which leads to tumor protein (p73) activity [38,39,40,41,42,43]; moesinezrin-radixin-like protein (Merlin) and Expanded (Ex) [44,45,46] [[22354087]]; Crumb (Crb) that regulates Ex levels and localization thus affecting cell polarity [47,48,49]; Dachsous (Ds) and Fat (Ft) [50,51,52,53,54]; Four-jointed (Fj) via modulation of Ds and Ft [55,56]; Kibra via interactions with large tumor

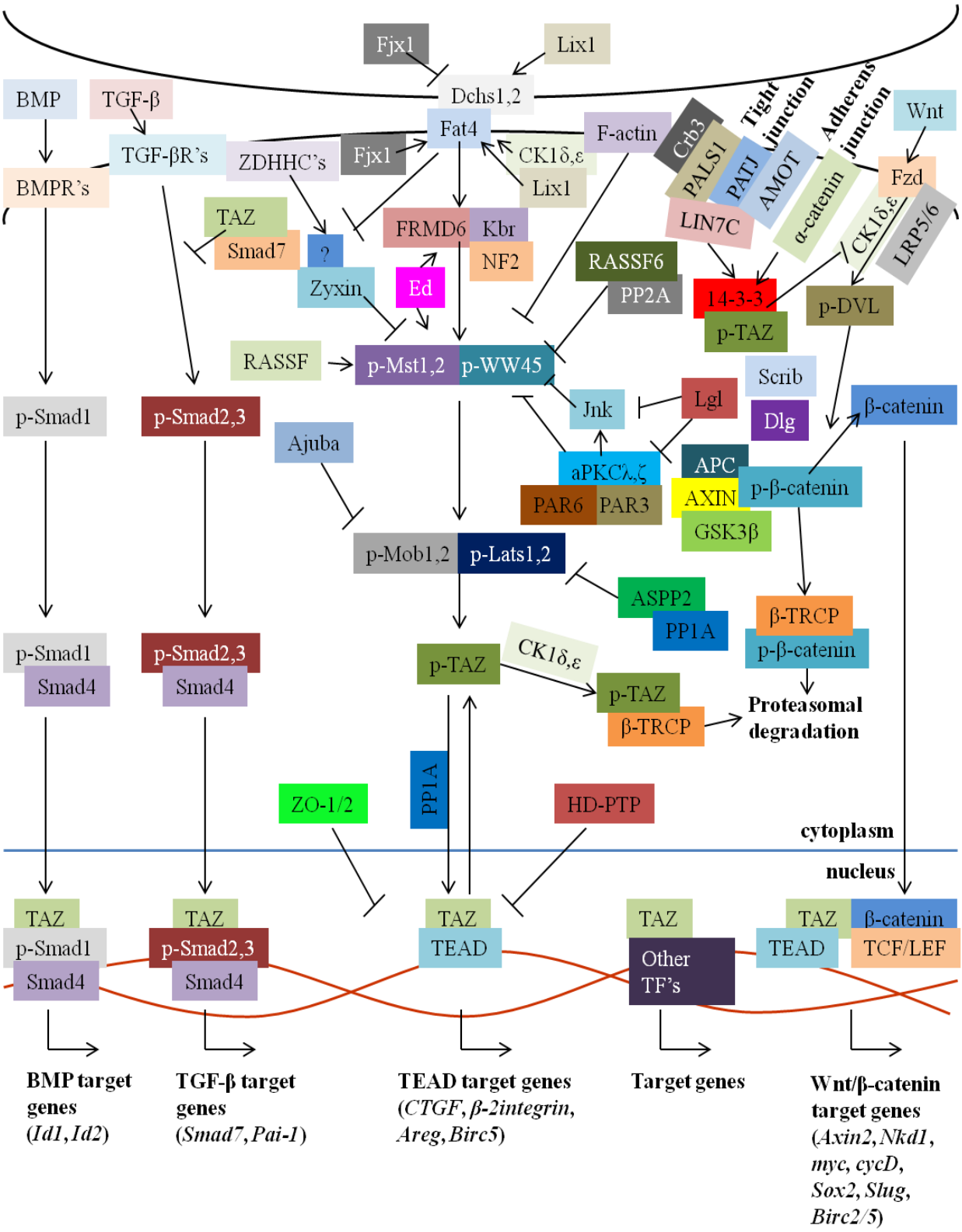

Figure 1: The Hippo pathway. Diagram shows interconnection between the Hippo pathway and the BMP, TGF-β, and Wnt/β-catenin pathways. Arrows indicate activation and blunt heads indicate inhibition.

suppressor (LATS) [57,58,59,60] or Pez [61]; E-cadherin [62]; Ajuba LIM proteins (Ajuba, LIMD1, and WTIP) [63]; and most recently Echinoid (Ed) [9]. The phosphatase complex *Drosophila* Striatin-interacting phosphatase and kinase (dSRIPAK) prevents Hippo activation during development [64] and recently, a group identified a class of endocytic neoplastic tumor suppressor genes in *Drosophila* that regulates the Hippo pathway [65]. Cellular detachment from the ECM also appears to regulate the Hippo pathway by activating LATS1/2, thus inhibiting YAP/TAZ downstream to initiate anoikis [66].

The Hippo pathway regulates cell polarity complexes by controlling the apical polarity complexes atypical protein kinase C (aPKC), Crb, and Patj [67,68,69] and is important in dendrite morphogenesis [70] and axis specification by interaction with the Notch pathway [71,72,73,74,75,76]. The Hippo pathway has also been linked to the Akt pathway via MST1/2 and YAP [77,78] and the Rb pathway, possibly through LATS2 [79], to maintain the terminally differentiated states in the *Drosophila* eye [80]. In mammals, the Hippo pathway plays a vital role in organ size and tumorigenesis [81] as well as intestinal stem cell regeneration [82,83,84] and tissue regeneration [85,86]. The Hippo pathway may also play a role in mantle cell lymphoma [87] and glial cell proliferation [88].

In *Drosophila*, Hpo is required for the cell death response triggered by Ionizing Radiations (IR) or *Drosophila melanogaster* p53 (Dmp53) [89] and is regulated by dimerization and cytoplasmic localization [90]. Hpo encodes a sterile20 (Ste-20) family protein kinase that binds to and phosphorylates Salvador (Sav), a tumor suppressor that interacts with Warts (Wts) [91]. Mob as tumor suppressor (Mats) acts downstream of Hpo to regulate cell growth, organ size, and tumor suppression [92,93,94,95].

In mammals, Mps one binder (Mob) 1A and 1B, the homologs of Mats, are tumor suppressers that regulate mitotic exit and cytokinesis [96] as well as cell polarity [97]. LATS, the Warts kinase homolog, has been shown to increase chemosensitivity by stabilizing p73 [98], to promote apoptosis-stimulating of p53 protein 1 (ASPP1) nuclear localization to promote cell death via p53 [99], and to repress cellular reprogramming, thus preventing cells from transitioning from a differentiated state to a pluripotent state [100]. Heat shock protein 90 (Hsp90) inhibitors [101], Itch [102,103], forkhead box P3 (FOXP3) [104], nephronophthisis 4 (NPHP4) [105], and angiomotin-like 2 (AMOTL2) [106] can affect LATS1 and 2 function. LATS is also a novel Snail1 regulator [107]. Crb interacts with TAZ/YAP to relay cell density information by promoting TAZ/YAP phosphorylation and TGF-β signaling suppression [108]. The main components of the Hippo pathway can be found in **Table 2**.

Many proteins have been linked to the Hippo pathway including division abnormally delayed (dally) and dally-like protein (dlp) that are two targets of Ft and Ds [109], Scribbled [110], cluster of differentiation 44 (CD44) [111], filamentous (F)-actin [112,113,114,115], Zyxin [116], Runt box domain DNA-binding transcription factor 3 (Runx3) [117], and Tao-1 [118,119].

TAZ, YAP, and TEAD

Much is known about Yki, the TAZ/YAP homolog, which is well-studied in *Drosophila*. Homothorax (Hth) and teashirt (Tsh) promote cell proliferation and protect eye progenitor cells from apoptosis by interacting with Yki [120], which leads to an up-regulation of the microRNA bantam [121,122,123,124]. In the midgut, Yki regulates stem cell

Table 2: The Hippo pathway components

Drosophila protein	Vertebrate homologues
Fat pathway	
Dachsous (Ds)	Dchs1, 2
Fat	Fat4
Lowfat (Lft)	Lix1, Lix1L
Four-jointed (Fj)	Fjx1
Discs overgrown (Dco)	CK1δ, ε
Dachs	?
Approximated (App)	ZDHHC's
Zyx102 (Zyx)	Zyxin, Lpp, Trip6
Ex-Mer complex	
Crumbs (Crb)	Crb1-3
Expanded (Ex)	FRMD6 (Willin)
Merlin (Mer)	NF2
Kibra (Kbr)	Kibra
Kinase cassette	
Hippo (Hpo)	Mst1, 2
Salvador (Sav)	WW45
Warts (Wts)	Lats1, 2
Mob as tumor suppressor (Mats)	Mob1, 2
Other regulators	
RASSF	RASSF1-6
PP2A (dSTRIPAK)	PP2A (STRIPAK)
Jub	Ajuba, Limd1, Wtip
Lgl	Lgl
Scrib	Scrib
Dlg	Dlg
Jnk	Jnk
Myopic (Mop)	HD-PTP
aPKC	aPKCλ, ζ
Par6	Par6
Baz	Par3
Veli	LIN7C
Patj	Patj
Transcription factors	
Yorkie (Yki)	Yap, Taz
Scalloped (Sd)	TEAD/TEF
Mad	Smad

proliferation and intestinal regeneration [125]. Yki also interacts with dMyc in a regulatory feedback mechanism to control growth and regulate organ size [126,127,128]; with WW domain-binding protein 2 (Wbp2) to drive tissue growth [129,130]; and with dE2F1 to bypass the cell cycle exit [131]. Regulation may occur through direct physical interaction with other proteins upstream in the Hippo pathway in addition to phosphorylation [132,133]. Also, myopic controls Yki endosomal association and protein levels, thus influencing Yki target gene expression [134].

In mammals, TAZ is a WW domain-containing molecule that is located at chromosome 3q23 that functions as a transcriptional co-activator by binding to proline-proline-any amino acid-tyrosine (PPXY) motifs present on transcription factors and is normally expressed highly in heart, lung, kidney and placenta [135,136]. TAZ also binds to the regulatory 14-3-3 proteins [135]. 14-3-3 proteins bind to serine/threonine-phosphorylated residues in a context specific manner and bind and regulate key proteins involved in intracellular signaling, cell cycling, apoptosis, and transcription regulation [137]. TAZ binds 14-3-3 proteins when phosphorylated on four specific serine residues (S66, S89, S117, S311), serine 89 being the most important. Phosphorylation results in TAZ being exported out of the nucleus to the cytoplasm [135]. TAZ also contains a post-synaptic density, *Drosophila* disc large tumor suppressor, and zonula occludens-1 (PDZ)-binding motif in the C-terminus that localizes TAZ to discrete nuclear foci and is vital for TAZ-stimulated gene transcription [135].

YAP is located on chromosome 11q13 and is highly expressed in placenta, prostate, ovary, and testis, but undetectable in peripheral blood leukocytes [138]. YAP binds to the Src homology domain 3 (SH3) of the Yes proto-oncogene product [139] and interacts with many proteins including ezrin/radixin/moesin (ERM)-binding phosphoprotein 50 kD (EBP50) in the

apical compartment of the airway epithelia [140]; p53-binding protein-2 (p53BP-2) [141]; Smad7 to promote the inhibitory effect against TGF-β signaling [142]; the full-length erythroblastosis oncogene B 4 (ErbB4) receptor at the membrane and the C-terminal fragment that translocates to the nucleus to regulate transcription [143,144]; Runx2 to suppress its function [145]; heterogeneous nuclear ribonuclear protein U (hnRNP U), an RNA- and DNA-binding protein that plays a role in the regulation of gene expression, via a proline-rich amino terminus not present in TAZ [146]; proline-rich γ-carboxyglutamic acid protein 2 (PRGP2) [147]; early growth response-1 (EGR-1) to upregulate B-cell leukemia/lymphoma 2 (Bcl2)-associated X (Bax) expression in irradiated prostate carcinoma cells [148]; amphiregulin (AREG) whose induction contributes to YAP-mediated cell proliferation and migration, but not epithelial-to-mesenchymal transition (EMT) [149]; ΔNp63α [150,151]; anterior gradient homolog 2 (AGR2) in adenocarcinomas [152]; FatJ to restrict the neural progenitor cells (NPC) pool size [153]; Rous sarcoma virus (RSV) [154]; and p73, which enhances its transcriptional activity [155]. Many groups have shown that promyelocytic leukemia gene (PML) is required for YAP to interact with p73 [156,157] and another showed that YAP competes with Itch thus preventing Itch-mediated ubiquitination of p73 [158]. Phosphorylation by c-Abl at position Y357 in response to DNA damage stabilizes YAP and creates a higher affinity to p73 [159].

TAZ contains one WW domain, unlike YAP, which contains 2 [160,161,162]; however, a group recently discovered a TAZ isotype with two WW domains [163]. The WW motif, a sequence of 38 amino acids containing two widely spread tryptophans, mediates protein-protein interactions and binds to PPXY motifs on proteins [164,165]. The WW motif lacks disulfide bridges, forms a three-stranded antiparallel β-sheet [166], and has distinct regulatory roles in different cell types [167]. PPXY motifs are found on many transcription factors including jun proto-oncogene (c-Jun) [168], activating enhancer binding protein 2 (AP-2) [169], nuclear

factor erythroid-derived 2 (NF-E2) [170], C/EBPα [171], early growth response 2 (EGR2) [172], myocyte enhancer binding factor 2 (MEF2) [173], and polyomavirus enhancer binding protein 2 (PEBP2), which suggests that it is a transcription activation domain that functions by recruiting TAZ/YAP as strong transcription activators to target genes [174].

The regulation of TAZ is still being elucidated. The Hippo pathway regulates TAZ via two mechanisms: 1) phosphorylating a phosphodegron and recruiting the S-phase kinase-associated protein 1 (Skp1)-cullin-F-box protein beta-transducin repeat-containing protein ($SCF^{\beta\text{-}TrCP}$) E3 ligase to promote degradation [175] and 2) LATS phosphorylation on the previously mentioned serine residues to promote cytoplasmic sequestration [135]. When these serine sites are replaced by an amino acid residue that cannot be phosphorylated (alanine), TAZ is constitutively active within the nucleus, which promotes cell proliferation, cell migration, invasion, and EMT in breast cancer cells [176,177]. EMT promotes the invasive and metastatic properties of tumor cells [178,179,180] and this model may provide insight into PMT seen in GBM. Physical interaction with angiomotin (AMOT) and AMOTL1 also promotes cytoplasmic retention thereby restricting TAZ activity [181]. Recently, it was discovered that protein phosphatase 1 alpha (PP1A) and ASPP2 promote TAZ dephosphorylation by antagonizing LATS, thus promoting TAZ function [182]. TAZ is also involved in other pathways including BMP2 signaling pathway [32] and Wnt/β-catenin signaling pathway via interaction with disheveled (DVL) in the cytoplasm where it inhibits Wnt signaling by regulating β-catenin translocation to the nucleus [34,35].

Similar to TAZ, multiple regulatory mechanisms of YAP have been elucidated. YAP is inhibited by cell density via the Hippo pathway and phosphorylation of serine residues by LATS1 leads to cytoplasmic translocation of YAP and binding to 14-3-3

[183,184,185,186,187,188,189]. Akt [190], Jun N-terminal kinase 1 and 2 (JNK1 and JNK2) [191], and α-catenin [192,193] act as negative regulators of YAP by phosphorylating YAP as well. YAP is also regulated by phosphorylation of a phosphodegron thus recruiting the $SCF^{\beta\text{-}TrCP}$ E3 ligase to promote degradation [194]. In hepatocellular carcinoma (HCC), microRNA 375 (miR-375) inhibits YAP [195] and AXL receptor tyrosine kinase drives YAP-dependent oncogenic activities [196]. miR-375 also inhibits YAP in lung cancer with neuroendocrine features [197]. The PDZ-binding motif is necessary for YAP localization in the nucleus [198] since zonula occludens 2 (ZO-2) was found to bind to YAP via the PDZ-binding motif to promote nuclear localization of YAP [199]. Cytoplasmic ASPP inhibits the interaction of YAP with LATS1, thus enhancing nuclear accumulation of YAP, which leads to inhibition of apoptosis [200]. In addition to phosphorylation, AMOTL1 and AMOTL2 regulate YAP via direct protein-protein interaction independent of YAP phosphorylation status and promote cytoplasmic retention [201,202,203]. Dobutamine has also been shown to inhibit YAP-dependent gene transcription [204] as well as 4.1/ezrin/radixin/moesin (FERM) domain containing 6 (Willin/FRMD6) that also antagonizes YAP activity [205]. Thus far, PP1A is the only protein shown to dephosphorylate YAP [206].

It is interesting to note that TAZ plays a role in mesenchymal stem cell (MSC) and human pulp stem cell differentiation by activating Runx2 [136,207,208] and repressing peroxisome proliferator–activated receptor γ (PPAR- γ) [136]. Groups have shown that TGF-β [209] or ephrin B1 [210] may also interact with TAZ to promote this osteogenic differentiation and that dexamethasone may inhibit TAZ to promote adipogenesis [[22374070]]. TAZ is similar to β-catenin by integrating extracellular, membrane, and cytoskeletal-derived signals to influence MSC outcome [211]. One group studied MSCs of multiple myeloma patients and found that TAZ expression was suppressed by tumor necrosis factor α (TNF-α), which resulted

in decreased osteogenic potential [212]. Different from these results, TNF-α enhanced osteogenic differentiation of human adipose stromal cells (hADSC) by activating nuclear factor of kappa light polypeptide gene enhancer in B-cells (NF-κB), which then resulted in an increase of TAZ expression [213]. Another group found that fibroblast growth factor-2 (FGF-2), a protein that inhibits bone mineralization and stimulates cell proliferation, reduced the TAZ protein expression level in the osteoblast-like cells MC3T3-E1 [214]. Molecular mechanisms for osteoporosis have also shown the involvement of TAZ with the disease process [215].

YAP has many roles including being a major effector of Merlin/Neurofibromatosis type-2 (NF2) in growth regulation [216], tissue growth, and cell transformation [217]. YAP also maintains stem cell pluripotency and basal epidermal progenitors [218]; regulates hair follicle morphogenesis [219]; modulates epidermal stem cell proliferation and tissue expansion [192,220]; plays a role in postnatal liver development [221]; and regulates vascular smooth muscle cells by interacting with myocardin [[22411986]]. YAP over-expression in primary human keratinocytes also appears to induce cell immortalization, but not malignant transformation [222].

TAZ has been shown to interact with many transcription factors including thyroid transcription factor-1 (TTF-1) to regulate surfactant protein-C levels [223]; polyomavirus T antigens [224]; paired box 3 (Pax3) within the paraxial mesoderm, limb buds, and the neural tube during embryogenesis [225]; T-box transcription factor (TBX5) during cardiac and limb development [226]; Pax8 and TTF-1 in thyroid to regulate thyroid development and differentiation [227]; myogenic differentiation 1 (MyoD) to promote myogenic gene expression during myoblast differentiation [228]; cell cycle and apoptosis regulatory protein 1 (CARP-1) to inhibit CARP-1 dependent apoptosis in breast cancer cells [229]; ZO-1 and ZO-2 that

negatively regulate TAZ via control of nuclear translocation and activity [230]; WW domain-binding protein 2 (Wbp2) via the WW domain of TAZ to promote the transforming ability of TAZ [231]; msh homeobox 2 interacting nuclear target 3 (Mint3) to mediate signaling of amyloid precursor like proteins 1 and 2 (APLP1 and APLP2) [232]; and Krüppel-like factor 5 (KLF5) to promote breast cell growth [233].

TAZ is also part of a Hemolysis, Elevated Liver enzymes and Low platelets (HELLP) syndrome molecular signature [234] as well as a pancreatic ductal adenocarcinoma molecular signature [235]. In addition, TAZ plays a role in papillary thyroid carcinoma [236], non-small cell lung cancer [237], epithelioid hemangioendothelioma via a gene fusion with calmodulin binding transcription activator 1 (CAMTA1) [238] [[22429593]], and infantile fibrosarcoma [[22374738]]. In breast cancer, TAZ appears to play a role in Taxol resistance [239]; is required for self-renewal, cell proliferation, and tumor-initiation capacities in breast cancer stem cells [233,240]; and is vital to the nuclear accumulation of the mothers against decapentaplegic homologs 2/3-4 (Smad2/3-4) complex via TGF-β stimulation [33]. TAZ is also involved in *Xenopus* development and is expressed in the migrating hypaxial myoblasts, presomitic mesoderm, trunk neural crest cells, facial connective tissues, brachial arch, and brain and is transiently expressed in the edges of the hypaxial myoblasts in the muscle lineage, presomitic mesoderm, and proliferation cells [241]. It has also been shown that TAZ is down-regulated during decidualization [242]. Interestingly, a group recently showed that, independent of the Hippo pathway, TAZ plays a role in mechanotransduction by relaying signals exerted by the cellular microenvironment (i.e.—ECM rigidity and cell shape) [243].

Expression of YAP is altered in several cancers including metastatic murine squamous carcinoma cells [244], oral squamous cell carcinoma [245,246] and esophageal squamous-cell

carcinoma (ESCC) [247]. YAP is also over-expressed in pancreatic cancer [248] [[22396793]], ependymoma [249], meningioma [250], medulloblastoma via Sonic hedgehog (Shh) signaling and Akt activation [251,252], gliomas [253], mesothelioma [254,255,256,257], HCC [258,259,260,261,262,263,264,265,266], clear cell renal cell carcinoma (ccRCC) via downregulation of Sav [267], gastric carcinoma [268,269,270,271,272], colorectal carcinoma via Wnt/β-catenin [273,274], non-small cell lung cancer [275,276], small-cell lung cancer [277], head and neck squamous cell carcinomas (HNSCCs) [278,279], soft tissue sarcomas [280], Ewing sarcoma via B lymphoma Mo-MLV insertion region 1 (BMI-1) [281], epithelial ovarian cancer [282,283], invasive breast carcinoma [284,285], and ovarian serous cystadenocarcinoma [286,287]. In nontransformed mammary epithelial cells, over-expression of human YAP induced EMT, apoptosis suppression, growth factor-independent proliferation, and anchorage-independent growth in soft agar [288], but other groups suggest that YAP acts as a tumor suppressor in breast cancer [289]. The effect on apoptosis may be different due to cellular context [290].

Mouse models show that TAZ -/- mice present with renal cysts that eventually lead to end-stage renal disease due to loss of cilia integrity [291]. The cilia integrity may be dependent on GLI-similar 3 (Glis3), a Kruppel-like zinc finger protein, since it localizes to primary cilium and binds to TAZ [292]. Another group showed that TAZ -/- mice develop polycystic kidney disease due to lack of polycystin 2 (PC2) degradation via a $SCF^{\beta -Trcp}$ E3 ubiquitin ligase pathway [293]. The PC2 channel may be regulated by TAZ and the Protein Associated with Lin Seven 1 (PALS1)-associated tight junction (PATJ) protein [294]. A different group suggests that TAZ and never in mitosis gene a (NIMA)-related kinase 1 (Nek1) form a negative feedback loop that maintains PC2 at the level needed for proper ciliogenesis [295]. These mice present with severe urinary concentrating defects and polyuria [296]. Other groups show that

TAZ -/- mice also develop emphysema due to abnormal alveolarization during development [293,297].

Likewise, animal models have provided insight into the various roles of YAP. In mice, YAP regulates embryonic stem cell self-renewal [298], promotes embryonic cardiac growth [299] by Wnt signaling inhibition [300], enhances proliferation in the postnatal mouse retina [185], regulates myogenesis [301], supports Smad1-dependent transcription, and is required for BMP suppression of neural differentiation. Over-expression of YAP also leads to an increase in organ size and aberrant tissue expansion [302]. YAP -/- mice show an arrest in development around E8.5, indicating that YAP plays an important role in yolk sac vasculogenesis, chorioallantoic attachment, and embryonic axis elongation [303]. In zebrafish embryogenesis, YAP is required for the brain, eyes, and neural crest development [304].

Prior literature indicates that TAZ is an important signaling molecule that interacts with TEAD/TEF transcription factors to activate downstream targets [305]. TEAD proteins bind to MCAT (muscle C, A and T sites) and A/T-rich sites in promoters active in cardiac, skeletal and smooth muscle, placenta, and neural crest [305]. Mutations preventing TEAD1 binding to TAZ also results in Sveinsson's chorioretinal atrophy (SCRA), an autosomal dominant eye disease characterized by bilateral chorioretinal degeneration [306]. YAP also interacts with TEAD, which is essential in facilitating YAP-dependent gene expression [307,308,309,310,311,312]. The YAP-TEAD interaction plays a vital role in regulating NPC number by affecting proliferation, fate choice, and cell survival [313] and by Pax3 expression in the neural plate border zone [314]. YAP also induces gene expression and exerts its biological functions by interacting with transcription factors through the WW domain in addition to the TEAD-binding domain [315].

TEAD-1, -2, -3, and -4 show different, but overlapping, spatiotemporal expression patterns. This would suggest that they are redundant, but differ in their control of development and regulation of specific tissues [316,317]. They share a highly conserved 68-amino acid TEA/ATTS DNA-binding domain, which binds to many motifs with the predominate consensus of GGAATG [318]. The TEAD family regulates Hippo pathway-responsive genes [319,320,321]. In *Drosophila*, the TEAD homolog Scalloped (Sd) functions to regulate cell-specific gene expression during development, especially in the nervous system differentiation [322]. TEAD-1/TEF-1 has been shown to activate human papillomavirus in cervical carcinoma cells [323], regulate vascular smooth muscle α-actin gene in myoblasts and fibroblasts [324,325,326,327], and plays an important role in cardiac development [328,329,330]. TEAD-2/TEF-4/ETF was first identified in mouse neural progenitor cells and expression in developing embryos was restricted to certain tissue such as the hindbrain [331], gut, and nephrogenic region of the kidney [332]. TEAD-3/TEF-5/DTEF-1 is strongly expressed in placenta [333,334] as well as cardiac muscle [335,336] while TEAD-4/TEF-3/RTEF-1 plays an important role in trophectoderm [337,338] and embryonic development of skeletal muscle [332,339,340], and cardiac muscle in mice [341] and was also found to be aberrantly expressed in lung adenocarcinomas [342] and in hypoxic endothelial cells [343,344].

Silencing TEAD or even preventing the TAZ-TEAD interaction blocked the ability of TAZ to promote cell proliferation and to induce EMT in breast cancer cells [177,345]. TAZ and TEAD1 have been shown to up-regulate zinc finger E-box binding homeobox 1 (Zeb1), a well-known transcription factor involved in EMT, in retinal pigment epithelial (RPE) cells, which then results in dedifferentiation, cell proliferation and EMT [346]. EMT is a normal biological process vital for morphogenesis during embryonic development that goes awry in neoplastic cells [347,348]. EMT describes the event of polarized epithelial cells undergoing

morphologic changes into non-polarized mesenchymal cells, thus allowing improved abilities to migrate, invade, and resist apoptosis [347,349].

EMT versus PMT

EMT is initiated by changes in expression of certain transcription factors (some discussed below), cell surface and cytoskeletal proteins, and enzymes that degrade the ECM [347]. EMT can be subdivided into three groups that are separated based on the cellular activities at the time of EMT. Type 1 occurs during implantation, embryogenesis, and organ development; Type 2 occurs during tissue regeneration and organ fibrosis; and Type 3, occurs during cancer and metastasis [347]. Five common steps to EMT are first, a group of cells to undergo EMT; second, intercellular adhesion loss is mediated by cadherins at adherens junctions; third, polarity markers are lost; fourth, cytoskeletal reorganization drives delamination; and fifth, the basement membrane degrades [350]. EMT plays an important role in early development, such as gastrulation and neural crest formation as well as in cardiac and musculoskeletal development [178,351,352]. One group showed that induction of EMT in immortalized human mammary epithelial cells resulted in the gain of mesenchymal traits as well as stem cell marker expression [353]. EMT plays many roles in carcinogenesis, including invasion, resistance to cell death and senescence, resistance to chemotherapy and immunotherapy, immunosuppression, inflammation, resistance to immune surveillance, and confers stem cell properties [178]. Activation of EMT is a critical mechanism for acquisition of malignant phenotype by cancer cells and facilitates aggressive dissemination since cells acquire stem cell features, invasiveness, and resistance to chemotherapy [347].

The loss of E-cadherin is central to EMT and leads to loss of cell-cell adhesion. E-cadherin is down-regulated during carcinoma by epigenetics, including transcriptional repression and promoter hypermethylation [354,355,356,357,358,359,360]. Sometimes a mutation leads to the absence or expression of a non-functional protein [361]. MicroRNAs have also been shown to play a role in E-cadherin regulation. The miR-200 family was found to directly target the mRNA of the E-cadherin transcriptional repressors ZEB1 and ZEB2 (also known as Smad-interacting protein 1 SIP1) [362,363]. E-cadherin is then replaced by expression of N-cadherin, a mesenchymal cadherin, implying a "cadherin switch" is important to initiating EMT. N-cadherin plays an opposite role of E-cadherin by promoting cell motility and migration. Changes in cadherin expression may modulate tumor cell adhesion and affect signal transduction [364]. Loss of E-cadherin contributes to metastases by inducing transcriptional and functional changes [365].

A number of pathways regulate EMT including TGF-β signaling, Wnt signaling, the Notch pathway, and tyrosine kinase receptors [352]. TGF-β signaling is a primary inducer of EMT and uses multiple distinct signaling mechanisms, such as direct phosphorylation by ligand-activated receptors of Smad transcription factors and by certain cytoplasmic proteins regulating cell polarity and tight junction formation [352,366]. EMT can occur through the Wnt signaling pathway via inhibition of phosphorylation of β-catenin by glycogen synthase kinase-3β (GSK3β). This decrease in β-catenin phosphorylation prevents degradation in the cytoplasm and leads to an increase of β-catenin in the nucleus, thus inducing Wnt target genes that are involved in EMT [367]. Notch signaling may trigger EMT via its regulation of stem cell function and maintenance of stem cell-like traits [368,369]. RTKs also play a role in EMT. Normally, they are involved in embryonic processes (i.e.—Type 1 EMT), but become mutated and constitutively active in cancer [352,370,371,372].

Numerous transcription factors are involved in EMT as well. A few well-studied proteins include Snail1, Slug, Twist, Zeb2/SIP1, and FOXC2. Snail1 is a well-studied zinc-finger transcription factor that triggers EMT by inducing the loss of epithelial markers, changing the cell shape and increasing the expression of mesenchymal markers. These allow epithelial cells to develop migratory and invasive properties during both embryonic development and tumor progression [373]. Snail1-induced EMT has been shown to accelerate cancer metastasis through enhanced invasion and immunosuppression induction [374]. Snail1 has also been shown to induce basement membrane degradation and perforation as well as initiate angiogenesis in cancer [375]. In addition to cancer cells, Snail1 regulates normal mesenchymal cell function [376]. For EMT induction, Snail1 requires binding to its co-repressor, Ajuba, via 14-3-3 interaction [377]. Slug is associated with breast cancer tumors from patients with metastatic disease or disease recurrence [378] and plays a role in semi-differentiated tubules within ductal carcinomas [379]. Twist expression leads to a loss of cell-cell adhesion and activates mesenchymal markers and induces cell motility [380]. Twist1 and Twist2 may also contribute to early tumor progression by preventing *ras*-induced senescence [381]. Zeb2 is up-regulated after Snail1-induced EMT [382] and is a Smad-interacting, multi-zinc finger protein that is triggered by TGF-β and acts as a transcriptional repressor of E-cadherin by binding to the promoter [383]. FOXC2 plays a role in invasion and metastasis and also promotes mesenchymal differentiation during EMT [384]; however, cytoplasmic FOXC2 has been shown to promote epithelial differentiation in injured tubular cells [385]. Twist1, Twist2, and Zeb1 have also been shown to regulate EMT, senescence, motility, and invasion [386].

Hypoxia can also induce EMT via up-regulation of hypoxia inducible factor 1α (HIF1α) and hepatocyte growth factor (HGF) up-regulation, DNA hypomethylation induction, and NF-

κB pathway activation [387]. In fact, a group showed that in hypoxia-induced EMT, different chromatin modifiers are induced to control EMT and that histone deacetylase 3 (hdac3) is vital for this type of EMT [388]. Alternative splicing of several genes has also been correlated with EMT progression and in an established breast cancer cell line, a group found an alternative splicing signature [389]. Other transcription factors shown to play a role in EMT, include KLF17, which was shown to be a negative regulator of EMT and metastasis in breast cancer [390] and secreted clusterin induced by TGF-β that acts as an important extracellular EMT promoter [391]. Other new players in EMT include Pez [392], PRL-3 [393,394], Aurora-A [395], Podoplanin [396,397], L1 cell adhesion molecule [398], interleukin-related molecule [399], interleukin-6 [400,401], and Thymosin β4 [402].

Similarities between PMT seen in gliomas and EMT can be drawn. Resistance to chemotherapy is commonly seen in EMT and this resistance to chemotherapy is also seen in gliomas that were originally defined as proneural and later became more mesenchymal over time [24]. Another similarity is the aggressive behavior of the tumor; those with a proneural tumor survived longer than those with a mesenchymal tumor, implying the transition to mesenchymal increases aggressiveness. This change in gene expression profiles is similar to the change seen in EMT when mesenchymal gene expression increases and epithelial gene expression decreases. Although the two processes are similar, differences exist. EMT is characterized by a loss of E-cadherin expression and a gain of Snail1, Slug, Twist, and/or ZEB2 [348]. These major EMT players seem not to play a large role in PMT and were not found to be significantly associated with mesenchymal gene expression in GBM [24]. Most of EMT is a direct result of E-cadherin loss [179,347,348,349]. A similar loss of a single protein has not been elucidated in PMT. EMT and PMT have similarities and while it would be convenient to hypothesize PMT is exactly the same as EMT, PMT likely has distinct differences that have yet

to be established, including the role of mesenchymal gene up-regulation in PMT. The role of mesenchymal gene up-regulation can only be speculated at this point. One can hypothesize that this up-regulation allows for an increase in tumor aggressiveness by increasing expression of genes involved in angiogenesis, cell motility, and ECM. This up-regulation of mesenchymal genes may also play a role in down-regulating proneural gene expression, which could then potentially lead to neural de-differentiation helping to promote tumorigenesis.

Hypothesis and Significance

Based on this information, TAZ appeared to be the most promising candidate as a transcriptional regulator that promotes the mesenchymal gene expression signature. Despite the well-established role of YAP in numerous tumors, it was not as highly correlated to the mesenchymal gene signature, thus I chose to further study TAZ. The main **hypothesis is that the TAZ-TEAD complex is critically important in PMT and aggressive clinical behavior in GBM.** Elucidating the mechanism of PMT in GBM is an important research question that needs to be answered. To ascertain the mechanism, both *in vitro* and *in vivo* studies must be done to characterize TAZ and establish its role in PMT in gliomas. TAZ expression will be stably knocked-down and over-expressed. The TAZ-TEAD interaction will also be prevented. *In vitro* studies will include invasion and proliferation assays and *in vivo* models will test for tumorigenesis as well as PMT. To study a possible molecular mechanism behind PMT, the Replication-Competent ASLV long terminal repeat with Splice acceptor (RCAS)/*Ntv-a* mouse model will be used. In this model, the expression of retrovirus-encoded genes can be directed to express in NPCs [403]. In published literature, it has been shown that the platelet-derived growth factor-β (PDGF-β) gene when over-expressed in *Nestin*$^{+}$ NPCs generates grade II

gliomas [404]. This model will be used to determine if over-expressing TAZ alone or in concert with PDGF-β is enough to drive the tumor from a lower grade, proneural phenotype to a higher grade, mesenchymal one. Using this model will be an important tool to further understand PMT in GBM.

Completion of this project will show an important mechanism that drives the aggressive nature of GBM. This research is significant because in the long-term it will contribute to the understanding of the molecular process driving the aggressive clinical behavior of GBM. TAZ could be used as a biomarker to estimate prognosis and stratify patients into clinically relevant subgroups. Also, establishing that the TAZ pathway is responsible for the cellular change seen in GBM may lead to new directions in alternative treatment options for patients. The high degree of clinical interest in attacking this pathway suggests that new concepts on elucidating the molecular mechanisms by which this pathway works will likely lead to a focused clinical trial on patients whose tumors show pathway activation. This study may also provide a rationale for developing inhibitors that directly target TAZ-TEAD and the downstream target genes.

CHAPTER 2: METHODS

Bioinformatic analyses. The ARACNe algorithm, as implemented in the geWorkBench suite (https://cabig.nci.nih.gov/tools/geWorkbench), was performed on the TCGA Affymetrix expression dataset (downloaded 04/28/2011, n=385), which was processed using a custom CDF and RMA normalization using R and Bioconductor (http://www.R-project.org/). The resulting matrix of data was processed with the following ARACNe settings: p-value of 0.01, adaptive partitioning, and DPI Tolerance of 0.1. For hub markers and the DPI target list, a composite set of transcription factors was generated from the TRANSFAC website and genes with the term 'transcription factor' in their parent GO term. The initial resulting ARACNe network was limited to GBM MES genes by combining the gene lists from Phillips [24] and Verhaak [25], and then selecting the immediately adjacent hub genes. Genes that were identified to be associated with TAZ by ARACNe analysis were processed using the DAVID webtool (http://david.abcc.ncifcrf.gov/), to obtain association of these genes with GO functional categories. Default processing was done, except the analysis was limited to DAVID's Gene Ontology biological processes FAT (GOTERM_BP_FAT) category. The resulting GO terms were ranked from smallest to largest p-values after removing terms that had 10 or less overlapping genes. To determine if a TCGA GBM was PN or MES, first a metagene score for MES or PN was generated, using a union of the respective Phillips [24] and Verhaak [25] genesets. The two metagene scores were then compared, with class being assigned based on the bigger metagene score. Tumors that had both Illumina Infinium methylation data and Affymetrix gene expression data were subsequently analyzed for correlation of TAZ methylation with TAZ expression and GBM subtype.

Cell Culture. Glioma stem cells (GSCs) were isolated from patients undergoing surgery at MDACC and grown in neural basal media (NBM) made from Dulbecco's Modified Eagle Medium (DMEM)/F12 50/50 (Cellgro) supplemented with B27 (Invitrogen), 20 ng/ml EGF (Chemicon), and 20 ng/ml FGF (Akron-Biotech). Antibiotics/antimycotics (Cellgro) were also added to the media at 1% final concentration.

To split cells, cells were collected in 50 mL Falcon tubes and centrifuged down at 4000 rpm for 5 minutes. Media was aspirated off then 1 mL Accutase (Sigma-Aldrich) was added to the cell pellet. Cells were incubated with Accutase at 37°C for 5 minutes then triturated prior to centrifugation. After centrifugation (same settings as above), Accutase was aspirated off and cells were resuspended in NBM and placed in a fresh cell culture flask.

Methyl light assay. DNA was extracted from cell lines using a DNA isolation kit (Epicentre). Proteinase K (1 μL of 50 μg/μL) was diluted into 300 μL of Tissue and Cell Lysis Solution for each sample. The cells were pelleted by centrifugation at 4000 rpm for 5 minutes and the supernatant was discarded. The Tissue and Cell Lysis Solution containing Proteinase K (300 μL) was added to each sample and mixed thoroughly then incubated at 65˚C for 15 minutes with vortexing every 5 minutes. The samples were cooled to 37˚C and RNase A (1 μL of 5 μg/μL) was added to each and mixed thoroughly then incubated at 37˚C for 30 minutes. The samples were placed on ice for 5 minutes then MPC Protein Precipitation Reagent (150 μL) was added to the 300 μL lysed sample and vortexed vigorously for 10 seconds. The debris was pelleted by centrifugation for 10 minutes at 10,000 x g in a microcentrifuge. The supernatant was transferred to a clean microcentrifuge tube and 500 μL of isopropanol was added then the tube was inverted 40 times. The DNA was pelleted by centrifugation at 4˚C for 10 minutes

then the isopropanol was carefully poured off without dislodging the pellet. The pellet was then washed twice with 70% ethanol with residual ethanol removed with a pipet. The DNA was then resuspended in 35 μL of TE buffer.

DNA was then bisulfite converted using the EZ DNA Methylation-Gold kit (Zymo). The prepared CT Conversion Reagent (130 μL) was added to 20 μL of DNA sample and mixed. The reaction was then incubated at 98˚C for 10 minutes, 64˚C for 2.5 hours, then held at 4˚C. The M-Binding Buffer (600 μL) was added to a Zymo-Spin IC Column then the sample was added and inverted several times to mix. The sample was centrifuged at maximum speed for 30 seconds and the flow-through was discarded. The M-Wash Buffer (100 μL) was added to the column, which was then centrifuged at maximum speed for 30 seconds. The M-Desulphonation Buffer (200 μL) was added to the column and incubated for 20 minutes at room temperature. After incubation, the sample was centrifuged at maximum speed for 30 seconds. The M-Wash Buffer (200 μL) was added to the column and centrifuged at maximum speed for 30 seconds; this step was repeated once more. The M-Elution Buffer (30 μL) was added directly to the column matrix placed in a fresh microcentrifuge tube. This was then centrifuged briefly to elute the DNA. The DNA concentration as then measured using the Nanodrop.

Primers (Forward: 5'-TTA TTA CGT TTC GAT TTC GGA AGT TCG-3' and R: 5'-CGC CCA AAT AAT ACC CGC TAA AAC-3') and probe (6FAM-CGC GCT CAT CCG ACA CCA CTC CAA-BHQ-1) were designed against the 2nd CpG island in the TAZ promoter using Primer Express software (Applied Biosystems) against the amplicon; 5'-GGG TAA GAG GAG ACG GGT GTT TTT TAT TTA TTT TTT TCG GTC GCG CGG ATT TTT TTC GTT TAG ATT TGT ATT TGT ATT TTT TTG AGT TTA TTA CGG ATT TGG GGC GGG ATT-3'.

To increase sensitivity, pre-amplification of 10 cycles was performed prior to real-time PCR. Real-time PCR was performed using a 96-well optical tray and optical caps with the 25 µL reaction mixture composed of 600 nM forward primer, 600 nM reverse primer, 200 nM probe, 200 µM dATP, 200 µM dCTP, 200 µM dGTP, and 400 µM dUTP, 3.5 mM $MgCl_2$, 1x TaqMan Buffer A containing a reference dye, and bisulfite-converted DNA. The reaction mixtures were then incubated at 50°C for 2 minutes for 1 cycle, 95°C for 10 minutes for 1 cycle, then 95°C for 15 seconds and 60°C for 1 minute for 40 cycles. The DNA methylation level was calculated using ΔC_T values of *WWTR1* to the *COL2A1* reference gene using the ABI 7900 Sequence Detection System (Perkin-Elmer).

Western Blot Analysis (WB). Western blot analysis was performed using standard protocols. To make the gel, two glass plates were cleaned using 70% ethanol and 1.5 mm spacers were used between the plates and locked into WB apparatus. The 15% resolving gel was made in a 50 mL Falcon tube adding 4.4 mL ddH_2O, 15 mL 30% Acrylamide (ISC Bioexpress), 2.6 mL 1% Bis-acrylamide (ISC Bioexpress), 7.5 mL 1.5M Tris (pH 8.8), 300 µL 10% SDS, 150 µL 10% APS, and 30 µL TEMED. The resolving gel was added between the two plates and ddH_2O was added on top to ensure an even top. The gel was allowed to set for 20 minutes. The stacking gel was made in a 15 mL Falcon tube adding 7 mL stacking gel solution (22.1 mL ddH_2O, 12.5 mL 0.5 M Tris (pH 6.8), 0.5 mL 10% SDS, 8.4 mL 30% Acrylamide, 6.5 mL 1% Bis-acrylamide; stored at 4°C), 70 µL 10% APS, and 7 µL TEMED. The ddH_2O on top of the resolving gel was poured off prior to the stacking gel. Either a 15 lane or 20 lane come (1.5 mm) was placed prior to pouring the stacking gel. Once poured, the stacking gel was allowed to set for 30 minutes.

Protein extraction of GSCs was performed using 0.5% NP-40 lysis buffer containing 50 mM Tris-HCl (pH7.5), 150 mM NaCl, 50 mM NaF, and supplemented with protease inhibitors (Roche) and PMSF just before use. A Lowry assay (Bio-rad) was performed to determine protein concentration. A BSA standard was used to calculate the unknown protein concentrations. Bio-Rad D_c Protein assay Reagent A (1 mL) and Bio-Rad D_c Protein assay Reagent S (20 µL) were added together to make a solution ("A + S") to add to each lysate. Using a 96-well flat bottom plate, 5 µL of lysate were placed in each well. To each well containing lysate, 25 µL A + S was added. Bio-Rad D_c Protein assay Reagent B (200 µL) was then added to each well. The assay was read using a plate reader and SoftMax Pro program. Protein concentration was then calculated and a final volume of 45 µL was used for each WB lane. NP40 buffer was used to increase the volume when needed. Prior to loading, each sample was placed in a microcentrifuge tube and 5 µL of 5x SDS + DTT was added. Each sample was then heated at 95°C for 5 minutes then loaded into the gel. The ladder (Precision Plus Protein Kaleidoscope standard) was loaded as well at 5 µL. The running buffer was 1x SDS PAGE. The gel was run at 220 V for 2 hours or at 40 V for overnight.

Prior to transfer, four chromatography paper pieces (16 cm x 14.5 cm) were soaked in transfer buffer (50 mL 5x Transfer buffer, 150 mL ddH_2O, 50 mL methanol) along with the nitrocellulose membrane. Two chromatography paper pieces were placed in the Amersham Biosciences Hoefer TE 70 semi-dry transfer unit then the nitrocellulose paper was added. The gel without the stacking gel portion was placed on top of the nitrocellulose. The last two chromatography papers were added on top of the gel. The transfer was run at 0.2 Amps for 1 hour. After the transfer, the nitrocellulose was blocked using 10% milk solution (10 g milk in 100 mL PBS). The primary antibody was added then left at 4°C overnight on a rocker.

To determine protein expression I used the following antibodies: from Sigma-Aldrich—TAZ (1:2500), NF2 (1:1000), MST1 (1:1000), p-MST1 (1:1000), MOB1 (1:500), LATS1 (1:1000), p-LATS1 (1:1000), 14-3-3-ε (1:1000), Flag (1:1000), Runx2 (1:1000), and SMA (1:1000); from Santa Cruz Biotechnology—YAP (1:500), TEAD1 (1:1000), TEAD2 (1:1000), TEAD3 (1:1000), TEAD4 (1:1000), SMAD2 (1:2000), p-TAZ (1:1000), p-YAP (1:1000), C/EBP-β (1:500), GFAP (1:1000), and Lamin (1:1000); from Bethyl Labs—LATS2 (1:1000); from Calbiochem—Actin (1:10,000); from BD Biosciences—FN1 (1:5000), CAV2 (1:1000), Mash1 (1:1000), SATB1 (1:1000), SATB2 (1:1000); from Abcam—CTGF (1:500); from Cell Signaling Technologies—CD44 (1:1000), Cyclin A (1:1000), Cyclin E (1:1000), Cyclin B1 (1:1000), MST2 (1:1000), p-cdk1 (1:1000), p-cdk4 (1:1000), STAT3 (1:1000), TCF3 (1:1000); and from IBL—Olig2 (1:1000).

The next day, the milk was poured off and washed with tap water once. Then the membranes were washed three times with PBST (1 L PBS with 1 mL Tween 20) for 5 minutes each wash on a shaker. The secondary antibody (Santa Cruz Biotechnology anti-rabbit or anti-mouse, as appropriate) was added to the milk (1:5000) and added to each membrane and rocked at room temperature for 1 hour. The secondary antibody was then removed and the membranes were washed four times with PBST for 15 minutes each wash on a shaker.

To develop, the SuperSignal West Dura Extended Duration Substrate Kit (ThermoScientific) was used. Equal volumes of the SuperSignal West Dura Stable Peroxide Buffer and the SuperSignal West Dura Luminol/Enhancer Solution were used. Each membrane was exposed to this solution for 3 minutes. The membranes were placed in a cassette and exposed to Basic Blue Autorad film (Gene Mate) then the film was developed.

For human glioma specimens, frozen tumors were dissected out and lysed with buffer containing 7M urea, 2M thiourea, 1% CHAPS, and 50 mM Tris-HCl (pH 7.5). Protein concentrations were determined using the CB-X Protein Assay (G Biosciences). The CB-X was chilled at -20°C prior to start. The protein samples (5 µL each) were transferred to microcentrifuge tubes and 1 mL pre-chilled CB-X was added to each sample and vortexed to mix. The samples were centrifuged at 13,500 rpm for 5 minutes and the supernatant was carefully removed without disturbing the protein pellet. CB-X Solubilization Buffer-I (50 µL) and CB-X Solubilization Buffer-II (50 µL) were added to the tube and vortexed to dissolve the protein pellet. The CB-X Assay Dye was mixed prior to use by gently inverting the bottle several times and 1 mL was added to the tube and vortexed briefly. The samples were incubated at room temperature for 5 minutes. The sample (200 µL assay solution) was transferred to a microtiter well and the absorbance was read at 595 nm against dH_2O. The CB-X Table was used to determine the amount of protein in the samples. The protein concentration was calculated by dividing the amount of protein by the sample volume.

Immunohistochemistry (IHC). IHC analyses were performed on paraffin blocks, deparaffinized at 65°C for 10 minutes, and hydrated through an ethanol series. The slides were placed in Xylene twice for 2 minutes each, then 100% ethanol for 2 minutes, 95% ethanol for 2 minutes, and 70% ethanol for 2 minutes. Slides were washed in PBS once then washed twice with tap water. The slides were then placed in 196 mL ddH_2O and 4 mL 0.5 M sodium citrate. The slides were placed in a crockpot (all vents completely closed) containing some tap water and microwaved for 10 minutes at high power then 12 minutes at medium low power. The slides were allowed to cool for 30 minutes then were placed in 180 mL PBS + 20 mL 20%

H_2O_2 + 50 µL Tween 20 for 30 minutes. Primary antibody was diluted in FBS (9:1 PBS:FBS). The slides were washed ten times with tap water then placed in a slide developer containing some water. Excess water was removed using KimWipes then 100-150 µL primary antibody was added to each slide and evenly spread to ensure all tissue was exposed to the antibody. Antibodies against TAZ (1:33; Novus), FN1 (1:4000; BD Biosciences), or CD44 (1:5000; Cell Signaling Technologies) were incubated with the slides overnight at 4°C.

The next day the slides were washed twice with PBS then excess liquid was removed using KimWipes and slides were placed in the slide developer. Staining was performed using the DAKO Envision kit according to the manufacturer's instructions (DAKO, Carpentaria, CA). The slides were covered with secondary antibody (DAKO labeled polymer-hrp anti-rabbit) and allowed to sit for 30 minutes. The slides were then washed twice with PBS and placed in the slide developer after removal of excess liquid. The slides were covered with 100 µL of dye (1 drop DAB+ chromogen per 1 mL DAB+ substrate buffer) and allowed to sit for 5 minutes. The slides were immediately added to tap water to stop the reaction. The slides were placed in fresh hematoxylin and washed with tap water until the water was clear. The slides were then dehydrated in 70% ethanol for 2 minutes, 95% ethanol for 2 minutes, 100% ethanol for 2 minutes, and finally, Xylene twice for 2 minutes each. Excess liquid was removed from each slide then covered with PerMount and covered with a 24 x 40 mm cover slip. The slides then dried for two hours.

Nuclear and Cytoplasmic Extraction. The compartment proteins were extracted from cultured cells using the Compartmental Protein Extraction Kit (Millipore). The cells were pelleted at 4000 rpm for 5 minutes then counted using the ViCell counter. Ice cold buffer C

was added to the cells at a concentration of 2 mL per 20 million cells and mixed well. The mixture was rotated at 4˚C for 20 minutes. A syringe with a needle gauged between 26.5 and 30 was prepared. The cell mixture was passed through the needle base 50-90 times to disrupt the cell membrane and release the nuclei from the cells. The cell mixture was centrifuged at 15,000 x g for 20 minutes at 4˚C. The cytoplasmic proteins were in the supernatant and saved in another tube then kept on ice. The pellet was resuspended with ice cold buffer W at 4 mL per 20 million cells and rotated at 4˚C for 5 minutes. The mixture was then centrifuged at 15,000 x g for 20 minutes at 4˚C. The nuclear proteins are in the supernatant and saved in another tube. The proteins were stored at -80˚C until ready to be analyzed by WB.

Bisulfite sequencing. Genomic DNA isolated from GSCs using the Epicentre kit, described above, was bisulfite converted using the Zymo kit, also described above. The DNA was then inserted into a Topo vector using the TOPO TA Cloning Kit for Sequencing (Invitrogen). The cloning reaction was composed of the following: 4 μL Fresh Purified PCR product, 1 μL Salt Solution, and 1 μL TOPO vector. The reaction was gently mixed and incubated for 5 minutes at room temperature then placed on ice. The TOPO Cloning reaction (6 μL) was added into a vial of One Shot Chemically Competent *E. coli* and gently mixed then incubated on ice for 30 minutes. The cells were heat shocked for 30 seconds at 42˚C without shaking then immediately transferred to ice. Room temperature S.O.C. Medium (150 μL) was added the cells then the cells were horizontally shaken in the tube at 37˚C for 1 hour. Each transformation (125 μL) was spread on pre-warmed LB Ampicillin plates then incubated overnight at 37˚C.

Colonies were picked the next day and grown in 2 mL LB Ampicillin (1:1000) overnight at 37˚C while shaking. After overnight culture, plasmids were isolated using the QIAprep

Miniprep kit (Qiagen). In a fresh microcentrifuge tube, cells (1.5 mL) were pelleted down at 6000g for 15 minutes. The pelleted bacterial cells were resuspended in 250 μL Buffer P1 and 250 μL Buffer P2 then mixed thoroughly by inverting the tube 6 times. Buffer N3 (350 μL) was then added and mixed immediately and thoroughly by inverting the tube 6 times. The cells were centrifuged for 10 minutes at 13,000 rpm in a table-top microcentrifuge. The supernatant was applied to the QIAprep spin column by pipetting and centrifuged for 1 minute at 13,000 rpm; the flow-through was discarded. The QIAprep spin column was washed by adding 0.5 mL Buffer PB and centrifuged for 1 minute at 13,000 rpm; the flow-through was discarded. The QIAprep spin column was then washed again by adding 0.75 mL Buffer PE and centrifuged 1 minute at 13,000 rpm; the flow-through was discarded. The samples were centrifuged for an additional minute at 13,000 rpm to remove the residual buffer. The DNA was eluted by placing the QIAprep column in a clean microcentrifuge tube and adding 50 μL Buffer EB to the center of each column. This was allowed to sit for 1 minute then was centrifuged for 1 minute at 13,000 rpm. The eluted DNA was sequenced at the MD Anderson Cancer Center core facility using the available M13 Forward (5'-GTA AAA CGA CGG CCAG-3') and Reverse (5'-CAG GAA ACA GCT ATG AC-3') primers. Sequencing was compared to the promoter sequence available on the Transcriptional Regulatory Element Database website (http://rulai.cshl.edu/cgi-bin/TRED/tred.cgi?process=home) to identify methylated CpG pairs.

Real-Time Reverse transcriptase PCR (qRT-PCR). mRNA was obtained using the QIAshredder kit (Qiagen) and the RNeasy Plus Mini Kit (Qiagen) followed by a two-step qRT-PCR method. Cells were collected via centrifugation for 5 minutes at 4000 rpm. The cells

were then disrupted by adding 350 µL Buffer RLT Plus with β-mercaptoethanol (β-ME; 10 µL β-mercaptoethanol per 1 mL Buffer RLT Plus). The lysates were homogenized using the QIAshredder spin column placed in a 2 mL collection tube and centrifuged for 2 minutes at maximum speed. The homogenized lysate was then transferred to a gDNA Eliminator spin column placed in a 2 mL collection tube and centrifuged for 30 seconds at 10,000 rpm. The column was discarded and the flow-through was saved. One volume (350 µL) of 70% ethanol was added to the flow-through and mixed well by pipetting. The 700 µL sample was transferred to an RNeasy spin column placed in a 2 mL collection tube and centrifuged for 15 seconds at 10,000 rpm; the flow-through was discarded. Buffer RW1 (700 µL) was added to the RNeasy spin column and centrifuged for 15 seconds at 10,000 rpm; the flow-through was discarded. Buffer RPE (500 µL) was added to the RNeasy spin column and centrifuged for 15 seconds at 10,000 rpm; the flow-through was discarded. Buffer RPE (500 µL) was added to the RNeasy spin column and centrifuged for 2 minutes at 10,000 rpm. The RNeasy spin column was placed in a new 1.7 mL collection tube. RNase-free water (40 µL) was directly added to the spin column membrane and centrifuged for 1 minute at 10,000 rpm to elute the RNA. The RNA concentration was found using the Nanodrop.

A total of 1 µg RNA was reverse transcribed to generate first strand DNA (Invitrogen). The RNA/primer mixture was prepared in sterile 0.5 mL tubes as follows: 1 µg RNA, 2 µL random hexamers (50 ng/µL), 1 µL 10 mM dNTP mix, and DEPC-treated water to bring the volume up to 10 µL. Each sample was incubated at 65˚C for 5 minutes then incubated on ice for at least 1 minute. For each sample, the following reaction mixture was prepared by adding each component in the indicated order: 2 µL 10X RT buffer, 4 µL 25 mM $MgCl_2$, 2 µL 0.1 M DTT, and 1 µL RNaseOUT Recombinant Ribonuclease Inhibitor. The reaction mixture (9 µL) was added to each RNA/primer mixture and mixed gently then collected by brief centrifugation.

The samples were then incubated at 25˚C for 2 minutes. SuperScript II RT (1 µL; 50 units) was added to each tube then mixed. The tubes were placed in a PCR machine and incubated at 25˚C for 10 minutes, 42˚C for 50 minutes, 70˚C for 15 minutes, and 4˚C forever. The reactions were collected by brief centrifugation and 1 µL RNase H was added to each tube and incubated for 20 minutes at 37˚C before amplifying the target cDNA.

To amplify the cDNA, Taqman primer probes in conjunction with 2x Taqman Universal PCR Master Mix (Applied Biosystems) were used for the following genes: *WWTR1*, *CTGF*, *CD44*, *FN1*, *YAP*, *CHI3L1*, *ACTG2*, *SMA*, *CXCL2*, *SERPINE1*, *SMAD7*, *TCF3*, *ADAMTS1*, *IL8*, and *Actin*. RNase inhibitor (0.4 units/µl; Roche) was included in every reaction. Each reaction was done in triplicate wells and the final volume was 20 µL per well (10 µL Master Mix, 1 µL TaqMan primer probe mix, 8 µL ddH_2O, 1 µL cDNA). Reaction mixtures were incubated at 95°C for 10 minutes for 1 cycle then 15 seconds at 95°C and 1 minute at 60°C for 40 cycles. The fluorescent signal was measured using the Applied Biosystems 7500 and the relative level of fold changes were calculated using the absolute $\Delta\Delta C_T$ method.

For the RCAS samples, RNA was isolated from tissue in Tissue-Tek O.C.T. First, everything used including the bench was cleaned with RNase Zap (Ambion). The bench was covered with a blue pad and a block of dry ice was covered with foil then placed on a Styrofoam top. Autoclaved microcentrifuge tubes were labeled (2 per sample) with 1 kept on dry ice and the other in liquid nitrogen. Thoroughly cleaned mortars and pestles were used (1 each per sample). A Thermoflask was filled with liquid nitrogen and the centrifuge was set to 4˚C prior to start. PBS was placed in a 50 mL Falcon tube and placed on ice. To isolate the tumors from the tissue, the frozen tissue was placed next to the dry ice block to soften the O.C.T. The O.C.T. was cut from the tissue (as much as possible) and the isolated tumor was placed in an

microcentrifuge tube then kept on dry ice. For each sample, a fresh scalpel was used and the foil surrounding the dry ice block was replaced. Each sample was washed once with cold PBS (1 mL) then shaken until the O.C.T. was no longer white; the samples were kept on dry ice for as much as possible). The tubes were then centrifuged for 5 minutes at maximum speed. The PBS was removed then the sample was placed on dry ice. Liquid nitrogen was poured into a mortar and the tissue was scooped out from the microcentrifuge tube. The tumor was then ground to a fine powder (liquid nitrogen was added as needed) then the powder was transferred to the microcentrifuge tube that was kept in the liquid nitrogen. The liquid nitrogen was allowed to evaporate from the powder substance before the microcentrifuge tube top was closed and the tube was placed back into the liquid nitrogen. The RNA was then isolated as above using the Qiagen RNeasy kit.

Small interfering RNA transfection. Transient knockdown was performed using siRNA constructs from Dharmacon against: scrambled control (D-001810-10), TAZ (L-016083-00), STAT3 (L-003544-00), C/EBP-β (L-006423-00), and SMAD2 (L-003561-00). Cells were cultured on laminin (BD Biosciences)/poly-L-ornithine coated plates. The laminin solution was made from 45 mL filtered DMEM/F12 plus 5 mL poly-L-ornithine and 50 μL laminin. Plates were coated with enough volume to cover the surface and sat at room temperature for 30 minutes. After coating, the plates were washed three times with PBS. Cells were allowed to attach to plates overnight in antibiotic free media. The next day the antibiotic free media was removed and the cells were washed twice with PBS. For a 6-well plate, each well had 700 μL OptiMem (Gibco) added after PBS wash. Two solutions were then made: 1) siRNA mixture and 2) Lipofectamine 2000 (Invitrogen) mixture. For the siRNA mixture, 6 μL of 10 μM

siRNA was added to 144 µL OptiMem and allowed to sit at room temperature for 5 minutes. For the Lipofectamine 2000 mixture, 5 µL Lipofectamine 2000 was added to 145 µL OptiMem and allowed to sit at room temperature for 5 minutes. After the 5 minute incubation for both, the mixtures were added together and allowed to sit for 30 minutes at room temperature. After the 30 minute incubation, the siRNA/Lipofectamine 2000 mixture was added to the cells suspended in 700 µL OptiMem (final siRNA concentration was 60 nM) and the cells were incubated at 37˚C for 6 hours. After 6 hours, the media was changed to regular media containing antibiotics and cells were collected and analyzed 48-72 hrs later.

Transfection. For lentivial transduction, pGIPZ vectors expressing shRNA against mRNA of *WWTR1*, *TEAD*, and *CTGF* were used. Viral particles were generated using the Trans-lentiviral packing system (Open Biosystems). 293FT Cells were cultured in 6-well plates overnight at a concentration of 1.2 x 10^6 cells in 2 mL media. For each well of a 6-well plate, the following two mixtures were made: 1) 9 µg leniviral transfer vector DNA, 26 µL Trans-lentiviral packaging mix, and serum free media to bring the volume up to 1 mL; 2) 187.5 µL Arrest-In and 812.5 µL serum free media. Both mixtures sat for 5 minutes at room temperature before being added together. The mixed solutions then incubated at room temperature for 30 minutes. Serum free media was added to the 293FT cells then the lentiviral/Arrest-In mixtures. After 6 hours, the media was changed to normal media containing serum. The viral particles were collected by harvesting the supernatant, which was centrifuged at 1600 x g for 10 minutes at 4˚C to remove cell debris. The supernatant was carefully removed and transferred to a fresh centrifuge tube. The particles were filtered using a 0.45 µm filter, aliquoted, and stored at -80˚C or used immediately. The GSCs were grown overnight in antibiotic free media in laminin

coated (described above) P100 plates. For each plate of cells, equal volumes of viral supernatant and NBM plus polybrene (Chemicon) was added. For example, 2 mL viral supernatant, 2 mL NBM, and 0.8 μL of 10 μg/μL polybrene stock (final concentration 2 μg/mL) were added to the cells. The cells were incubated with this mixture for 6 hours then the media was changed to NBM. The cells were analyzed microscopically for the presence of GFP then selected in NBM containing puromycin (4 μg/mL) for generation of stable clones.

Phoenix Ampho (for GSCs) obtained from a commercial source (Orbigen) and grown in DMEM/F12 plus 10% fetal bovine serum (FBS) were transfected with 16 μg of DNA (pBABE vector containing wild type TAZ, 4SA, 4SA-S51A) using Lipofectamine 2000 (Invitrogen) according to manufacturer instructions. Two mixtures were made: 1) 16 μg DNA in 500 μL OptiMem; 2) 20 μL Lipofectamine 2000 in 500 μL OptiMem. These two mixtures incubated separately for 5 minutes at room temperature before being added together. Once mixed together, the solution incubated for 30 minutes prior to adding to the cells. The cells incubated with 1 mL DNA/Lipofectamine plus 2 mL antibiotic free media for 6 hours then the media was changed to regular media. Viral supernatants were collected 48 hours after transfection, filtered using at 0.45 μm filter, and immediately used for transduction of GSCs. Cells were cultured on laminin coated plates (described above) then transduced with viral supernatant plus polybrene at a final concentration of 2 μg/mL. After 6 hours, the media viral supernatant was aspirated off then replaced with NBM. The pBABE transduced GSCs were selected in NBM containing puromycin (4 μg/ml) for generation of stable clones.

The pBABE-4SA-S51A plasmid was made using the QuikChange II XL Site-Directed Mutatgenesis Kit (Stratagene) and primers designed to introduce serine to alanine mutation (5'-CGG AAG AAG ATC CTG CCG GAG GCC TTC TTT AAG GAG CCTG-3'; 5'-CAGG CTC

CTT AAA GAA GGC CTC CGG CAG GAT CTT CTT CCG-3'). The sample reaction was prepared as follows: 5 μL of 10x reaction buffer, 10 ng or 50 ng of dsDNA template, 1.25 μL forward primer (10 μM stock), 1.25 μL reverse primer (10 μM stock), 1 μL of dNTP mix, 3 μL of QuikSolution, and ddH_2O to a final volume of 50 μL. Then 1 μL of *PfuUltra* HF DNA polymerase (2.5 U/μL) was added to the sample. The samples were amplified using the following program: 95˚C for 1 minute for 1 cycle, then for 18 cycles at 95˚C for 50 seconds, 60˚C for 50 seconds, and 68˚C for 7.5 minutes, followed by 68˚C for 7 minutes and 4˚C forever. To each amplification reaction, 1 μL of *Dpn* I restriction enzyme (10 U/μL) was added. The reaction was gently and thoroughly mixed by pipetting then centrifuged for 1 minute at maximum speed. The reactions were then incubated immediately at 37˚C for 1 hour to digest the parental dsDNA. XL 10-Gold ultracompetent cells were thawed on ice and for each reaction to be transformed, 45 μL of the cells were aliquoted to pre-chilled 14-mL BD Falcon polypropylene round-bottom tubes. β-ME (2 μL) were added to the 45 μL of cells then swirled to gently mix. The cells were incubated on ice for 10 minutes and swirled gently every 2 minutes. The *Dpn* I-treated DNA (5 μL) were added to the cells and swirled to gently mix then incubated on ice for 30 minutes. The S.O.C. Medium was preheated in a 42˚C water bath during this incubation. The cells were heat shocked at 42˚C for 30 seconds then immediately incubated on ice for 2 minutes. The preheated S.O.C. Medium (0.1 mL) was added to each tube then the tubes were incubated at 37˚C for 1 hour with shaking. The entire reaction was plated on LB Ampicillin plates then incubated at 37˚C overnight.

Colonies were picked the next day and grown in 2 mL LB Ampicillin (1:1000) overnight at 37˚C while shaking. After overnight culture, plasmids were isolated using the QIAprep Miniprep kit (Qiagen) as described above. The eluted DNA was sequenced at the MD

Anderson Cancer Center core facility using the following primer sequences: 5'-CGC TCG CAC GCG TCG CCC GCG-3' and 5'-CGC GGG CGA CGC GTG CGA GCG-3'.

Matrigel Invasion Assay. Matrigel (BD Biosciences) aliquots were thawed overnight in 4˚C then diluted down to 0.7 mg/mL using cold serum-free media and kept on ice. This diluted solution was plated on a transwell (200 µL/well; ISC Bioexpress) and allowed to sit at room temperature for at least 20 minutes. Then the medium was removed from the transwell prior to plating cells. Cells were split as described above and resuspended in serum-free media then counted using the ViCell counter (described below). The cells were washed at least 3 times in serum-free media and resuspended in serum-free media (one million cells in 500 µL are needed to plate on each transwell). Each transwell had a final volume of 700 µL (500 µL of cells plated plus 200 µL serum-free media). Serum-containing media (1 mL) was added below each transwell then the cells incubated overnight in a 37˚C incubator.

The next day the medium from the transwell and the well below was removed. Hema 3 staining kit (Thermo Fisher) was used to stain the cells that invaded through the Matrigel. Stain 1 (fixative) was added to the transwell (200 µL) and the well below (500 µL) and allowed to sit for 20 minutes. The stain was removed and Stain 2 was added as above. After 20 minutes, Stain 2 was removed and Stain 3 was added as above. At the end of 20 minutes, Stain 3 was removed and each transwell was removed and dipped in a beaker of tap water. A Q-tip was used to remove the Matrigel and the transwell were left to dry overnight.

The last day the transwell membranes were cut and placed in individual microcentrifuge tubes. Each tube had 250 µL of 5% Sodium Deoxycholate (Sigma-Aldrich) added and allowed to

rotate on a belly-dancer for 20 minutes to extract the dye. For the OD reading, 200 μL of each sample was plated in a 96-well flat bottom plate and read at 595 nm using the SoftMax Pro program. The control reading was set to 100% and the experimental arms were calculated relative to the control.

Neurosphere Assay. Cells were split as described above and resuspended in diluted propidium iodide (50 μg/mL) then filtered through a filtered cap flow tube. Viable cells were fluorescence-activated cell sorted (FACS) using an MD Anderson Cancer Center core facility then centrifuged to collect the cells. The cells were resuspended in 1.25 mL NBM then 250 μL of the cell suspension was added to 750 μL NBM in a ViCell vial. Viability was calculated using the ViCell counter and 3 cells were plated per well in a 96-well flat bottom plate in triplicate. Cells were allowed to grow for three weeks with the addition of fresh media as needed. The number of wells containing neurospheres was counted three weeks after plating.

EdU labeling and flow cytometric analysis. After trituration, cells were chased with 30 μM EdU (stock 100 mM) for 2 hours at 37˚C. The cells were then centrifuged and accutized after EdU treatment. S phase cells were detected using the Click-iT EdU kit (Invitrogen) per kit instructions. After accutizing, the cells were washed once with 1% BSA in PBS and pelleted by centrifugation at 500 x g for 5 minutes; the supernatant was removed. The cells were resuspended at 1 x 10^7 cells/mL in 1% BSA in PBS. The cell suspension (100 μL) was added to flow tubes along with 100 μL of Click-iT fixative (Component D); the pellet was dislodged and mixed well to ensure a homogenous sample. The tubes were covered with foil and

incubated at room temperature for 15 minutes. The cells were washed once with 3 mL of 1% BSA in PBS then pelleted as above; the supernatant was removed. The cell pellet was dislodged and mixed will to ensure a homogenous sample. Triton X-100 based permeabilization reagent (100 µL; Component F) was added and mixed well then incubated for 30 minutes at room temperature protected from light. Each tube was washed with 3 mL of 1% BSA in PBS then pelleted as above; the supernatant was removed. The pellet was dislodged and mixed well to ensure a homogenous sample. The Click-iT reaction cocktail was made from the following components and was used within 15 minutes: for 1 reaction, 438 µL 1x Click-iT Reaction Buffer, 10 µL $CuSO_4$ (Component H), 2.5 µL Fluorescent dye azide, and 50 µL Reaction Buffer Additive. The Click-iT reaction cocktail (0.5 mL) was added to each tube then mixed well and incubated at room temperature for 30 minutes protected from light. The cells were washed once with 3 mL of 1% BSA in PBS, then pelleted as above; the supernatant was removed. To the cells, 1% BSA in PBS (0.5 mL) was added along with 5 µL of Ribonuclease A (Component L) to each tube and mixed. CellCycle 405-blue (2 µL) was added to each tube and mixed well then incubated at room temperature for 30 minutes protected from light. The final product was filtered through the top of a filtered flow tube prior to FACS analysis at an MD Anderson Cancer Center core facility. For the detection of EdU with Alexa Fluor 647 azide, 633/635-nm excitation with red emission filter (660/20-nm) was used. The fluorescent signal generated by the Alexa Fluor 647 azide was best detected with logarithmic amplification. For the detection of DNA content, blue emission filter (450/50-nm) was used. The fluorescent signal generated by the CellCycle stain was best detected with linear amplification.

Intracranial Mouse Injections. Cells were split as described above and counted using the ViCell counter. The cells were resuspended in serum free media at a concentration of 10K cells/μL. SCID mice were bolted as previously described [405] and injected with cells (10K/μL) in serum free media. Five mice were injected for each group. Mice were sacrificed using carbon dioxide once they showed neurological symptoms or appeared moribund. Brains were immediately fixed in 4% paraformaldehyde (PFA) and processed for hematoxylin and eosin staining or IHC.

Immunofluorescence (IF). IF was performed on GSCs plated on laminin (described above) coated chamber slides overnight. The media was aspirated off the cells and the cells were washed twice in PBS at room temperature. The cells were fixed in freshly prepared 3% PFA in PBS for 10 minutes at room temperature. The cells were then rinsed once in PBS to remove the PFA. The cells were then permeabilized in PBS/0.2% Triton X-100 for 5 minutes at 4˚C followed by two PBS washes to remove the Triton. The cells were then blocked in blocking solution made from PBS and 0.5% bovine serum albumin (BSA) for 30 minutes at room temperature with gentle shaking. The blocking solution was aspirated off then the primary antibody diluted in the blocking solution (Smad2/3 1:5000) was added (total volume 200 μL/well) and incubated for 1 hour with gentle shaking at room temperature. The cells were washed 3 times with PBS for 10 minutes per wash at room temperature while gently shaking. The secondary fluorescent antibody was diluted to 1:100 in blocking solution and added to the cells then incubated for 30 minutes at room temperature with gentle shaking (the chamber slide was covered with foil at this time). The cells were washed 3 times with PBS for 10 minutes at room temperature while gently shaking and covered with foil. The chambers were removed

and the cells were covered with 1 drop of ProLong Gold (Invitrogen) mounting solution followed by a cover slip. The slide was analyzed using an Olympus microscope.

Immunoprecipitation (IP). Prior to start, the Protein G dynabeads (Invitrogen) were rocked (not vortexed) for 20 minutes. After 20 minutes, the Protein B dynabeads were aliquoted (50 µL) into microcentrifuge tubes (2 tubes per sample) and the buffer was removed. The beads were then resuspended in 400 µL of 0.5% NP40 lysis buffer and 4 µL of the primary antibody (or IgG) was added as appropriate to each tube to cross link the beads to the antibody. The tubes rotated on a belly dancer for 1 hour at room temperature. During the hour incubation, the cells were prepped. Each IP used 1 confluent P150 of cells. The cells were pelleted and washed with PBS for 5 minutes at 4000 rpm. Cells were lysed using the lysis solution mentioned above (1.5 mL 0.5% NP40 lysis buffer per P150). The lysed cells were aliquoted (1.5 mL cells in a microcentrifuge tube) and rotated in the cold room for 30 minutes. The cells were then spun down at maximum speed at 4˚C for 10 minutes. The Input was aliquoted at this time (5 µL supernatant per P150). The 0.5% NP40 lysis buffer was then removed from the beads and the 1.5 mL lysed cells were added to the beads and left in the cold room overnight to rotate.

The next day the beads were washed 4 times with 0.5% NP40 lysis buffer (1 mL per wash per tube). The first wash was immediate and the next 3 washes were 30 minutes each on the belly dancer at room temperature. After the washes, 50 µL of 2x loading buffer dye was added to each tube and vortexed very well then spun down at maximum speed for 5 seconds. The Input samples were prepared by adding 30 µL PBS, 10 µL 5x loading buffer dye, and 10 µL Input.

The samples were then boiled for 5 minutes at 95˚C and loaded onto a WB gel then ran overnight at 55 V.

Osteogenesis and chondrogenesis assays. Cells were seeded at a density of $5x10^4$ cells in a 6-well plate. After 24 hours, cell differentiation was induced with Complete Osteogenesis Differentiation Medium (Lonza). Cells were fed every 3-4 days by completely replacing the medium with fresh Osteogenesis Differentiation Medium. After 3-4 weeks, cells were rinsed in PBS, fixed with 4% formaldehyde solution for 30 minutes then rinsed twice with dH_2O and stained with 2% Alizarin Red S Solution (pH 4.2) for 2-3 minutes. The wells were rinsed three times with dH_2O then visualized under light microscopy for analysis.

For the chondrogenesis assay, cell pellets were prepared by spinning down $3x10^5$ cells in 15 ml polypropylene tubes and grown in Complete Chondrogenesis Differentiation Medium (Lonza). Cell pellets were fed every 2-3 days by completely replacing the medium with freshly prepared Complete Chondrogenesis Differentiation Medium. After 3-4 weeks, pellets were fixed in buffered 10% formalin and embedded in paraffin. Sections (5 μm) were slide-mounted and stained for glycosaminoglycans with Safranin O.

Microarray analyses. 15 μg of cRNA was used in the hybridizations to U133A 2.0 human GeneChip expression arrays done according to the specifications of the manufacturer (Affymetrix). Intensity data were obtained from array images and data was analyzed using R Suite as previously described.

Chromatin Immunoprecipitation (ChIP) assay. The ChIP assay was done using the Imprint ChIP kit from Sigma-Aldrich. For each ChIP sample assay well, 1 x 10^5 cells were used. The cells were centrifuged at 180 x g for 5 minutes then the supernatant was discarded. The cells were washed once with 10 mL of PBS by centrifugation as above. The cells were then resuspended in 9 mL fresh culture medium and 270 µL of 37% formaldehyde was added to the sample, which was then mixed by inverting the tube several times immediately following formaldehyde addition. This mixture was incubated for 10 minutes at room temperature on a rocking platform. The cross-linking was quenched by adding 1 mL of 1.25 M glycine for every 9 mL cross-linking solution and mixed then centrifuged at 180 x g for 5 minutes. The medium was removed and the cells were washed three times with 10 mL ice-cold PBS by centrifugation. The Nuclei Preparation Buffer was added to resuspend the cell pellet (200 µL/10^6 cells) and transferred to a microcentrifuge tube then incubated on ice for 10 minutes. After incubation, the sample was vortexed vigorously for 10 seconds and centrifuged at 180 x g for 5 minutes. The supernatant was carefully removed and the nuclear pellet was resuspended in Shearing Buffer (100 µL/10^6 cells) containing Protease Inhibitor Cocktail (PIC; 10 µL PIC/1 mL Shearing Buffer). The samples were incubated on ice for 10 minutes with occasional vortexing. DNA was sonicated using an Ultrasonic Processor (GE130, Sorvall) at 25 cycles of 10 pulses each at 80% power with 1 min interval between cycles. Sonicated DNA was then centrifuged at 14,000 rpm for 15 minutes at 4^{o}C. The clarified supernatant was transferred to microcentrifuge tubes in 50 µL aliquots and stored at -80˚C until use.

The Stripwells were washed once with 150 µL of Antibody Buffer prior to start. Antibody Buffer (100 µL) was mixed with 2 µg of antibody (mouse IgG, BD Biosciences TAZ, or Novus

TEAD2) then added to each well as appropriate. The Stripwells were then covered with Parafilm and shaken at 50-100 rpm for 60-90 minutes at room temperature. The clarified supernatant was diluted with Dilution Buffer at a ratio of 1:9. The diluted supernatant (5 µL) was set aside on ice as Input (5%) control. The incubated antibody solution was removed from the wells and the wells were washed 3 times with 150 µL of Antibody Buffer by pipetting up and down. The diluted supernatant (100 µL) was added to each well and the wells were covered with Parafilm then incubated on an orbital shaker at 4˚C overnight.

The supernatant was removed the next day then the wells were washed 6 times with 150 µL of IP Wash Buffer for 2 minutes each wash. The washes were removed by inverting and striking the wells onto a paper towel 10 times. The wells were washed once with 150 µL of 1x Tris-EDTA Buffer. DNA Release Buffer (40 µL) containing Proteinase K (1 µL Proteinase K/40 µL DNA Release Buffer) was added to each sample including Input then mixed well by pipetting. The sample wells were covered with Stripcaps then incubated along with the Input vial at 65˚C for 15 minutes. Reversing Solution (40 µL) was added to the samples and Input then mixed, covered, and incubated at 65˚C for 90 minutes. The samples were then transferred and stored in microcentrifuge tubes at -20˚C overnight.

A GenElute Binding Column G was placed in a Collection Tube then the column was equilibrated by adding 500 µL of Column Preparation Solution. The column was centrifuged for 1 minute at 12,000 x g and the flow-through was removed. All subsequent centrifugations were done at 12,000 x g. In a separate vessel, 400 µL of Binding Solution and the ChIP lysate were added together and briefly vortexed. The mixed solution was then transferred to an equilibrated binding column and centrifuged for 1 minute; the flow-through was removed. Diluted Wash Solution Concentrate (500 µL) was added to each spin column then centrifuged

for 1 minute; the flow-through was removed. The columns were centrifuged for an additional 2 minutes to thoroughly dry the column. The spin column was then transferred to a new collection tube and 50 µL of Elution Solution was added directly to the membrane in the column then incubated for at least 1 minute. The column was centrifuged for 1 minute then the DNA was stored for downstream applications at -20˚C.

ChIP DNA was analyzed by PCR. Each reaction had the following: 12.5 µL AmpliTaq Gold Master Mix (Applied Biosystems), 1.25 µL 10 µM forward primer, 1.25 µL 10 µM reverse primer, 9 µL sterile H_2O, and 1 µL DNA. Reaction mixtures were incubated at 95°C for 2 minutes for 1 cycle then 30 seconds at 95°C, 30 seconds at 58°C, and 30 seconds at 72˚C for 40 cycles. PCR products were run on 0.5% Tris base, acetic acid, and EDTA (TAE) agarose gel containing ethidium bromide (1:10,000) after the addition of 5 µL dye to each PCR sample. The ladder (100 bp; 5 µL) was diluted with ddH_2O (30 µL) and 6x loading dye (7 µL). The gel was run for 1 hour at 100 V. Pictures of the gel were taken using the UVP BioImaging Systems unit and the VisionWorksLS program. Primer sequences for each gene are shown in **Table 5**.

RCAS Mice. Prior to start, the genes of interest were in the pBABE vector. These were transferred to pENTR using the pENTR Directional TOPO Cloning Kit (Invitrogen) before transferring to the RCAS vector. The genes in the pBABE vector were PCR amplified prior to the pENTR transfer using the following primers: for 4SA and 4SA-S51A (Forward: 5'-CAC CAT GAA TCC GGC CTC GGC GCCC-3'; Reverse: 5'-TTA CAG CCA GGT TAG AAA GGG-3') and for WT-YAP (Forward: 5'-CAC CAT GGA TCC CGG GCA GCA GCCG-3'; Reverse: 5'-CTA TAA CCA TGT AAG AAA GCT-3'). Each PCR reaction was composed of

100 ng DNA Template, 5 µL 10x PCR Buffer (appropriate for Pfu), 0.5 µL dNTP Mix, 1 µL forward primer, 1 µL reverse primer, 1 µL Pfu, and sterile water to bring the volume up to 50 µL. The reactions were amplified using the following parameters: 94˚C for 2 minutes for 1 cycle, 94˚C for 1 minute, 55˚C for 1 minute, and 72˚C for 1 minute for 25 cycles, then 72˚C for 7 minutes for 1 cycle. The reaction (10 µL) was run on a 1.5% agarose gel to ensure a single discrete band was present. The band was excised from the agarose gel and purified using the PureLink Quick Gel Extraction and PCR Purification Combo Kit (Invitrogen). The gel slice containing the DNA fragment was weighed then placed into a microcentrifuge tube. Three volumes of the Gel Solubilization Buffer (L3) was added to one gel volume. The tube was then incubated at 50˚C for 10 minutes with mixing by inverting every 3 minutes. After the gel slice can no longer be seen, the tube was incubated for an additional 5 minutes. One gel volume of isopropanol was added and mixed well. The dissolved gel mixture with DNA was loaded onto the center of the PureLink Clean-up Spin Column inside a Wash Tube and centrifuged at 13,000 rpm for 1 minute; the flow-through was discarded. The Wash Buffer (W1; 700 µL) was added then centrifuged for 13,000 rpm for 1 minute; the flow-through was discarded. The tube was centrifuged an additional 3 minutes at maximum speed to remove any residual Wash Buffer. The Wash Tube was then discarded and the Spin Column was placed in an Elution Tube. The Elution Buffer (E1; 50 µL) was added to the center of the column and incubated at room temperature for 1 minute then centrifuged at 13,000 rpm for 1 minute to elute the purified DNA. The TOPO Cloning reaction was set up from the following: 4 µL fresh PCR product, 1 µL Salt solution, and 1 µL TOPO vector. The sample was mixed gently and incubated for 30 minutes at room temperature then placed on ice. The TOPO Cloning reaction (6 µL) was added to a vial of One Shot chemically competent *E. coli* cells and mixed gently then incubated on ice for 30 minutes. The cells were heat shocked for 30 seconds at 42˚C without shaking then

immediately transferred to ice. Room temperature S.O.C. Medium (250 μL) was added to the tube then incubated at 37˚C for 1 hour with shaking. All of the bacterial culture was spread on pre-warmed LB kanamycin plates then incubated overnight at 37˚C.

Colonies were picked the next day and grown in 2 mL LB Kanamycin (1:1000) overnight at 37˚C while shaking. After overnight culture, plasmids were isolated using the QIAprep Miniprep kit (Qiagen) as described above. The eluted DNA was sequenced at the MD Anderson Cancer Center core facility using the available M13 Forward (5'-GTA AAA CGA CGG CCAG-3') and Reverse (5'-CAG GAA ACA GCT ATG AC-3') primers. Once the correct sequence was confirmed, the gene of interest was transferred from pENTR to RCAS.

The RCAS model for somatic gene transfer has been previously described in detail [406,407]. The Gateway LR Clonase II Enzyme Mix Kit was used for the LR reaction to transfer the gene of interest from a pENTR vector to the RCAS vector. The following was added to a microcentrifuge tube: 1 μL Entry clone (150 ng/μL), 1.09 μL RCAS-DV (1:10 dilution stock from Rao laboratory), 5.91 μL TE buffer. The LR Clonase mix was then thawed on ice for 2 minutes and vortexed twice for 2 seconds each time. The LR Clonase mix (2 μL) was added to each sample and vortexed twice then microcentrifuged. The reaction incubated overnight at room temperature.

The next day Proteinase K (1 μL) was added to the reaction mixture and vortexed then incubated at 37˚C for 10 minutes. After the incubation, 50 μL DH5α cells were aliquoted into a fresh microcentrifuge tube and 1 μL of the LR reaction was added to the cells then incubated on ice for 30 minutes. The cells were then heat-shocked at 42˚C for 30 seconds and placed on ice. S.O.C. Medium (250 μL) was then added to each sample and incubated at 37˚C with shaking

for 1 hour. The cells (40 μL) were then plated on LB containing Ampicillin plates and incubated overnight at 37˚C.

Colonies were picked the next day and grown in 2 mL LB Ampicillin (1:1000) overnight at 37˚C while shaking. After overnight culture, plasmids were isolated using the QIAprep Miniprep kit (Qiagen) as described above. The eluted DNA was sequenced at the MD Anderson Cancer Center core facility using the following primer sequences: RCAS forward (5'-GAG CTG AGC TGA CTC TGC TGG TGGC-3'); TAZ reverse (5'-CTT CCA GGA ACA AAC GTT GA-3'); YAP reverse (5'-TGC CAT GAA CCA GAG AAT CA-3').

After sequencing confirmed proper insertion of the gene into the RCAS vector, a maxi prep (QIAGEN Plasmid Purification kit) was performed. The remaining 500 μL from the original culture was added to 200 mL LB Ampicillin (1:1000) broth and grown overnight in a 37˚C shaker. All the media was centrifuged at 6000 x g for 15 minutes at 4˚C. The bacterial pellet was homogeneously resuspended in 10 mL Buffer P1 then 10 mL Buffer P2 was added and mixed thoroughly by vigorously inverting 6 times. This solution incubated at room temperature for 5 minutes then 10 mL of pre-chilled Buffer P3 was added and mixed thoroughly by vigorously inverting 6 times. This solution then incubated on ice for 20 minutes. The solution was then centrifuged at 20,000 x g for 30 minutes at 4˚C. During the centrifugation, the QIAGEN-tip 500 was equilibrated by applying 10 mL Buffer QBT, which was allowed to empty the column by gravity flow. The supernatant from the spun down cells was then applied to the QIAGEN-tip and allowed to enter the resin by gravity flow. The QIAGEN-tip was washed twice with 30 mL Buffer QC, which was allowed to move through the tip by gravity flow. The DNA was eluted with 15 mL Buffer QF into a clean 50 mL Falcon tube. The DNA was precipitated by adding 10.5 mL isopropanol at room temperature. The

sample was divided into two 14 mL round bottom tubes (Falcon) and centrifuged at 5000 x g for 1 hour at 4˚C. The supernatant was carefully removed and 200 µL 70% ethanol was added to each tube. The samples were collected in a fresh microcentrifuge tube and vortexed gently then centrifuged at maximum speed for 5 minutes. The supernatant was removed and the pellet was allowed to air dry before it was resuspended in water. DNA concentration was determined by a Nanodrop.

DF-1 cells were transfected by using Fugene (Promega). The cells were grown to 50-70% confluency in a 100 mm plate. In a microcentrifuge tube, 582 µL DMEM without antibiotics or serum was added together with 18 µL Fugene. The tube was flicked to mix and incubated for 5 minutes at room temperature. DNA (6 µg) was then added to the tube and flicked to mix. This mixture then incubated for 15 minutes at room temperature. After the incubation, the mixture was added in a drop-wise manner to the cells and the plate was swirled to ensure even distribution over the entire plate surface. The cells were incubated until confluent. WB was used to confirm over-expression of the gene of interest.

To prepare the DF-1 transfected cells for injection, the cells were rinsed in 3 mL PBS and trypsinized in 2 mL trypsin for each plate. The cells were pooled together from all plates and placed in a 15 mL Falcon tube then pelleted down at 1000 rpm for 10 minutes. The supernatant was discarded by aspiration and the cells were resuspended in 11 mL cold PBS. Of the 11 mL, 1 mL was used for counting using the ViCell counter while the remaining 10 mL were spun down at 1000 rpm for 10 minutes. The supernatant was discarded and the cells were resuspended in PBS (enough to make the final concentration 1 x 10^4 cells/µL). The resuspended cells were transferred to a sterile microcentrifuge tube and kept on ice until the

injections. For two genes, both were at the concentration of 1 x 10^4 cells/μL then mixed at equal volumes into a microcentrifuge tube.

To inject the mice, 2-day old pups were removed from the cage and placed on a gauze in the hood. The Hamilton syringe was rinsed with cold PBS before every injection. For 1 gene, 1 μL of cells was drawn up into the syringe and directly injected intracranially on each side (i.e.—1 μL of cells per hemisphere). For 2 genes, 2 μL of cells was intracranially injected on both sides (i.e.—2 μL of cells per hemisphere).

Mice were sacrificed using carbon dioxide when neurological symptoms were present (i.e. hydrocephalus, seizures, inactivity, and/or ataxia). Mice were sacrificed after 90 days post-injection if they did not show symptoms. Brains were fixed in formalin and embedded in paraffin blocks for further analyses.

To make new breeding pairs, the mice were genotyped from DNA isolated from their tails. The tip of their tails were cut and each tail tip was placed into a fresh microcentrifuge tube. The Proteinase K Buffer (50 μg/μL) was prepared from the following and stored at room temperature: 500 μL 1M Tris pH 8.0, 1 mL 5 M NaCl, 1 mL 0.5 M EDTA pH 8.0, 2.5 mL 10% SDS, and 45 mL H_2O. The Proteinase K buffer was diluted to a final concentration of 250 μg/mL and 500 μL of the diluted buffer was added to each tail sample. The samples were incubated overnight at 50˚C.

The mouse tail samples were then centrifuged at 11,000 rpm for 10 minutes and the supernatant was removed to a fresh tube. Saturated (6M) NaCl (250 μL) was added to each tube and vortexed. The samples were placed on ice for 10 minutes then centrifuged at 10,000 rpm for 10 minutes at 4˚C. Some of the supernatant (500 μL) was removed and added to a fresh

microcentrifuge tube containing 1 mL cold 100% ethanol. The two liquids were mixed by inversion then centrifuged at 4˚C for 10 minutes at maximum speed. The pellets were washed with cold 70% ethanol to remove the salt. The non-resuspended pellets were centrifuged at 4˚C for 5 minutes at maximum speed. The supernatant was decanted with any residual removed by a pipet. The pellet was resuspended in 200 µL TE buffer overnight at 4˚C.

The DNA was amplified using PCR. Each reaction had the following: 22.7 µL AmpliTaq Gold Master Mix (Applied Biosystems), 2.25 µL 10 µM forward primer (5'-CTG CTG CCC GGT AAC GTG ACC GG-3'), 2.25 µL 10 µM reverse primer (5'-GCC CTG GGG AAG GTC CTG CCC-3'), 17.1 µL sterile H_2O, and 1 µL DNA. Reaction mixtures were incubated at 94°C for 5 minutes for 1 cycle then 30 seconds at 94°C, 30 seconds at 55°C, and 30 seconds at 72˚C for 30 cycles followed by 72˚C for 10 minutes then 4˚C forever. The PCR products (15 µL + 3 µL 6x dye) were then run on a 2% agarose gel. The TVA band runs around 500 bp.

Statistical analyses. For all experiments, biological triplicates were performed. Means are expressed as mean +/- standard error. A p-value less than or equal to 0.05 is considered significant. Student's t-test or ANOVA was performed as appropriate. Sample size was calculated using power analysis.

CHAPTER 3: RESULTS—SPECIFIC AIM 1

TAZ is associated with both the mesenchymal signature and GBM.

To ascertain the role of TAZ in the mesenchymal transition, we first needed to establish the association of TAZ with mesenchymal activities. To establish this association, we used ARACNe, as described previously [408], on TCGA data to find transcription factors highly associated with the mesenchymal gene signature. Based on this initial list, I chose to further characterize TAZ because of its established role in EMT in breast cancer [176] as well as its ability to predict survival (**Fig. 2A**). Although YAP involvement has been established in numerous tumors, it was not as highly correlated to the mesenchymal gene signature and did not predict survival as well as TAZ based on TCGA glioma data (**Fig. 2B**). To further show that TAZ plays a role in mesenchymal activities, we produced a list of genes predicted to be regulated by TAZ and analyzed this list using DAVID [409,410], which then produced a list of biological activities of these genes (**Table 3**). The biological activities included wound healing and inflammatory response, which supports the role of TAZ in mesenchymal activities. *TAZ*/*WWTR1* expression in the TCGA data was also found to be highly correlated with a mesenchymal metagene score created by combining the Phillips [24] and Verhaak [25] mesenchymal genes (**Fig. 3**). Taking everything together, we found a positive correlation of TAZ with the mesenchymal gene signature.

Next, we speculated that *WWTR1* was regulated by methylation of CpG islands in its promoter region since it is well-established that methylation can affect expression [411]; therefore, we analyzed its methylation status along with other genes in the Hippo pathway (**Figs. 4, 5, and 6**). **Fig. 4** shows the basic Hippo pathway and the main proteins involved in the pathway. The CpG islands in the *WWTR1* promoter (**Fig. 5A**) were highly methylated in the proneural subgroup compared to the mesenchymal subgroup (**Fig. 5B**) and the methylation status inversely correlated with *WWTR1* expression (**Fig. 5C**). *YAP1*, *LATS2*, and *MST1*

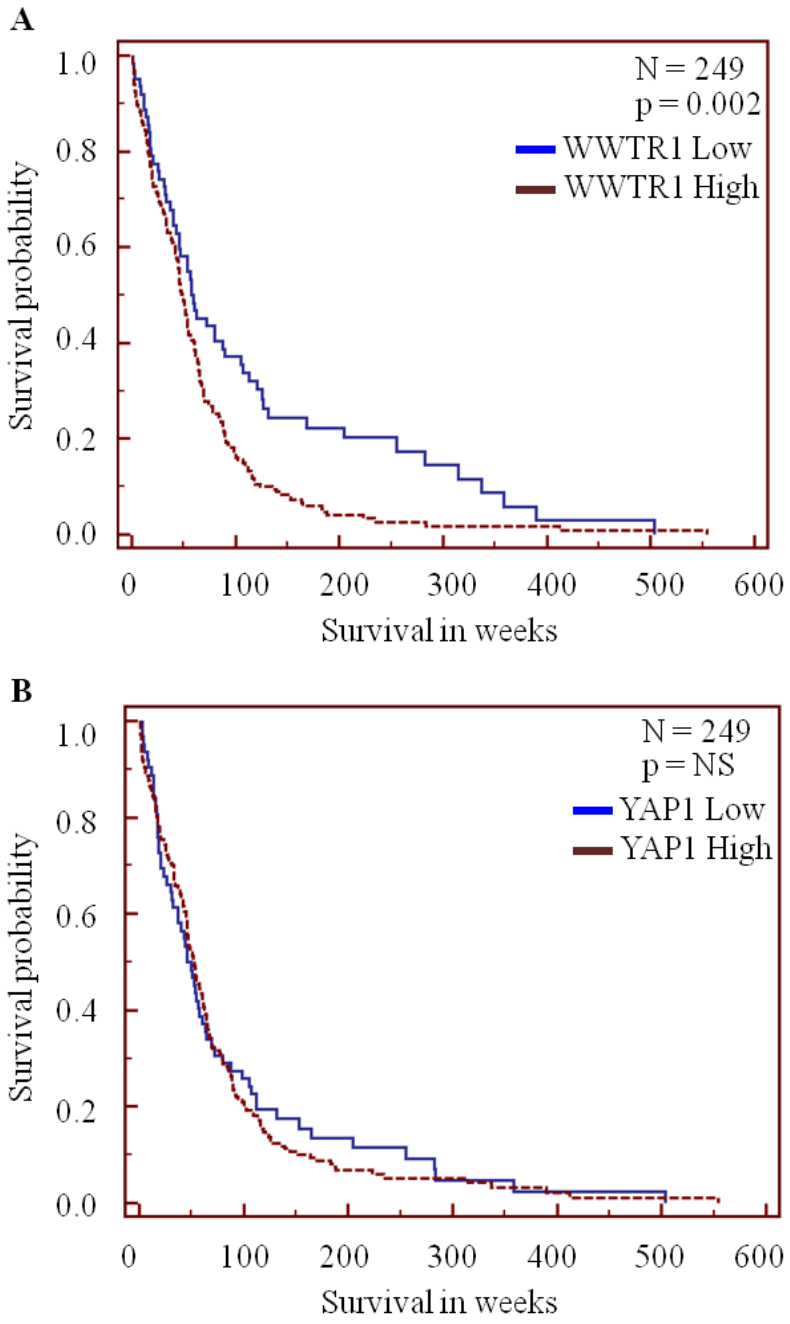

Figure 2: Kaplan-Meier analyses of patient survival in TCGA datasets. (A) Survival based on *TAZ*/*WWTR1* expression. (B) Survival based on *YAP1* expression. Expression was compared between lowest 25th quantile (Low) and remaining 75th quantile (High). NS = not significant. Data analyzed by EP Sulman. Reprinted with permission, Bhat, Salazar, Balasubramaniyan, et al., Genes Dev 25:2594-2609 [412], Copyright © 2011, Cold Spring Harbor Laboratory Press.

Table 3: Functional gene analysis of genes regulated by TAZ

Functional Annotation	p-value
response to wounding	5.5E-8
inflammatory response	4.9E-5
defense response	1.7E-3
wound healing	1.6E-3
acute inflammatory	2.5E-4

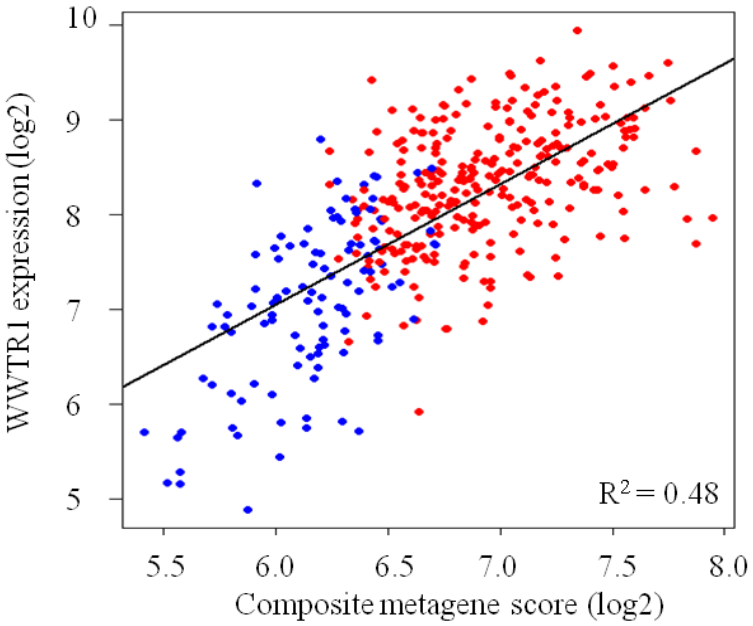

Figure 3: *TAZ*/*WWTR1* expression versus mesenchymal metagene score. Blue dots indicate proneural tumors and red dots indicate mesenchymal tumors from the TCGA data set. Gene signatures of tumors were established by composite metagenes defined by Phillips [24] and Verhaak [25]. Data analyzed by BD Vaillant. Reprinted with permission, Bhat, Salazar, Balasubramaniyan, et al., Genes Dev 25:2594-2609 [412], Copyright © 2011, Cold Spring Harbor Laboratory Press.

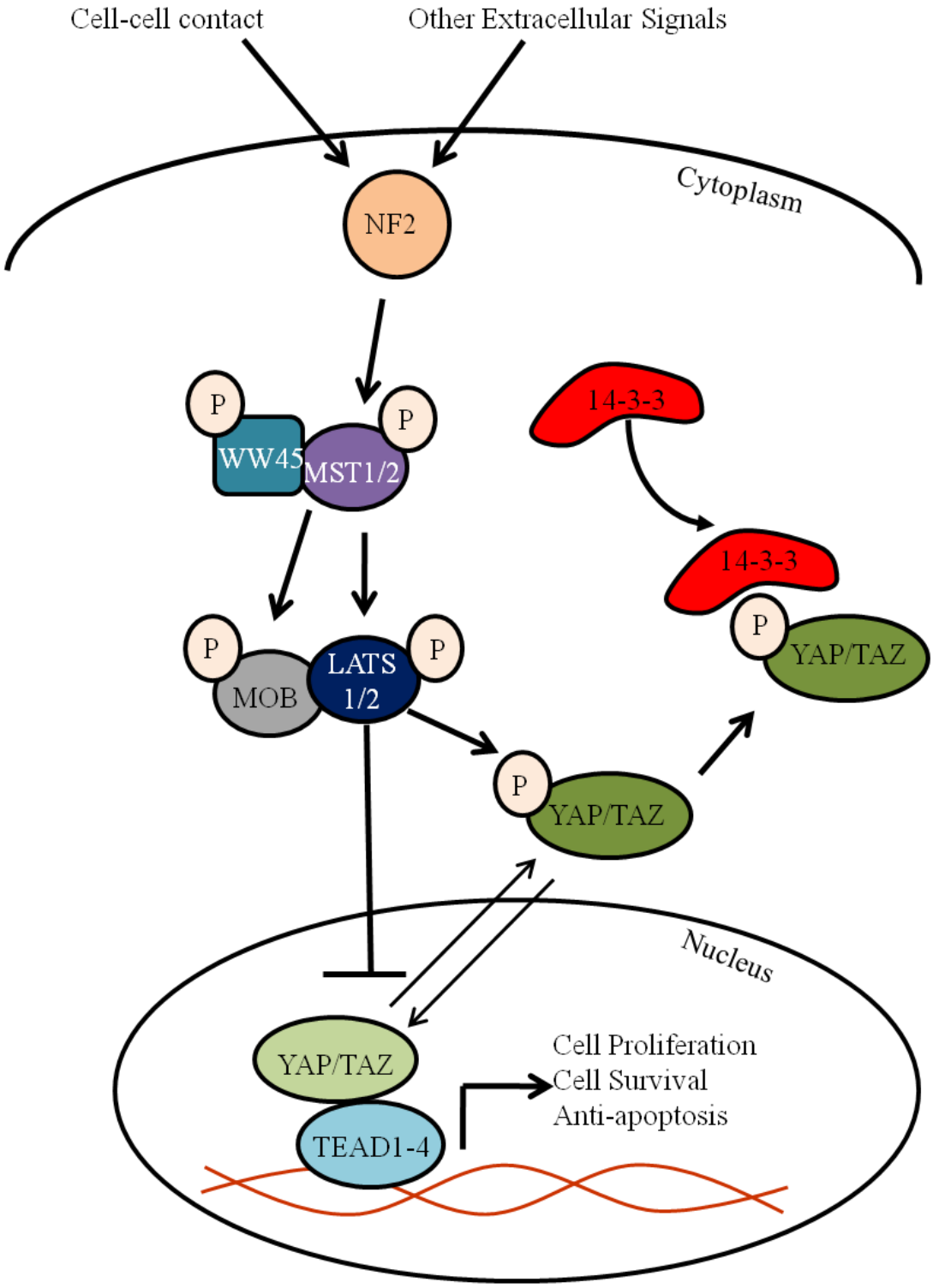

Figure 4: The Hippo pathway (simplified). Thin arrows indicate movement, thick arrows indicate activation, and blunt heads indicate inhibition. "P" indicates phosphorylation.

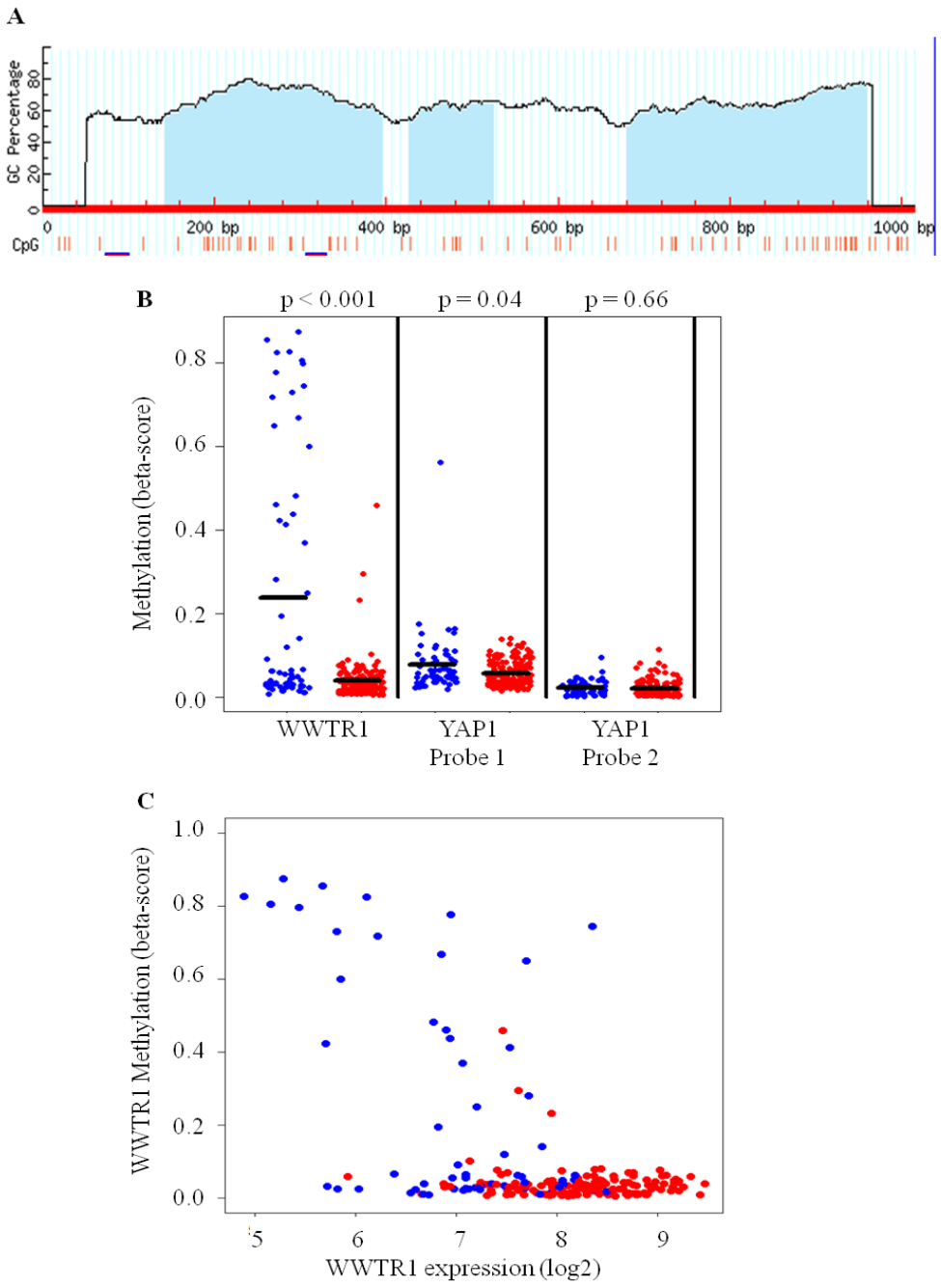

Figure 5: Methylation status of *WWTR1* and *YAP1*. (A) Diagram of CpG islands (highlighted blue regions) within the *TAZ/WWTR1* promoter. (B) Methylation of *WWTR1* and *YAP1* sub-divided into proneural or mesenchymal tumors. Blue dots indicate proneural and red dots indicate mesenchymal samples. Gene signatures of tumors were established by composite metagenes defined by Phillips [24] and Verhaak [25]. Black bars show the methylation β-score mean. (C) *WWTR1* methylation status versus *WWTR1* expression. Blue dots represent proneural samples while red dots represent mesenchymal samples. Data analyzed by BD Vaillant. Reprinted with permission, Bhat, Salazar, Balasubramaniyan, et al., Genes Dev 25:2594-2609 [412], Copyright © 2011, Cold Spring Harbor Laboratory Press.

showed significant methylation in the proneural subgroup as well, but not to the degree seen in *WWTR1* (**Figs. 5B and 6**). *TEAD1* was also methylated, but no significant difference was seen between the proneural and the mesenchymal subgroups (**Fig. 6**). *LATS1*, *TEAD2*, and *TEAD4* showed no significant difference in methylation status between the proneural and mesenchymal subgroups (**Fig. 6**).

We next analyzed the *WWTR1* methylation status of all glioma grades and found that lower grade gliomas (grades II and III) were more frequently methylated relative to GBM (grade IV) tumors (**Fig. 7**). Since lower grade gliomas tend to be proneural nature [413,414] while GBMs can be either proneural or mesenchymal, we suspect this association of TAZ methylation with lower grade gliomas to be due to the gene expression signature rather than differences in grades. Based on microarray data, TAZ expression was higher in GBM relative to grades II/III (**Fig. 8A**) and in short-term survivors (≤ 2 years) compared to long-term survivors (> 2 years; **Fig. 8B**). Consistent with this data, TAZ expression was higher in GBM compared to lower grade gliomas at the protein level (**Fig. 9**). A similar pattern was seen with phospho-TAZ, YAP, TEAD4, MST1, LATS1/2, and the mesenchymal marker fibronectin1 (FN1; **Fig. 9**). The WB analyses of MST1 and LATS2 were consistent with the methylation data (**Fig. 6**). Although expression was higher for both MST1 and LATS2, the activated form of both proteins (i.e.—phosphorylated) was not significantly different between lower and high grade gliomas (**Fig. 9**). MOB1 showed higher expression in grades II/III (**Fig. 9**), which may indicate signals to promote activation of the LATS1/2 that is present, despite the low levels, in order to regulate TAZ localization. No other proteins in the Hippo pathway that were examined showed significant expression differences between grades II/III and GBM (**Fig. 9**). In addition to FN1, smooth muscle actin (SMA) was also used as a mesenchymal markers while oligodendrocyte lineage transcription factor 2 (Olig2) was used as a proneural marker.

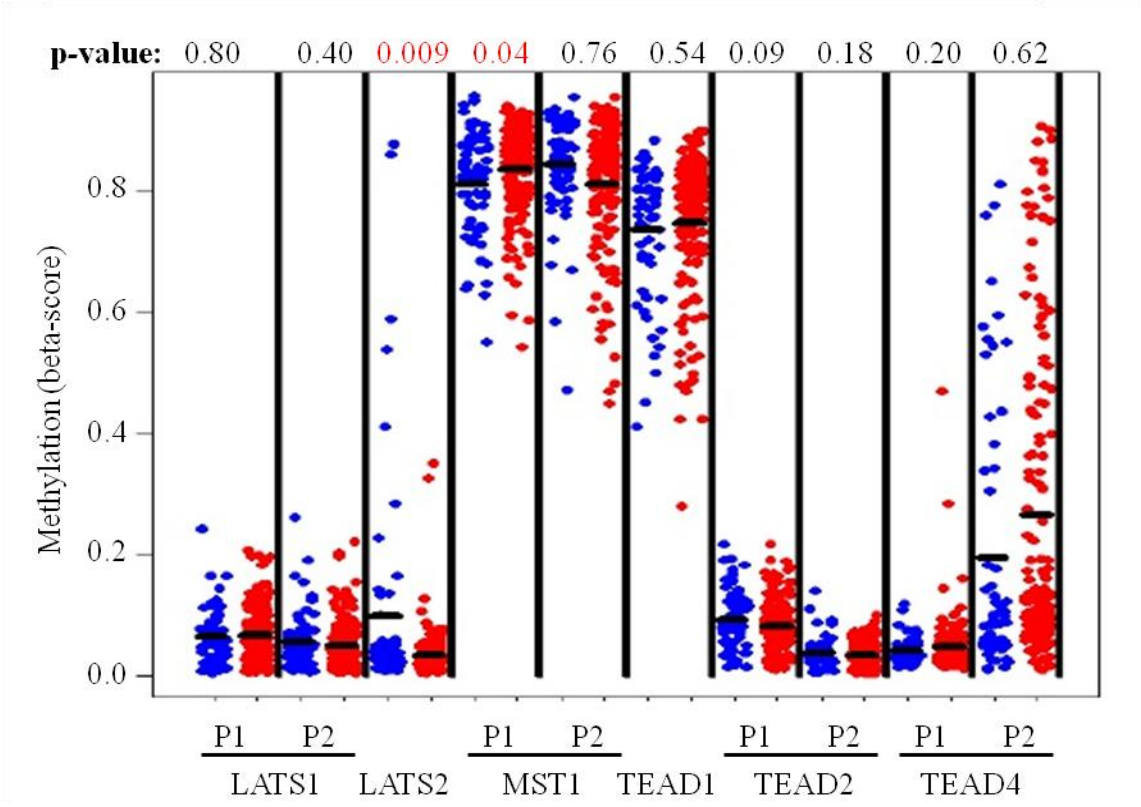

Figure 6: Methylation status of Hippo pathway genes. Methylation of *LATS1, LATS2, MST1, TEAD1, TEAD2,* and *TEAD4* sub-divided into proneural or mesenchymal tumors. Blue dots indicate proneural and red dots indicate mesenchymal samples. Gene signatures of tumors were established by composite metagenes defined by Phillips [24] and Verhaak [25]. Black bars show the methylation β-score mean. P1 = Probe 1 and P2 = Probe 2. Data analyzed by BD Vaillant. Reprinted with permission, Bhat, Salazar, Balasubramaniyan, et al., Genes Dev 25:2594-2609 [412], Copyright © 2011, Cold Spring Harbor Laboratory Press.

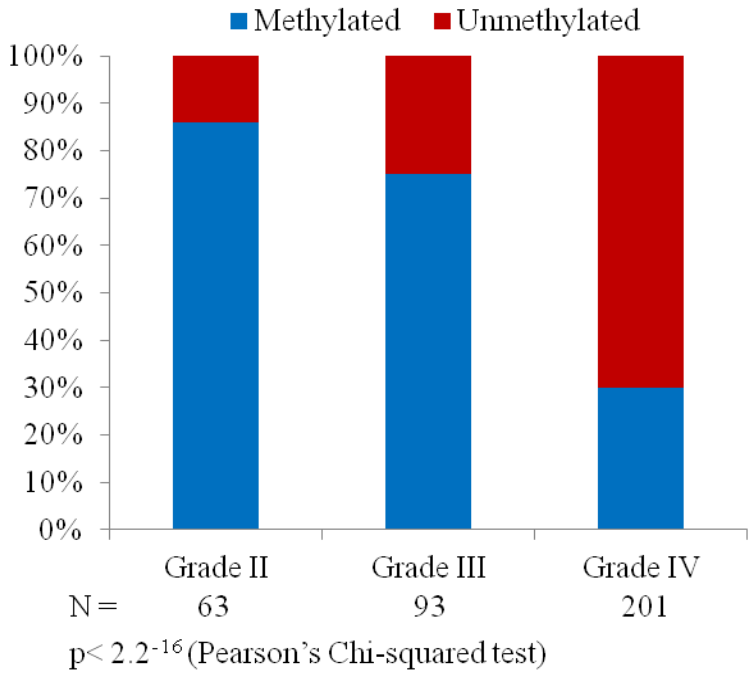

Figure 7: Methylation frequency of *WWTR1* CpG sites in grades II, III, and IV gliomas. Bar graph shows percentage of tumors within each group to have a methylated (blue) or unmethylated (red) 2nd CpG island in the *WWTR1* promoter region. Experiment performed by KL Diefes. Reprinted with permission, Bhat, Salazar, Balasubramaniyan, et al., Genes Dev 25:2594-2609 [412], Copyright © 2011, Cold Spring Harbor Laboratory Press.

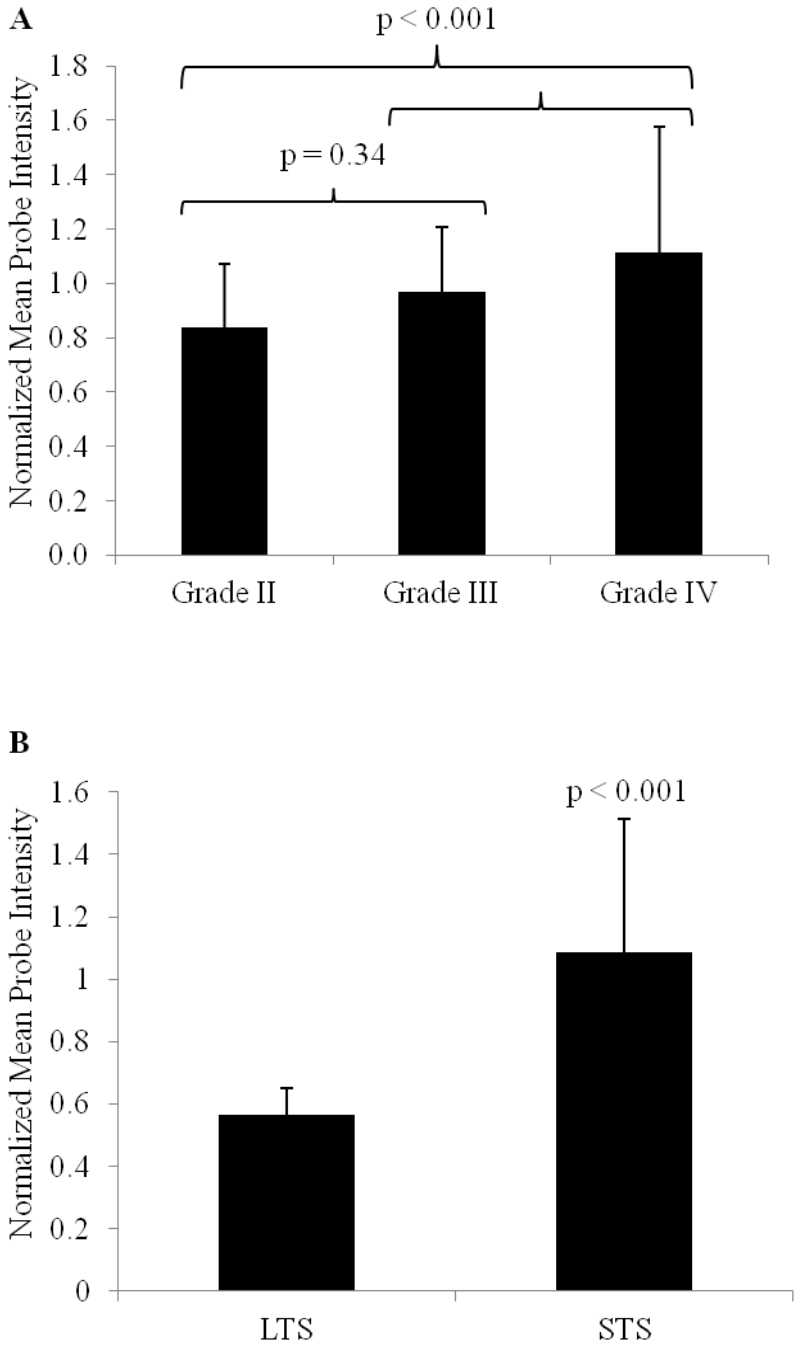

Figure 8: *WWTR1* expression in microarray dataset of 783 diffuse glioma samples. (A) Bar graphs show normalized mean probe intensity of *WWTR1* across glioma grades. (B) Bar graphs show normalized mean probe intensity of *WWTR1* in long-term survivors (LTS; > 2 years) and short-term survivors (STS; ≤ 2 years). Data analyzed by KD Aldape. Reprinted with permission, Bhat, Salazar, Balasubramaniyan, et al., Genes Dev 25:2594-2609 [412], Copyright © 2011, Cold Spring Harbor Laboratory Press.

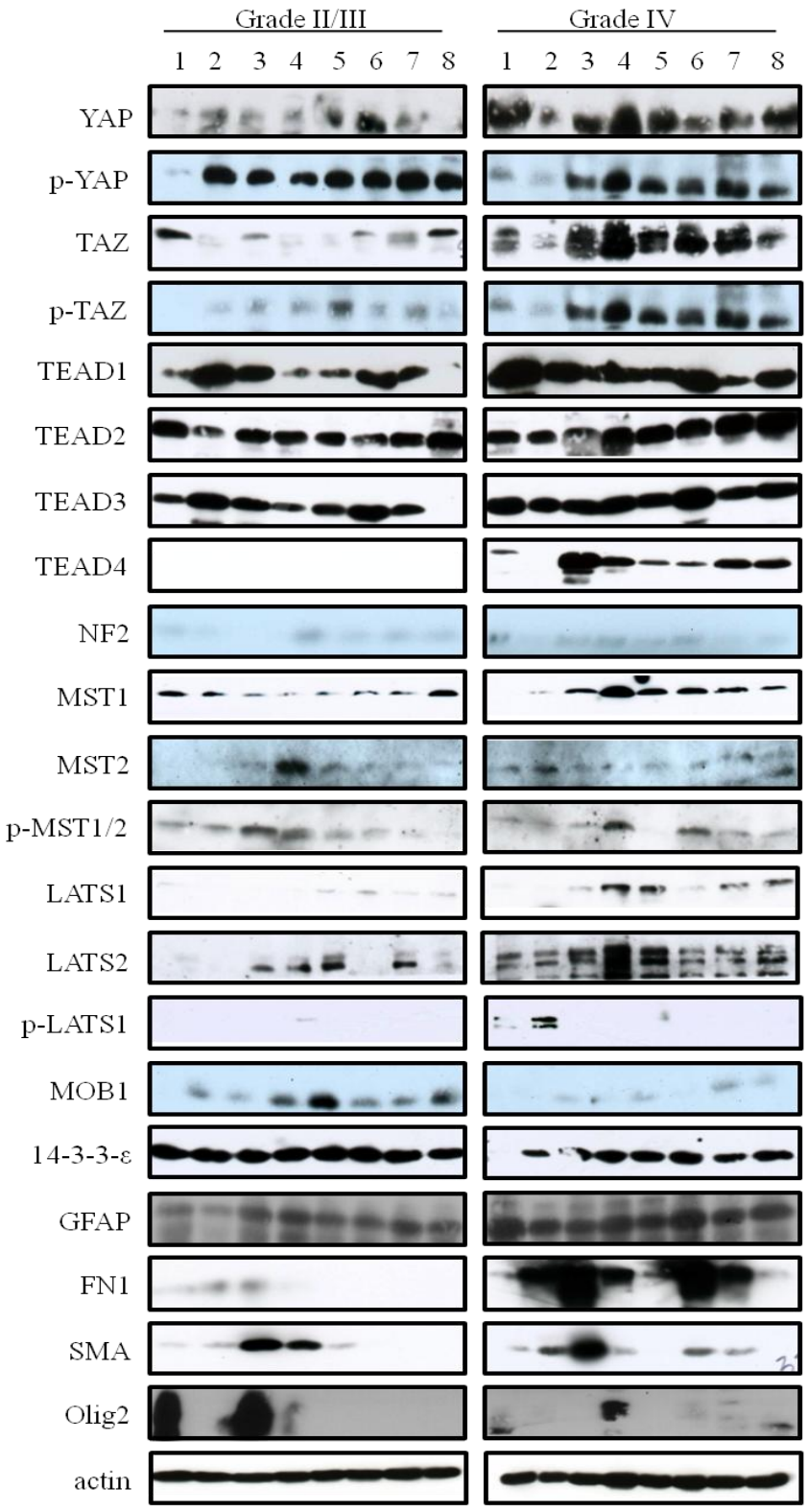

Figure 9: Western analyses of lysate from frozen grade II-IV gliomas. Most proteins in the Hippo pathway were analyzed. FN1 and SMA were used as mesenchymal markers while Olig2 was used as a proneural marker. Reprinted with permission, Bhat, Salazar, Balasubramaniyan, et al., Genes Dev 25:2594-2609 [412], Copyright © 2011, Cold Spring Harbor Laboratory Press.

SMA showed expression in more GBM samples than grades II/III, although the sample size is quite small (**Fig. 9**). Olig2 showed expression in some grades II/III and GBM samples, but higher expression was seen in the grades II/III samples (**Fig. 9**). Since FN1 is associated with endothelial cells [415], the increase in expression seen in the GBM samples could be due to an increase in vasculature rather than a mesenchymal shift. To rule this out, we did IHC and found FN1 expression in unequivocal GBM tumor cells, unlike lower grade tumors, where FN1 was only expressed around vessels (**Fig. 10**).

To determine the clinical significance of TAZ subcellular localization, I analyzed 189 gliomas using IHC. TAZ was highly expressed in the GBM samples, but was mostly undetectable in the lower grade gliomas (**Fig. 11A**). TAZ showed localization in both the nucleus and cytoplasm (score = 2^+) in some GBM samples and these patients had a shorter survival compared to those who only had TAZ expression in either the nucleus or the cytoplasm (score = 1^+) or to those with no expression (score = 0; **Fig. 11B**). Taken together, TAZ is strongly associated with the mesenchymal signature and is regulated via both phosphorylation and methylation. In addition, its expression correlates with the mesenchymal signature, higher grade gliomas, and worse overall prognosis.

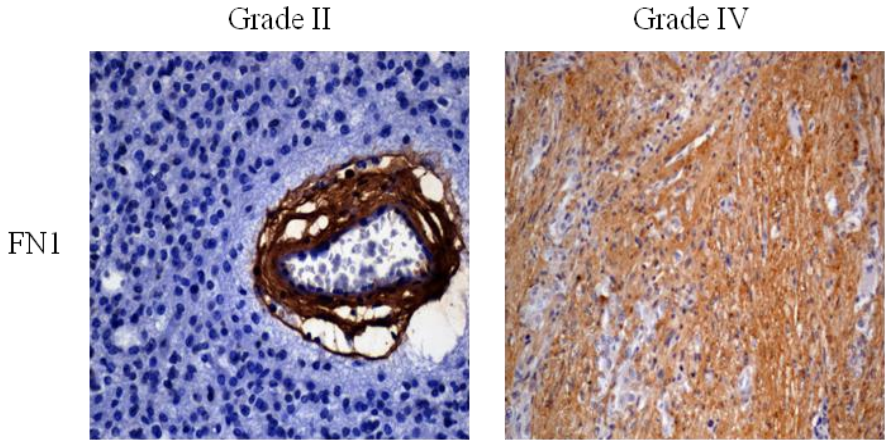

Figure 10: IHC staining of FN1 on grade II and IV gliomas. 40x magnification. Experiment performed by EF Hollingsworth. Reprinted with permission, Bhat, Salazar, Balasubramaniyan, et al., Genes Dev 25:2594-2609 [412], Copyright © 2011, Cold Spring Harbor Laboratory Press.

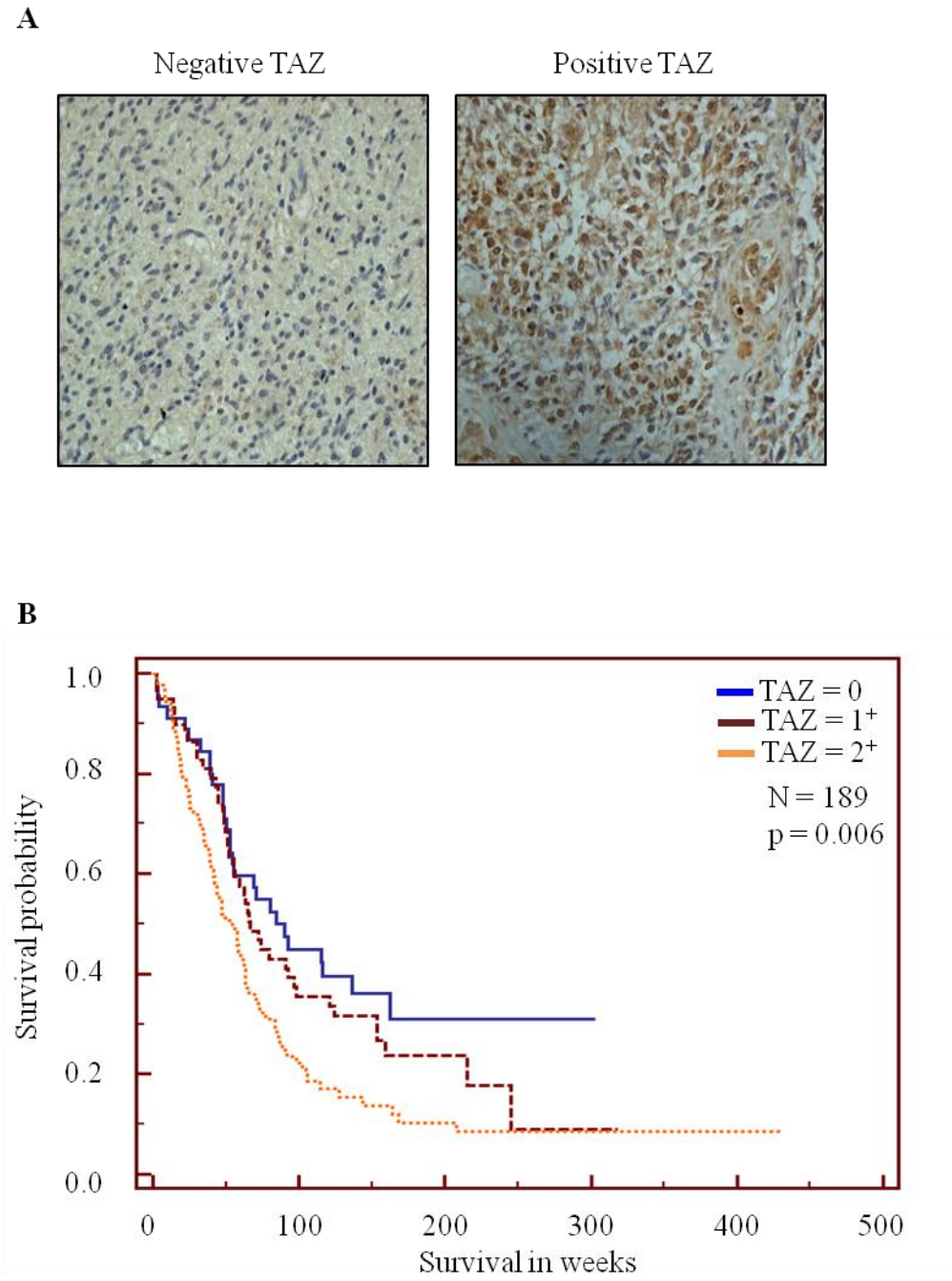

Figure 11: Clinical significance of TAZ expression. (A) Representative IHC pictures of TAZ stained glioma samples (40x magnification). (B) Kaplan-Meier survival analysis based on IHC staining pattern of TAZ. No expression was scored 0 while expression in the nucleus or the cytoplasm scored 1^+ and expression in both scored 2^+. Reprinted with permission, Bhat, Salazar, Balasubramaniyan, et al., Genes Dev 25:2594-2609 [412], Copyright © 2011, Cold Spring Harbor Laboratory Press.

TAZ is essential for PMT and aggressive behavior in glioma stem cells (GSCs).

I next tested TAZ expression in GSCs. Some of these lines have been established to be proneural (GSC 7-11, GSC 8-11, GSC 11, and GSC 23) while others have been established to be mesenchymal (GSC 6-27 and GSC 20). Consistent with the data from human tumors, TAZ expression is higher in the cell lines identified as mesenchymal compared to those identified as proneural; a similar pattern is seen in the mesenchymal marker CD44 (**Fig. 12**). Of note, YAP expression did not correlate with the proneural or mesenchymal signature (i.e.—similar expression levels in the proneural line GSC 23 and in the mesenchymal line GSC 20). In contrast to the glioma samples, LATS1 and LATS2 expression were higher in the proneural lines (**Fig. 12**). Alterations in expression of established cell lines from that of the original tumors are common [416] and may be the cause of this discrepancy. The increase in LATS1/2 expression may help regulate TAZ via phosphorylation, thus promoting cytoplasmic localization and ubiquitination. This type of regulation, in addition to methylation, may play a role in the low levels of TAZ seen in the proneural cell lines. CTGF and FN1 appear to show no difference between lines (**Fig. 12**). We also show that TAZ expression is higher in the nuclear fraction isolated from the mesenchymal cell lines compared to the nuclear fraction isolated from the proneural cell lines (**Fig. 13**). This also holds true for the cytosolic fraction, but to a lesser extent (**Fig. 13**). This result may reflect ubiquitination once TAZ localizes to the cytoplasm. I performed bisulfite sequencing of the *WWTR1* promoter, which showed hypermethylation in GSC 7-11 and GSC 8-11 and hypomethylation in GSC 6-27 and GSC 20 (**Fig. 14A**). I followed that up with demethylation treatment using 5-aza-2'-deoxycytidine (DAC) on GSC 7-11 and GSC 8-11 and found an increase in TAZ expression at the protein level for both cell lines (**Fig. 14B**), but with a greater increase in GSC 8-11. We also saw an increase in the relative mRNA expression level in GSC 8-11 with a subsequent increase in the

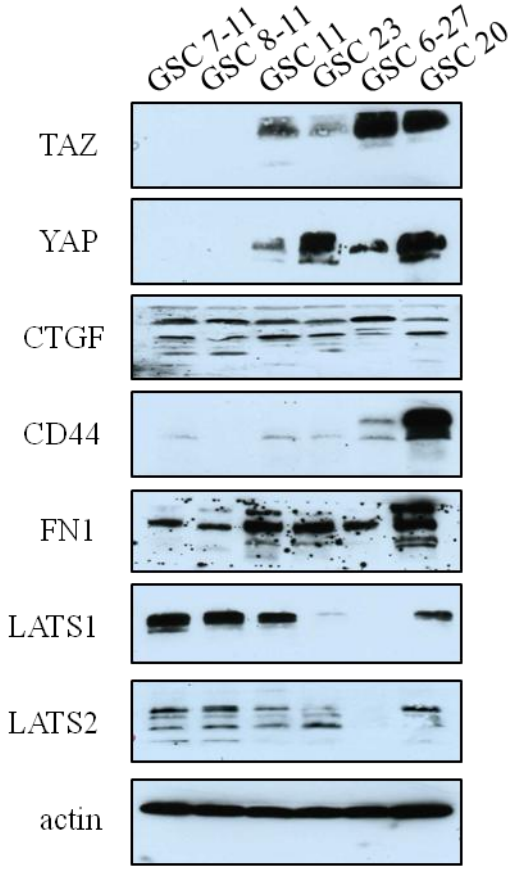

Figure 12: Western analyses of established GSC lines. Western analyses of TAZ, YAP, CTGF, CD44, FN1, LATS1, and LATS2 in the proneural lines GSC 7-11, GSC 8-11, GSC 11, GSC 23 and the mesenchymal lines GSC 6-27 and GSC 20. Reprinted with permission, Bhat, Salazar, Balasubramaniyan, et al., Genes Dev 25:2594-2609 [412], Copyright © 2011, Cold Spring Harbor Laboratory Press.

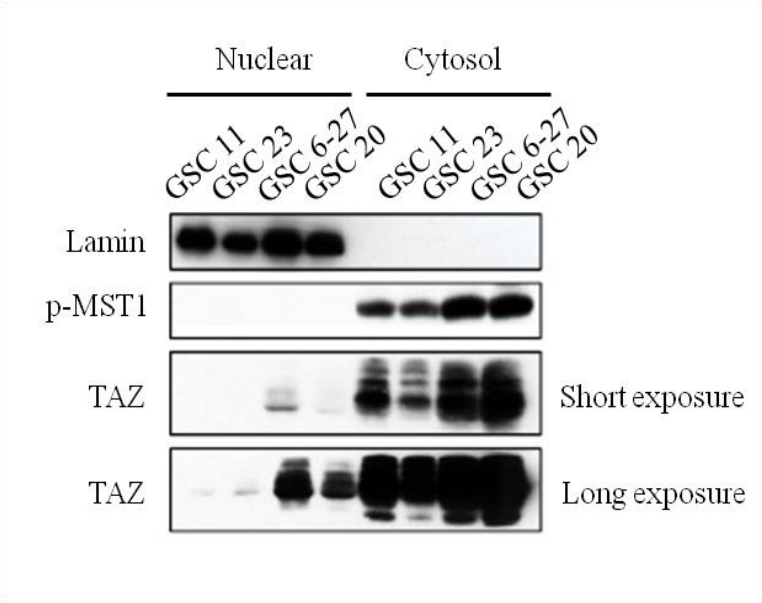

Figure 13: Cellular fractionation of proneural and mesenchymal cell lines. Comparison of p-MST1 and TAZ expression in the nuclear and cytosolic fractions of proneural lines (GSC 11 and GSC 23) and of mesenchymal lines (GSC 6-27 and GSC 20). Lamins are intermediate filament components of the nuclear envelope. Experiment performed by KP Bhat. Reprinted with permission, Bhat, Salazar, Balasubramaniyan, et al., Genes Dev 25:2594-2609 [412], Copyright © 2011, Cold Spring Harbor Laboratory Press.

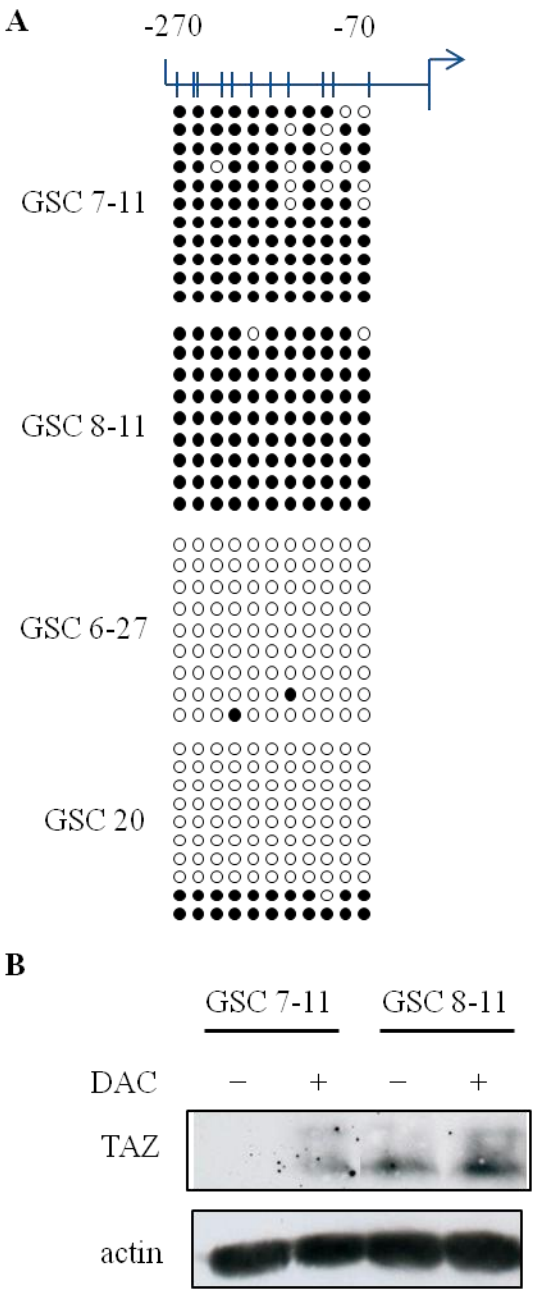

Figure 14: DNA methylation analysis of glioma cell lines. (A) Bisulfite conversion followed by sequencing of cloned PCR products. Methylated CG pairs are indicated by black circles while unmethylated CG pairs are indicated by white circles. Each column represents 11 CpG sites proximal to the transcription start site of TAZ (shown on top). Each row represents the methylation status of a clone. (B) Western analyses of TAZ expression in GSC 7-11 and GSC 8-11 after demethylation treatment with 10 μM DAC for 72 hrs. Reprinted with permission, Bhat, Salazar, Balasubramaniyan, et al., Genes Dev 25:2594-2609 [412], Copyright © 2011, Cold Spring Harbor Laboratory Press.

mesenchymal gene targets *CD44* and *CTGF* (**Fig. 15A**). For GSC 7-11, the increase in *WWTR1* post-DAC treatment was not as dramatic as GSC 8-11 (**Fig. 15B**), which is consistent with the WB data (**Fig. 14B**). I tested the same principle using two different cell lines, HL60 and Raji. HL60 showed hypomethylation while Raji was hypermethylated (data not shown). After DAC treatment, Raji showed a slight increase in TAZ expression at both the mRNA level and the protein level while HL60 did not show any difference (**Fig. 16A and B**). Taken together, the data elucidate a novel mechanism of *WWTR1* regulation via CpG island methylation.

To test whether expression of mesenchymal proteins in GSC 2 and GSC 20 were TAZ-dependent, I transiently knocked down *WWTR1* in these cells using siRNA and found that silencing *WWTR1* for 72 hours led to a decrease in expression of the mesenchymal markers FN1 at the protein level (**Fig. 17A**) and CD44 at both the protein and mRNA levels (**Fig. 17A and B**). At the mRNA level, I also observed a decrease in *CTGF*, an increase in *CHI3L1*, and no significant change in *YAP* expression (**Fig. 17B**). To further characterize the effect of silencing *WWTR1 in vitro*, I stably silenced *WWTR1* using shRNA. Two independent shRNA constructs targeting different regions of the *WWTR1* transcript were used in GSC 20 and found to significantly decrease the expression of TAZ at the protein level; however, these clones did not affect YAP levels (**Fig. 18A**). Compared to the non-targeting control, the stably silenced *WWTR1* clones showed a significant decrease in invasion across matrigel (**Fig. 18B**) and a significant decrease in self-renewal as tested by neurosphere formation (**Fig. 19A**). These data suggest that TAZ is required for the invasive and self-renewal capacity of GSC 20. These stably silenced *WWTR1* clones did not appear to affect the proliferation of GSC 20 (**Fig. 19B**). I therefore reasoned that the decrease in invasive and self-renewal capabilities was not due to a decrease in proliferation. Next we characterized the effect of silencing *WWTR1 in vivo* by

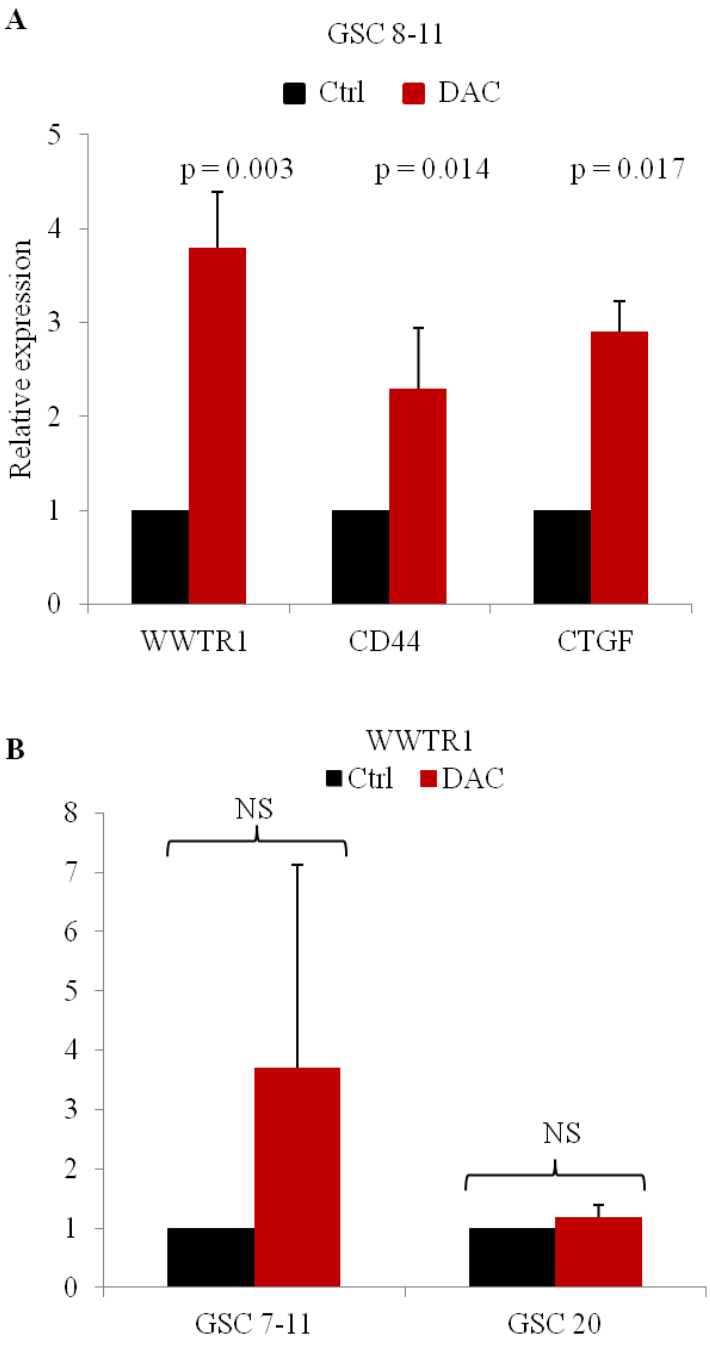

Figure 15: Real-time qPCR analysis after demethylation treatment. (A) Real-time qPCR of *WWTR1*, *CD44*, and *CTGF* expression in GSC 8–11 after treatment with 10 μM DAC for 72 hrs. To compare transcript levels, fold change before and after treatment was used. Experiment performed by KP Bhat. (B) Real-time qPCR of *WWTR1* expression in GSC 7-11 and GSC 20 after treatment with 10 μM DAC for 72 hrs. To compare transcript levels, fold change before and after treatment was used. NS = not significant. Reprinted with permission, Bhat, Salazar, Balasubramaniyan, et al., Genes Dev 25:2594-2609 [412], Copyright © 2011, Cold Spring Harbor Laboratory Press.

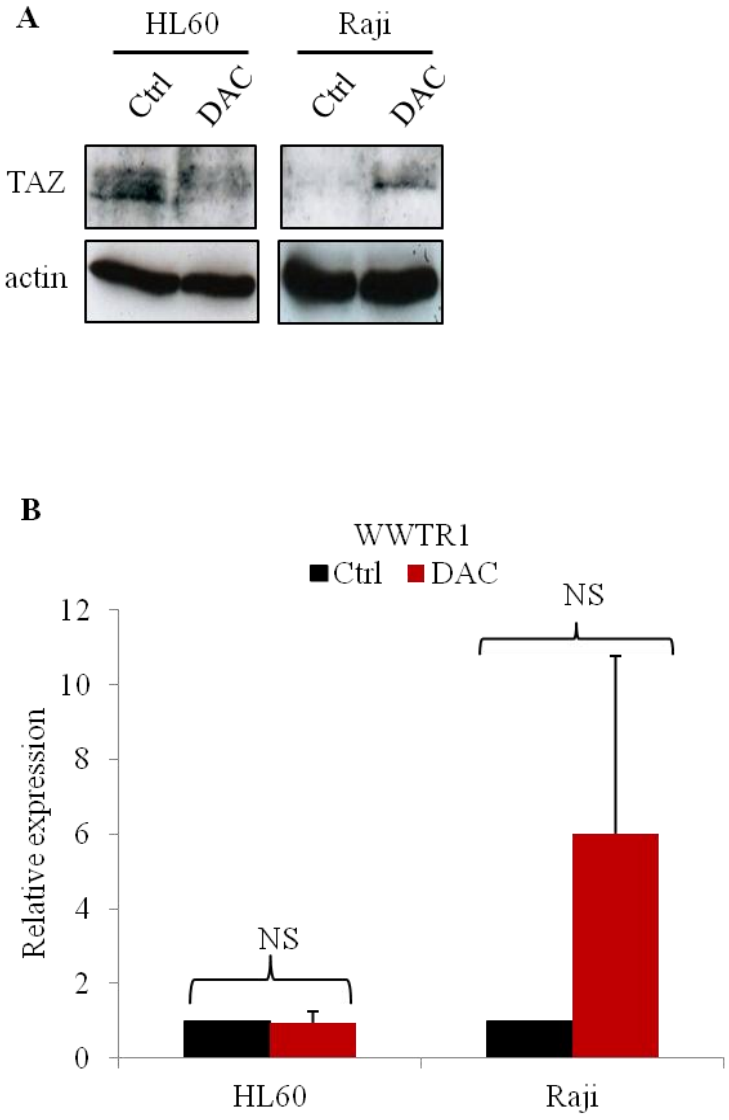

Figure 16: Western and real-time qPCR analyses after demethylation treatment. (A) Western analyses of TAZ expression in HL60 and Raji after treatment with 10 μM DAC for 72 hrs. (B) Real-time qPCR of *WWTR1* expression in HL60 and Raji after treatment with 10 μM DAC for 72 hrs. To compare transcript levels, fold change before and after treatment was used. NS = not significant.

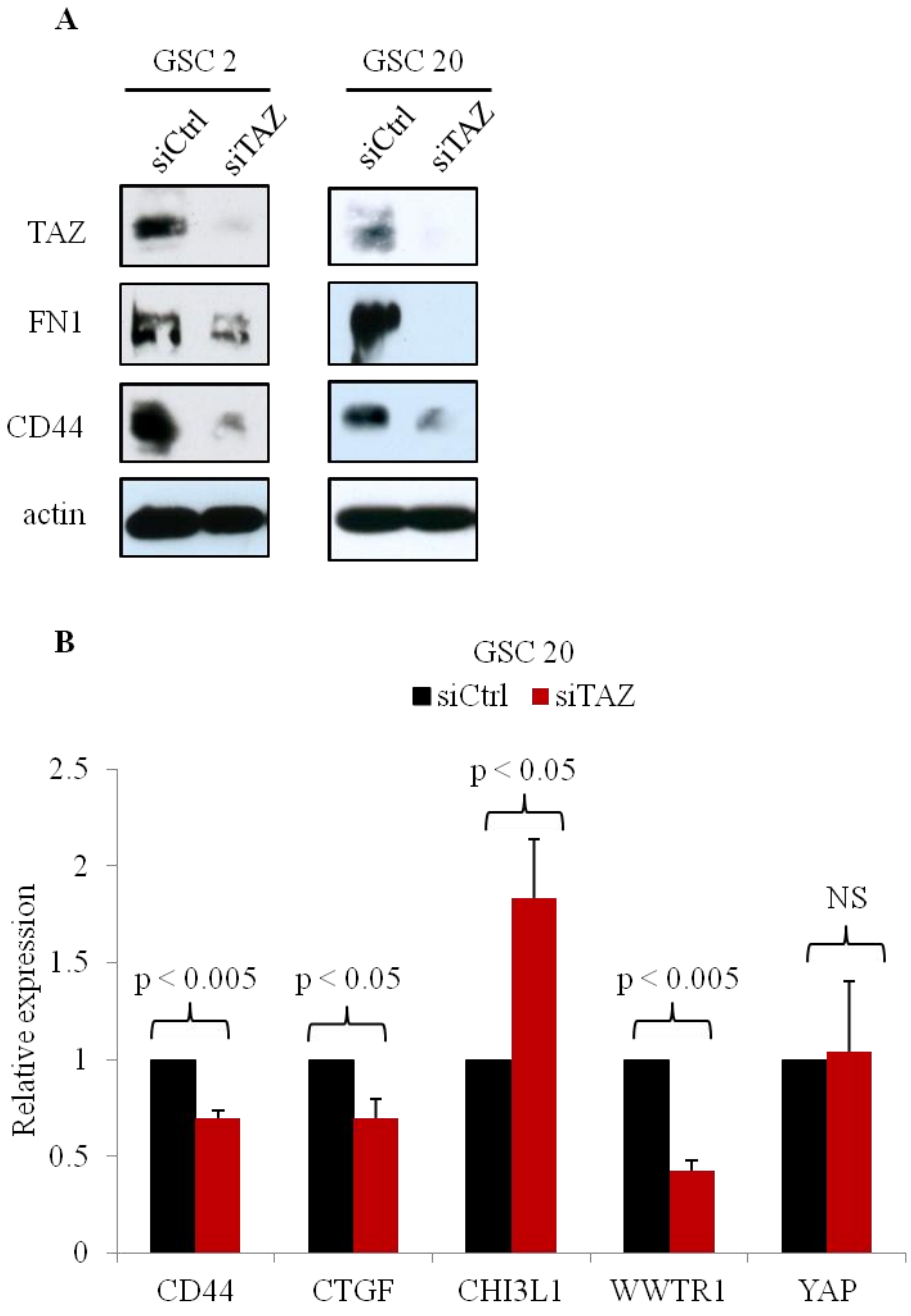

Figure 17: Western and real-time qPCR analyses after transient knockdown of *WWTR1*. (A) Western analysis of TAZ, FN1, and CD44 expression after transient knockdown of *WWTR1* in GSC 2 and GSC 20. Cells were cultured in laminin and poly-L-ornithine-coated plates and transfected with siRNA for 48 hrs. (B) Real-time qPCR of *CD44*, *CTGF*, *CHI3L1*, *WWTR1*, and *YAP* expression in GSC 20 after transient knockdown of *WWTR1*. To compare transcript levels, fold change with siCtrl and with siTAZ was used. NS = not significant. Reprinted with permission, Bhat, Salazar, Balasubramaniyan, et al., Genes Dev 25:2594-2609 [412], Copyright © 2011, Cold Spring Harbor Laboratory Press.

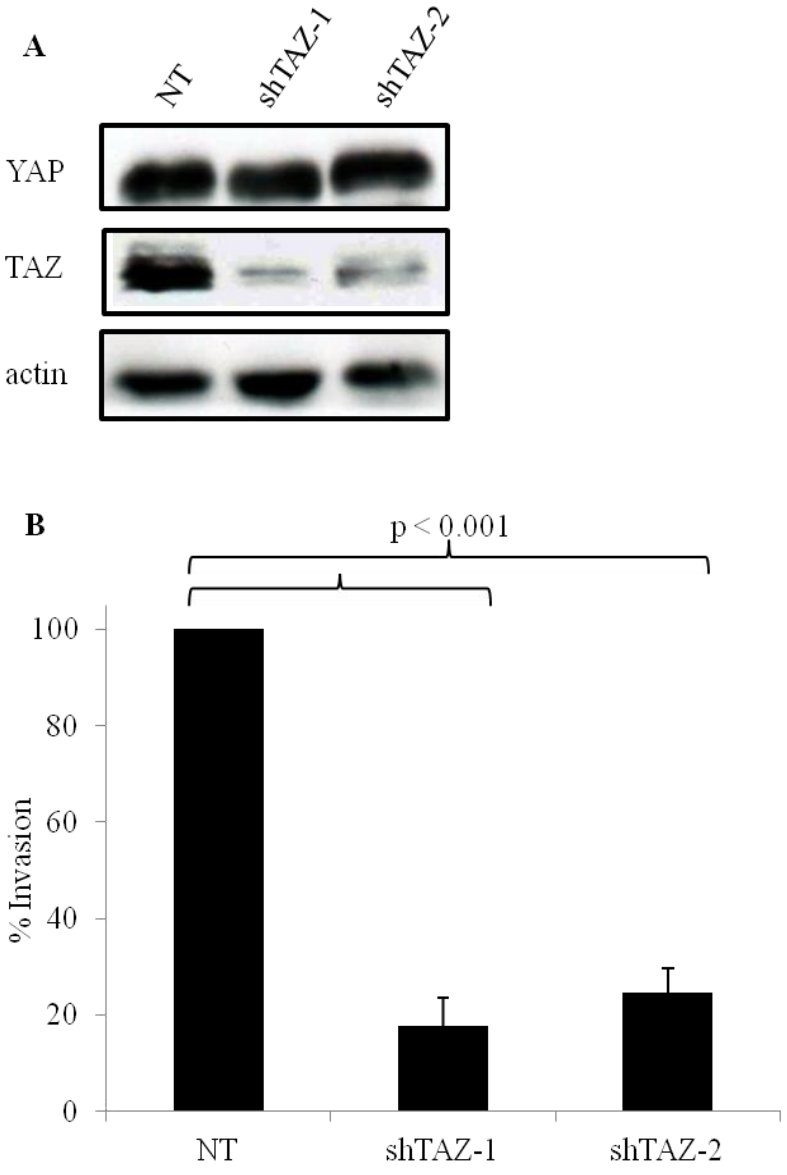

Figure 18: Invasive capacity of stable TAZ knockdown clones. (A) Western analysis of YAP and TAZ expression in GSC 20 stable TAZ knockdown clones. NT is the non-targeting control; shTAZ-1 and shTAZ-2 are independent, non-overlapping constructs that target different portions of the *WWTR1* transcript. (B) Invasion assay of GSC 20 stable TAZ knockdown clones. The invasion efficiency of the non-targeting control was set to100% for comparison. Reprinted with permission, Bhat, Salazar, Balasubramaniyan, et al., Genes Dev 25:2594-2609 [412], Copyright © 2011, Cold Spring Harbor Laboratory Press.

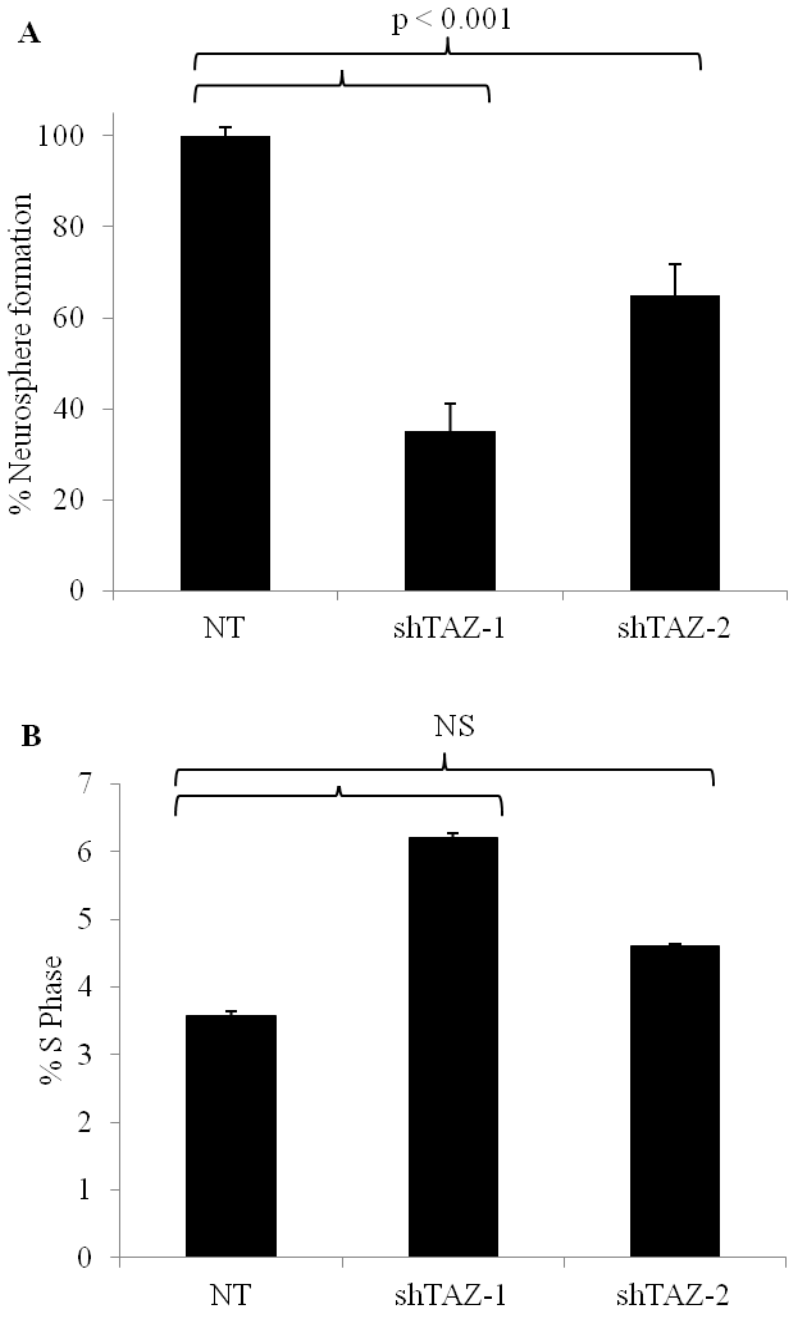

Figure 19: Self-renewal and proliferation capabilities in stable TAZ knockdown clones. (A) Neurosphere assay of TAZ knockdown clones. Bar graphs indicate percentage of neurosphere formation. The self-renewal ability of the NT construct was set to 100% for comparison. NT is the non-targeting control; shTAZ-1 and shTAZ-2 are independent, non-overlapping constructs that target different portions of the *WWTR1* transcript. (B) Proliferation assay of TAZ knockdown clones. Bar graphs indicate percentage of cells in S phase. NS = not significant. Reprinted with permission, Bhat, Salazar, Balasubramaniyan, et al., Genes Dev 25:2594-2609 [412], Copyright © 2011, Cold Spring Harbor Laboratory Press.

intracranially injecting the non-targeting and stably silenced clones into severe combined immunodeficiency (SCID) mice with the hypothesis that the tumor-initiating ability of the stably silenced clones would be decreased compared to the non-targeting clone. All five mice injected with the non-targeting control formed tumors with pseudopalisading necrosis and microvascular proliferation, two pathognomonic characteristics of GBM (**Fig. 20A**). None of the mice injected with shTAZ-1 formed tumors while only two of the five mice injected with shTAZ-2 formed tumors. The tumors that formed in the shTAZ-2 group were smaller and lacked the pathognomonic signs of GBM (**Fig. 20A**). They also lacked expression of TAZ and CD44 compared to the tumors that formed in the non-targeting control group as tested by IHC (**Fig. 20B**). The percent of animals tumor-free as well as the overall survival proportion was improved in those mice injected with the stably silenced clones compared to those injected with the non-targeting control (**Fig. 21A and B**). Taken together, these data show that TAZ increases tumor-initiating ability and negatively affects overall survival in this mouse model. In GSCs, TAZ is epigenetically silenced and is required for mesenchymal marker expression, invasion, self-renewal, and tumor initiation; however, I observed no effect on proliferation by TAZ.

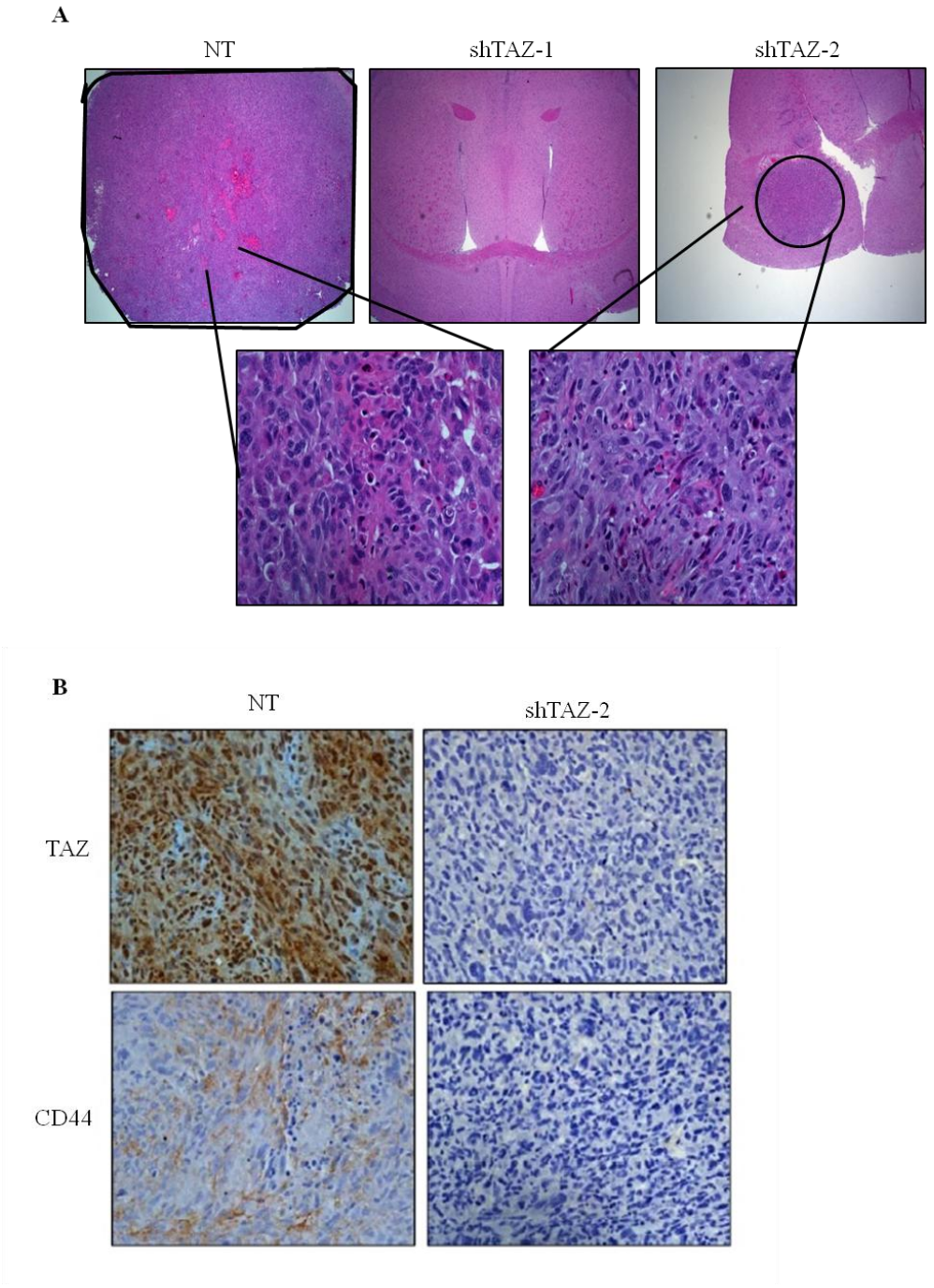

Figure 20: Stable TAZ knockdown clones in an orthotopic intracranial mouse model. (A) Representative pictures of hematoxylin and eosin stained brain slides from SCID mice injected with stable TAZ knockdown clones. NT is the non-targeting control; shTAZ-1 and shTAZ-2 are independent, non-overlapping constructs that target different portions of the *WWTR1* transcript. Top row is 2x magnification and bottom row is 40x magnification of top images. Mice injected by J Gumin. (B) IHC staining for CD44 and TAZ. Representative images of negative staining or strong positive staining are shown (40x magnification). Experiment performed by EF Hollingsworth. Reprinted with permission, Bhat, Salazar, Balasubramaniyan, et al., Genes Dev 25:2594-2609 [412], Copyright © 2011, Cold Spring Harbor Laboratory Press.

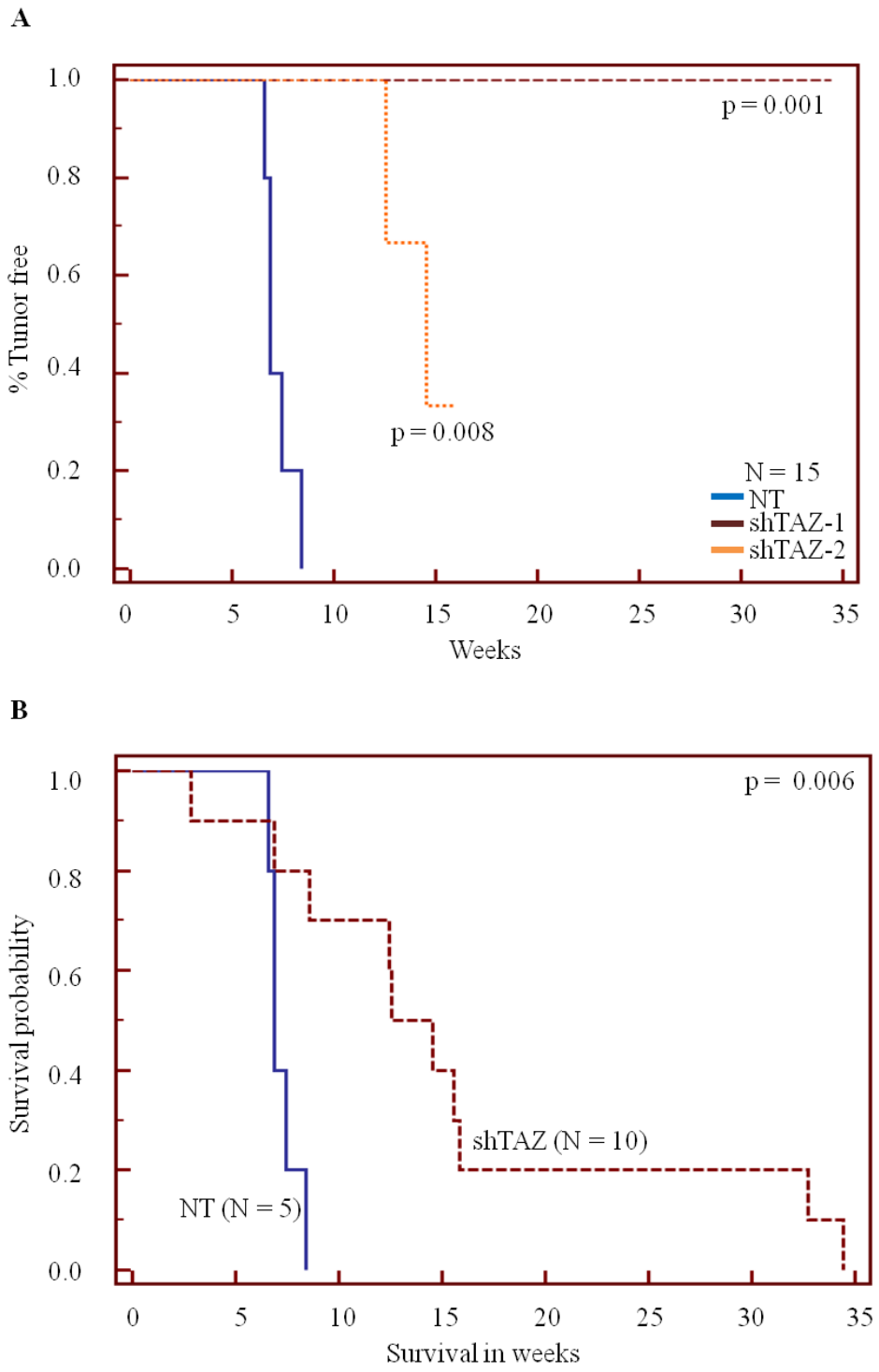

Figure 21: Kaplan-Meier analysis of tumor-free progression and overall survival. (A) Kaplan-Meier analysis of tumor-free progression of SCID mice injected with stable TAZ knockdown clones (shTAZ-1 and shTAZ-2) compared to those injected with non-targeting control (NT). (B) Kaplan-Meier analysis of survival probability of SCID mice injected with stable TAZ knockdown clones (shTAZ) compared to those injected with non-targeting control (NT). Reprinted with permission, Bhat, Salazar, Balasubramaniyan, et al., Genes Dev 25:2594-2609 [412], Copyright © 2011, Cold Spring Harbor Laboratory Press.

CHAPTER 4: RESULTS—SPECIFIC AIM 2

The mesenchymal transition is controlled by TAZ interacting with TEAD.

Using proneural GSCs to further characterize TAZ and its role in the mesenchymal transition, I stably over-expressed a mutant that always localized to the nucleus (4SA). TAZ can be phosphorylated on four serine residues (S66, S89, S117, and S311) and when this occurs, TAZ is shuttled out of the nucleus into the cytoplasm where it is sequestered by 14-3-3 [135]. Muation of these serine residues to alanine, results in absence of phosphorylation, nuclear sequestration, and increased transcriptional activity of TAZ (**Fig. 22A and B**). I hypothesized that when TAZ is localized to the nucleus, it would increase the mesenchymal behavior of normally proneural GSCs. Next, I further hypothesized that the TAZ-TEAD interaction was important for the mesenchymal transition in gliomas due to its established role in EMT in breast cancer [176,345]. To test this hypothesis, I created an additional mutation in the 4SA construct at the S51 site located in the TEAD binding domain to prevent the TAZ-TEAD interaction. To our knowledge, TEAD is the only transcription factor that binds to TAZ in the TEAD binding domain. With this construct (4SA-S51A), TAZ is localized to the nucleus, but cannot bind to TEAD (**Fig. 22A and B**). I created stable clones in GSC 11 (**Fig. 23A**), GSC 7-11 and GSC 8-11 (**Fig. 23B**) using a retrovirus-expressing Flag-tagged vector and used an empty vector as the vector contol. Most studies were completed using GSC 11 unless otherwise noted. Immunofluorescence (IF) showed predominently nuclear localization of 4SA while 4SA-S51A showed localization to both the cytoplasm and nucleus (**Fig. 23C**). This is likely due to the fact that TEAD also helps with the nuclear retention of TAZ [417]. To show the S51A mutation prevents TEAD binding, I did immunoprecipitation (IP) using Flag antibody that showed interaction of TEAD4 and Runx2 with 4SA, but only Runx2 interacted with 4SA-S51A (**Fig. 24A**). Western analysis showed an increase in expression of CD44, FN1, CTGF, and Cav2 in 4SA that was abrogated in 4SA-S51A (**Fig. 24B**), suggesting that the

A

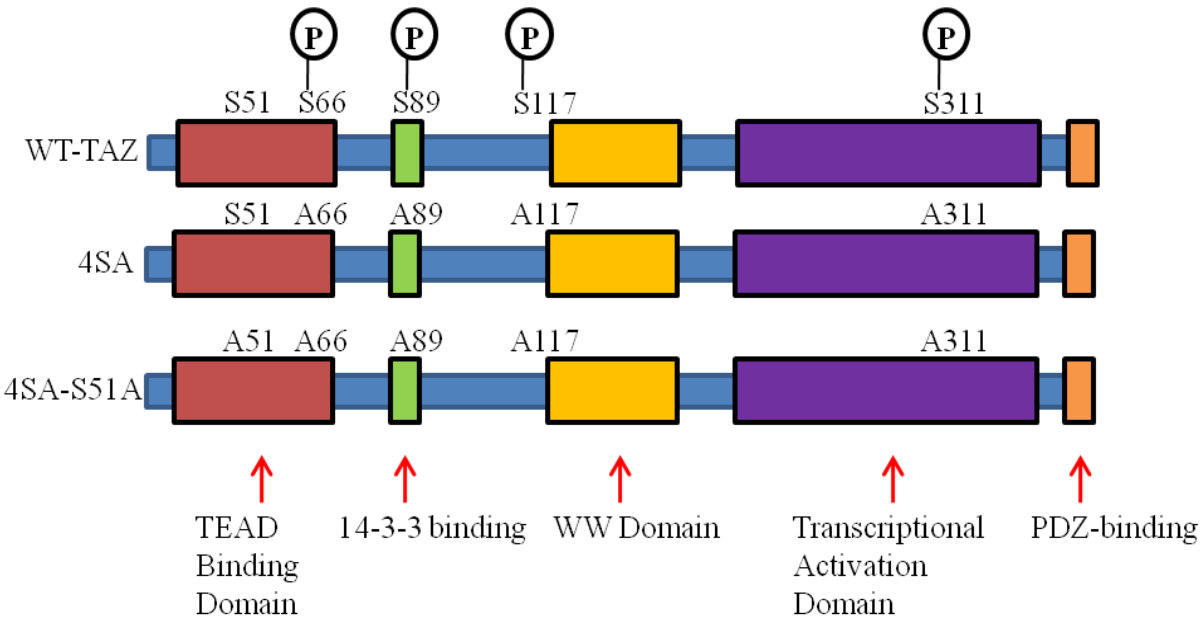

B

Construct	Localization	TEAD Binding
WT-TAZ	Cytoplasm, Nucleus	Yes
4SA	Nucleus	Yes
4SA-S51A	Nucleus	No

Figure 22: Mutant constructs 4SA and 4SA-S51A. (A) Diagram showing the locations of the serine sites that are normally phosphorylated in WT-TAZ and that are converted to alanine in 4SA and in 4SA-S51A. "P" indicates phosphorylation. (B) Table describing location and TEAD binding ability of each construct.

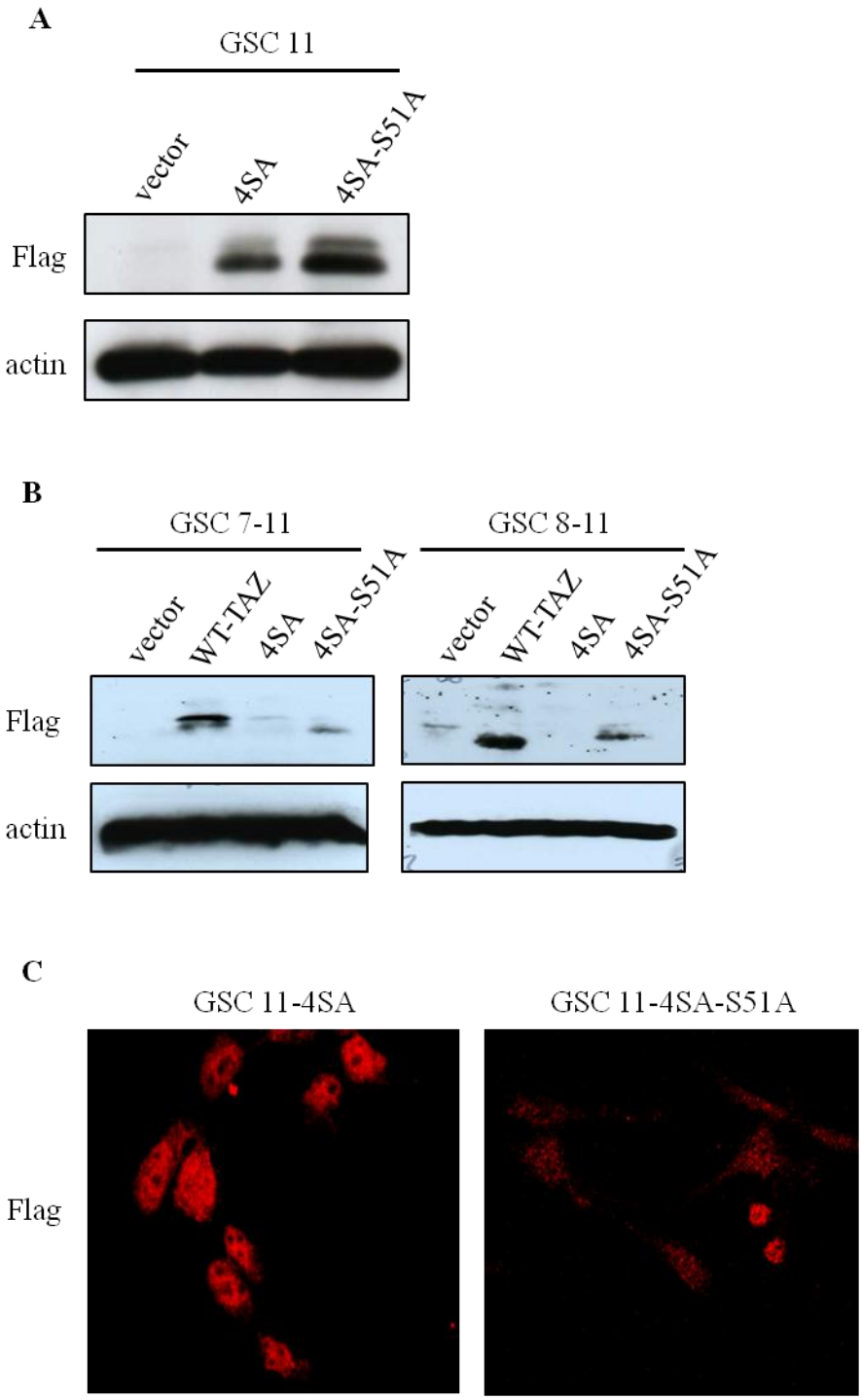

Figure 23: Stable 4SA and 4SA-S51A clones in GSCs. (A) Western analysis of Flag in GSC 11 expressing a Flag-tagged empty vector, 4SA or 4SA-S51A. (B) Western analysis of Flag in GSC 7-11 and GSC 8-11 expressing a Flag-tagged empty vector, WT-TAZ, 4SA or 4SA-S51A. (C) IF analysis of Flag in GSC 11-4SA and GSC 11-4SA-S51A. Reprinted with permission, Bhat, Salazar, Balasubramaniyan, et al., Genes Dev 25:2594-2609 [412], Copyright © 2011, Cold Spring Harbor Laboratory Press.

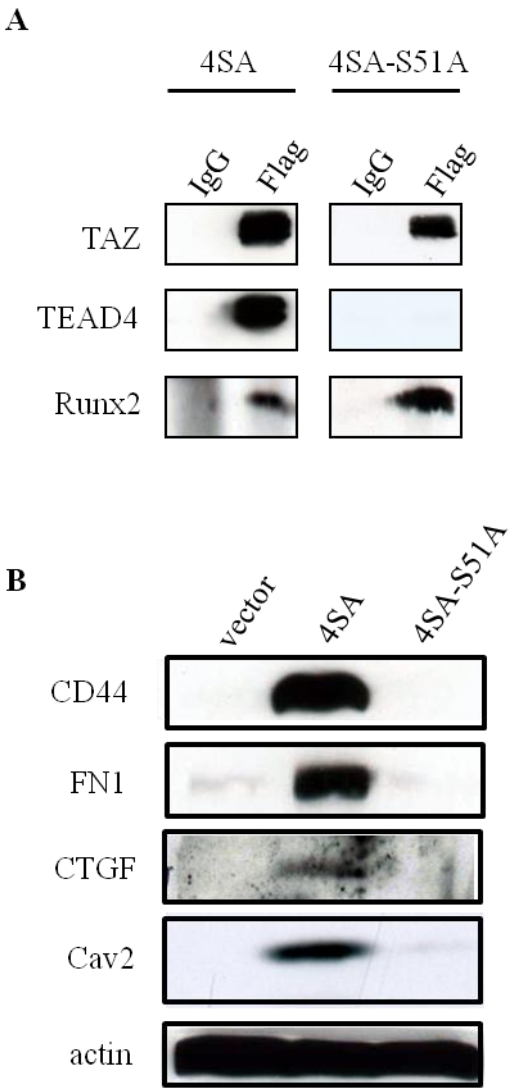

Figure 24: IP and Western analyses of 4SA and 4SA-S51A. (A) IP (Flag)-WB (TAZ, TEAD4, Runx2) of GSC 11-4SA and GSC 11-4SA-S51A. (B) Western analysis of CD44, FN1, CTGF, and Cav2 in GSC 11-4SA and GSC 11-4SA-S51A compared to GSC 11 empty vector control. Reprinted with permission, Bhat, Salazar, Balasubramaniyan, et al., Genes Dev 25:2594-2609 [412], Copyright © 2011, Cold Spring Harbor Laboratory Press.

TAZ-TEAD interaction is important in mesenchymal protein expression. These constructs also affected invasion capacity, but not self-renewal abilities (**Fig. 25A and B**). Invasion increased in 4SA, but this was decreased to almost control levels in 4SA-S51A (**Fig. 25A**), suggesting that the TAZ-TEAD interaction is important for the invasive properties of GSCs. Self-renewal does not appear to be affected by 4SA (**Fig. 25B**), which is unexpected based on findings from another publication using breast cancer stem cells [240]. It is possible that the 4SA mutation affects self-renewal in GSCs through an unknown mechanism, but it has been noted that self-renewal does not necessarily predict tumor potential in murine models [418]. Another cell line expressing 4SA, GSC 23, (**Fig. 26A**) also showed an increase in invasive capabilities (**Fig. 26B**). Next, these GSC 11 constructs were also tested for changes in proliferation. Using EdU incorporation, neither 4SA nor 4SA-S51A showed a significant change in proliferation compared to vector control (**Fig. 27A**), suggesting that in GSCs, TAZ does not appear to enhance proliferation. Consistent with these findings, western analysis showed no difference in expression of proteins involved in the proliferation between vector control, 4SA or 4SA-S51A (**Fig. 27B**). Stable knockdown constructs of *TEAD* were also used in 4SA as another way to test the importance of the TAZ-TEAD interaction. I also stably knocked down *CTGF*, a well-known downstream target of TAZ-TEAD, to rule out the possibility that the changes seen *in vitro* were specifically due to TAZ-TEAD-CTGF rather than TAZ-TEAD affecting many downstream targets. Invasive capacity decreased when *TEAD* was stably knocked down in 4SA; however, this was not seen when *CTGF* was stably knocked down (**Fig. 28A**), suggesting that it is the TAZ-TEAD interaction that subsequently activates *CTGF* in addition to many other target genes that is important to invasion in GSCs. Western analysis of FN1, CD44, CTGF, and Cav2 in 4SA-shTEAD also showed a decrease in expression similar to that seen in 4SA-S51A (**Fig. 28B**); however, no signficant decrease was seen in CD44 or Cav2 in

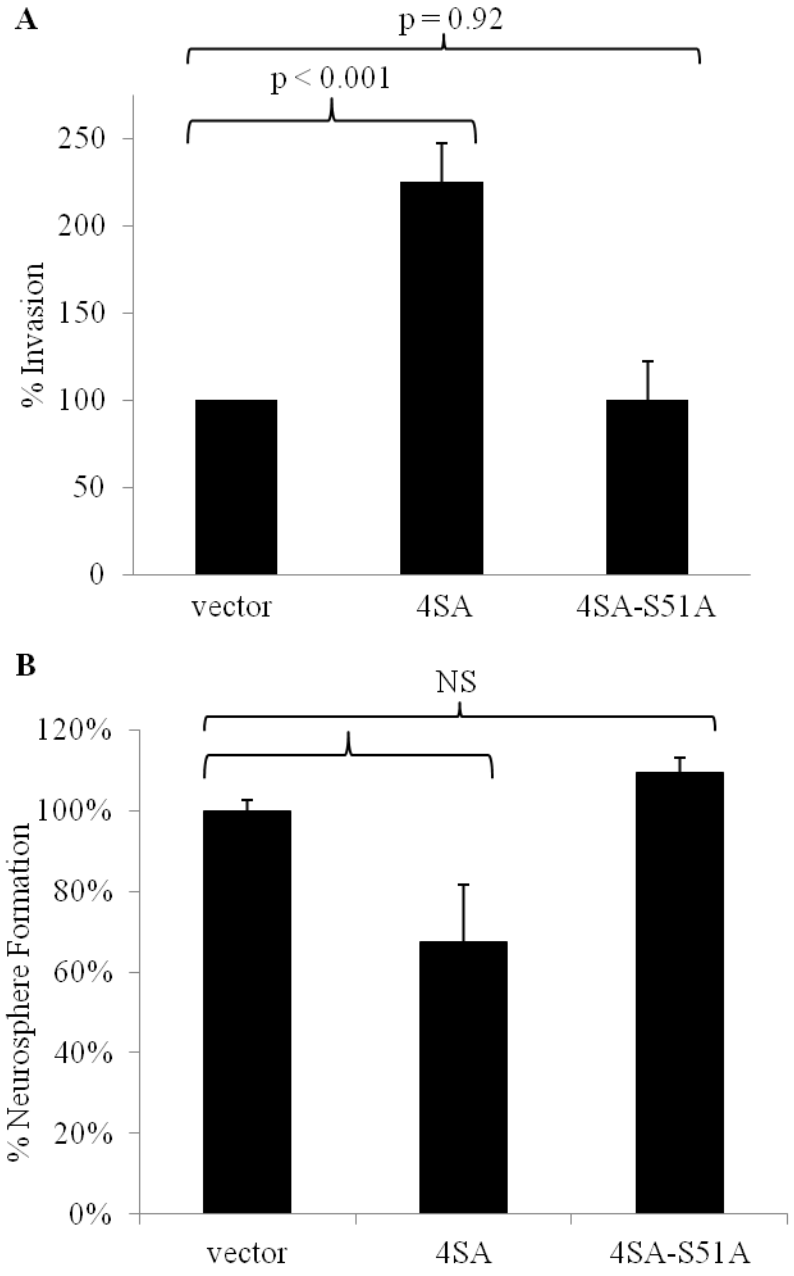

Figure 25: Invasive and self-renewal abilities of 4SA and 4SA-S51A. (A) Invasion assay of GSC 11 vector control, 4SA, and 4SA-S51A. The invasion efficiency of the vector control was set to100% for comparison. (B) Neurosphere assay of GSC 11 vector control, 4SA, and 4SA-S51A. Bar graphs indicate percentage of neurosphere formation. The self-renewal ability of the vector control was set to 100% for comparison. NS = not significant. Reprinted with permission, Bhat, Salazar, Balasubramaniyan, et al., Genes Dev 25:2594-2609 [412], Copyright © 2011, Cold Spring Harbor Laboratory Press.

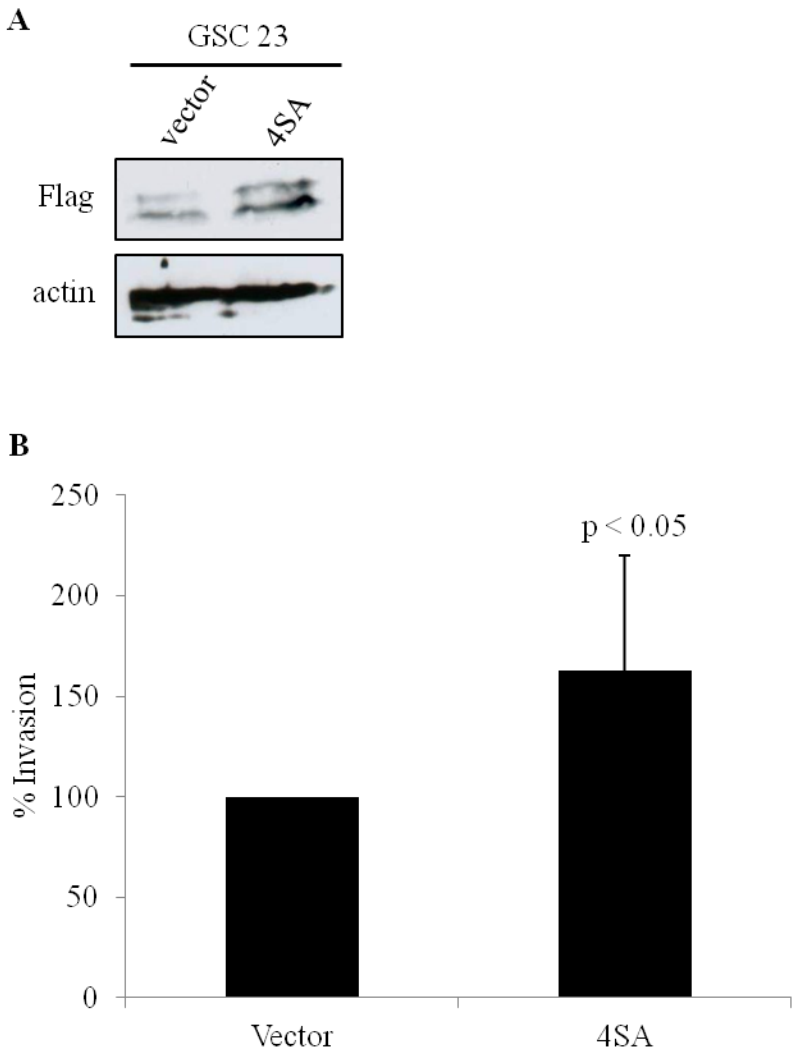

Figure 26: Western and invasion analyses of 4SA in GSC 23. (A) Western analysis of Flag in GSC 23 expressing a Flag-tagged empty vector or 4SA. (B) Invasion assay of GSC 23 vector control and 4SA. The invasion efficiency of the vector control was set to100% for comparison.

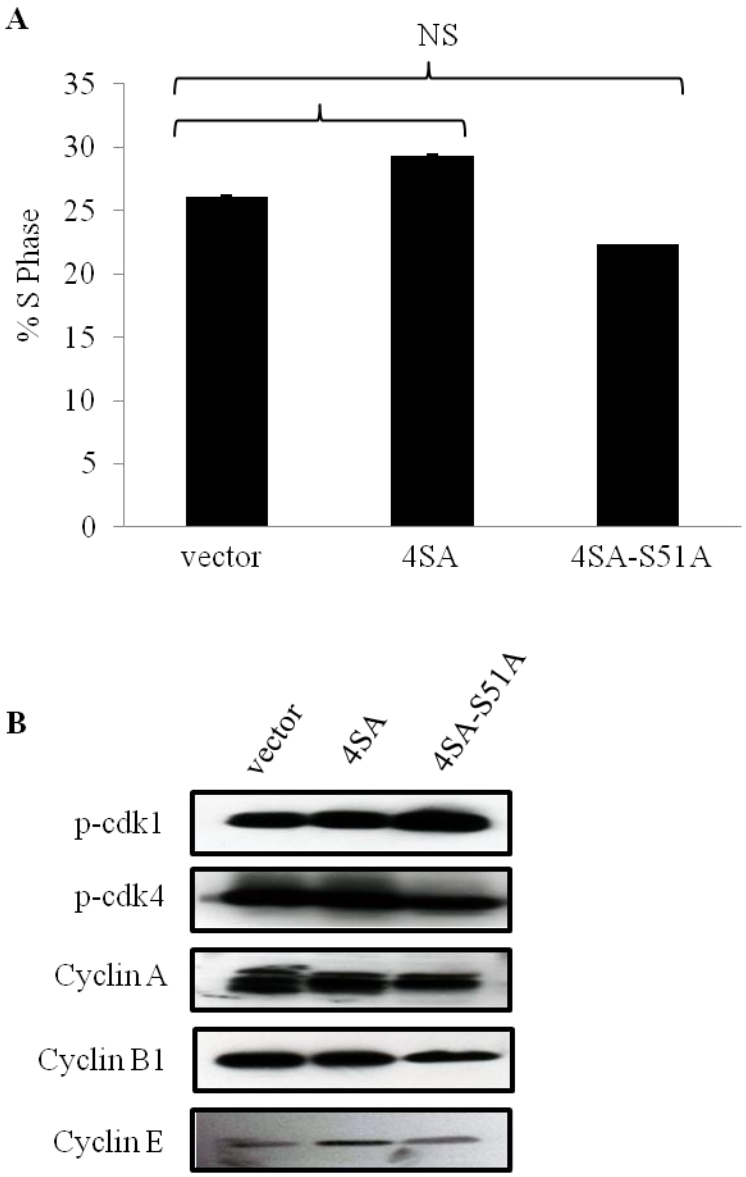

Figure 27: Proliferation in 4SA and 4SA-S51A. (A) Proliferation assay of vector control, 4SA and 4SA-S51A in GSC 11. Bar graphs indicate percentage of cells in S phase. NS = not significant. (B) Western analyses of p-cdk1, p-cdk4, Cyclin A, Cyclin B1, and Cyclin E in GSC 11 vector control, 4SA, and 4SA-S51A. Reprinted with permission, Bhat, Salazar, Balasubramaniyan, et al., Genes Dev 25:2594-2609 [412], Copyright © 2011, Cold Spring Harbor Laboratory Press.

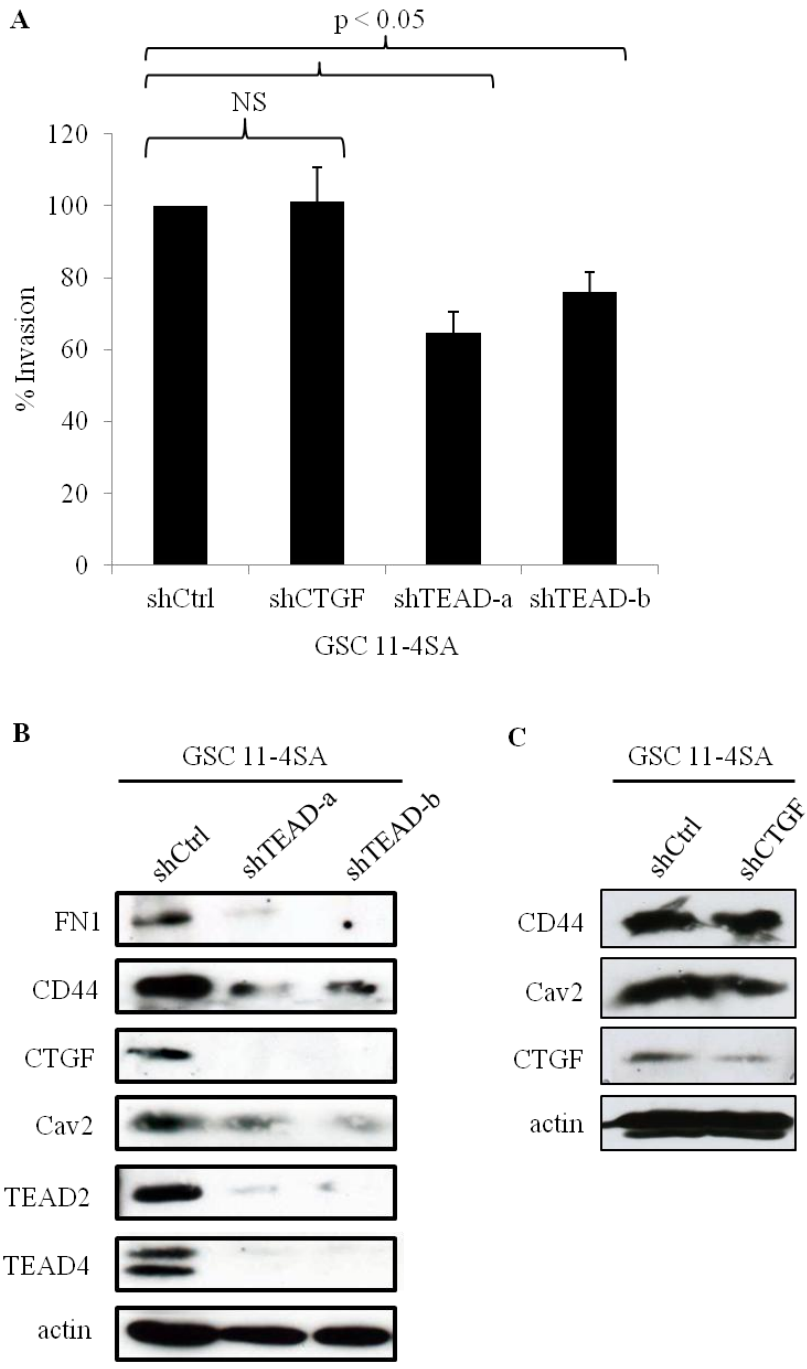

Figure 28: Stable knockdown of TEAD and CTGF in 4SA. (A) Invasion assay of GSC 11-4SA expressing the stable knockdown of *TEAD* or *CTGF*. The invasion efficiency of GSC 11-4SA expressing the non-targeting control was set to100% for comparison. shTEAD-a and shTEAD-b are independent constructs that target different *TEAD* transcripts. (B) Western analysis of FN1, CD44, CTGF, Cav2, TEAD2, and TEAD4 in GSC 11-4SA expressing stable *TEAD* knockdown constructs. (C) Western analysis of CD44, Cav2, and CTGF in GSC 11-4SA expressing a stable *CTGF* knockdown construct. Reprinted with permission, Bhat, Salazar, Balasubramaniyan, et al., Genes Dev 25:2594-2609 [412], Copyright © 2011, Cold Spring Harbor Laboratory Press.

4SA-shCTGF (**Fig. 28C**).

From previous publications, I knew that TAZ plays a role in mesenchymal stem cell differentation by interacting with Runx2 to promote differentiation into osteoblasts [136]. I hypothesized that something similar would occur in GSCs expressing nuclear TAZ. To test this hypothesis, we performed osteogenesis and chondrogenesis differentiation assays on GSC 11-4SA and GSC 11-4SA-S51A. For osteogenesis differentation, both constructs were subjected to osteogenic conditions for 30 days then fixed and stained with alizarin red, a dye that binds specifically to calcium matrix formations. Only 4SA showed significant red staining while vector control and 4SA-S51A lacked staining (**Fig. 29A**). For chondrocytic differentation, vector control and 4SA-transduced cells were subjected to chondrogenic conditions for 30 days then fixed and stained with safranin O, a stain used for the detection of cartilage. Safranin O staining was positive in the 4SA construct compared to vector control (**Fig. 29B**). Taken together, these data show that TAZ-TEAD interaction induces the mesenchymal transition in GSCs. Next we characterized the effect of 4SA and 4SA-S51A *in vivo* by intracranially injecting the vector control, 4SA, and 4SA-S51A into SCID mice with the hypothesis that the tumor-initiating ability of 4SA would be increased when compared to the vector control followed by a subsequent decrease in 4SA-S51A. Those mice injected with vector control showed smaller tumors that lacked the pathognomonic characteristics of GBM (i.e.—microvascular proliferation and pseudopalisading necrosis) while those injected with 4SA developed large tumors that showed the signs of GBM (**Fig. 30A**). None of the mice injected with 4SA-S51A formed tumors (**Fig. 30A**). Overall survival was also decreased in those mice injected with 4SA compared to those injected with vector control (**Fig. 30B**). Collectively, the data show that the TAZ-TEAD interaction is important for mesenchymal protein expression, invasion, differentiation, and tumor-initiating abilities, but not

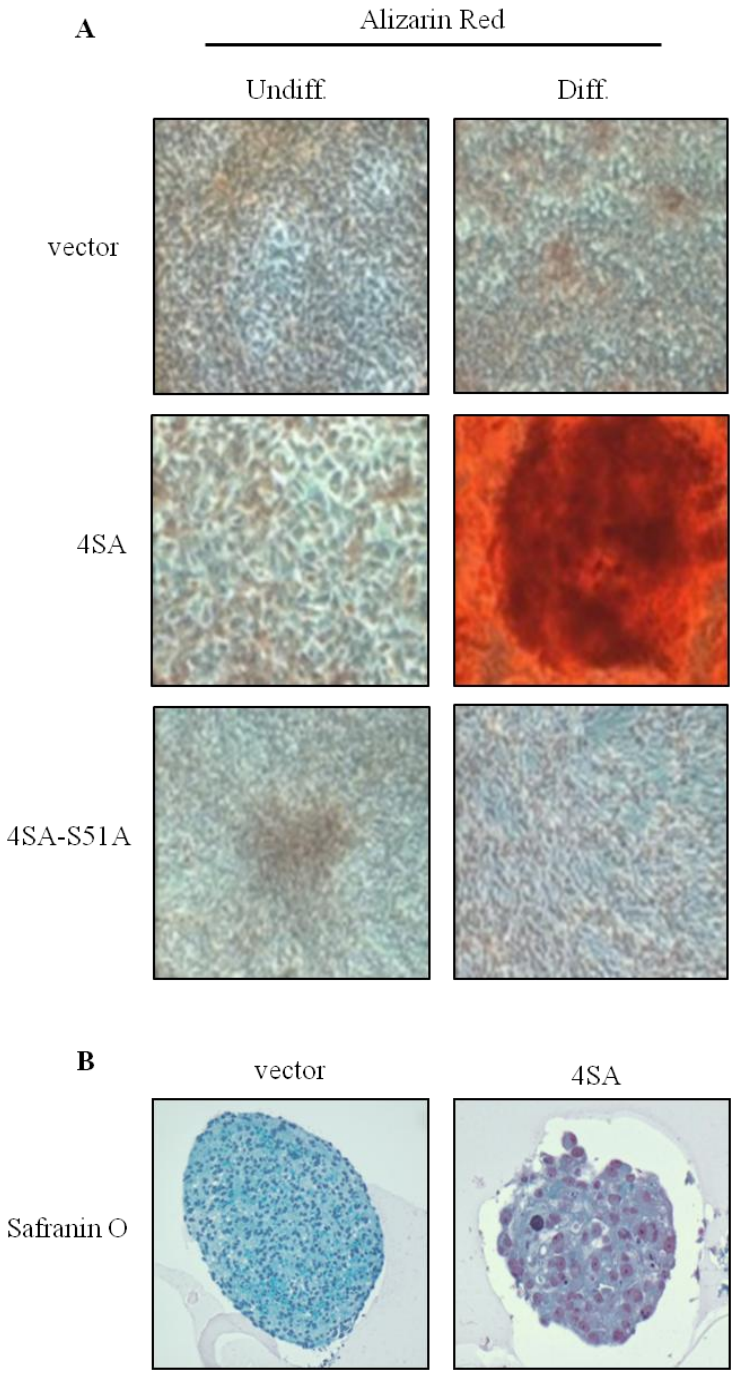

Figure 29: Osteogenic and chondrogenic differentiation of 4SA and 4SA-S51A. (A) Osteogenic differentiation of vector control, 4SA, and 4SA-S51A after growth in control media (Undiff. column) or osteogenic conditions (Diff. column) for 30 days. Cells were fixed then stained with alizarin red to identify calcium matrix formation. Experiment performed by J Gumin. (B) Chondrogenic differentiation of vector control and 4SA after growth in chondrogenic conditions for 30 days. Cells were fixed and stained with safranin O to identify cartilage. Experiment performed by J Gumin. Reprinted with permission, Bhat, Salazar, Balasubramaniyan, et al., Genes Dev 25:2594-2609 [412], Copyright © 2011, Cold Spring Harbor Laboratory Press.

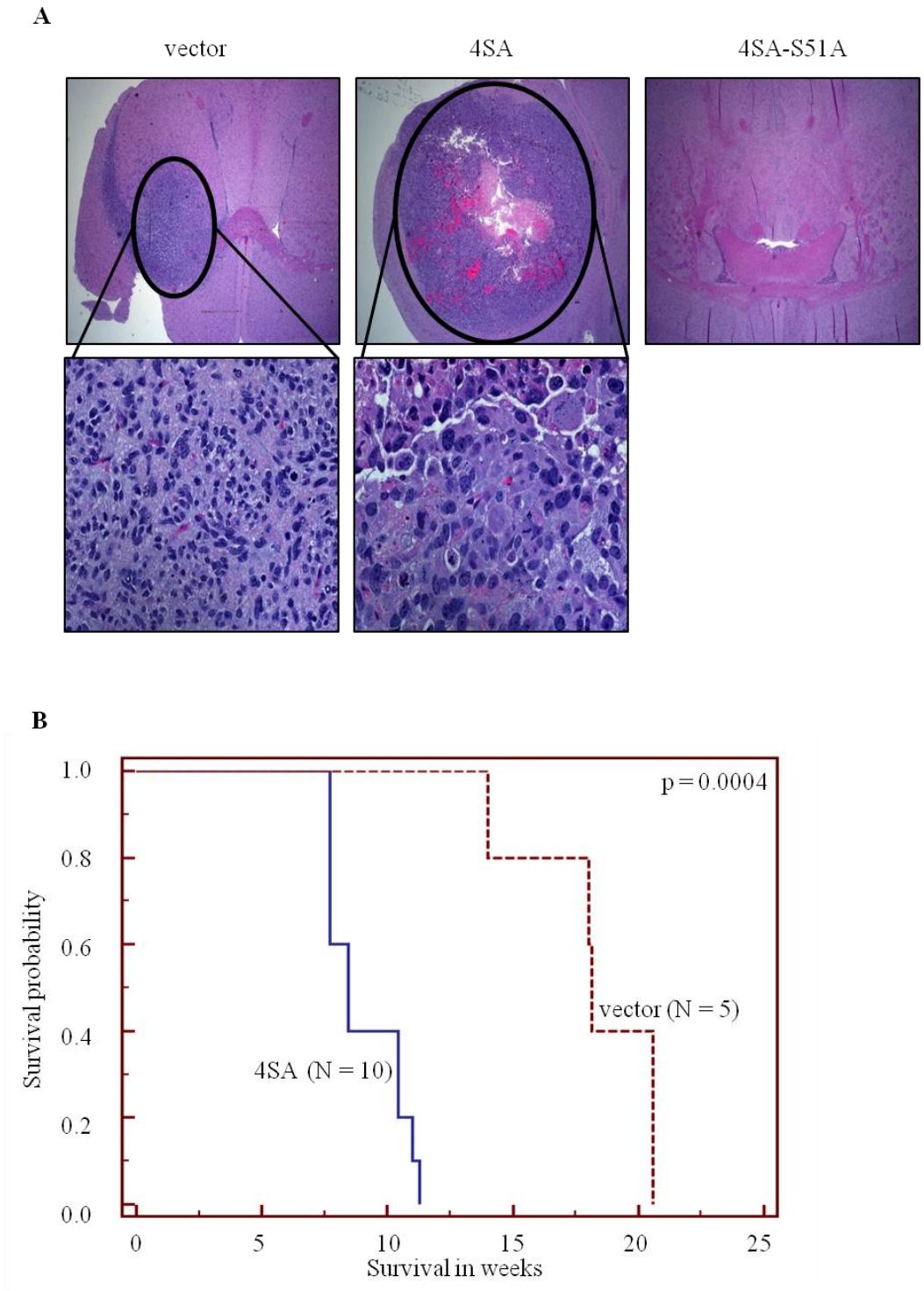

Figure 30: 4SA and 4SA-S51A in an orthotopic intracranial mouse model. (A) Representative pictures of hematoxylin and eosin stained brain slides from SCID mice injected with GSC 11 vector control, 4SA or 4SA-S51A. Top row is 2x magnification and bottom row is 40x magnification of top images. Mice injected by J Gumin. (B) Kaplan-Meier analysis of survival probability of SCID mice injected with GSC 11-4SA compared to those injected with GSC 11 vector control.

proliferation and self-renewal.

TAZ-TEAD directly binds the promoters of target genes to induce mesenchymal transition.

It is possible that the mesenchymal transition seen with TAZ is due to interaction with other transcription factors established in mesenchymal transition in gliomas, specificially STAT3 and C/EBP-β [28]. To determine if such an interaction exists, *STAT3*, *C/EBP-β*, and *WWTR1* were transiently knocked down in GSC 20. Western analysis of STAT3, C/EBP-β, and TAZ showed no interdependence of expression between these proteins (**Fig. 31A**), suggesting that although STAT3 and C/EBP-β also lead to mesenchymal transition in gliomas, they likely do so via an independent pathway of TAZ. Next I asked if this transition could also be due to activation of TAZ via TGF-β upstream since this has been established in other models [33]. I looked at Smad2 in GSC 11-4SA and interestingly saw a decrease in expression on western (**Fig. 31B**). One would expect similar or greater expression of Smad2 between vector control and 4SA if TGF-β played an important role the mesenchymal transition in gliomas. To further show that the TAZ-TEAD induced mesenchymal transition was independent of the TGF-β pathway or STAT3 and C/EBP-β, I transiently knocked down *SMAD2*, or *STAT3* and *C/EBP-β* in GSC 11-4SA. Real-time qPCR of *ACTG2*, *CD44*, *SMA*, and *WWTR1* showed no significant difference in expression between control and transient knockdown of *SMAD2* or *STAT3* + *C/EBP-β* (**Fig. 32**). This suggests that although these pathways ultimately result in the mesenchymal shift, they are working independently of each other in our glioma model.

To test if the TAZ-TEAD interaction is responsible for up-regulating mesenchymal genes, we analyzed GSC 11 vector control, 4SA, and 4SA-S51A using microarray. We found

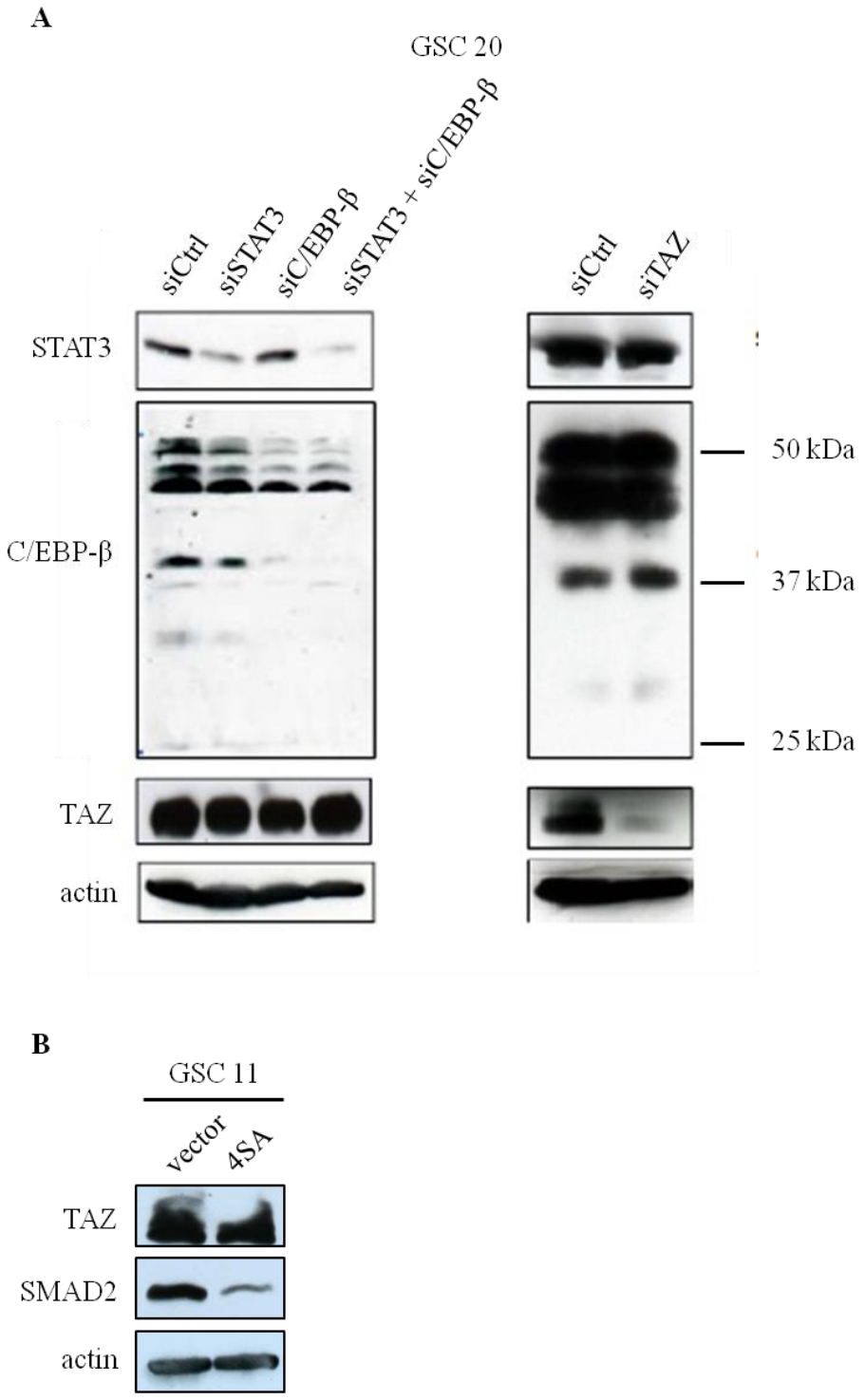

Figure 31: Western analyses of transient knockdown of *STAT3*, *C/EBP-β*, and *SMAD2*. (A) Western analysis of STAT3, C/EBP-β, and TAZ in GSC 20 after transient knockdown of *STAT3* and/or *C/EBP-β* and *WWTR1*. (B) Western analysis of TAZ and Smad2 in GSC 11 vector control and 4SA after transient knockdown of *SMAD2*. Reprinted with permission, Bhat, Salazar, Balasubramaniyan, et al., Genes Dev 25:2594-2609 [412], Copyright © 2011, Cold Spring Harbor Laboratory Press.

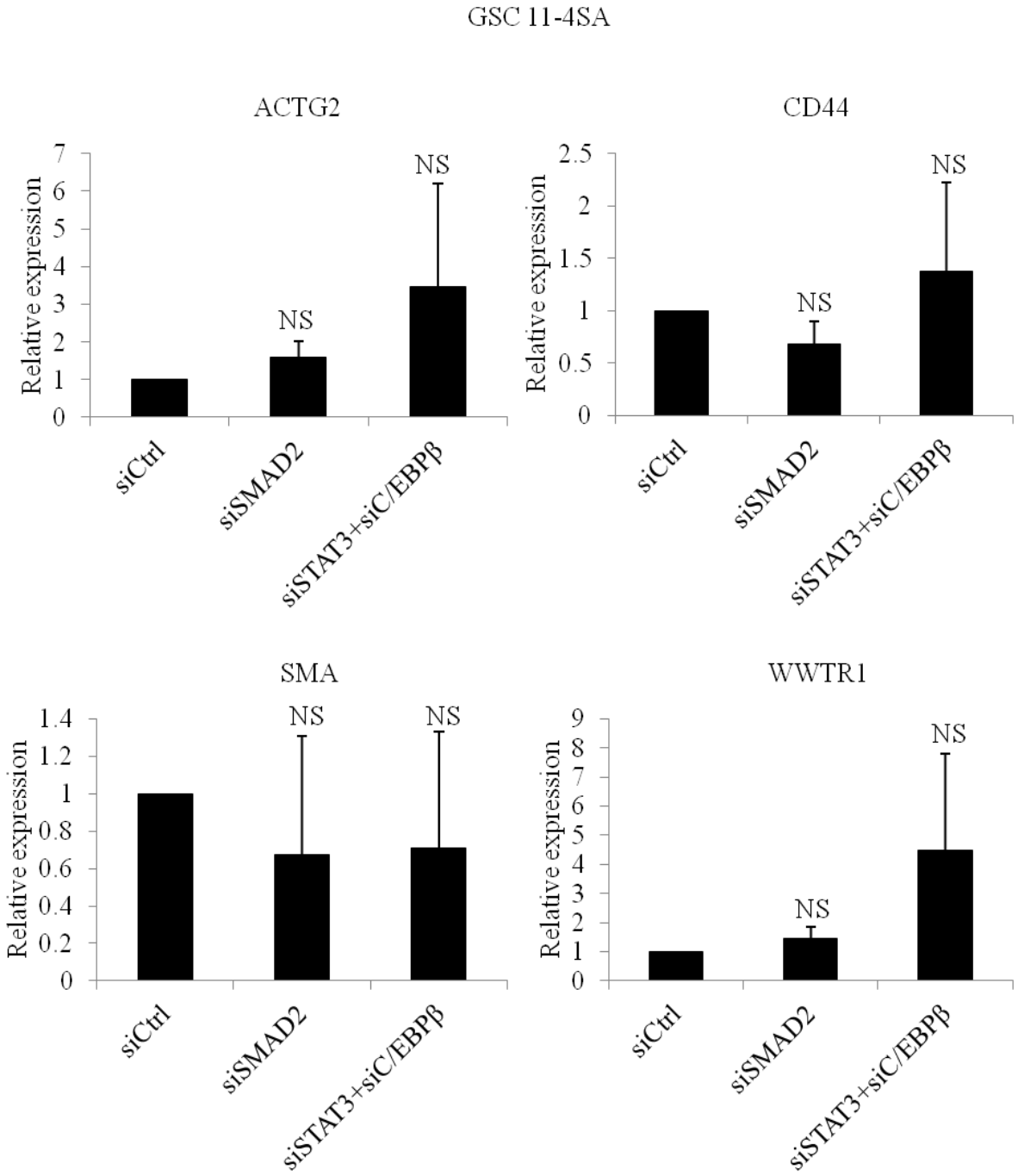

Figure 32: Real-time qPCR after transient knockdown of *SMAD2*, *STAT3*, and *C/EBP-β*. Real-time qPCR of *ACTG2*, *CD44*, *SMA*, and *WWTR1* expression in GSC 11-4SA after transient knockdown of *SMAD2* or *STAT3* + *C/EBP-β*. To compare transcript levels, fold change with siCtrl and with siRNA was used. NS = not significant.

hundreds of genes that were up-regulated by 4SA (i.e.—fold change > 1.5 compared to vector control) and this induction was abrogated in the 4SA-S51A cells (i.e.—similar to vector control levels), suggesting that TAZ-TEAD interaction is important for up-regulation of specific mesenchymal genes (since these genes are down-regulated when the TAZ-TEAD interaction is prevented in 4SA-S51A; **Fig. 33**). To confirm the microarray results, I used real-time qPCR to analyze the following mesenchymal genes: *WWTR1*, *CD44*, *ADAMTS1*, *CTGF*, *IL8*, and *FN1*. The real-time qPCR data are consistent with the microarray data (**Fig. 34**), further suggesting that the TAZ-TEAD interaction is important for the mesenchymal shift via up-regulation of numerous mesenchymal genes. The collective set of genes that were up-regulated in 4SA cells were analyzed using DAVID and these genes were found to have mesenchymal biological activities, including vasculature development, response to wound healing, and regulation of cell motion (**Table 4**). These data further support the importance of TAZ in the mesenchymal shift seen in gliomas. Conversely, when we looked at the genes that were down-regulated in 4SA and subsequently up-regulated in 4SA-S51A, we found predominantly proneural genes (**Fig. 35A**). DAVID analysis showed that these genes have proneural biological activities, including gliogenesis, neurogenesis regulation, and glial cell differentiation (**Fig. 35B**). Western analysis of TAZ, Olig2, and achaete-scute complex homolog 1 (Mash1) was consistent with the microarray data (**Fig. 35C**), suggesting that TAZ-TEAD is important to the proneural-mesenchymal shift seen in gliomas.

To show that these genes are up-regulated directly by TAZ-TEAD, ChIP-PCR was performed. Genomatix was used to analyze 3 kb portions proximal to the transcription start site of sixteen mesenchymal genes. Primer3 was used to design primers around putative TEAD consensus sequences (GGAATG [318]) in these mesenchymal genes (**Table 5**). GSC 11-4SA was used for the ChIP-PCR experiment and both IP-TAZ and IP-TEAD was performed. PCR

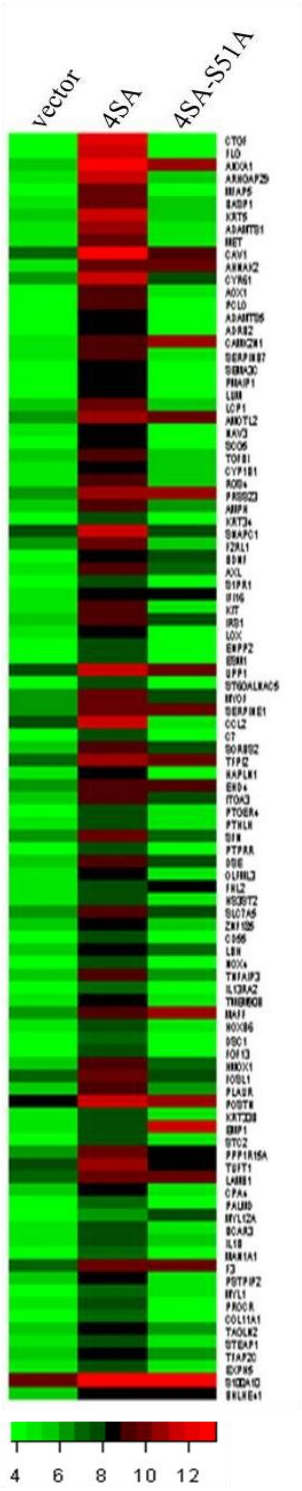

Figure 33: Microarray of vector control, 4SA, and 4SA-S51A. Heat map showing genes induced in GSC 11-4SA compared to GSC 11 vector control. Gene expression levels in GSC 11-4SA-S51A are relative to GSC 11 vector control as well. Plots are the log2 of Affymetrix expression values. Data analyzed by BD Vaillant. Reprinted with permission, Bhat, Salazar, Balasubramaniyan, et al., Genes Dev 25:2594-2609 [412], Copyright © 2011, Cold Spring Harbor Laboratory Press.

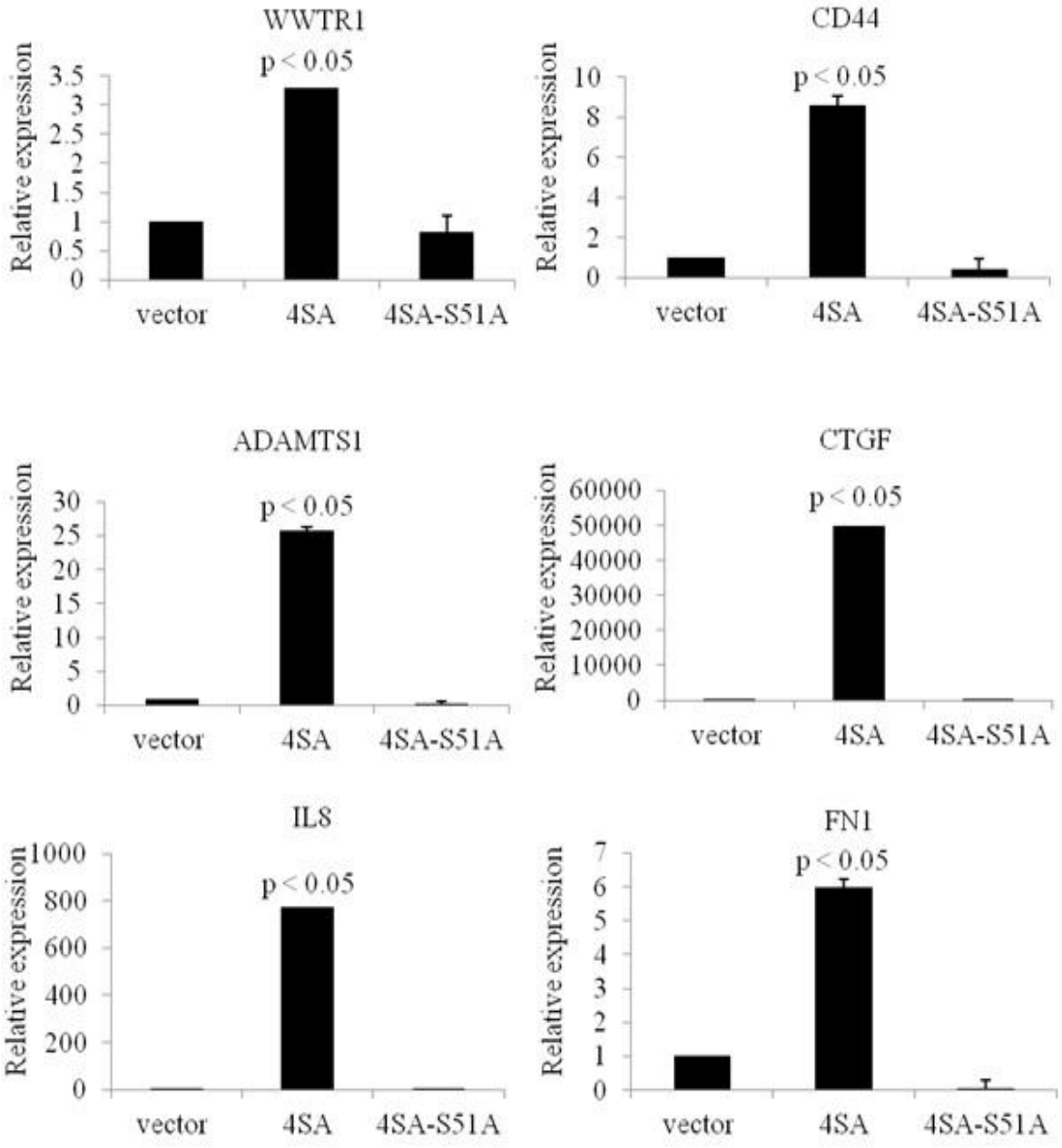

Figure 34: Real-time qPCR of vector control, 4SA, and 4SA-S51A. Real-time qPCR results of *WWTR1*, *CD44*, *ADAMTS1*, *CTGF*, *IL8*, and *FN1* expression in GSC 11 vector control, 4SA, and 4SA-S51A. To compare transcript levels, fold change with vector control and with 4SA or with 4SA-S51A was used. Reprinted with permission, Bhat, Salazar, Balasubramaniyan, et al., Genes Dev 25:2594-2609 [412], Copyright © 2011, Cold Spring Harbor Laboratory Press.

Table 4: Functional gene analysis of genes up-regulated by 4SA

Functional Annotation	p-value
blood vessel development	1.0E-8
vasculature development	1.4E-8
positive regulation of phosphorylation	3.3E-7
blood vessel morphogenesis	3.7E-7
positive regulation of phosphorus metabolic process	4.4E-7
positive regulation of phosphate metabolic process	4.4E-7
response to wounding	6.7E-7
regulation of cell motion	8.3E-7

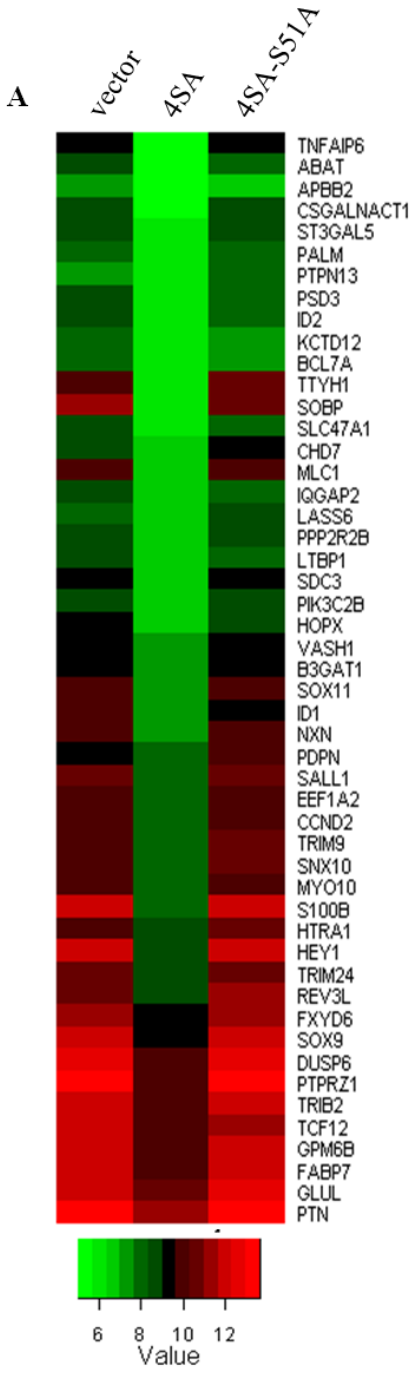

B

Functional Annotation	p-value
gliogenesis	3.4E-8
regulation of neurogenesis	8.1E-8
glial cell differentiation	3.9E-7
regulation of cell development	4.2E-7
developmental protein	5.4E-7
regulation of nervous system development	7.3E-7
transcription factor activity	1.7E-6
regulation of neuron differentiation	3.3E-6

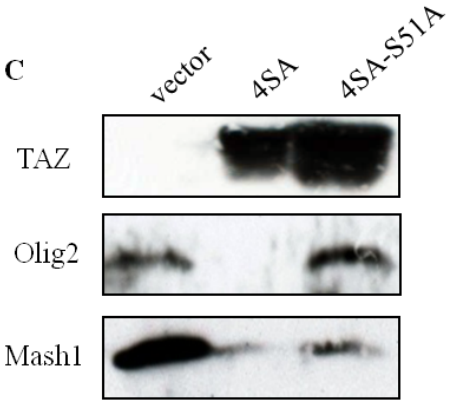

Figure 35: Down-regulation of proneural genes in 4SA. (A) Heat map showing genes down-regulated in GSC 11-4SA compared to GSC 11 vector control. Gene expression levels in GSC 11-4SA-S51A are relative to GSC 11 vector control as well. Plots are the log2 of Affymetrix expression values. Data analyzed by BD Vaillant. (B) Functional gene analysis by DAVID of genes down-regulated by GSC 11-4SA. (C) Western analysis of TAZ, Olig2, and Mash1 in GSC 11 vector control, 4SA, and 4SA-S51A. Reprinted with permission, Bhat, Salazar, Balasubramaniyan, et al., Genes Dev 25:2594-2609 [412], Copyright © 2011, Cold Spring Harbor Laboratory Press.

Table 5: ChIP-PCR Primer Designs

Gene	Forward	Reverse
ACTG2	TGTTTATCGACTGGCTGTGC	AAGCTCCCCCTCTGATTCTC
ACTN1	CAGGGACTATGGCTTTTTCATC	GATATCGGATGGTGTCTCTGG
ADAMTS1	TTGAGTGAAAGCACGCAGAC	GCCACCTCTTCACCAGAGAC
CAV2	TGGATTCCCATAAGGATTCAT	CATCACCCTGCTTACCCATT
CD44	AAGACTGCCTGGTGTTCTCC	AGAAATGCACCCAGCCATC
COL1A1	CCCCATCATTTTTCATCACC	AGGAGGCAGGAGTTTCCACT
COL11A1	ATTAACGAACAAAAAGGAGTCAA	GATCCTGGATGAGGGGGTA
CTGF	TTCTGTGAGCTGGAGTGTGC	GCCAATGAGCTGAATGGAGT
CXCL2	TCAGCTAAACAGGCTTGGAAA	AAGGCCATAGACACCACCAG
IL4R	ACTATCCAAATGTGGCTGGAG	TCCTCCTCCCCTTCCTAACA
LAMP1	AAGCCAGTCCACGTGTCAGT	GACAGGACCAGGCACTCACT
LUM	ATGCTCTGAAACGCACAAAA	GCTCTTGTTAGAAAAACTCCACCT
MYL1	GCCCTGACCCTTTAGATTCC	GATCCACAGCCCAGTGTCTT
PLAUR	ACTACGCCCGGCTAATTTTT	TTAACCCTTGCTTTGCTTCC
TAGLN2	TACTAGGGCTCGGCTACCAG	GACTCACCTAGGGGGTCAGC
TUBB6	GACCTCCCCAAACCTACTCC	TCCTCGTTGATTTGCATCAG

bands were seen in both IP-TAZ and IP-TEAD, but not IgG, in the following genes: *ACTN1*, *COL1A1*, *CTGF*, and *CXCL2* (**Fig 36**). Some genes (*ACTG2*, *CD44*, *COL11A1*, and *MYL1*) demonstrated inconclusive data (**Fig. 36**). Other genes (*CAV2*, *IL4R*, *LAMP1*, *LUM*, *PLAUR*, *TAGLN2*, and *TUBB6*) displayed positive bands following TAZ IP, but not TEAD IP (**Fig. 36**). These data suggest that at least a subset of these genes is directly activated by TAZ-TEAD. However, it is possible that some of these results are due to technical issues and with changes, such as alternative primer design, more conclusive outcomes could be drawn. Overall, these data show that TAZ-TEAD is important for activation of mesenchymal genes and de-activation of proneural genes independent of the TGF-β pathway or STAT3 and C/EBP-β.

TAZ-TEAD interaction decreases survival and increases glioma grade in a mouse model.

To supplement the SCID mice data, I used the RCAS/*N-tva* mouse model system due to its advantages including the ability to control the cell of origin, to combine specific gene alterations, and to know the earliest time of onset (i.e.—day of injection). Also, this system allows for tumors to develop in a normal cellular environment (i.e.—normal microenvironment with a competent immune system) and the tumors that form are similar to the human counterparts [419]. This system uses retrovirus-encoded genes that can be directed to express in *Nestin*$^{+}$ neural progenitor cells (NPCs) expressing the tv-a receptor on their cell surface. Chicken fibroblast (DF-1) cells were transfected with the RCAS vector containing specific genes of interest and directly injected into the *N-tva* mouse brains as described previously [406,407].

Since specific gene combinations can be studied in this model, PDGF-β was chosen as the baseline control and was common among the experimental groups. Tumors that form from

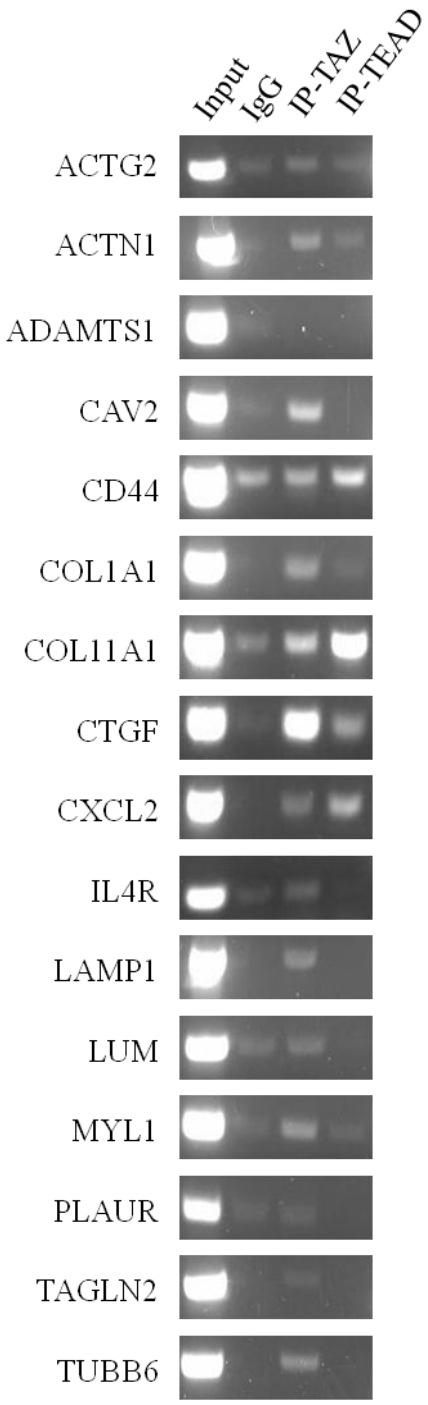

Figure 36: ChIP-PCR of inferred TAZ-TEAD target gene promoters using 4SA. IP was done with either TAZ or TEAD. Standard PCR was performed using designed primers in **Table 5** (above). PCR products were run on 0.5% TAE agarose gels with ethidium bromide. Pictures were taken using a UV-lamp light box.

the over-expression of PDGF-β in this mouse model are typically lower grade proneural tumors [420]. I hypothesized that the addition of WT-TAZ or 4SA to PDGF-β would induce a proneural-mesenchymal shift that would generate high grade gliomas. I further speculated that the addition of the 4SA-S51A allele, which lacks TEAD binding, to PDGF-β would result in tumors similar to PDGF-β alone. Mice were sacrificed once neurological symptoms (e.g.—seizures, hydrocephalus, ataxia, etc.) were present. I found that mice injected with WT-TAZ + PDGF-β or 4SA + PDGF-β had a significant decrease in overall survival compared to those injected with PDGF-β alone (**Fig. 37A and B**). Interestingly, when 4SA-S51A is injected along with PDGF-β in these mice, the overall survival improves compared to those injected with either WT-TAZ + PDGF-β or 4SA + PDGF-β (**Fig. 37A and B**). The median survival of WT-TAZ + PDGF-β and 4SA + PDGF-β was almost half of that of PDGF-β at 5 weeks compared to 11 weeks while the median survival of 4SA-S51A + PDGF-β was in between at 8 weeks (**Fig. 37C**). Mice injected with WT-TAZ, 4SA or 4SA-S51A alone survived more than 90 days post-injection and did not form tumors (**Figs. 37A and 38**). This is likely due to a known property of this mouse model when specific oncogenes are used in isolation. Others have shown that tumors fail to form when well-known oncogenes, such as Akt and Ras, are injected alone [421]. To our knowledge, PDGF-β is the only gene that can form tumors when over-expressed alone in this mouse model [422]. Over-expression of WT-TAZ + PDGF-β and of 4SA + PDGF-β also led to an overall shift in grade, meaning the predominate grade in PDGF-β alone was grade II (76%) while the predominate grades with the gene combinations was grades III (41-50%) or IV (43-45%; **Fig. 38**). Given more time without serious neurological symptoms, the mice could have transitioned from grade III to grade IV, thus increasing the predominant grade to grade IV in the WT-TAZ + PDGF-β and in the 4SA + PDGF-β groups. No shift in grade was seen in 4SA-S51A + PDGF-β since most of the tumors

A

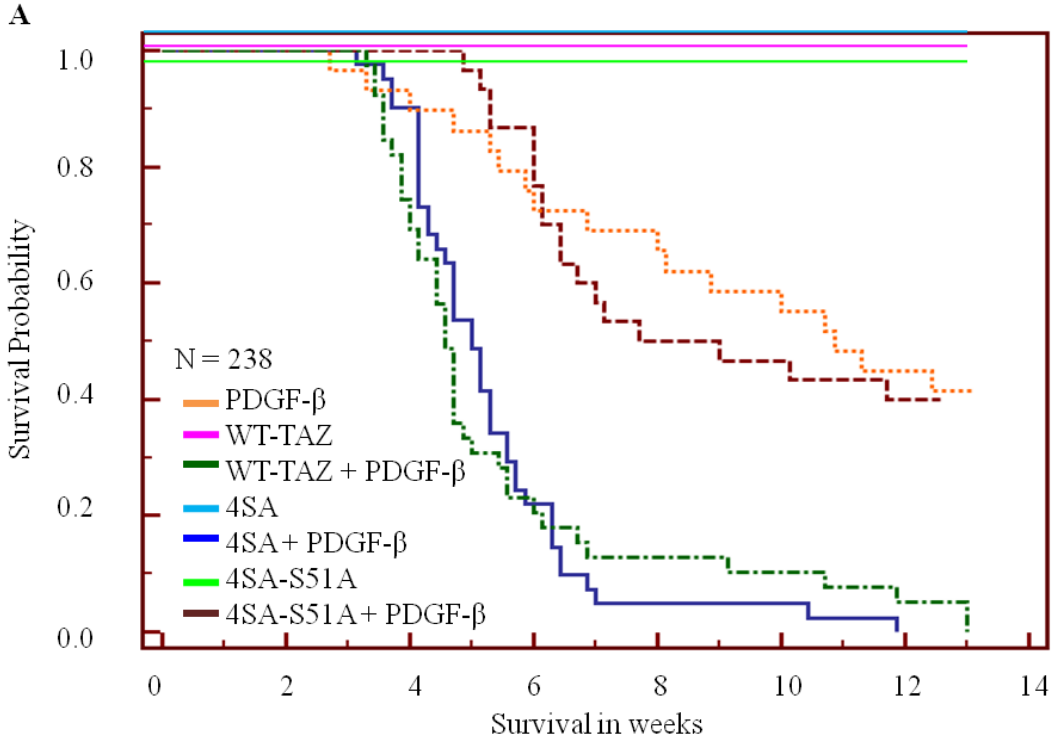

B

Comparison	p-value
PDGF-β vs. WT-TAZ + PDGF-β	3.0E-7
PDGF-β vs. 4SA + PDGF-β	1.3E-8
PDGF-β vs. 4SA-S51A + PDGF-β	0.0389
4SA + PDGF-β vs. 4SA-S51A + PDGF-β	3.2E-9

C

Gene(s)	Median Survival (weeks)
PDGF-β	10.9
WT-TAZ + PDGF-β	4.6
4SA + PDGF-β	5.0
4SA-S51A + PDGF-β	8.4

Figure 37: Kaplan-Meier of survival analyzing TAZ in the RCAS/*N-tva* mouse model. (A) Kaplan-Meier of survival probability of RCAS/*N-tva* mice injected with PDGF-β, WT-TAZ ± PDGF-β, 4SA ± PDGF-β or 4SA-S51A ± PDGF-β. (B) Table shows statistical significance between groups. (C) Table shows median survival of PDGF-β, WT-TAZ + PDGF-β, 4SA + PDGF-β, and 4SA-S51A + PDGF-β. Reprinted with permission, Bhat, Salazar, Balasubramaniyan, et al., Genes Dev 25:2594-2609 [412], Copyright © 2011, Cold Spring Harbor Laboratory Press.

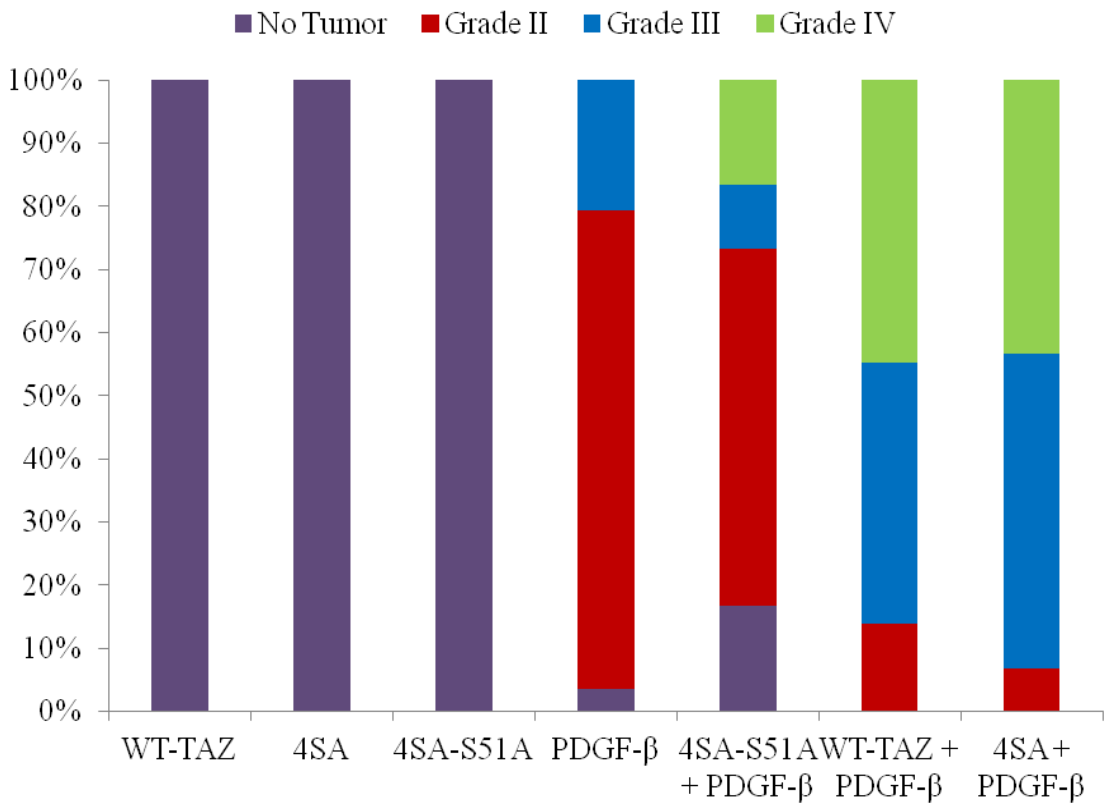

Figure 38: Grade frequency in the RCAS/*N-tva* mouse model. Bar graph shows percentage of each grade (no tumor = purple; grade II = red; grade III = blue; grade IV = green) within each group (PDGF-β, WT-TAZ ± PDGF-β, 4SA ± PDGF-β, and 4SA-S51A ± PDGF-β). Reprinted with permission, Bhat, Salazar, Balasubramaniyan, et al., Genes Dev 25:2594-2609 [412], Copyright © 2011, Cold Spring Harbor Laboratory Press.

were grade II (57%; **Fig. 38**). The grade IV tumors that formed in the WT-TAZ + PDGF-β and the 4SA + PDGF-β groups showed the pathognomonic characteristics of GBM (i.e.—pseudopalisading necrosis and microvascular proliferation) while these features were lacking in the majority of the tumors in the PDGF-β alone and the 4SA-S51A + PDGF-β groups (**Fig. 39**). Again, no tumors formed in the mice over-expressing WT-TAZ, 4SA or 4SA-S51A alone (**Fig. 39**). Next, I performed real-time qPCR of *CD44*, *CTGF*, *CXCL2*, and *FN1* on fresh frozen tumors isolated from the PDGF-β and the WT-TAZ + PDGF-β groups. I found no significant difference of relative expression of these genes between PDGF-β and WT-TAZ + PDGF-β (**Fig. 40**). This may be due to isolation methods where normal tissue was also removed and contaminated the samples. It is also possible that other mesnchymal gene targets not studied may show a difference between the two groups. Taken together, TAZ in conjunction with PDGF-β decreases overall survival and increases the predominant tumor grades in the RCAS/*N-tva* mouse model. Activation of *CD44*, *CTGF*, *CXCL2*, and *FN1* is inconclusive at this time.

In summary, the TAZ-TEAD interaction, independent of the TGF-β pathway or STAT3 and C/EBP-β, deactivates a proneural pathway and activates a mesenchymal pathway via direct binding to mesenchymal gene promoters that increases invasive capacity, promotes mesenchymal stem cell like properties, decreases survival, and increases tumor grade.

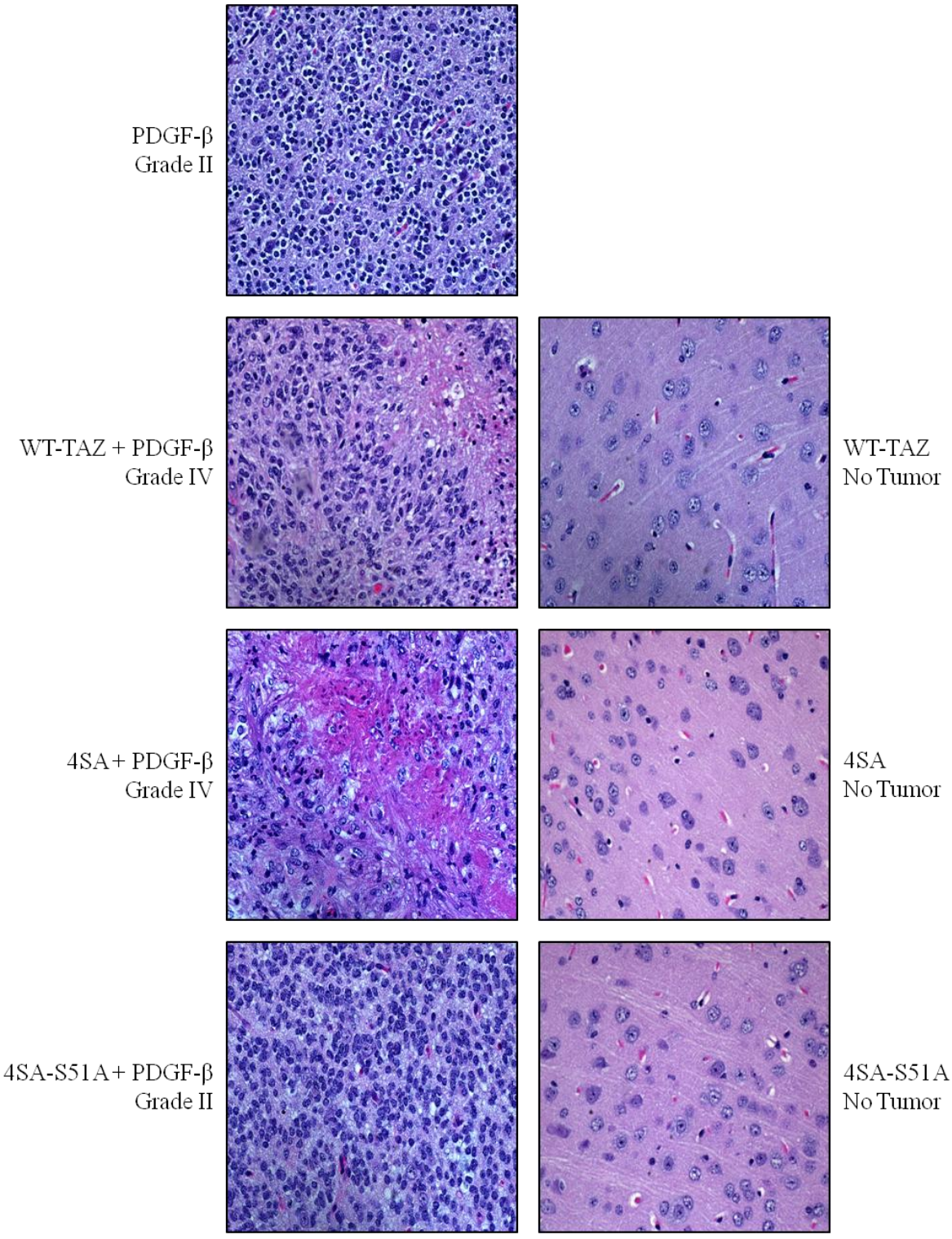

Figure 39: Representative pictures of hematoxylin and eosin stained RCAS/*N-tva* tumors. Representative tumors of each group (PDGF-β, WT-TAZ ± PDGF-β, 4SA ± PDGF-β, and 4SA-S51A ± PDGF-β) are pictured at 40x magnification. Reprinted with permission, Bhat, Salazar, Balasubramaniyan, et al., Genes Dev 25:2594-2609 [412], Copyright © 2011, Cold Spring Harbor Laboratory Press.

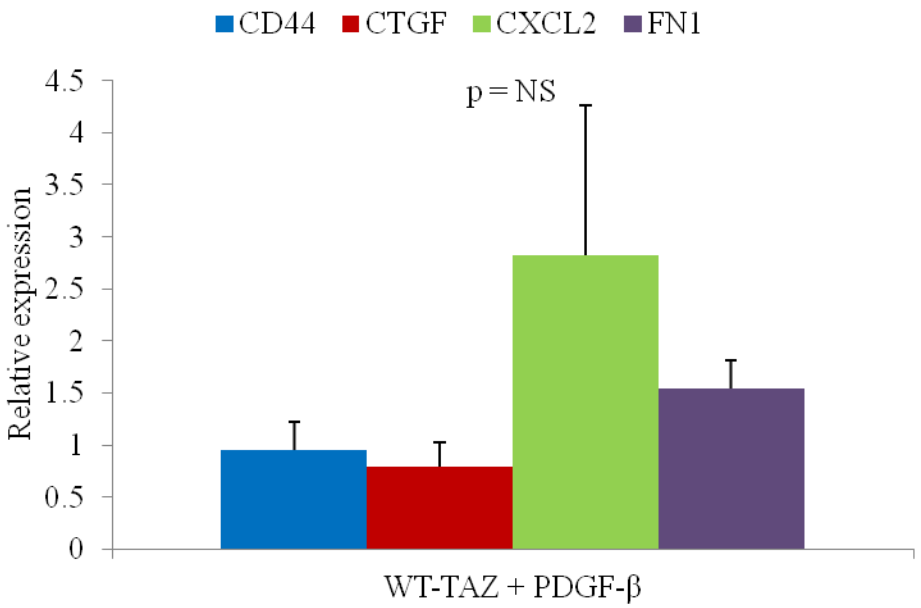

Figure 40: Real-time qPCR of PDGF-β and WT-TAZ + PDGF-β. Real-time qPCR of *CD44*, *CTGF*, *CXCL2*, and *FN1* expression tumors isolated from RCAS/*N-tva* mice injected with PDGF-β or WT-TAZ + PDGF-β. To compare transcript levels, the fold change compared to PDGF-β tumors is shown. NS = not significant.

CHAPTER 5: DISCUSSION

Summary

Our findings show the importance of TAZ in the mesenchymal shift seen in gliomas. We showed that TAZ is highly associated with the mesenchymal signature and is regulated by methylation in addition to phosphorylation and ubiquitination. I also showed that TAZ is important for the mesenchymal transition and aggressive behavior in GSCs. Next, I showed that the TAZ-TEAD interaction controls the mesenchymal transition and that the TAZ-TEAD complex directly binds to target gene promoters. Lastly, I showed that TAZ-TEAD increased grade and decreased survival in the RCAS/*N-tva* mouse model. Overall, I show that TAZ is another key modulator of the mesenchymal transition in gliomas.

Using a variety of different methods, we demonstrated that TAZ is associated with the mesenchymal gene signature seen in GBMs. We analyzed TCGA data and found that *WWTR1* expression was able to predict patient survival. We also looked at the functional activity of genes regulated by TAZ and found these genes to be involved in mesenchymal actions. Next, we examined the mesenchymal metagene score and found a positive correlation with *WWTR1* expression. We also able identified a novel regulatory mechanism of *WWTR1* via methylation of its promoter region in proneural tumors. This frequent promoter methylation in lower grade gliomas likely represents at least one mechanism that results in lower protein expression levels that is seen in clinical samples when compared to GBM. I found this same regulatory mechanism present in GSC lines deemed proneural. Analyzing hundreds of samples using microarray data, we also showed that *WWTR1* expression correlated strongly with GBM. I was also able to show this in clinical tumor samples. Lastly, I found that when TAZ expression was lowered, invasion, self-renewal, mesenchymal gene expression, and tumor potential decreased.

Taken together, these data support that TAZ is strongly connected to the mesenchymal gene signature and affects clinical behavior.

To further establish the role of TAZ in the mesenchymal gene signature, I over-expressed TAZ and found that this over-expression led to an increase in expression of mesenchymal markers. I also found that this increase was prevented when TAZ could not bind to TEAD, thus showing that it is not the over-expression of TAZ alone that is important to this mesenchymal shift, but that it is the interaction of TAZ with TEAD that causes this change to occur. I found an increase in invasion, self-renewal, mesenchymal stem cell differentiation, and tumor potential when TAZ was over-expressed, but all this was abrogated when TAZ could no longer bind to TEAD. Interestingly, I saw a concurrent decrease in proneural gene expression when TAZ was over-expressed, but again, this was prevented when TAZ could not bind to TEAD. Lastly, I observed that TAZ-TEAD directly bound to some mesenchymal gene targets to up-regulate their expression. Overall, I show that not only is TAZ associated with the mesenchymal signature, but that it is the interaction of TAZ with TEAD that causes this mesenchymal shift.

Others have also shown the importance of TAZ in cell proliferation, migration, invasion, self-renewal, and EMT in breast cancer [176,177,240]. Although we show that TAZ is important in invasion and self-renewal, we did not see an effect on proliferation. It is possible that in gliomas the main effect of TAZ is on the mesenchymal signature and not necessarily on cell growth like in breast. Gliomas and breast cancers are quite different, but it is possible that some signaling pathways are similar between the two, namely the TEAD interaction [177,345]. The TAZ-TEAD interaction likely leads to an increase in self-renewal, invasion, and EMT in both cancers, but the differences seen in the effect of TAZ on these

cancers may be due to different signaling mechanisms or possibly different downstream targets that are cancer specific. It is reassuring to see that TAZ-TEAD play an important role in other cancer models since it helps strengthen the importance of TAZ-TEAD on mesenchymal transition. However, it is likely that TAZ is involved with other pathways to induce the mesenchymal transformation in other cancers.

One group showed that in breast cancer TAZ was important in TGF-β signaling since TAZ controlled Smad localization, thus affecting TGF-β target gene induction [33]. Early on, an appealing idea was that TGF-β signaling was involved in the mesenchymal transition seen in gliomas. While I initially hypothesized the importance of the TGF-β pathway involvement in PMT (since it is associated with EMT [352,366]), interestingly, our results did not point to a role of this pathway in PMT. Due to the results I obtained, which are discussed in greater detail in the Appendix chapter, I chose to further characterize the role of TAZ and TEAD in PMT. It is possible that TGF-β may still play a role in the mesenchymal change, but further studies need to be done to establish this pathway in the mesenchymal shift seen in gliomas.

Another group showed that STAT3 and C/EBP-β also regulate the mesenchymal signature in gliomas [28], but we were able to show that this occurs independently of TAZ-TEAD. Although we asked similar questions, our study differed from theirs because we used a larger dataset of approximately 400 compared to their almost 200 profiles and we limited our analyses to only GBMs whereas they studied both grades III and IV. Their study may have emphasized the difference between grades III and IV whereas ours highlighted the differences within GBM. Overall, these findings show that more than one transcription factor can modulate the mesenchymal change with more regulators destined to be discovered.

We also showed that TAZ is regulated via methylation in lower grade gliomas. Normally in cancer, methylation is associated with the down-regulation of tumor suppressor genes important for cell cycle or growth regulation; therefore, methylation is thought to be central in the early tumor initiation phase of tumorigenesis [423,424,425]. We show that TAZ is normally methylated in normal brain and in lower grade gliomas, but when TAZ becomes demethylated in GBM, we see a higher expression of TAZ as well as an increase in invasion, but we see no effect on proliferation. Because of this, methylation of TAZ in GBM may be associated with later events in tumorigenesis. It is possible that in GBM, other mutations or gene alterations occur before the demethylation of TAZ. Other genes that show a similar methylation pattern in low grade gliomas and GBM are part of a glioma-CpG island methylator phenotype (G-CIMP) [426]. This hypermethylation is associated with low grade proneural gliomas in younger patients with an improved outcome. Some of the genes in the G-CIMP signature are mesenchymal in nature (e.g.—*CHI3L1*, *MMP9*, *LGALS3*, *PDPN*, etc.) and the silencing of these mesenchymal genes may be the reason for the better clinical outcome [412]. Although CIMP exists in numerous cancers, a few including colorectal [427], gastric [428], pancreatic adenocarcinoma [429], ovarian carcinoma [430], esophageal adenocarcinoma [431], HCC [432], and neuroblastoma [433], TAZ has not been shown to be methylated in these tumors. It is possible that TAZ is also methylated in these tumors, but it has not been studied yet in previous work. It would be interesting to see if TAZ is methylated in other cancers and if it affects early or late tumorigenesis. Both effects are possible and may be cancer specific.

This research gives us a working model of how gliomas become higher grade and more aggressive. TAZ-TEAD, in addition to STAT3 and C/EBP-β [28], can modulate this mesenchymal transition. In proneural tumors, TAZ is mediated via methylation of its promoter (**Fig. 41A**), but this is not the case in mesenchymal tumors. In mesenchymal gliomas, the

TAZ-TEAD complex directly binds to mesenchymal gene promoters, thus up-regulating gene expression (**Fig. 41B**). How the TAZ-TEAD complex can silence proneural genes is unknown, but one could hypothesize that the TAZ-TEAD complex either directly inhibits the proneural gene expression or the mesenchymal genes that are up-regulated somehow inhibit the expression of proneural genes (**Fig. 41B**). It is possible that TAZ binds to another unknown transcription factor to silence the proneural genes, but based on the 4SA and 4SA-S51A microarray data, the silencing likely occurs via the TAZ-TEAD interaction.

Future Directions, Clinical Implications, and Conclusions

A number of avenues could be pursued to follow up this work. The next step would be to identify potential drugs that target TAZ-TEAD function. This could be done by testing a drug panel using a *CTGF*-drive luciferase assay. The luciferase would be used as a read-out of TAZ activity and those drugs that decrease the luciferase level would indicate blocked TAZ activity. These drugs could then be tested *in vitro* using GSCs. Once the potential drugs have been narrowed down to the most promising, we could test them in animal models. Either multiple animal glioma models would need to be used or animal models of mechanism would be another option [434]. Multiple animal models would allow us to study if the drug is effective in more than one animal and hopefully ensures that the results we find are not animal specific. It is possible to use the same animal (i.e.—mouse), but have mice modeling different gliomas (proneural, mesenchymal, etc.). Another option would be to use animal models of mechanism, where the mechanism of TAZ is mimicked to induce tumors. This would allow us to study which drugs block the action of TAZ. Yet an additional model would be a humanized transgenic mouse that studies human drug metabolizing enzymes. This model would be ideal

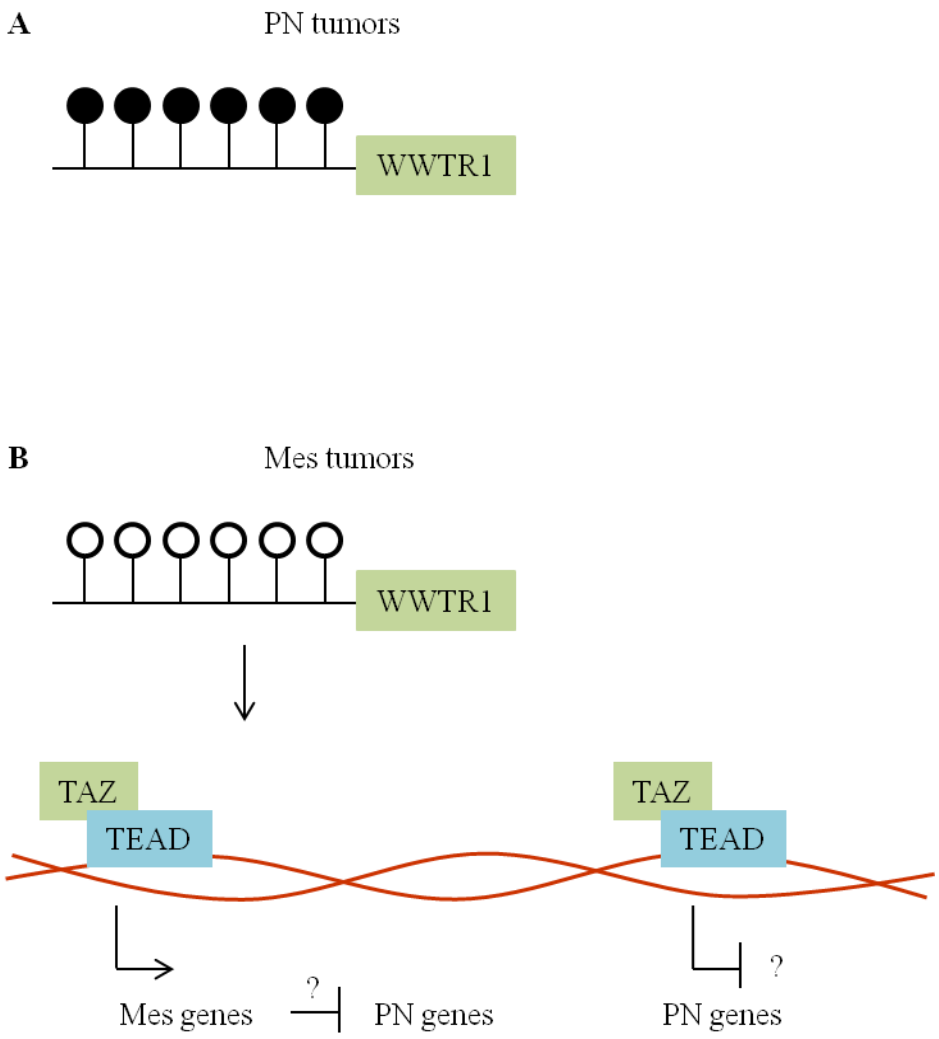

Figure 41: Proposed model of TAZ-TEAD regulating Mes and PN genes. (A) Gene regulation of *WWTR1* in PN tumors via promoter methylation, indicated by black circles. (B) Gene regulation of *WWTR1* in Mes tumors lacks promoter methylation, indicated by white circles. Gene activation of *WWTR1* eventually leads to binding with TEAD, thus activating Mes genes. PN gene down-regulation, indicated by a '?', is speculated at this point.

to test pharmacokinetics, drug clearance, and toxicity in humans [435]. The use of all these models would help find the best drug inhibitor to use in humans since it would test the drugs from multiple angles.

It would also be interesting to study if and/or how the regulation of TAZ via interaction with tight junction proteins (e.g.—AMOT, AMOTL1 [202], ZO-1, and ZO-2 [230]) or adherens junction proteins (e.g.—E-cadherin and α-catenin [62,192,193]) affects gliomagenesis. It is possible that this interaction with tight and/or adherens junction proteins, which results in cytoplasmic retention, is another regulatory mechanism of TAZ in gliomas. It would be interesting to find that a loss of these tight and/or adherens junction proteins results in high grade, mesenchymal gliomas due to the loss of cytoplasmic retention of TAZ. This regulation could also be exploited clinically as another way to regulate TAZ in gliomas.

Lastly, elucidating how TAZ down-regulates the proneural genes would also be interesting. Again, it likely occurs via TAZ-TEAD interaction, but if the down-regulation occurs due to TAZ-TEAD directly or due to mesenchymal genes remains to be determined. It seems that the proneural and mesenchymal phenotypes cannot co-exist, so if the tumor could switch to a proneural phenotype, the clinical outcome may be better. Preventing the down-regulation of proneural genes via TAZ/TAZ-TEAD may be yet another way this research could be used clinically. If we could doubly prevent the effect of TAZ on proneural genes (i.e.—down-regulation) and mesenchymal genes (i.e.—up-regulation) in the clinic, then patient survival may improve.

The glioma field is heading towards greater understanding of the molecular drivers of gliomagenesis and the mesenchymal signature. Many more modulators of the mesenchymal gene phenotype will be found in the future, including miRs along with other transcription

factors. Ideally, we would be able to translate this information in the clinic by developing treatments targeting these mesenchymal network regulators. Molecular profiling will be essential to personalized medicine by identifying patients who will do better clinically and identifying treatments to which they will respond. If personalized medicine advances greatly, it is possible that diagnostic gene marker panels will eventually identify cancer patients earlier than when they start to show symptoms.

Further investigation of the Hippo pathway is likely to lead to great advances in the next several years. This pathway will likely be connected to many more pathways besides BMP, TGF-β, and Wnt/β-catenin [32,34,35,108]. Understanding how these pathways are integrated is an important question. Additional proteins that dephosphorylate TAZ/YAP may also be identified as well as other downstream targets of TAZ/YAP. Like YAP, TAZ will likely be found to be important in numerous other cancers. Also, how the upstream regulators of MST1/2 regulate its activity and how these upstream regulators relate to one another will hopefully be elucidated in the near future. How cell polarity and cell adhesion proteins regulate the Hippo pathway are additional important questions that could be answered in the years to come. It is an exciting time for those studying the Hippo pathway since many aspects of this relatively new pathway have yet to be explored and fully understood.

Ideally, this research would be translated clinically and TAZ could be used as a biomarker, but much more research would need to be done in order for that to happen. To be the best biomarker, it must identify the disease throughout its development (i.e.—from early to late) and it would have to pass a Food and Drug Administration (FDA) process qualification [436]. Convincing biotechnology companies to develop this as a biomarker, it must show promise financially and be readily available for physicians in all settings from rural to urban

areas to use. The biomarker would show appeal to clinicians if it was cheap, fast, easy to use, accurate, and reimbursed by health insurance. To use as a screening tool, it would need high sensitivity and would have to be followed up with another test that has high specificity to rule out the false positives. To truly translate this research to the bedside, many obstacles exist and must be dealt with at each step.

If TAZ biomarker development is not possible, other tests could be established. Examples of potential studies include testing gene signatures or TAZ methylation status. The gene signature could be tested via microarray, but that would be difficult due to cost, variability between batch runs and the need for bioinformatics experts to decipher the data for clinicians. Microarrays would have to become cheaper to be used clinically. A biomarker panel could be developed to test for the overall gene signature, but that development faces the same problem as using TAZ as a biomarker. This kind of panel could be a cheaper option compared to microarray. Another option would be to test the methylation status of the TAZ promoter, but this would require DNA isolation followed by bisulfite conversion and PCR. These analyses have potential, but all would have to be streamlined to make it practical to use clinically.

Even if a biomarker test is developed, we must know what to do with this data once obtained and what it means for treatment. Without a drug inhibitor of TAZ, it will not help the patient by merely just knowing the TAZ levels of the tumor. Drug inhibitors would have to be identified and clinical trials would be needed before this data could be used clinically. A general start to this study would include testing a drug panel and using a CTGF driven luciferase assay to test the TAZ activity. Once potential drugs that silence TAZ activity are identified, we would need to test them both *in vitro* and *in vivo*. For the *in vivo* experiments,

we would need to find concentrations of the drugs that are both effective and could realistically be used on human subjects without numerous side effects.

This research is important because it provides a greater understanding of the molecular mechanism controlling mesenchymal transition. It shows that more than one transcription factor can regulate this transition and that the tumor cells have more than one pathway to transition to a mesenchymal signature. Realistically, it would be difficult to target all these modulators, but maybe it is possible to target more than one at a time. Another possibility is trying to both promote the proneural signature to mask or inhibit the mesenchymal signature as well as attempt to silence the mesenchymal phenotype. If we were to focus on TAZ alone, then it could be used as a drug target or methylation of its promoter could be tested. This research changed the field because it shows that TAZ is epigenetically regulated and that the mesenchymal shift is also due to TAZ-TEAD interaction. These data show that many transcription factors can regulate the mesenchymal transition in gliomas similar to the many transcription factors that affect EMT. In the end, TAZ-TEAD-related mechanisms represent an important part of the mesenchymal phenotype, but additional transcription factors and pathways are also likely to play an important role. The future has much potential to improve our understanding of the clinical aggressiveness of gliomas.

CHAPTER 6: APPENDIX

WT-YAP decreases survival and increases glioma grade in the RCAS/N-tva model.

In addition to TAZ and its role in gliomagenesis, I was also curious about the potential role of YAP in glioma formation. Although I chose to further characterize TAZ, I speculated that YAP may also play a role in gliomagenesis since they are comparable, but with some differences. I used the RCAS/*N-tva* mouse model to test the role of YAP in glioma formation and found that the over-expression of WT-YAP + PDGF-β also decreased overall survival compared to PDGF-β alone (**Fig. 42**). The mice injected with WT-YAP alone did not form tumors and survived more than 90 days (**Fig. 42**). Over-expression of WT-YAP + PDGF-β also led to an overall shift in grade, meaning the predominantly grade in PDGF-β alone was grade II (76%) while the predominate grade with the gene combinations was grade IV (69%; **Fig. 43A**). The grade IV tumors that formed in the WT-YAP + PDGF-β group showed the pathognomonic signs of GBM (i.e.—pseudopalisading necrosis and microvascular proliferation) while these features were lacking in the majority of the tumors in the PDGF-β alone group (**Fig. 43B**). Again, no tumors formed in the mice over-expressing WT-YAP alone (**Fig. 43B**).

The next step for this experiment is to develop mutants that are similar to 4SA and 4SA-S51A and test these mutants in the RCAS/*N-tva* mouse model as well. YAP is phosphorylated at S61, S109, S127, S164, and S381 [437]; mutations of these serine residues to alanine would create a mutant functionally similar to 4SA. Adding a mutation at S94 to an alanine would prevent TEAD binding [437], thus creating a mutant functionally similar to 4SA-S51A. It would be interesting to see similar results to those seen with TAZ; however, if results are different, then that would imply that YAP is involved in gliomagenesis, but through a mechanism not involving the interaction with TEAD.

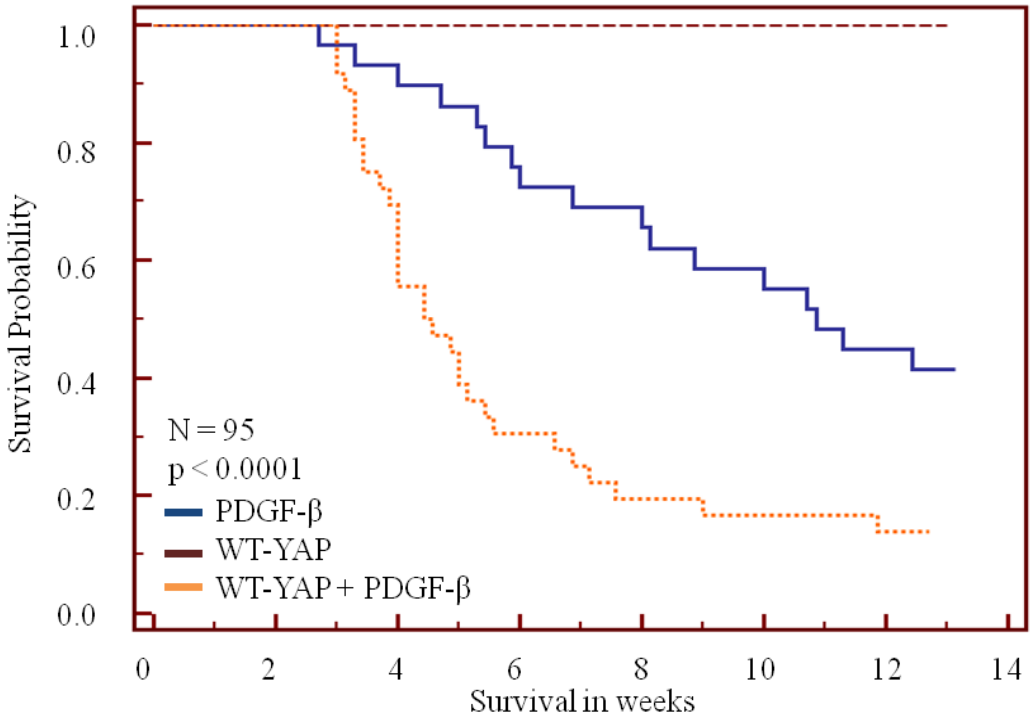

Figure 42: Kaplan-Meier of survival analyzing YAP in the RCAS/*N-tva* mouse model. Kaplan-Meier of survival probability of RCAS/*N-tva* mice injected with PDGF-β or WT-YAP ± PDGF-β.

A

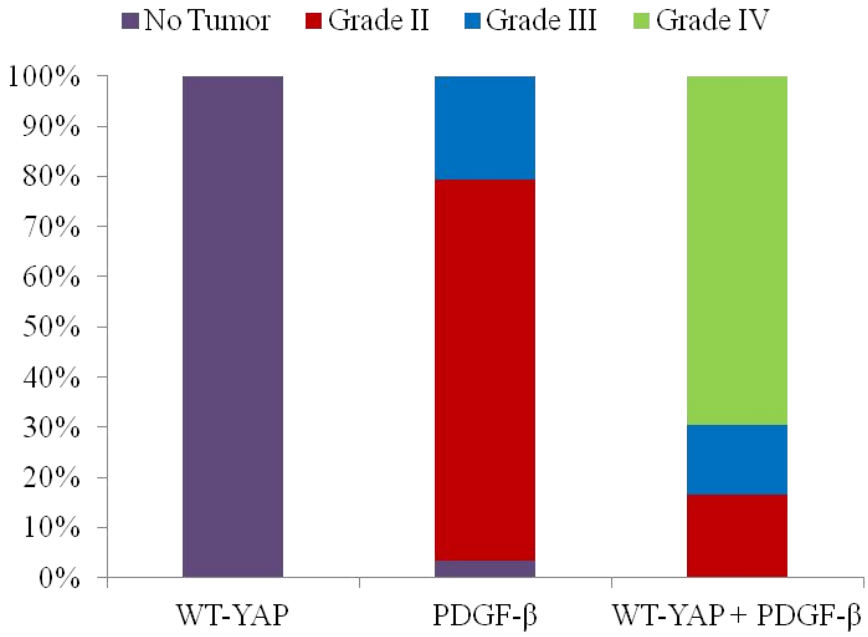

B

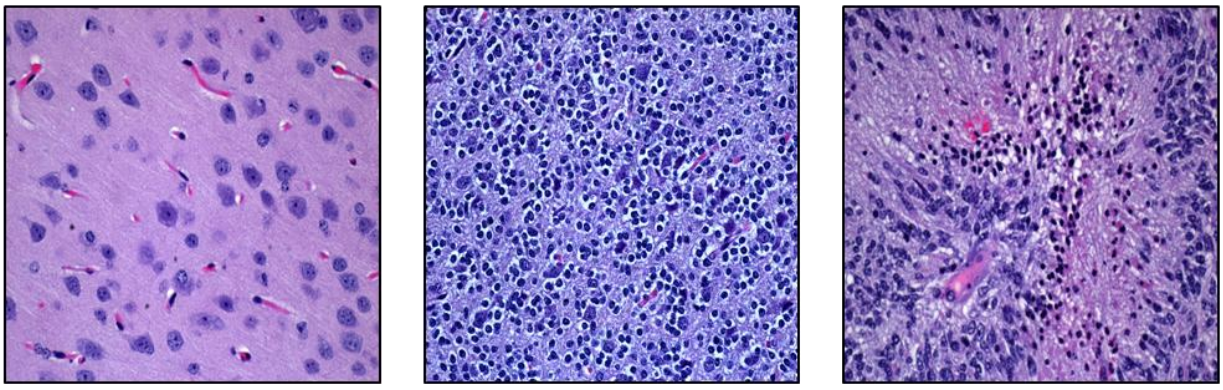

Figure 43: RCAS/*N-tva* mouse model studying WT-YAP. (A) Bar graph shows percentage of each grade (no tumor = purple; grade II = red; grade III = blue; grade IV = green) within each group (PDGF-β or WT-YAP ± PDGF-β). (B) Representative pictures of hematoxylin and eosin stained RCAS/*N-tva* tumors from each group (PDGF-β or WT-YAP ± PDGF-β) are pictured at 40x magnification.

TGF-β does not activate TAZ in GSCs.

In a paper written by Varelas, et. al., the group found that TAZ controlled Smad localization, thus affecting TGF-β induced genes [33]. When TAZ localized to the nucleus, the Smad complex was able to bind to TAZ and the promoter regions of TGF-β genes. When TAZ localized to the cytoplasm, the Smad complex was unable to induce TGF-β driven genes. The group also found that the TAZ-Smad interaction regulated human embryonic stem cell (ESC) self-renewal. Based on these findings, I hypothesized that something similar was occurring in GSCs. I first tested this hypothesis by IF of Smad2/3 in GSCs after TGF-β treatment (R&D Systems). In GSC 20 (high TAZ), Smad2/3 localized to the nucleus while this was not seen in GSC 23 (low TAZ; **Fig. 44**). This suggested that Smad2/3 localization depended on TAZ. I further tested this hypothesis by real-time qPCR of GSC 20 after transient knockdown of *WWTR1* and looked at two known downstream TGF-β targets, *SERPINE1* and *SMAD7* [438]. I found that there was no significant increase in expression of either gene after the addition of TGF-β to the siCtrl sample (**Fig. 45**). I also did not see a decrease in expression of either gene when *WWTR1* was transiently knocked down (**Fig. 45**). One would speculate that if these targets were TAZ dependent, then expression should decrease after transient *WWTR1* knockdown. Other real-time qPCR experiments showed inconsistent results when I tested the effect of TGF-β on GSCs (data not shown), thus I chose to study the TAZ-TEAD interaction instead. TGF-β may play a role in gliomagenesis via TAZ, but the genes I chose to study did not support this hypothesis. Of course if pursued in the future, TGF-β-TAZ dependent genes could be found to support the hypothesis.

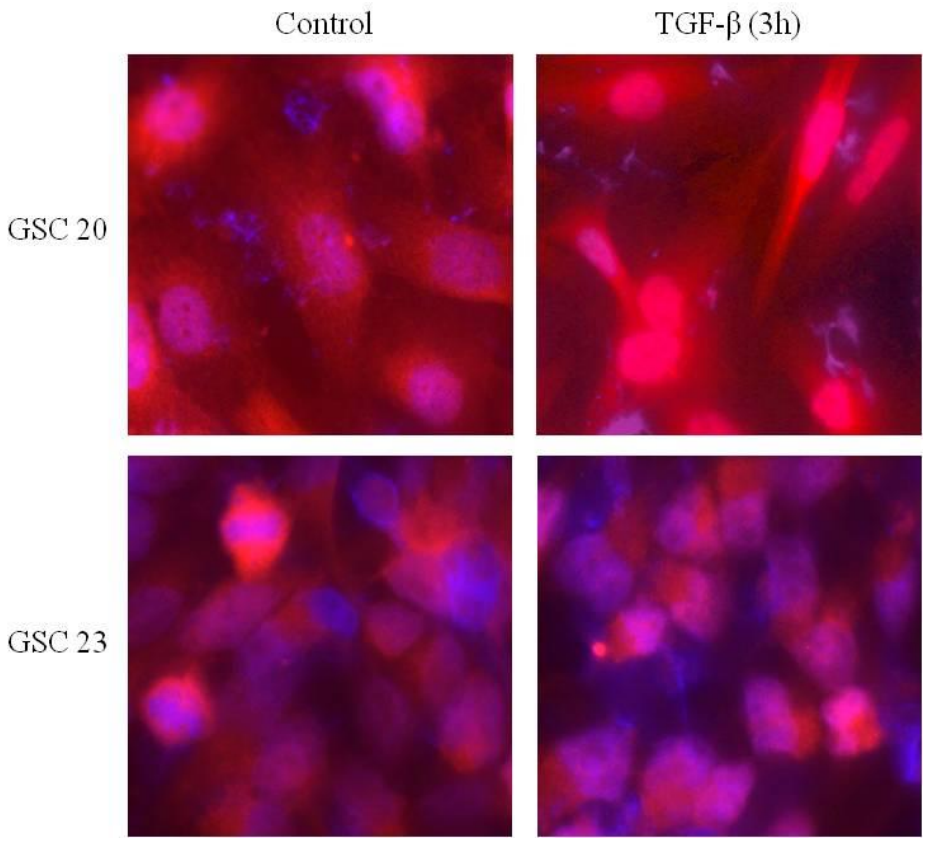

Figure 44: IF of Smad2/3 in GSCs after TGF-β treatment. IF of Smad2/3 localization after 100 pM TGF-β treatment for 3 hrs in GSC 20 (high TAZ) and GSC 23 (low TAZ).

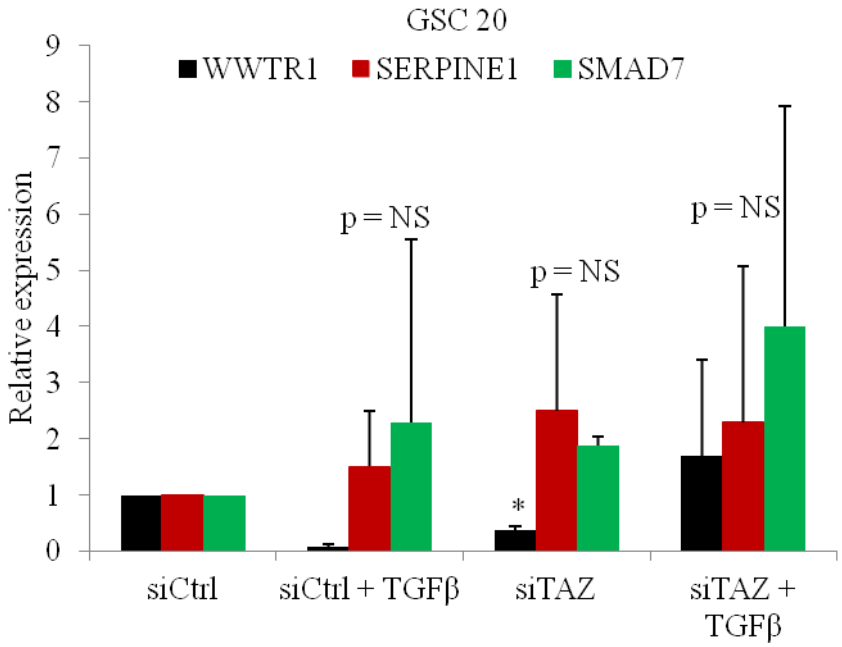

Figure 45: Real-time qPCR of transient *TAZ* knockdown with TGF-β treatment. Real-time qPCR of *WWTR1*, *SERPINE1*, and *SMAD7* expression in GSC 20 after transient knockdown of *WWTR1* followed by 100 pM TGF-β treatment for 3 hrs. To compare transcript levels, fold change before and after treatment was used. NS = not significant. '*' = p-value < 0.05.

In another angle, I also tested transcription factor 3 E2A immunoglobulin enhancer binding factors E12/E47 (TCF3) in GSCs after TGF-β treatment. TCF3 was found to be important for maintaining ESC self-renewal [439] and I found that TCF3 levels paralleled TAZ in GSCs (**Fig. 46A**). I hypothesized that TGF-β-TAZ-TCF3 played a role in regulating GSCs. To test this hypothesis, I used real-time qPCR to test *TCF3* expression after TGF-β treatment and after transient *WWTR1* knockdown followed by TGF-β treatment. I would expect *TCF3* levels to increase after TGF-β treatment and to be low after TGF-β treatment in transient *WWTR1* knockdown samples if *TCF3* expression was dependent on TAZ. I did not find a significant difference in *TCF3* expression after the addition of TGF-β or after the transient knockdown of *WWTR1* with the subsequent treatment with TGF-β (**Fig. 46B**). This suggests that TCF3 is independent of TAZ. Based these data, I chose not to further study TCF3 and its potential role in maintaining self-renewal in GSCs.

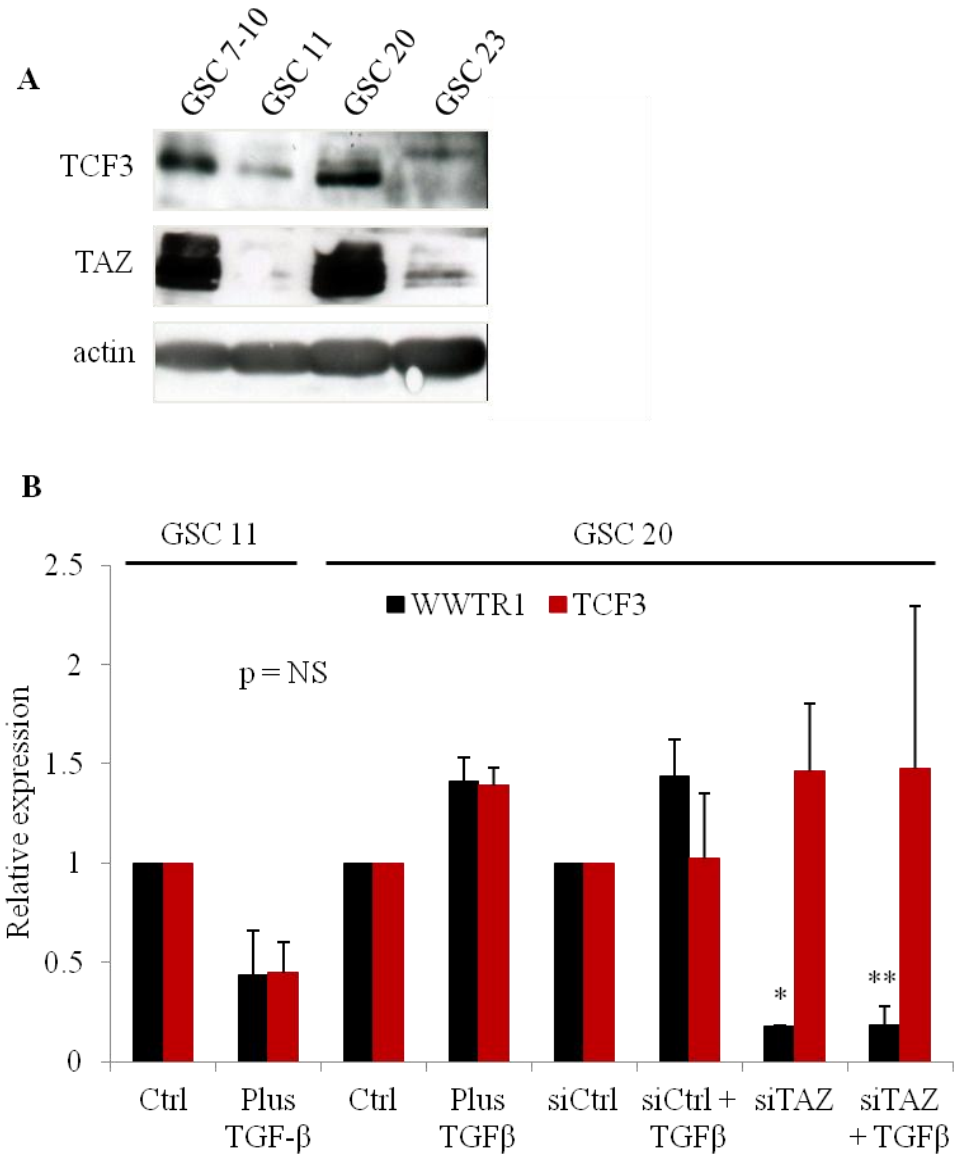

Figure 46: Western and real-time qPCR analyses studying TCF3 in GSCs. (A) Western analysis of TCF3 and TAZ in GSC 7-10, GSC 11, GSC 20, and GSC 23. (B) Real-time qPCR of *WWTR1* and *TCF3* in GSC 11 and GSC 20 after 100 pM TGF-β treatment for 3 hrs. *WWTR1* was transiently knocked down in GSC 20 and samples were subsequently treated with TGF-β. To compare transcript levels, fold change before and after treatment was used. All results are NS unless noted with an '*' or an '**'. NS = not significant. '*' = p-value < 0.05 and '**' = p-value < 0.005.

GSCs cultured with CTGF show an increase in growth.

It is well-established that CTGF is a downstream target of TAZ-TEAD [181,297,345]. Early on, I hypothesized that the mesenchymal transition seen in gliomas was due to TAZ-TEAD-CTGF. I wanted to test if CTGF was the primary reason that GSCs shifted to a mesenchymal phenotype, thus I tested the effect of adding CTGF (ThermoScientific) to cultures of GSCs with low basal expression of TAZ as a way to bypass TAZ-TEAD. I also wanted to test if CTGF could supplement EGF or FGF, growth factors that are important in culturing GSCs to maintain the original tumor phenotype [440]. I cultured GSC 11 and GSC 23 in neural basal media containing various combinations of EGF, FGF, and CTGF. Cells were split and counted prior to addition of the appropriate media. I found that adding CTGF increased the number of neurospheres in both GSC 11 and GSC 23 and could supplement EGF, but not FGF (**Fig. 47**). It is possible that the results were due to the addition of high, non-physiological levels of CTGF. The next step would be to add physiological levels of CTGF; however, based on other experiments mentioned earlier, I chose not to pursue this route and modified the hypothesis to its current form.

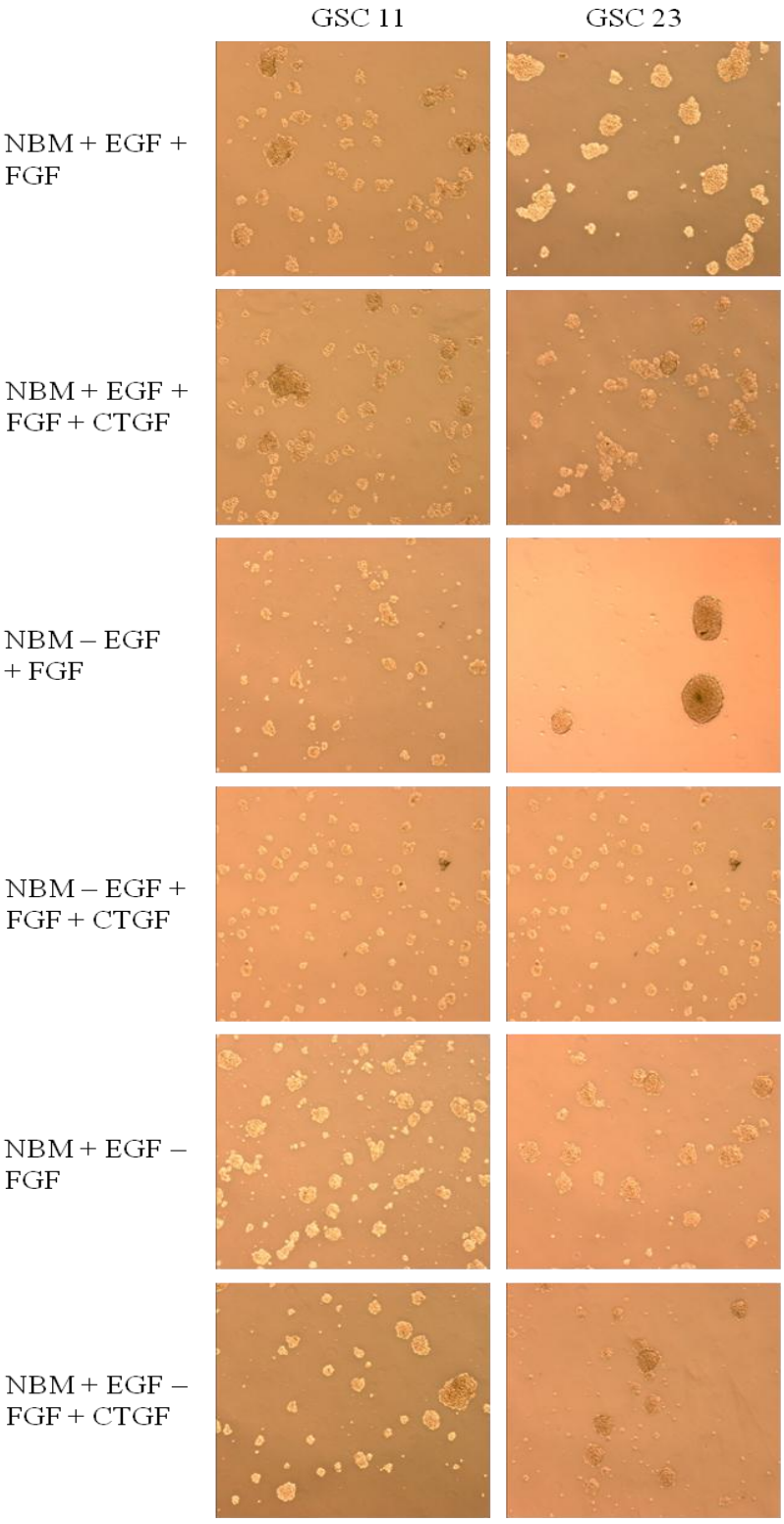

Figure 47: Effect on GSCs cultured with CTGF. GSC 11 and GSC 23 were cultured in neural basal media (NBM) with various combinations of EGF, FGF, and CTGF. EGF and FGF concentrations were based on [440] and CTGF was added at 25 μM. Cells were grown in this media for 14 days. Representative pictures were taken at 5x magnification.

TAZ-TEAD may recruit SATB1/2 to repress proneural genes.

As mentioned previously, TAZ-TEAD appears to down-regulate proneural genes. The mechanism of this repression is unknown; however, I hypothesized that special AT-rich sequence-binding protein 1 (SATB1) and SATB2 were potential mediators of proneural repression. SATB proteins are PDZ domain containing proteins that control nuclear gene expression by recruiting histone deacetylaces directly to the promoter of genes [441,442]. Since TAZ contains a C-terminal PDZ binding motif, I hypothesized that the TAZ-TEAD complex represses proneural genes by recruiting SATB1 and/or SATB2 to target promoters (**Fig. 48A**). To test this hypothesis, I first wanted to know the basal expression levels of SATB1 and SATB2 then I wanted to confirm the interaction of TAZ with SATB1 and/or SATB2 via IP-WB. I found no correlation between SATB1 or SATB2 expression and TAZ (**Fig. 48B**), but one would not necessarily expect different levels of SATB1 or SATB2, just different levels of TAZ-TEAD affecting proneural gene expression via recruitment of SATB1 and/or SATB2. Next I performed IP-WB to test the interaction of TAZ with SATB1 in GSC 20 and GSC 11-4SA. I found that TAZ and SATB1 may interact, but different antibodies need to be used for the experiment in the future since the IP-WB was not very clean (**Fig. 48C**). This hypothesis has potential to be pursued at a later time in order to discover the mechanism repressing proneural gene expression in GSCs.

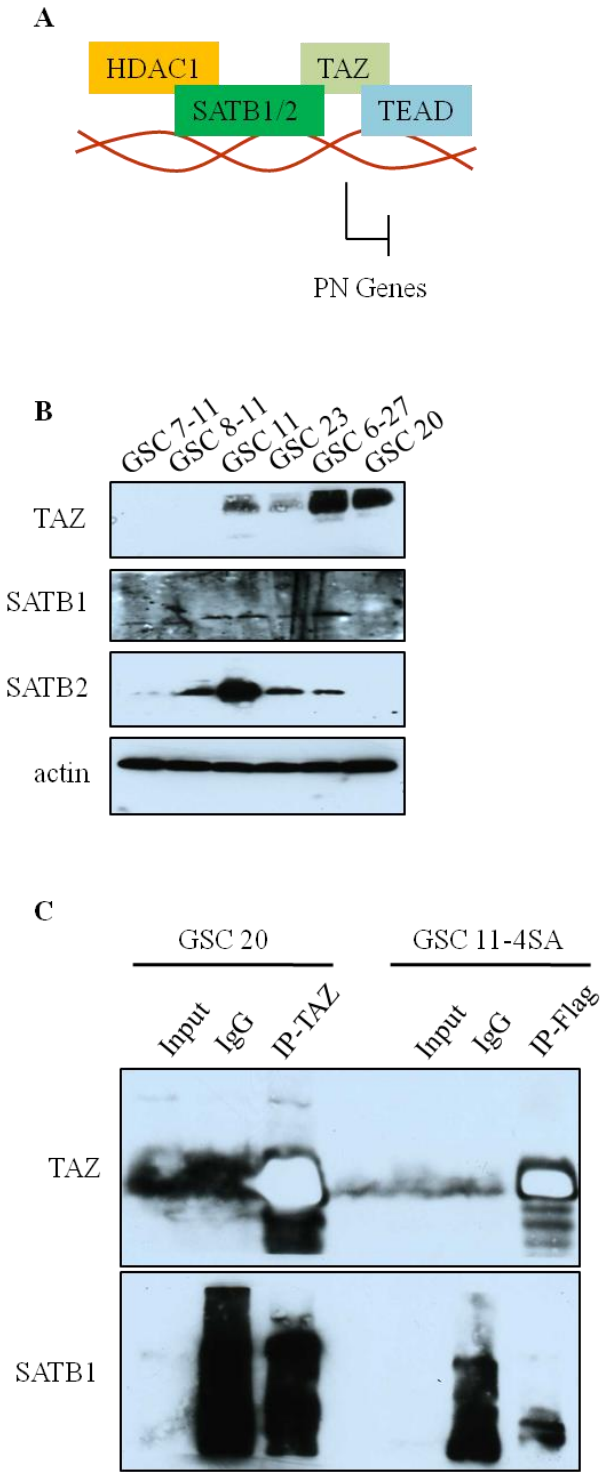

Figure 48: Western and IP-WB analyses of SATB1 and SATB2 in GSCs. (A) Proposed model of PN gene down-regulation via TAZ-TEAD. Blunt head indicates inhibition. (B) Western analysis of TAZ, SATB1 and SATB2 in GSC 7-11, GSC 8-11, GSC 11, GSC 23, GSC 6-27, and GSC 20. (C) IP-WB analysis of GSC 20 and GSC 11-4SA. IP-TAZ or IP-Flag was done and western analysis of TAZ and SATB1 was performed.

BIBLIOGRAPHY

[1] D.N. Louis, H. Ohgaki, O.D. Wiestler, W.K. Cavenee, P.C. Burger, A. Jouvet, B.W. Scheithauer, P. Kleihues, The 2007 WHO classification of tumours of the central nervous system, Acta Neuropathol 114 (2007) 97-109.

[2] Comprehensive genomic characterization defines human glioblastoma genes and core pathways, Nature 455 (2008) 1061-1068.

[3] F.B. Furnari, T. Fenton, R.M. Bachoo, A. Mukasa, J.M. Stommel, A. Stegh, W.C. Hahn, K.L. Ligon, D.N. Louis, C. Brennan, L. Chin, R.A. DePinho, W.K. Cavenee, Malignant astrocytic glioma: genetics, biology, and paths to treatment, Genes Dev 21 (2007) 2683-2710.

[4] C.L. Gladson, R.A. Prayson, W.M. Liu, The pathobiology of glioma tumors, Annu Rev Pathol 5 (2010) 33-50.

[5] J.T. Huse, E.C. Holland, Targeting brain cancer: advances in the molecular pathology of malignant glioma and medulloblastoma, Nat Rev Cancer 10 (2010) 319-331.

[6] L.M. Chow, R. Endersby, X. Zhu, S. Rankin, C. Qu, J. Zhang, A. Broniscer, D.W. Ellison, S.J. Baker, Cooperativity within and among Pten, p53, and Rb pathways induces high-grade astrocytoma in adult brain, Cancer Cell 19 (2011) 305-316.

[7] B.H. Ozer, G.J. Wiepz, P.J. Bertics, Activity and cellular localization of an oncogenic glioblastoma multiforme-associated EGF receptor mutant possessing a duplicated kinase domain, Oncogene 29 (2010) 855-864.

[8] J. Cho, S. Pastorino, Q. Zeng, X. Xu, W. Johnson, S. Vandenberg, R. Verhaak, A.D. Cherniack, H. Watanabe, A. Dutt, J. Kwon, Y.S. Chao, R.C. Onofrio, D. Chiang, Y. Yuza, S. Kesari, M. Meyerson, Glioblastoma-Derived Epidermal Growth Factor Receptor Carboxyl-Terminal Deletion Mutants Are Transforming and Are Sensitive to EGFR-Directed Therapies, Cancer Res 71 (2011) 7587-7596.

[9] T. Yue, A. Tian, J. Jiang, The Cell Adhesion Molecule Echinoid Functions as a Tumor Suppressor and Upstream Regulator of the Hippo Signaling Pathway, Dev Cell (2012).

[10] H. Yan, D.D. Bigner, V. Velculescu, D.W. Parsons, Mutant metabolic enzymes are at the origin of gliomas, Cancer Res 69 (2009) 9157-9159.

[11] D. Yin, W. Chen, J. O'Kelly, D. Lu, M. Ham, N.B. Doan, D. Xie, C. Wang, J. Vadgama, J.W. Said, K.L. Black, H.P. Koeffler, Connective tissue growth factor associated with oncogenic activities and drug resistance in glioblastoma multiforme, Int J Cancer 127 (2010) 2257-2267.

[12] J.H. Tchaicha, S.B. Reyes, J. Shin, M.G. Hossain, F.F. Lang, J.H. McCarty, Glioblastoma angiogenesis and tumor cell invasiveness are differentially regulated by beta8 integrin, Cancer Res 71 (2011) 6371-6381.

[13] B.M. Costa, J.S. Smith, Y. Chen, J. Chen, H.S. Phillips, K.D. Aldape, G. Zardo, J. Nigro, C.D. James, J. Fridlyand, R.M. Reis, J.F. Costello, Reversing HOXA9 oncogene activation by PI3K inhibition: epigenetic mechanism and prognostic significance in human glioblastoma, Cancer Res 70 (2010) 453-462.

[14] N. Zhang, P. Wei, A. Gong, W.T. Chiu, H.T. Lee, H. Colman, H. Huang, J. Xue, M. Liu, Y. Wang, R. Sawaya, K. Xie, W.K. Yung, R.H. Medema, X. He, S. Huang, FoxM1 promotes beta-catenin nuclear localization and controls Wnt target-gene expression and glioma tumorigenesis, Cancer Cell 20 (2011) 427-442.

[15] Y. Wang, J. Yang, H. Zheng, G.J. Tomasek, P. Zhang, P.E. McKeever, E.Y. Lee, Y. Zhu, Expression of mutant p53 proteins implicates a lineage relationship between neural stem cells and malignant astrocytic glioma in a murine model, Cancer Cell 15 (2009) 514-526.

[16] T.S. Jacques, A. Swales, M.J. Brzozowski, N.V. Henriquez, J.M. Linehan, Z. Mirzadeh, O.M. C, H. Naumann, A. Alvarez-Buylla, S. Brandner, Combinations of genetic mutations in the adult neural stem cell compartment determine brain tumour phenotypes, EMBO J 29 (2010) 222-235.

[17] N. Sanai, A. Alvarez-Buylla, M.S. Berger, Neural stem cells and the origin of gliomas, N Engl J Med 353 (2005) 811-822.

[18] C. Liu, J.C. Sage, M.R. Miller, R.G. Verhaak, S. Hippenmeyer, H. Vogel, O. Foreman, R.T. Bronson, A. Nishiyama, L. Luo, H. Zong, Mosaic analysis with double markers reveals tumor cell of origin in glioma, Cell 146 (2011) 209-221.

[19] M.E. Hegi, A.C. Diserens, T. Gorlia, M.F. Hamou, N. de Tribolet, M. Weller, J.M. Kros, J.A. Hainfellner, W. Mason, L. Mariani, J.E. Bromberg, P. Hau, R.O. Mirimanoff, J.G. Cairncross, R.C. Janzer, R. Stupp, MGMT gene silencing and benefit from temozolomide in glioblastoma, N Engl J Med 352 (2005) 997-1003.

[20] J.F. de Groot, M.R. Gilbert, K. Aldape, K.R. Hess, T.A. Hanna, S. Ictech, M.D. Groves, C. Conrad, H. Colman, V.K. Puduvalli, V. Levin, W.K. Yung, Phase II study of carboplatin and erlotinib (Tarceva, OSI-774) in patients with recurrent glioblastoma, J Neurooncol 90 (2008) 89-97.

[21] M. Squatrito, E.C. Holland, DNA damage response and growth factor signaling pathways in gliomagenesis and therapeutic resistance, Cancer Res 71 (2011) 5945-5949.

[22] E.C. Burton, K.R. Lamborn, B.G. Feuerstein, M. Prados, J. Scott, P. Forsyth, S. Passe, R.B. Jenkins, K.D. Aldape, Genetic aberrations defined by comparative genomic hybridization distinguish long-term from typical survivors of glioblastoma, Cancer Res 62 (2002) 6205-6210.

[23] W.A. Freije, F.E. Castro-Vargas, Z. Fang, S. Horvath, T. Cloughesy, L.M. Liau, P.S. Mischel, S.F. Nelson, Gene expression profiling of gliomas strongly predicts survival, Cancer Res 64 (2004) 6503-6510.

[24] H.S. Phillips, S. Kharbanda, R. Chen, W.F. Forrest, R.H. Soriano, T.D. Wu, A. Misra, J.M. Nigro, H. Colman, L. Soroceanu, P.M. Williams, Z. Modrusan, B.G. Feuerstein, K. Aldape, Molecular subclasses of high-grade glioma predict prognosis, delineate a pattern of disease progression, and resemble stages in neurogenesis, Cancer Cell 9 (2006) 157-173.

[25] R.G. Verhaak, K.A. Hoadley, E. Purdom, V. Wang, Y. Qi, M.D. Wilkerson, C.R. Miller, L. Ding, T. Golub, J.P. Mesirov, G. Alexe, M. Lawrence, M. O'Kelly, P. Tamayo, B.A. Weir, S. Gabriel, W. Winckler, S. Gupta, L. Jakkula, H.S. Feiler, J.G. Hodgson, C.D. James, J.N. Sarkaria, C. Brennan, A. Kahn, P.T. Spellman, R.K. Wilson, T.P. Speed, J.W. Gray, M. Meyerson, G. Getz, C.M. Perou, D.N. Hayes, Integrated genomic analysis identifies clinically relevant subtypes of glioblastoma characterized by abnormalities in PDGFRA, IDH1, EGFR, and NF1, Cancer Cell 17 (2010) 98-110.

[26] H. Colman, L. Zhang, E.P. Sulman, J.M. McDonald, N.L. Shooshtari, A. Rivera, S. Popoff, C.L. Nutt, D.N. Louis, J.G. Cairncross, M.R. Gilbert, H.S. Phillips, M.P. Mehta, A. Chakravarti, C.E. Pelloski, K. Bhat, B.G. Feuerstein, R.B. Jenkins, K. Aldape, A multigene predictor of outcome in glioblastoma, Neuro Oncol 12 (2010) 49-57.

[27] J.M. Nigro, A. Misra, L. Zhang, I. Smirnov, H. Colman, C. Griffin, N. Ozburn, M. Chen, E. Pan, D. Koul, W.K. Yung, B.G. Feuerstein, K.D. Aldape, Integrated array-comparative genomic hybridization and expression array profiles identify clinically relevant molecular subtypes of glioblastoma, Cancer Res 65 (2005) 1678-1686.

[28] M.S. Carro, W.K. Lim, M.J. Alvarez, R.J. Bollo, X. Zhao, E.Y. Snyder, E.P. Sulman, S.L. Anne, F. Doetsch, H. Colman, A. Lasorella, K. Aldape, A. Califano, A. Iavarone, The transcriptional network for mesenchymal transformation of brain tumours, Nature 463 (2010) 318-325.

[29] R.S. Udan, M. Kango-Singh, R. Nolo, C. Tao, G. Halder, Hippo promotes proliferation arrest and apoptosis in the Salvador/Warts pathway, Nat Cell Biol 5 (2003) 914-920.

[30] Y. Bao, Y. Hata, M. Ikeda, K. Withanage, Mammalian Hippo pathway: from development to cancer and beyond, J Biochem 149 (2011) 361-379.

[31] A. Sebé-Pedrós, Y. Zheng, I. Ruiz-Trillo, D. Pan, Premetazoan Origin of the Hippo Signaling Pathway, (2011).

[32] D. Hong, H.X. Chen, Y. Xue, D.M. Li, X.C. Wan, R. Ge, J.C. Li, Osteoblastogenic effects of dexamethasone through upregulation of TAZ expression in rat mesenchymal stem cells, J Steroid Biochem Mol Biol 116 (2009) 86-92.

[33] X. Varelas, R. Sakuma, P. Samavarchi-Tehrani, R. Peerani, B.M. Rao, J. Dembowy, M.B. Yaffe, P.W. Zandstra, J.L. Wrana, TAZ controls Smad nucleocytoplasmic shuttling and regulates human embryonic stem-cell self-renewal, Nat Cell Biol 10 (2008) 837-848.

[34] X. Varelas, B.W. Miller, R. Sopko, S. Song, A. Gregorieff, F.A. Fellouse, R. Sakuma, T. Pawson, W. Hunziker, H. McNeill, J.L. Wrana, L. Attisano, The Hippo pathway regulates Wnt/beta-catenin signaling, Dev Cell 18 (2010) 579-591.

[35] M. Imajo, K. Miyatake, A. Iimura, A. Miyamoto, E. Nishida, A molecular mechanism that links Hippo signalling to the inhibition of Wnt/beta-catenin signalling, EMBO J (2012).

[36] G. Hamilton, K.S. Yee, S. Scrace, E. O'Neill, ATM regulates a RASSF1A-dependent DNA damage response, Curr Biol 19 (2009) 2020-2025.

[37] N.A. Grzeschik, L.M. Parsons, M.L. Allott, K.F. Harvey, H.E. Richardson, Lgl, aPKC, and Crumbs regulate the Salvador/Warts/Hippo pathway through two distinct mechanisms, Curr Biol 20 (2010) 573-581.

[38] E. O'Neill, W. Kolch, Taming the Hippo: Raf-1 controls apoptosis by suppressing MST2/Hippo, Cell Cycle 4 (2005) 365-367.

[39] C. Polesello, S. Huelsmann, N.H. Brown, N. Tapon, The Drosophila RASSF homolog antagonizes the hippo pathway, Curr Biol 16 (2006) 2459-2465.

[40] C. Guo, S. Tommasi, L. Liu, J.K. Yee, R. Dammann, G.P. Pfeifer, RASSF1A is part of a complex similar to the Drosophila Hippo/Salvador/Lats tumor-suppressor network, Curr Biol 17 (2007) 700-705.

[41] E. Hwang, K.S. Ryu, K. Paakkonen, P. Guntert, H.K. Cheong, D.S. Lim, J.O. Lee, Y.H. Jeon, C. Cheong, Structural insight into dimeric interaction of the SARAH domains from Mst1 and RASSF family proteins in the apoptosis pathway, Proc Natl Acad Sci U S A 104 (2007) 9236-9241.

[42] D. Matallanas, D. Romano, K. Yee, K. Meissl, L. Kucerova, D. Piazzolla, M. Baccarini, J.K. Vass, W. Kolch, E. O'Neill, RASSF1A elicits apoptosis through an MST2 pathway directing proapoptotic transcription by the p73 tumor suppressor protein, Mol Cell 27 (2007) 962-975.

[43] M. Ikeda, A. Kawata, M. Nishikawa, Y. Tateishi, M. Yamaguchi, K. Nakagawa, S. Hirabayashi, Y. Bao, S. Hidaka, Y. Hirata, Y. Hata, Hippo pathway-dependent and -independent roles of RASSF6, Sci Signal 2 (2009) ra59.

[44] F. Hamaratoglu, M. Willecke, M. Kango-Singh, R. Nolo, E. Hyun, C. Tao, H. Jafar-Nejad, G. Halder, The tumour-suppressor genes NF2/Merlin and Expanded act through Hippo signalling to regulate cell proliferation and apoptosis, Nat Cell Biol 8 (2006) 27-36.

[45] Y. Feng, K.D. Irvine, Fat and expanded act in parallel to regulate growth through warts, Proc Natl Acad Sci U S A 104 (2007) 20362-20367.

[46] S. Sun, S. Zhao, Z. Wang, Genes of Hippo signaling network act unconventionally in the control of germline proliferation in Drosophila, Dev Dyn 237 (2008) 270-275.

[47] J. Menendez, A. Perez-Garijo, M. Calleja, G. Morata, A tumor-suppressing mechanism in Drosophila involving cell competition and the Hippo pathway, Proc Natl Acad Sci U S A 107 (2010) 14651-14656.

[48] B.S. Robinson, J. Huang, Y. Hong, K.H. Moberg, Crumbs regulates Salvador/Warts/Hippo signaling in Drosophila via the FERM-domain protein Expanded, Curr Biol 20 (2010) 582-590.

[49] C. Ling, Y. Zheng, F. Yin, J. Yu, J. Huang, Y. Hong, S. Wu, D. Pan, The apical transmembrane protein Crumbs functions as a tumor suppressor that regulates Hippo signaling by binding to Expanded, Proc Natl Acad Sci U S A 107 (2010) 10532-10537.

[50] E. Cho, Y. Feng, C. Rauskolb, S. Maitra, R. Fehon, K.D. Irvine, Delineation of a Fat tumor suppressor pathway, Nat Genet 38 (2006) 1142-1150.

[51] M. Willecke, F. Hamaratoglu, M. Kango-Singh, R. Udan, C.L. Chen, C. Tao, X. Zhang, G. Halder, The fat cadherin acts through the hippo tumor-suppressor pathway to regulate tissue size, Curr Biol 16 (2006) 2090-2100.

[52] E. Silva, Y. Tsatskis, L. Gardano, N. Tapon, H. McNeill, The tumor-suppressor gene fat controls tissue growth upstream of expanded in the hippo signaling pathway, Curr Biol 16 (2006) 2081-2089.

[53] F.C. Bennett, K.F. Harvey, Fat cadherin modulates organ size in Drosophila via the Salvador/Warts/Hippo signaling pathway, Curr Biol 16 (2006) 2101-2110.

[54] D.M. Tyler, N.E. Baker, Expanded and fat regulate growth and differentiation in the Drosophila eye through multiple signaling pathways, Dev Biol 305 (2007) 187-201.

[55] M. Willecke, F. Hamaratoglu, L. Sansores-Garcia, C. Tao, G. Halder, Boundaries of Dachsous Cadherin activity modulate the Hippo signaling pathway to induce cell proliferation, Proc Natl Acad Sci U S A 105 (2008) 14897-14902.

[56] A.L. Brittle, A. Repiso, J. Casal, P.A. Lawrence, D. Strutt, Four-jointed modulates growth and planar polarity by reducing the affinity of dachsous for fat, Curr Biol 20 (2010) 803-810.

[57] J. Yu, Y. Zheng, J. Dong, S. Klusza, W.M. Deng, D. Pan, Kibra functions as a tumor suppressor protein that regulates Hippo signaling in conjunction with Merlin and Expanded, Dev Cell 18 (2010) 288-299.

[58] A. Genevet, M.C. Wehr, R. Brain, B.J. Thompson, N. Tapon, Kibra is a regulator of the Salvador/Warts/Hippo signaling network, Dev Cell 18 (2010) 300-308.

[59] R. Baumgartner, I. Poernbacher, N. Buser, E. Hafen, H. Stocker, The WW domain protein Kibra acts upstream of Hippo in Drosophila, Dev Cell 18 (2010) 309-316.

[60] L. Xiao, Y. Chen, M. Ji, J. Dong, KIBRA regulates Hippo signaling activity via interactions with large tumor suppressor kinases, J Biol Chem 286 (2011) 7788-7796.

[61] I. Poernbacher, R. Baumgartner, S.K. Marada, K. Edwards, H. Stocker, Drosophila Pez Acts in Hippo Signaling to Restrict Intestinal Stem Cell Proliferation, Curr Biol (2012).

[62] N.G. Kim, E. Koh, X. Chen, B.M. Gumbiner, E-cadherin mediates contact inhibition of proliferation through Hippo signaling-pathway components, Proc Natl Acad Sci U S A 108 (2011) 11930-11935.

[63] M. Das Thakur, Y. Feng, R. Jagannathan, M.J. Seppa, J.B. Skeath, G.D. Longmore, Ajuba LIM proteins are negative regulators of the Hippo signaling pathway, Curr Biol 20 (2010) 657-662.

[64] P.S. Ribeiro, F. Josue, A. Wepf, M.C. Wehr, O. Rinner, G. Kelly, N. Tapon, M. Gstaiger, Combined functional genomic and proteomic approaches identify a PP2A complex as a negative regulator of Hippo signaling, Mol Cell 39 (2010) 521-534.

[65] B.S. Robinson, K.H. Moberg, Drosophila endocytic neoplastic tumor suppressor genes regulate Sav/Wts/Hpo signaling and the c-Jun N-terminal kinase pathway, Cell Cycle 10 (2011) 4110-4118.

[66] B. Zhao, L. Li, L. Wang, C.Y. Wang, J. Yu, K.L. Guan, Cell detachment activates the Hippo pathway via cytoskeleton reorganization to induce anoikis, Genes Dev 26 (2012) 54-68.

[67] F. Hamaratoglu, K. Gajewski, L. Sansores-Garcia, C. Morrison, C. Tao, G. Halder, The Hippo tumor-suppressor pathway regulates apical-domain size in parallel to tissue growth, J Cell Sci 122 (2009) 2351-2359.

[68] A. Genevet, C. Polesello, K. Blight, F. Robertson, L.M. Collinson, F. Pichaud, N. Tapon, The Hippo pathway regulates apical-domain size independently of its growth-control function, J Cell Sci 122 (2009) 2360-2370.

[69] C.L. Chen, K.M. Gajewski, F. Hamaratoglu, W. Bossuyt, L. Sansores-Garcia, C. Tao, G. Halder, The apical-basal cell polarity determinant Crumbs regulates Hippo signaling in Drosophila, Proc Natl Acad Sci U S A 107 (2010) 15810-15815.

[70] K. Emoto, J.Z. Parrish, L.Y. Jan, Y.N. Jan, The tumour suppressor Hippo acts with the NDR kinases in dendritic tiling and maintenance, Nature 443 (2006) 210-213.

[71] C. Meignin, I. Alvarez-Garcia, I. Davis, I.M. Palacios, The salvador-warts-hippo pathway is required for epithelial proliferation and axis specification in Drosophila, Curr Biol 17 (2007) 1871-1878.

[72] C. Polesello, N. Tapon, Salvador-warts-hippo signaling promotes Drosophila posterior follicle cell maturation downstream of notch, Curr Biol 17 (2007) 1864-1870.

[73] J. Yu, J. Poulton, Y.C. Huang, W.M. Deng, The hippo pathway promotes Notch signaling in regulation of cell differentiation, proliferation, and oocyte polarity, PLoS One 3 (2008) e1761.

[74] B.V. Reddy, C. Rauskolb, K.D. Irvine, Influence of fat-hippo and notch signaling on the proliferation and differentiation of Drosophila optic neuroepithelia, Development 137 (2010) 2397-2408.

[75] H.J. Chen, C.M. Wang, T.W. Wang, G.J. Liaw, T.H. Hsu, T.H. Lin, J.Y. Yu, The Hippo pathway controls polar cell fate through Notch signaling during Drosophila oogenesis, Dev Biol 357 (2011) 370-379.

[76] Y. Li, M.A. Hibbs, A.L. Gard, N.A. Shylo, K. Yun, Genome-Wide Analysis of N1ICD/RBPJ Targets in vivo Reveals Direct Transcriptional Regulation of Wnt, SHH, and Hippo Pathway Effectors by Notch1, Stem Cells (2012).

[77] Z. Yuan, D. Kim, S. Shu, J. Wu, J. Guo, L. Xiao, S. Kaneko, D. Coppola, J.Q. Cheng, Phosphoinositide 3-kinase/Akt inhibits MST1-mediated pro-apoptotic signaling through phosphorylation of threonine 120, J Biol Chem 285 (2010) 3815-3824.

[78] D. Kim, S. Shu, M.D. Coppola, S. Kaneko, Z.Q. Yuan, J.Q. Cheng, Regulation of proapoptotic mammalian ste20-like kinase MST2 by the IGF1-Akt pathway, PLoS One 5 (2010) e9616.

[79] K. Tschop, A.R. Conery, L. Litovchick, J.A. Decaprio, J. Settleman, E. Harlow, N. Dyson, A kinase shRNA screen links LATS2 and the pRB tumor suppressor, Genes Dev 25 (2011) 814-830.

[80] B.N. Nicolay, B. Bayarmagnai, N.S. Moon, E.V. Benevolenskaya, M.V. Frolov, Combined inactivation of pRB and hippo pathways induces dedifferentiation in the Drosophila retina, PLoS Genet 6 (2010) e1000918.

[81] J. Dong, G. Feldmann, J. Huang, S. Wu, N. Zhang, S.A. Comerford, M.F. Gayyed, R.A. Anders, A. Maitra, D. Pan, Elucidation of a universal size-control mechanism in Drosophila and mammals, Cell 130 (2007) 1120-1133.

[82] J. Cai, N. Zhang, Y. Zheng, R.F. de Wilde, A. Maitra, D. Pan, The Hippo signaling pathway restricts the oncogenic potential of an intestinal regeneration program, Genes Dev 24 (2010) 2383-2388.

[83] F. Ren, B. Wang, T. Yue, E.Y. Yun, Y.T. Ip, J. Jiang, Hippo signaling regulates Drosophila intestine stem cell proliferation through multiple pathways, Proc Natl Acad Sci U S A 107 (2010) 21064-21069.

[84] P. Karpowicz, J. Perez, N. Perrimon, The Hippo tumor suppressor pathway regulates intestinal stem cell regeneration, Development 137 (2010) 4135-4145.

[85] F.A. Grusche, J.L. Degoutin, H.E. Richardson, K.F. Harvey, The Salvador/Warts/Hippo pathway controls regenerative tissue growth in Drosophila melanogaster, Dev Biol 350 (2011) 255-266.

[86] G. Sun, K.D. Irvine, Regulation of Hippo signaling by Jun kinase signaling during compensatory cell proliferation and regeneration, and in neoplastic tumors, Dev Biol 350 (2011) 139-151.

[87] E.M. Hartmann, E. Campo, G. Wright, G. Lenz, I. Salaverria, P. Jares, W. Xiao, R.M. Braziel, L.M. Rimsza, W.C. Chan, D.D. Weisenburger, J. Delabie, E.S. Jaffe, R.D. Gascoyne, S.S. Dave, H.K. Mueller-Hermelink, L.M. Staudt, G. Ott, S. Bea, A. Rosenwald, Pathway discovery in mantle cell lymphoma by integrated analysis of high-resolution gene expression and copy number profiling, Blood 116 (2010) 953-961.

[88] B.V. Reddy, K.D. Irvine, Regulation of Drosophila glial cell proliferation by Merlin-Hippo signaling, Development 138 (2011) 5201-5212.

[89] J. Colombani, C. Polesello, F. Josue, N. Tapon, Dmp53 activates the Hippo pathway to promote cell death in response to DNA damage, Curr Biol 16 (2006) 1453-1458.

[90] Y. Jin, L. Dong, Y. Lu, W. Wu, Q. Hao, Z. Zhou, J. Jiang, Y. Zhao, L. Zhang, Dimerization and cytoplasmic localization regulate Hippo kinase signaling activity in organ size control, J Biol Chem (2012).

[91] S. Wu, J. Huang, J. Dong, D. Pan, hippo encodes a Ste-20 family protein kinase that restricts cell proliferation and promotes apoptosis in conjunction with salvador and warts, Cell 114 (2003) 445-456.

[92] X. Wei, T. Shimizu, Z.C. Lai, Mob as tumor suppressor is activated by Hippo kinase for growth inhibition in Drosophila, EMBO J 26 (2007) 1772-1781.

[93] T. Shimizu, L.L. Ho, Z.C. Lai, The mob as tumor suppressor gene is essential for early development and regulates tissue growth in Drosophila, Genetics 178 (2008) 957-965.

[94] L.L. Ho, X. Wei, T. Shimizu, Z.C. Lai, Mob as tumor suppressor is activated at the cell membrane to control tissue growth and organ size in Drosophila, Dev Biol 337 (2010) 274-283.

[95] H. Song, K.K. Mak, L. Topol, K. Yun, J. Hu, L. Garrett, Y. Chen, O. Park, J. Chang, R.M. Simpson, C.Y. Wang, B. Gao, J. Jiang, Y. Yang, Mammalian Mst1 and Mst2 kinases

play essential roles in organ size control and tumor suppression, Proc Natl Acad Sci U S A 107 (2010) 1431-1436.

[96] A. Chow, Y. Hao, X. Yang, Molecular characterization of human homologs of yeast MOB1, Int J Cancer 126 (2010) 2079-2089.

[97] A. Tavares, J. Goncalves, C. Florindo, A.A. Tavares, H. Soares, Mob1: defining cell polarity for proper cell division, J Cell Sci 125 (2012) 516-527.

[98] M. Kawahara, T. Hori, K. Chonabayashi, T. Oka, M. Sudol, T. Uchiyama, Kpm/Lats2 is linked to chemosensitivity of leukemic cells through the stabilization of p73, Blood 112 (2008) 3856-3866.

[99] Y. Aylon, Y. Ofir-Rosenfeld, N. Yabuta, E. Lapi, H. Nojima, X. Lu, M. Oren, The Lats2 tumor suppressor augments p53-mediated apoptosis by promoting the nuclear proapoptotic function of ASPP1, Genes Dev 24 (2010) 2420-2429.

[100] H. Qin, K. Blaschke, G. Wei, Y. Ohi, L. Blouin, Z. Qi, J. Yu, R.F. Yeh, M. Hebrok, M. Ramalho-Santos, Transcriptional Analysis of Pluripotency Reveals the Hippo Pathway as a Barrier to Reprogramming, Hum Mol Genet (2012).

[101] C.J. Huntoon, M.D. Nye, L. Geng, K.L. Peterson, K.S. Flatten, P. Haluska, S.H. Kaufmann, L.M. Karnitz, Heat shock protein 90 inhibition depletes LATS1 and LATS2, two regulators of the mammalian hippo tumor suppressor pathway, Cancer Res 70 (2010) 8642-8650.

[102] Z. Salah, G. Melino, R.I. Aqeilan, Negative regulation of the Hippo pathway by E3 ubiquitin ligase ITCH is sufficient to promote tumorigenicity, Cancer Res 71 (2011) 2010-2020.

[103] K.C. Ho, Z. Zhou, Y.M. She, A. Chun, T.D. Cyr, X. Yang, Itch E3 ubiquitin ligase regulates large tumor suppressor 1 stability [corrected], Proc Natl Acad Sci U S A 108 (2011) 4870-4875.

[104] W. Li, L. Wang, H. Katoh, R. Liu, P. Zheng, Y. Liu, Identification of a tumor suppressor relay between the FOXP3 and the Hippo pathways in breast and prostate cancers, Cancer Res 71 (2011) 2162-2171.

[105] S. Habbig, M.P. Bartram, R.U. Muller, R. Schwarz, N. Andriopoulos, S. Chen, J.G. Sagmuller, M. Hoehne, V. Burst, M.C. Liebau, H.C. Reinhardt, T. Benzing, B. Schermer, NPHP4, a cilia-associated protein, negatively regulates the Hippo pathway, J Cell Biol 193 (2011) 633-642.

[106] M. Paramasivam, A. Sarkeshik, J.R. Yates, 3rd, M.J. Fernandes, D. McCollum, Angiomotin family proteins are novel activators of the LATS2 kinase tumor suppressor, Mol Biol Cell 22 (2011) 3725-3733.

[107] K. Zhang, E. Rodriguez-Aznar, N. Yabuta, R.J. Owen, J.M. Mingot, H. Nojima, M.A. Nieto, G.D. Longmore, Lats2 kinase potentiates Snail1 activity by promoting nuclear retention upon phosphorylation, EMBO J 31 (2012) 29-43.

[108] X. Varelas, P. Samavarchi-Tehrani, M. Narimatsu, A. Weiss, K. Cockburn, B.G. Larsen, J. Rossant, J.L. Wrana, The Crumbs complex couples cell density sensing to Hippo-dependent control of the TGF-beta-SMAD pathway, Dev Cell 19 (2010) 831-844.

[109] L.A. Baena-Lopez, I. Rodriguez, A. Baonza, The tumor suppressor genes dachsous and fat modulate different signalling pathways by regulating dally and dally-like, Proc Natl Acad Sci U S A 105 (2008) 9645-9650.

[110] K. Skouloudaki, M. Puetz, M. Simons, J.R. Courbard, C. Boehlke, B. Hartleben, C. Engel, M.J. Moeller, C. Englert, F. Bollig, T. Schafer, H. Ramachandran, M. Mlodzik,

T.B. Huber, E.W. Kuehn, E. Kim, A. Kramer-Zucker, G. Walz, Scribble participates in Hippo signaling and is required for normal zebrafish pronephros development, Proc Natl Acad Sci U S A 106 (2009) 8579-8584.

[111] Y. Xu, I. Stamenkovic, Q. Yu, CD44 attenuates activation of the hippo signaling pathway and is a prime therapeutic target for glioblastoma, Cancer Res 70 (2010) 2455-2464.

[112] B.G. Fernandez, P. Gaspar, C. Bras-Pereira, B. Jezowska, S.R. Rebelo, F. Janody, Actin-Capping Protein and the Hippo pathway regulate F-actin and tissue growth in Drosophila, Development 138 (2011) 2337-2346.

[113] L. Sansores-Garcia, W. Bossuyt, K. Wada, S. Yonemura, C. Tao, H. Sasaki, G. Halder, Modulating F-actin organization induces organ growth by affecting the Hippo pathway, EMBO J 30 (2011) 2325-2335.

[114] K. Wada, K. Itoga, T. Okano, S. Yonemura, H. Sasaki, Hippo pathway regulation by cell morphology and stress fibers, Development 138 (2011) 3907-3914.

[115] C. Bras-Pereira, T. Zhang, F. Pignoni, F. Janody, Homeostasis of the Drosophila adult retina by actin-capping protein and the Hippo pathway, Commun Integr Biol 4 (2011) 612-615.

[116] C. Rauskolb, G. Pan, B.V. Reddy, H. Oh, K.D. Irvine, Zyxin links fat signaling to the hippo pathway, PLoS Biol 9 (2011) e1000624.

[117] B. Min, M.K. Kim, J.W. Zhang, J. Kim, K.C. Chung, B.C. Oh, G.S. Stein, Y.H. Lee, A.J. van Wijnen, S.C. Bae, Identification of RUNX3 as a component of the MST/Hpo signaling pathway, J Cell Physiol 227 (2012) 839-849.

[118] J.C. Boggiano, P.J. Vanderzalm, R.G. Fehon, Tao-1 phosphorylates Hippo/MST Kinases to regulate the Hippo-Salvador-Warts tumor suppressor pathway, Dev Cell 21 (2011) 888-895.

[119] C.L. Poon, J.I. Lin, X. Zhang, K.F. Harvey, The sterile 20-like kinase Tao-1 controls tissue growth by regulating the Salvador-Warts-Hippo pathway, Dev Cell 21 (2011) 896-906.

[120] T. Zhang, Q. Zhou, F. Pignoni, Yki/YAP, Sd/TEAD and Hth/MEIS control tissue specification in the Drosophila eye disc epithelium, PLoS One 6 (2011) e22278.

[121] B.J. Thompson, S.M. Cohen, The Hippo pathway regulates the bantam microRNA to control cell proliferation and apoptosis in Drosophila, Cell 126 (2006) 767-774.

[122] R. Nolo, C.M. Morrison, C. Tao, X. Zhang, G. Halder, The bantam microRNA is a target of the hippo tumor-suppressor pathway, Curr Biol 16 (2006) 1895-1904.

[123] H.W. Peng, M. Slattery, R.S. Mann, Transcription factor choice in the Hippo signaling pathway: homothorax and yorkie regulation of the microRNA bantam in the progenitor domain of the Drosophila eye imaginal disc, Genes Dev 23 (2009) 2307-2319.

[124] H. Oh, K.D. Irvine, Cooperative regulation of growth by Yorkie and Mad through bantam, Dev Cell 20 (2011) 109-122.

[125] B.K. Staley, K.D. Irvine, Warts and Yorkie mediate intestinal regeneration by influencing stem cell proliferation, Curr Biol 20 (2010) 1580-1587.

[126] M. Ziosi, L.A. Baena-Lopez, D. Grifoni, F. Froldi, A. Pession, F. Garoia, V. Trotta, P. Bellosta, S. Cavicchi, dMyc functions downstream of Yorkie to promote the supercompetitive behavior of hippo pathway mutant cells, PLoS Genet 6 (2010).

[127] R.M. Neto-Silva, S. de Beco, L.A. Johnston, Evidence for a growth-stabilizing regulatory feedback mechanism between Myc and Yorkie, the Drosophila homolog of Yap, Dev Cell 19 (2010) 507-520.

[128] H. Stocker, Growth control: Myc and Yorkie get connected, Curr Biol 21 (2011) R37-39.

[129] X. Zhang, C.C. Milton, C.L. Poon, W. Hong, K.F. Harvey, Wbp2 cooperates with Yorkie to drive tissue growth downstream of the Salvador-Warts-Hippo pathway, Cell Death Differ 18 (2011) 1346-1355.

[130] S.K. Lim, M. Orhant-Prioux, W. Toy, K.Y. Tan, Y.P. Lim, Tyrosine phosphorylation of transcriptional coactivator WW-domain binding protein 2 regulates estrogen receptor alpha function in breast cancer via the Wnt pathway, FASEB J 25 (2011) 3004-3018.

[131] B.N. Nicolay, B. Bayarmagnai, A.B. Islam, N. Lopez-Bigas, M.V. Frolov, Cooperation between dE2F1 and Yki/Sd defines a distinct transcriptional program necessary to bypass cell cycle exit, Genes Dev 25 (2011) 323-335.

[132] C. Badouel, L. Gardano, N. Amin, A. Garg, R. Rosenfeld, T. Le Bihan, H. McNeill, The FERM-domain protein Expanded regulates Hippo pathway activity via direct interactions with the transcriptional activator Yorkie, Dev Cell 16 (2009) 411-420.

[133] H. Oh, B.V. Reddy, K.D. Irvine, Phosphorylation-independent repression of Yorkie in Fat-Hippo signaling, Dev Biol 335 (2009) 188-197.

[134] M.M. Gilbert, M. Tipping, A. Veraksa, K.H. Moberg, A screen for conditional growth suppressor genes identifies the Drosophila homolog of HD-PTP as a regulator of the oncoprotein Yorkie, Dev Cell 20 (2011) 700-712.

[135] F. Kanai, P.A. Marignani, D. Sarbassova, R. Yagi, R.A. Hall, M. Donowitz, A. Hisaminato, T. Fujiwara, Y. Ito, L.C. Cantley, M.B. Yaffe, TAZ: a novel transcriptional co-activator regulated by interactions with 14-3-3 and PDZ domain proteins, EMBO J 19 (2000) 6778-6791.

[136] J.H. Hong, E.S. Hwang, M.T. McManus, A. Amsterdam, Y. Tian, R. Kalmukova, E. Mueller, T. Benjamin, B.M. Spiegelman, P.A. Sharp, N. Hopkins, M.B. Yaffe, TAZ, a

transcriptional modulator of mesenchymal stem cell differentiation, Science 309 (2005) 1074-1078.

[137] G. Tzivion, Y.H. Shen, J. Zhu, 14-3-3 proteins; bringing new definitions to scaffolding, Oncogene 20 (2001) 6331-6338.

[138] M. Sudol, P. Bork, A. Einbond, K. Kastury, T. Druck, M. Negrini, K. Huebner, D. Lehman, Characterization of the mammalian YAP (Yes-associated protein) gene and its role in defining a novel protein module, the WW domain, J Biol Chem 270 (1995) 14733-14741.

[139] M. Sudol, Yes-associated protein (YAP65) is a proline-rich phosphoprotein that binds to the SH3 domain of the Yes proto-oncogene product, Oncogene 9 (1994) 2145-2152.

[140] P.J. Mohler, S.M. Kreda, R.C. Boucher, M. Sudol, M.J. Stutts, S.L. Milgram, Yes-associated protein 65 localizes p62(c-Yes) to the apical compartment of airway epithelia by association with EBP50, J Cell Biol 147 (1999) 879-890.

[141] X. Espanel, M. Sudol, Yes-associated protein and p53-binding protein-2 interact through their WW and SH3 domains, J Biol Chem 276 (2001) 14514-14523.

[142] O. Ferrigno, F. Lallemand, F. Verrecchia, S. L'Hoste, J. Camonis, A. Atfi, A. Mauviel, Yes-associated protein (YAP65) interacts with Smad7 and potentiates its inhibitory activity against TGF-beta/Smad signaling, Oncogene 21 (2002) 4879-4884.

[143] A. Komuro, M. Nagai, N.E. Navin, M. Sudol, WW domain-containing protein YAP associates with ErbB-4 and acts as a co-transcriptional activator for the carboxyl-terminal fragment of ErbB-4 that translocates to the nucleus, J Biol Chem 278 (2003) 33334-33341.

[144] J. Omerovic, E.M. Puggioni, S. Napoletano, V. Visco, R. Fraioli, L. Frati, A. Gulino, M. Alimandi, Ligand-regulated association of ErbB-4 to the transcriptional co-activator YAP65 controls transcription at the nuclear level, Exp Cell Res 294 (2004) 469-479.

[145] S.K. Zaidi, A.J. Sullivan, R. Medina, Y. Ito, A.J. van Wijnen, J.L. Stein, J.B. Lian, G.S. Stein, Tyrosine phosphorylation controls Runx2-mediated subnuclear targeting of YAP to repress transcription, EMBO J 23 (2004) 790-799.

[146] M. Howell, C. Borchers, S.L. Milgram, Heterogeneous nuclear ribonuclear protein U associates with YAP and regulates its co-activation of Bax transcription, J Biol Chem 279 (2004) 26300-26306.

[147] J.D. Kulman, J.E. Harris, L. Xie, E.W. Davie, Proline-rich Gla protein 2 is a cell-surface vitamin K-dependent protein that binds to the transcriptional coactivator Yes-associated protein, Proc Natl Acad Sci U S A 104 (2007) 8767-8772.

[148] M. Zagurovskaya, M.M. Shareef, A. Das, A. Reeves, S. Gupta, M. Sudol, M.T. Bedford, J. Prichard, M. Mohiuddin, M.M. Ahmed, EGR-1 forms a complex with YAP-1 and upregulates Bax expression in irradiated prostate carcinoma cells, Oncogene 28 (2009) 1121-1131.

[149] J. Zhang, J.Y. Ji, M. Yu, M. Overholtzer, G.A. Smolen, R. Wang, J.S. Brugge, N.J. Dyson, D.A. Haber, YAP-dependent induction of amphiregulin identifies a non-cell-autonomous component of the Hippo pathway, Nat Cell Biol 11 (2009) 1444-1450.

[150] A. Chatterjee, T. Sen, X. Chang, D. Sidransky, Yes-associated protein 1 regulates the stability of DeltaNp63alpha, Cell Cycle 9 (2010) 162-167.

[151] M. Yuan, P. Luong, C. Hudson, K. Gudmundsdottir, S. Basu, c-Abl phosphorylation of DeltaNp63alpha is critical for cell viability, Cell Death Dis 1 (2010) e16.

[152] A. Dong, A. Gupta, R.K. Pai, M. Tun, A.W. Lowe, The human adenocarcinoma-associated gene, AGR2, induces expression of amphiregulin through Hippo pathway co-activator YAP1 activation, J Biol Chem 286 (2011) 18301-18310.

[153] N.J. Van Hateren, R.M. Das, G.M. Hautbergue, A.G. Borycki, M. Placzek, S.A. Wilson, FatJ acts via the Hippo mediator Yap1 to restrict the size of neural progenitor cell pools, Development 138 (2011) 1893-1902.

[154] L. Garnier, J.W. Wills, M.F. Verderame, M. Sudol, WW domains and retrovirus budding, Nature 381 (1996) 744-745.

[155] S. Strano, E. Munarriz, M. Rossi, L. Castagnoli, Y. Shaul, A. Sacchi, M. Oren, M. Sudol, G. Cesareni, G. Blandino, Physical interaction with Yes-associated protein enhances p73 transcriptional activity, J Biol Chem 276 (2001) 15164-15173.

[156] S. Strano, O. Monti, N. Pediconi, A. Baccarini, G. Fontemaggi, E. Lapi, F. Mantovani, A. Damalas, G. Citro, A. Sacchi, G. Del Sal, M. Levrero, G. Blandino, The transcriptional coactivator Yes-associated protein drives p73 gene-target specificity in response to DNA Damage, Mol Cell 18 (2005) 447-459.

[157] E. Lapi, S. Di Agostino, S. Donzelli, H. Gal, E. Domany, G. Rechavi, P.P. Pandolfi, D. Givol, S. Strano, X. Lu, G. Blandino, PML, YAP, and p73 are components of a proapoptotic autoregulatory feedback loop, Mol Cell 32 (2008) 803-814.

[158] D. Levy, Y. Adamovich, N. Reuven, Y. Shaul, The Yes-associated protein 1 stabilizes p73 by preventing Itch-mediated ubiquitination of p73, Cell Death Differ 14 (2007) 743-751.

[159] D. Levy, Y. Adamovich, N. Reuven, Y. Shaul, Yap1 phosphorylation by c-Abl is a critical step in selective activation of proapoptotic genes in response to DNA damage, Mol Cell 29 (2008) 350-361.

[160] M. Sudol, H.I. Chen, C. Bougeret, A. Einbond, P. Bork, Characterization of a novel protein-binding module--the WW domain, FEBS Lett 369 (1995) 67-71.

[161] B. Andre, J.Y. Springael, WWP, a new amino acid motif present in single or multiple copies in various proteins including dystrophin and the SH3-binding Yes-associated protein YAP65, Biochem Biophys Res Commun 205 (1994) 1201-1205.

[162] C.B. McDonald, S.K. McIntosh, D.C. Mikles, V. Bhat, B.J. Deegan, K.L. Seldeen, A.M. Saeed, L. Buffa, M. Sudol, Z. Nawaz, A. Farooq, Biophysical analysis of binding of WW domains of the YAP2 transcriptional regulator to PPXY motifs within WBP1 and WBP2 adaptors, Biochemistry 50 (2011) 9616-9627.

[163] C. Webb, A. Upadhyay, F. Giuntini, I. Eggleston, M. Furutani-Seiki, R. Ishima, S. Bagby, Structural features and ligand binding properties of tandem WW domains from YAP and TAZ, nuclear effectors of the Hippo pathway, Biochemistry 50 (2011) 3300-3309.

[164] H.I. Chen, M. Sudol, The WW domain of Yes-associated protein binds a proline-rich ligand that differs from the consensus established for Src homology 3-binding modules, Proc Natl Acad Sci U S A 92 (1995) 7819-7823.

[165] M.J. Macias, M. Hyvonen, E. Baraldi, J. Schultz, M. Sudol, M. Saraste, H. Oschkinat, Structure of the WW domain of a kinase-associated protein complexed with a proline-rich peptide, Nature 382 (1996) 646-649.

[166] G.T. Ibragimova, R.C. Wade, Stability of the beta-sheet of the WW domain: A molecular dynamics simulation study, Biophys J 77 (1999) 2191-2198.

[167] X. Zhang, C.C. Milton, P.O. Humbert, K.F. Harvey, Transcriptional output of the Salvador/warts/hippo pathway is controlled in distinct fashions in Drosophila melanogaster and mammalian cell lines, Cancer Res 69 (2009) 6033-6041.

[168] V.R. Baichwal, R. Tjian, Control of c-Jun activity by interaction of a cell-specific inhibitor with regulatory domain delta: differences between v- and c-Jun, Cell 63 (1990) 815-825.

[169] T. Williams, R. Tjian, Analysis of the DNA-binding and activation properties of the human transcription factor AP-2, Genes Dev 5 (1991) 670-682.

[170] E.A. Mosser, J.D. Kasanov, E.C. Forsberg, B.K. Kay, P.A. Ney, E.H. Bresnick, Physical and functional interactions between the transactivation domain of the hematopoietic transcription factor NF-E2 and WW domains, Biochemistry 37 (1998) 13686-13695.

[171] C. Nerlov, E.B. Ziff, Three levels of functional interaction determine the activity of CCAAT/enhancer binding protein-alpha on the serum albumin promoter, Genes Dev 8 (1994) 350-362.

[172] C. Vesque, P. Charnay, Mapping functional regions of the segment-specific transcription factor Krox-20, Nucleic Acids Res 20 (1992) 2485-2492.

[173] J.D. Molkentin, A.B. Firulli, B.L. Black, J.F. Martin, C.M. Hustad, N. Copeland, N. Jenkins, G. Lyons, E.N. Olson, MEF2B is a potent transactivator expressed in early myogenic lineages, Mol Cell Biol 16 (1996) 3814-3824.

[174] R. Yagi, L.F. Chen, K. Shigesada, Y. Murakami, Y. Ito, A WW domain-containing yes-associated protein (YAP) is a novel transcriptional co-activator, EMBO J 18 (1999) 2551-2562.

[175] C.Y. Liu, Z.Y. Zha, X. Zhou, H. Zhang, W. Huang, D. Zhao, T. Li, S.W. Chan, C.J. Lim, W. Hong, S. Zhao, Y. Xiong, Q.Y. Lei, K.L. Guan, The hippo tumor pathway promotes TAZ degradation by phosphorylating a phosphodegron and recruiting the SCF{beta}-TrCP E3 ligase, J Biol Chem 285 (2010) 37159-37169.

[176] Q.Y. Lei, H. Zhang, B. Zhao, Z.Y. Zha, F. Bai, X.H. Pei, S. Zhao, Y. Xiong, K.L. Guan, TAZ promotes cell proliferation and epithelial-mesenchymal transition and is inhibited by the hippo pathway, Mol Cell Biol 28 (2008) 2426-2436.

[177] S.W. Chan, C.J. Lim, K. Guo, C.P. Ng, I. Lee, W. Hunziker, Q. Zeng, W. Hong, A role for TAZ in migration, invasion, and tumorigenesis of breast cancer cells, Cancer Res 68 (2008) 2592-2598.

[178] J.P. Thiery, H. Acloque, R.Y. Huang, M.A. Nieto, Epithelial-mesenchymal transitions in development and disease, Cell 139 (2009) 871-890.

[179] K. Polyak, R.A. Weinberg, Transitions between epithelial and mesenchymal states: acquisition of malignant and stem cell traits, Nat Rev Cancer 9 (2009) 265-273.

[180] T. Tsuji, S. Ibaragi, G.F. Hu, Epithelial-mesenchymal transition and cell cooperativity in metastasis, Cancer Res 69 (2009) 7135-7139.

[181] S.W. Chan, C.J. Lim, Y.F. Chong, A.V. Pobbati, C. Huang, W. Hong, Hippo pathway-independent restriction of TAZ and YAP by angiomotin, J Biol Chem 286 (2011) 7018-7026.

[182] C.Y. Liu, X. Lv, T. Li, Y. Xu, X. Zhou, S. Zhao, Y. Xiong, Q.Y. Lei, K.L. Guan, PP1 cooperates with ASPP2 to dephosphorylate and activate TAZ, J Biol Chem 286 (2011) 5558-5566.

[183] B. Zhao, X. Wei, W. Li, R.S. Udan, Q. Yang, J. Kim, J. Xie, T. Ikenoue, J. Yu, L. Li, P. Zheng, K. Ye, A. Chinnaiyan, G. Halder, Z.C. Lai, K.L. Guan, Inactivation of YAP oncoprotein by the Hippo pathway is involved in cell contact inhibition and tissue growth control, Genes Dev 21 (2007) 2747-2761.

[184] H. Oh, K.D. Irvine, In vivo regulation of Yorkie phosphorylation and localization, Development 135 (2008) 1081-1088.

[185] J. Zhang, G.A. Smolen, D.A. Haber, Negative regulation of YAP by LATS1 underscores evolutionary conservation of the Drosophila Hippo pathway, Cancer Res 68 (2008) 2789-2794.

[186] T. Oka, V. Mazack, M. Sudol, Mst2 and Lats kinases regulate apoptotic function of Yes kinase-associated protein (YAP), J Biol Chem 283 (2008) 27534-27546.

[187] H. Oh, K.D. Irvine, In vivo analysis of Yorkie phosphorylation sites, Oncogene 28 (2009) 1916-1927.

[188] F. Ren, L. Zhang, J. Jiang, Hippo signaling regulates Yorkie nuclear localization and activity through 14-3-3 dependent and independent mechanisms, Dev Biol 337 (2010) 303-312.

[189] B. Schumacher, M. Skwarczynska, R. Rose, C. Ottmann, Structure of a 14-3-3sigma-YAP phosphopeptide complex at 1.15 A resolution, Acta Crystallogr Sect F Struct Biol Cryst Commun 66 (2010) 978-984.

[190] S. Basu, N.F. Totty, M.S. Irwin, M. Sudol, J. Downward, Akt phosphorylates the Yes-associated protein, YAP, to induce interaction with 14-3-3 and attenuation of p73-mediated apoptosis, Mol Cell 11 (2003) 11-23.

[191] V. Tomlinson, K. Gudmundsdottir, P. Luong, K.Y. Leung, A. Knebel, S. Basu, JNK phosphorylates Yes-associated protein (YAP) to regulate apoptosis, Cell Death Dis 1 (2010) e29.

[192] K. Schlegelmilch, M. Mohseni, O. Kirak, J. Pruszak, J.R. Rodriguez, D. Zhou, B.T. Kreger, V. Vasioukhin, J. Avruch, T.R. Brummelkamp, F.D. Camargo, Yap1 acts downstream of alpha-catenin to control epidermal proliferation, Cell 144 (2011) 782-795.

[193] M.R. Silvis, B.T. Kreger, W.H. Lien, O. Klezovitch, G.M. Rudakova, F.D. Camargo, D.M. Lantz, J.T. Seykora, V. Vasioukhin, alpha-catenin is a tumor suppressor that controls cell accumulation by regulating the localization and activity of the transcriptional coactivator Yap1, Sci Signal 4 (2011) ra33.

[194] B. Zhao, L. Li, K. Tumaneng, C.Y. Wang, K.L. Guan, A coordinated phosphorylation by Lats and CK1 regulates YAP stability through SCF(beta-TRCP), Genes Dev 24 (2010) 72-85.

[195] A.M. Liu, R.T. Poon, J.M. Luk, MicroRNA-375 targets Hippo-signaling effector YAP in liver cancer and inhibits tumor properties, Biochem Biophys Res Commun 394 (2010) 623-627.

[196] M.Z. Xu, S.W. Chan, A.M. Liu, K.F. Wong, S.T. Fan, J. Chen, R.T. Poon, L. Zender, S.W. Lowe, W. Hong, J.M. Luk, AXL receptor kinase is a mediator of YAP-dependent oncogenic functions in hepatocellular carcinoma, Oncogene 30 (2011) 1229-1240.

[197] E. Nishikawa, H. Osada, Y. Okazaki, C. Arima, S. Tomida, Y. Tatematsu, A. Taguchi, Y. Shimada, K. Yanagisawa, Y. Yatabe, S. Toyokuni, Y. Sekido, T. Takahashi, miR-375 is activated by ASH1 and inhibits YAP1 in a lineage-dependent manner in lung cancer, Cancer Res 71 (2011) 6165-6173.

[198] T. Oka, M. Sudol, Nuclear localization and pro-apoptotic signaling of YAP2 require intact PDZ-binding motif, Genes Cells 14 (2009) 607-615.

[199] T. Oka, E. Remue, K. Meerschaert, B. Vanloo, C. Boucherie, D. Gfeller, G.D. Bader, S.S. Sidhu, J. Vandekerckhove, J. Gettemans, M. Sudol, Functional complexes between YAP2 and ZO-2 are PDZ domain-dependent, and regulate YAP2 nuclear localization and signalling, Biochem J 432 (2010) 461-472.

[200] A.M. Vigneron, R.L. Ludwig, K.H. Vousden, Cytoplasmic ASPP1 inhibits apoptosis through the control of YAP, Genes Dev 24 (2010) 2430-2439.

[201] W. Wang, J. Huang, J. Chen, Angiomotin-like proteins associate with and negatively regulate YAP1, J Biol Chem 286 (2011) 4364-4370.

[202] B. Zhao, L. Li, Q. Lu, L.H. Wang, C.Y. Liu, Q. Lei, K.L. Guan, Angiomotin is a novel Hippo pathway component that inhibits YAP oncoprotein, Genes Dev 25 (2011) 51-63.

[203] T. Oka, A.P. Schmitt, M. Sudol, Opposing roles of angiomotin-like-1 and zona occludens-2 on pro-apoptotic function of YAP, Oncogene 31 (2012) 128-134.

[204] Y. Bao, K. Nakagawa, Z. Yang, M. Ikeda, K. Withanage, M. Ishigami-Yuasa, Y. Okuno, S. Hata, H. Nishina, Y. Hata, A cell-based assay to screen stimulators of the Hippo pathway reveals the inhibitory effect of dobutamine on the YAP-dependent gene transcription, J Biochem 150 (2011) 199-208.

[205] L. Angus, S. Moleirinho, L. Herron, A. Sinha, X. Zhang, M. Niestrata, K. Dholakia, M.B. Prystowsky, K.F. Harvey, P.A. Reynolds, F.J. Gunn-Moore, Willin/FRMD6 expression activates the Hippo signaling pathway kinases in mammals and antagonizes oncogenic YAP, Oncogene 31 (2012) 238-250.

[206] P. Wang, Y. Bai, B. Song, Y. Wang, D. Liu, Y. Lai, X. Bi, Z. Yuan, PP1A-mediated dephosphorylation positively regulates YAP2 activity, PLoS One 6 (2011) e24288.

[207] C.B. Cui, L.F. Cooper, X. Yang, G. Karsenty, I. Aukhil, Transcriptional coactivation of bone-specific transcription factor Cbfa1 by TAZ, Mol Cell Biol 23 (2003) 1004-1013.

[208] J.S. Suh, K.S. Kim, J.Y. Lee, Y.J. Choi, C.P. Chung, Y.J. Park, A cell-permeable fusion protein for the mineralization of human dental pulp stem cells, J Dent Res 91 (2012) 90-96.

[209] L. Zhao, S. Jiang, B.M. Hantash, Transforming growth factor beta1 induces osteogenic differentiation of murine bone marrow stromal cells, Tissue Eng Part A 16 (2010) 725-733.

[210] W. Xing, J. Kim, J. Wergedal, S.T. Chen, S. Mohan, Ephrin B1 regulates bone marrow stromal cell differentiation and bone formation by influencing TAZ transactivation via complex formation with NHERF1, Mol Cell Biol 30 (2010) 711-721.

[211] J.H. Hong, M.B. Yaffe, TAZ: a beta-catenin-like molecule that regulates mesenchymal stem cell differentiation, Cell Cycle 5 (2006) 176-179.

[212] B. Li, M. Shi, J. Li, H. Zhang, B. Chen, L. Chen, W. Gao, N. Giuliani, R.C. Zhao, Elevated tumor necrosis factor-alpha suppresses TAZ expression and impairs osteogenic potential of Flk-1+ mesenchymal stem cells in patients with multiple myeloma, Stem Cells Dev 16 (2007) 921-930.

[213] H.H. Cho, K.K. Shin, Y.J. Kim, J.S. Song, J.M. Kim, Y.C. Bae, C.D. Kim, J.S. Jung, NF-kappaB activation stimulates osteogenic differentiation of mesenchymal stem cells derived from human adipose tissue by increasing TAZ expression, J Cell Physiol 223 (2010) 168-177.

[214] H. Eda, K. Aoki, K. Marumo, K. Fujii, K. Ohkawa, FGF-2 signaling induces downregulation of TAZ protein in osteoblastic MC3T3-E1 cells, Biochem Biophys Res Commun 366 (2008) 471-475.

[215] B. Hopwood, A. Tsykin, D.M. Findlay, N.L. Fazzalari, Gene expression profile of the bone microenvironment in human fragility fracture bone, Bone 44 (2009) 87-101.

[216] N. Zhang, H. Bai, K.K. David, J. Dong, Y. Zheng, J. Cai, M. Giovannini, P. Liu, R.A. Anders, D. Pan, The Merlin/NF2 tumor suppressor functions through the YAP oncoprotein to regulate tissue homeostasis in mammals, Dev Cell 19 (2010) 27-38.

[217] X. Zhang, F.A. Grusche, K.F. Harvey, Control of tissue growth and cell transformation by the salvador/warts/hippo pathway, PLoS One 7 (2012) e31994.

[218] I. Lian, J. Kim, H. Okazawa, J. Zhao, B. Zhao, J. Yu, A. Chinnaiyan, M.A. Israel, L.S. Goldstein, R. Abujarour, S. Ding, K.L. Guan, The role of YAP transcription coactivator in regulating stem cell self-renewal and differentiation, Genes Dev 24 (2010) 1106-1118.

[219] H. Zhang, H.A. Pasolli, E. Fuchs, Yes-associated protein (YAP) transcriptional coactivator functions in balancing growth and differentiation in skin, Proc Natl Acad Sci U S A 108 (2011) 2270-2275.

[220] T. Bertero, C. Gastaldi, I. Bourget-Ponzio, V. Imbert, A. Loubat, E. Selva, R. Busca, B. Mari, P. Hofman, P. Barbry, G. Meneguzzi, G. Ponzio, R. Rezzonico, miR-483-3p controls proliferation in wounded epithelial cells, FASEB J 25 (2011) 3092-3105.

[221] S. Septer, G. Edwards, S. Gunewardena, A. Wolfe, H. Li, J. Daniel, U. Apte, Yes-associated protein is involved in Proliferation and Differentiation During Postnatal Liver Development, Am J Physiol Gastrointest Liver Physiol (2011).

[222] I. D'Addario, C. Abbruzzese, M. Lo Iacono, M. Teson, O. Golisano, V. Barone, Overexpression of YAP1 induces immortalization of normal human keratinocytes by blocking clonal evolution, Histochem Cell Biol 134 (2010) 265-276.

[223] K.S. Park, J.A. Whitsett, T. Di Palma, J.H. Hong, M.B. Yaffe, M. Zannini, TAZ interacts with TTF-1 and regulates expression of surfactant protein-C, J Biol Chem 279 (2004) 17384-17390.

[224] Y. Tian, D. Li, J. Dahl, J. You, T. Benjamin, Identification of TAZ as a binding partner of the polyomavirus T antigens, J Virol 78 (2004) 12657-12664.

[225] M. Murakami, J. Tominaga, R. Makita, Y. Uchijima, Y. Kurihara, O. Nakagawa, T. Asano, H. Kurihara, Transcriptional activity of Pax3 is co-activated by TAZ, Biochem Biophys Res Commun 339 (2006) 533-539.

[226] M. Murakami, M. Nakagawa, E.N. Olson, O. Nakagawa, A WW domain protein TAZ is a critical coactivator for TBX5, a transcription factor implicated in Holt-Oram syndrome, Proc Natl Acad Sci U S A 102 (2005) 18034-18039.

[227] T. Di Palma, B. D'Andrea, G.L. Liguori, A. Liguoro, T. de Cristofaro, D. Del Prete, A. Pappalardo, A. Mascia, M. Zannini, TAZ is a coactivator for Pax8 and TTF-1, two transcription factors involved in thyroid differentiation, Exp Cell Res 315 (2009) 162-175.

[228] H. Jeong, S. Bae, S.Y. An, M.R. Byun, J.H. Hwang, M.B. Yaffe, J.H. Hong, E.S. Hwang, TAZ as a novel enhancer of MyoD-mediated myogenic differentiation, FASEB J 24 (2010) 3310-3320.

[229] Y. Jiang, V.T. Puliyappadamba, L. Zhang, W. Wu, A. Wali, M.B. Yaffe, J.A. Fontana, A.K. Rishi, A novel mechanism of cell growth regulation by Cell Cycle and Apoptosis Regulatory Protein (CARP)-1, J Mol Signal 5 (2010) 7.

[230] E. Remue, K. Meerschaert, T. Oka, C. Boucherie, J. Vandekerckhove, M. Sudol, J. Gettemans, TAZ interacts with zonula occludens-1 and -2 proteins in a PDZ-1 dependent manner, FEBS Lett 584 (2010) 4175-4180.

[231] S.W. Chan, C.J. Lim, C. Huang, Y.F. Chong, H.J. Gunaratne, K.A. Hogue, W.P. Blackstock, K.F. Harvey, W. Hong, WW domain-mediated interaction with Wbp2 is important for the oncogenic property of TAZ, Oncogene 30 (2011) 600-610.

[232] M.E. Orcholski, Q. Zhang, D.E. Bredesen, Signaling via amyloid precursor-like proteins APLP1 and APLP2, J Alzheimers Dis 23 (2011) 689-699.

[233] D. Zhao, X. Zhi, Z. Zhou, C. Chen, TAZ antagonizes the WWP1-mediated KLF5 degradation and promotes breast cell proliferation and tumorigenesis, Carcinogenesis 33 (2012) 59-67.

[234] M. Buimer, R. Keijser, J.M. Jebbink, D. Wehkamp, A.H. van Kampen, K. Boer, J.A. van der Post, C. Ris-Stalpers, Seven placental transcripts characterize HELLP-syndrome, Placenta 29 (2008) 444-453.

[235] S. Balasenthil, N. Chen, S.T. Lott, J. Chen, J. Carter, W.E. Grizzle, M.L. Frazier, S. Sen, A.M. Killary, A migration signature and plasma biomarker panel for pancreatic adenocarcinoma, Cancer Prev Res (Phila) 4 (2011) 137-149.

[236] T. de Cristofaro, T. Di Palma, A. Ferraro, A. Corrado, V. Lucci, R. Franco, A. Fusco, M. Zannini, TAZ/WWTR1 is overexpressed in papillary thyroid carcinoma, Eur J Cancer 47 (2011) 926-933.

[237] Z. Zhou, Y. Hao, N. Liu, L. Raptis, M.S. Tsao, X. Yang, TAZ is a novel oncogene in non-small cell lung cancer, Oncogene 30 (2011) 2181-2186.

[238] C. Errani, L. Zhang, Y.S. Sung, M. Hajdu, S. Singer, R.G. Maki, J.H. Healey, C.R. Antonescu, A novel WWTR1-CAMTA1 gene fusion is a consistent abnormality in epithelioid hemangioendothelioma of different anatomic sites, Genes Chromosomes Cancer 50 (2011) 644-653.

[239] D. Lai, K.C. Ho, Y. Hao, X. Yang, Taxol resistance in breast cancer cells is mediated by the hippo pathway component TAZ and its downstream transcriptional targets Cyr61 and CTGF, Cancer Res 71 (2011) 2728-2738.

[240] M. Cordenonsi, F. Zanconato, L. Azzolin, M. Forcato, A. Rosato, C. Frasson, M. Inui, M. Montagner, A.R. Parenti, A. Poletti, M.G. Daidone, S. Dupont, G. Basso, S. Bicciato, S.

Piccolo, The Hippo transducer TAZ confers cancer stem cell-related traits on breast cancer cells, Cell 147 (2011) 759-772.

[241] S. Nejigane, Y. Haramoto, M. Okuno, S. Takahashi, M. Asashima, The transcriptional coactivators Yap and TAZ are expressed during early Xenopus development, Int J Dev Biol 55 (2011) 121-126.

[242] Z. Strakova, J. Reed, I. Ihnatovych, Human transcriptional coactivator with PDZ-binding motif (TAZ) is downregulated during decidualization, Biol Reprod 82 (2010) 1112-1118.

[243] S. Dupont, L. Morsut, M. Aragona, E. Enzo, S. Giulitti, M. Cordenonsi, F. Zanconato, J. Le Digabel, M. Forcato, S. Bicciato, N. Elvassore, S. Piccolo, Role of YAP/TAZ in mechanotransduction, Nature 474 (2011) 179-183.

[244] G. Dong, E. Loukinova, Z. Chen, L. Gangi, T.I. Chanturita, E.T. Liu, C. Van Waes, Molecular profiling of transformed and metastatic murine squamous carcinoma cells by differential display and cDNA microarray reveals altered expression of multiple genes related to growth, apoptosis, angiogenesis, and the NF-kappaB signal pathway, Cancer Res 61 (2001) 4797-4808.

[245] A.M. Snijders, B.L. Schmidt, J. Fridlyand, N. Dekker, D. Pinkel, R.C. Jordan, D.G. Albertson, Rare amplicons implicate frequent deregulation of cell fate specification pathways in oral squamous cell carcinoma, Oncogene 24 (2005) 4232-4242.

[246] L. Zhang, D.X. Ye, H.Y. Pan, K.J. Wei, L.Z. Wang, X.D. Wang, G.F. Shen, Z.Y. Zhang, Yes-associated protein promotes cell proliferation by activating Fos Related Activator-1 in oral squamous cell carcinoma, Oral Oncol 47 (2011) 693-697.

[247] T. Muramatsu, I. Imoto, T. Matsui, K. Kozaki, S. Haruki, M. Sudol, Y. Shimada, H. Tsuda, T. Kawano, J. Inazawa, YAP is a candidate oncogene for esophageal squamous cell carcinoma, Carcinogenesis 32 (2011) 389-398.

[248] J. Guo, J. Kleeff, Y. Zhao, J. Li, T. Giese, I. Esposito, M.W. Buchler, M. Korc, H. Friess, Yes-associated protein (YAP65) in relation to Smad7 expression in human pancreatic ductal adenocarcinoma, Int J Mol Med 17 (2006) 761-767.

[249] P. Modena, E. Lualdi, F. Facchinetti, J. Veltman, J.F. Reid, S. Minardi, I. Janssen, F. Giangaspero, M. Forni, G. Finocchiaro, L. Genitori, F. Giordano, R. Riccardi, E.F. Schoenmakers, M. Massimino, G. Sozzi, Identification of tumor-specific molecular signatures in intracranial ependymoma and association with clinical characteristics, J Clin Oncol 24 (2006) 5223-5233.

[250] K. Striedinger, S.R. VandenBerg, G.S. Baia, M.W. McDermott, D.H. Gutmann, A. Lal, The neurofibromatosis 2 tumor suppressor gene product, merlin, regulates human meningioma cell growth by signaling through YAP, Neoplasia 10 (2008) 1204-1212.

[251] L.A. Fernandez, P.A. Northcott, J. Dalton, C. Fraga, D. Ellison, S. Angers, M.D. Taylor, A.M. Kenney, YAP1 is amplified and up-regulated in hedgehog-associated medulloblastomas and mediates Sonic hedgehog-driven neural precursor proliferation, Genes Dev 23 (2009) 2729-2741.

[252] L.A. Fernandez, M. Squatrito, P. Northcott, A. Awan, E.C. Holland, M.D. Taylor, Z. Nahle, A.M. Kenney, Oncogenic YAP promotes radioresistance and genomic instability in medulloblastoma through IGF2-mediated Akt activation, Oncogene (2011).

[253] B.A. Orr, H. Bai, Y. Odia, D. Jain, R.A. Anders, C.G. Eberhart, Yes-associated protein 1 is widely expressed in human brain tumors and promotes glioblastoma growth, J Neuropathol Exp Neurol 70 (2011) 568-577.

[254] T. Yokoyama, H. Osada, H. Murakami, Y. Tatematsu, T. Taniguchi, Y. Kondo, Y. Yatabe, Y. Hasegawa, K. Shimokata, Y. Horio, T. Hida, Y. Sekido, YAP1 is involved in mesothelioma development and negatively regulated by Merlin through phosphorylation, Carcinogenesis 29 (2008) 2139-2146.

[255] H. Murakami, T. Mizuno, T. Taniguchi, M. Fujii, F. Ishiguro, T. Fukui, S. Akatsuka, Y. Horio, T. Hida, Y. Kondo, S. Toyokuni, H. Osada, Y. Sekido, LATS2 is a tumor suppressor gene of malignant mesothelioma, Cancer Res 71 (2011) 873-883.

[256] T. Mizuno, H. Murakami, M. Fujii, F. Ishiguro, I. Tanaka, Y. Kondo, S. Akatsuka, S. Toyokuni, K. Yokoi, H. Osada, Y. Sekido, YAP induces malignant mesothelioma cell proliferation by upregulating transcription of cell cycle-promoting genes, Oncogene (2012).

[257] M. Fujii, T. Toyoda, H. Nakanishi, Y. Yatabe, A. Sato, Y. Matsudaira, H. Ito, H. Murakami, Y. Kondo, E. Kondo, T. Hida, T. Tsujimura, H. Osada, Y. Sekido, TGF-beta synergizes with defects in the Hippo pathway to stimulate human malignant mesothelioma growth, J Exp Med (2012).

[258] M.Z. Xu, T.J. Yao, N.P. Lee, I.O. Ng, Y.T. Chan, L. Zender, S.W. Lowe, R.T. Poon, J.M. Luk, Yes-associated protein is an independent prognostic marker in hepatocellular carcinoma, Cancer 115 (2009) 4576-4585.

[259] D. Zhou, C. Conrad, F. Xia, J.S. Park, B. Payer, Y. Yin, G.Y. Lauwers, W. Thasler, J.T. Lee, J. Avruch, N. Bardeesy, Mst1 and Mst2 maintain hepatocyte quiescence and suppress hepatocellular carcinoma development through inactivation of the Yap1 oncogene, Cancer Cell 16 (2009) 425-438.

[260] L. Lu, Y. Li, S.M. Kim, W. Bossuyt, P. Liu, Q. Qiu, Y. Wang, G. Halder, M.J. Finegold, J.S. Lee, R.L. Johnson, Hippo signaling is a potent in vivo growth and tumor suppressor pathway in the mammalian liver, Proc Natl Acad Sci U S A 107 (2010) 1437-1442.

[261] K.P. Lee, J.H. Lee, T.S. Kim, T.H. Kim, H.D. Park, J.S. Byun, M.C. Kim, W.I. Jeong, D.F. Calvisi, J.M. Kim, D.S. Lim, The Hippo-Salvador pathway restrains hepatic oval cell proliferation, liver size, and liver tumorigenesis, Proc Natl Acad Sci U S A 107 (2010) 8248-8253.

[262] M.A. Kowalik, C. Saliba, M. Pibiri, A. Perra, G.M. Ledda-Columbano, I. Sarotto, E. Ghiso, S. Giordano, A. Columbano, Yes-associated protein regulation of adaptive liver enlargement and hepatocellular carcinoma development in mice, Hepatology 53 (2011) 2086-2096.

[263] R. Urtasun, M.U. Latasa, M.I. Demartis, S. Balzani, S. Goni, O. Garcia-Irigoyen, M. Elizalde, M. Azcona, R.M. Pascale, F. Feo, P. Bioulac-Sage, C. Balabaud, J. Muntane, J. Prieto, C. Berasain, M.A. Avila, Connective tissue growth factor autocriny in human hepatocellular carcinoma: oncogenic role and regulation by epidermal growth factor receptor/yes-associated protein-mediated activation, Hepatology 54 (2011) 2149-2158.

[264] C. Wang, L. Zhang, Q. He, X. Feng, J. Zhu, Z. Xu, X. Wang, F. Chen, X. Li, J. Dong, Differences in Yes-associated protein and mRNA levels in regenerating, Mol Med Report 5 (2012) 410-414.

[265] S. Benhamouche, M. Curto, I. Saotome, A.B. Gladden, C.H. Liu, M. Giovannini, A.I. McClatchey, Nf2/Merlin controls progenitor homeostasis and tumorigenesis in the liver, Genes Dev 24 (2010) 1718-1730.

[266] A.M. Liu, Z. Xu, J.M. Luk, An update on targeting Hippo-YAP signaling in liver cancer, Expert Opin Ther Targets (2012).

[267] K. Matsuura, C. Nakada, M. Mashio, T. Narimatsu, T. Yoshimoto, M. Tanigawa, Y. Tsukamoto, N. Hijiya, I. Takeuchi, T. Nomura, F. Sato, H. Mimata, M. Seto, M. Moriyama, Downregulation of SAV1 plays a role in pathogenesis of high-grade clear cell renal cell carcinoma, BMC Cancer 11 (2011) 523.

[268] C.L. Da, Y. Xin, J. Zhao, X.D. Luo, Significance and relationship between Yes-associated protein and survivin expression in gastric carcinoma and precancerous lesions, World J Gastroenterol 15 (2009) 4055-4061.

[269] W. Kang, J.H. Tong, A.W. Chan, T.L. Lee, R.W. Lung, P.P. Leung, K.K. So, K. Wu, D. Fan, J. Yu, J.J. Sung, K.F. To, Yes-associated protein 1 exhibits oncogenic property in gastric cancer and its nuclear accumulation associates with poor prognosis, Clin Cancer Res 17 (2011) 2130-2139.

[270] Z. Zhou, J.S. Zhu, Z.P. Xu, Q. Zhang, Lentiviral vector-mediated siRNA knockdown of the YAP gene inhibits growth and induces apoptosis in the SGC7901 gastric cancer cell line, Mol Med Report 4 (2011) 1075-1082.

[271] Z. Zhou, J.S. Zhu, Z.P. Xu, RNA Interference Mediated YAP Gene Silencing Inhibits Invasion and Metastasis of Human Gastric Cancer Cell Line SGC-7901, Hepatogastroenterology 58 (2011) 2156-2161.

[272] D. Zhou, Y. Zhang, H. Wu, E. Barry, Y. Yin, E. Lawrence, D. Dawson, J.E. Willis, S.D. Markowitz, F.D. Camargo, J. Avruch, Mst1 and Mst2 protein kinases restrain intestinal stem cell proliferation and colonic tumorigenesis by inhibition of Yes-associated protein (Yap) overabundance, Proc Natl Acad Sci U S A 108 (2011) E1312-1320.

[273] W.M. Konsavage, S.L. Kyler, S.A. Rennoll, G. Jin, G.S. Yochum, Wnt/beta-catenin signaling regulates Yes-associated protein (YAP) gene expression in colorectal carcinoma cells, J Biol Chem (2012).

[274] J. Avruch, D. Zhou, N. Bardeesy, YAP oncogene overexpression supercharges colon cancer proliferation, Cell Cycle 11 (2012).

[275] Y. Wang, Q. Dong, Q. Zhang, Z. Li, E. Wang, X. Qiu, Overexpression of yes-associated protein contributes to progression and poor prognosis of non-small-cell lung cancer, Cancer Sci 101 (2010) 1279-1285.

[276] J.M. Kim, D.W. Kang, L.Z. Long, S.M. Huang, M.K. Yeo, E.S. Yi, K.H. Kim, Differential expression of Yes-associated protein is correlated with expression of cell cycle markers and pathologic TNM staging in non-small-cell lung carcinoma, Hum Pathol 42 (2011) 315-323.

[277] C. Wu, B. Xu, P. Yuan, X. Miao, Y. Liu, Y. Guan, D. Yu, J. Xu, T. Zhang, H. Shen, T. Wu, D. Lin, Genome-wide interrogation identifies YAP1 variants associated with survival of small-cell lung cancer patients, Cancer Res 70 (2010) 9721-9729.

[278] R. Ehsanian, M. Brown, H. Lu, X.P. Yang, A. Pattatheyil, B. Yan, P. Duggal, R. Chuang, J. Doondeea, S. Feller, M. Sudol, Z. Chen, C. Van Waes, YAP dysregulation by phosphorylation or DeltaNp63-mediated gene repression promotes proliferation, survival and migration in head and neck cancer subsets, Oncogene 29 (2010) 6160-6171.

[279] L. Ge, M. Smail, W. Meng, Y. Shyr, F. Ye, K.H. Fan, X. Li, H.M. Zhou, N.A. Bhowmick, Yes-associated protein expression in head and neck squamous cell carcinoma nodal metastasis, PLoS One 6 (2011) e27529.

[280] Z. Helias-Rodzewicz, G. Perot, F. Chibon, C. Ferreira, P. Lagarde, P. Terrier, J.M. Coindre, A. Aurias, YAP1 and VGLL3, encoding two cofactors of TEAD transcription factors, are amplified and overexpressed in a subset of soft tissue sarcomas, Genes Chromosomes Cancer 49 (2010) 1161-1171.

[281] J.H. Hsu, E.R. Lawlor, BMI-1 suppresses contact inhibition and stabilizes YAP in Ewing sarcoma, Oncogene 30 (2011) 2077-2085.

[282] C.A. Hall, R. Wang, J. Miao, E. Oliva, X. Shen, T. Wheeler, S.G. Hilsenbeck, S. Orsulic, S. Goode, Hippo pathway effector Yap is an ovarian cancer oncogene, Cancer Res 70 (2010) 8517-8525.

[283] X. Zhang, J. George, S. Deb, J.L. Degoutin, E.A. Takano, S.B. Fox, D.D. Bowtell, K.F. Harvey, The Hippo pathway transcriptional co-activator, YAP, is an ovarian cancer oncogene, Oncogene 30 (2011) 2810-2822.

[284] R. Tufail, M. Jorda, W. Zhao, I. Reis, Z. Nawaz, Loss of Yes-associated protein (YAP) expression is associated with estrogen and progesterone receptors negativity in invasive breast carcinomas, Breast Cancer Res Treat 131 (2012) 743-750.

[285] X. Wang, L. Su, Q. Ou, Yes-associated protein promotes tumour development in luminal epithelial derived breast cancer, Eur J Cancer (2011).

[286] D.M. Lam-Himlin, J.A. Daniels, M.F. Gayyed, J. Dong, A. Maitra, D. Pan, E.A. Montgomery, R.A. Anders, The hippo pathway in human upper gastrointestinal dysplasia and carcinoma: a novel oncogenic pathway, Int J Gastrointest Cancer 37 (2006) 103-109.

[287] A.A. Steinhardt, M.F. Gayyed, A.P. Klein, J. Dong, A. Maitra, D. Pan, E.A. Montgomery, R.A. Anders, Expression of Yes-associated protein in common solid tumors, Hum Pathol 39 (2008) 1582-1589.

[288] M. Overholtzer, J. Zhang, G.A. Smolen, B. Muir, W. Li, D.C. Sgroi, C.X. Deng, J.S. Brugge, D.A. Haber, Transforming properties of YAP, a candidate oncogene on the chromosome 11q22 amplicon, Proc Natl Acad Sci U S A 103 (2006) 12405-12410.

[289] M. Yuan, V. Tomlinson, R. Lara, D. Holliday, C. Chelala, T. Harada, R. Gangeswaran, C. Manson-Bishop, P. Smith, S.A. Danovi, O. Pardo, T. Crook, C.A. Mein, N.R. Lemoine, L.J. Jones, S. Basu, Yes-associated protein (YAP) functions as a tumor suppressor in breast, Cell Death Differ 15 (2008) 1752-1759.

[290] K.K. Lee, S. Yonehara, Identification of a mechanism that couples multisite phosphorylation of Yes-Associated Protein (YAP) with transcriptional coactivation and regulation of apoptosis, J Biol Chem (2012).

[291] Z. Hossain, S.M. Ali, H.L. Ko, J. Xu, C.P. Ng, K. Guo, Z. Qi, S. Ponniah, W. Hong, W. Hunziker, Glomerulocystic kidney disease in mice with a targeted inactivation of Wwtr1, Proc Natl Acad Sci U S A 104 (2007) 1631-1636.

[292] H.S. Kang, J.Y. Beak, Y.S. Kim, R. Herbert, A.M. Jetten, Glis3 is associated with primary cilia and Wwtr1/TAZ and implicated in polycystic kidney disease, Mol Cell Biol 29 (2009) 2556-2569.

[293] Y. Tian, R. Kolb, J.H. Hong, J. Carroll, D. Li, J. You, R. Bronson, M.B. Yaffe, J. Zhou, T. Benjamin, TAZ promotes PC2 degradation through a SCFbeta-Trcp E3 ligase complex, Mol Cell Biol 27 (2007) 6383-6395.

[294] K. Duning, D. Rosenbusch, M.A. Schluter, Y. Tian, K. Kunzelmann, N. Meyer, U. Schulze, A. Markoff, H. Pavenstadt, T. Weide, Polycystin-2 activity is controlled by transcriptional coactivator with PDZ binding motif and PALS1-associated tight junction protein, J Biol Chem 285 (2010) 33584-33588.

[295] H. Yim, C.K. Sung, J. You, Y. Tian, T. Benjamin, Nek1 and TAZ interact to maintain normal levels of polycystin 2, J Am Soc Nephrol 22 (2011) 832-837.

[296] R. Makita, Y. Uchijima, K. Nishiyama, T. Amano, Q. Chen, T. Takeuchi, A. Mitani, T. Nagase, Y. Yatomi, H. Aburatani, O. Nakagawa, E.V. Small, P. Cobo-Stark, P.

Igarashi, M. Murakami, J. Tominaga, T. Sato, T. Asano, Y. Kurihara, H. Kurihara, Multiple renal cysts, urinary concentration defects, and pulmonary emphysematous changes in mice lacking TAZ, Am J Physiol Renal Physiol 294 (2008) F542-553.

[297] A. Mitani, T. Nagase, K. Fukuchi, H. Aburatani, R. Makita, H. Kurihara, Transcriptional coactivator with PDZ-binding motif is essential for normal alveolarization in mice, Am J Respir Crit Care Med 180 (2009) 326-338.

[298] C. Tamm, N. Bower, C. Anneren, Regulation of mouse embryonic stem cell self-renewal by a Yes-YAP-TEAD2 signaling pathway downstream of LIF, J Cell Sci 124 (2011) 1136-1144.

[299] M. Xin, Y. Kim, L.B. Sutherland, X. Qi, J. McAnally, R.J. Schwartz, J.A. Richardson, R. Bassel-Duby, E.N. Olson, Regulation of insulin-like growth factor signaling by Yap governs cardiomyocyte proliferation and embryonic heart size, Sci Signal 4 (2011) ra70.

[300] T. Heallen, M. Zhang, J. Wang, M. Bonilla-Claudio, E. Klysik, R.L. Johnson, J.F. Martin, Hippo pathway inhibits Wnt signaling to restrain cardiomyocyte proliferation and heart size, Science 332 (2011) 458-461.

[301] K.I. Watt, R. Judson, P. Medlow, K. Reid, T.B. Kurth, J.G. Burniston, A. Ratkevicius, C. De Bari, H. Wackerhage, Yap is a novel regulator of C2C12 myogenesis, Biochem Biophys Res Commun 393 (2010) 619-624.

[302] F.D. Camargo, S. Gokhale, J.B. Johnnidis, D. Fu, G.W. Bell, R. Jaenisch, T.R. Brummelkamp, YAP1 increases organ size and expands undifferentiated progenitor cells, Curr Biol 17 (2007) 2054-2060.

[303] E.M. Morin-Kensicki, B.N. Boone, M. Howell, J.R. Stonebraker, J. Teed, J.G. Alb, T.R. Magnuson, W. O'Neal, S.L. Milgram, Defects in yolk sac vasculogenesis,

chorioallantoic fusion, and embryonic axis elongation in mice with targeted disruption of Yap65, Mol Cell Biol 26 (2006) 77-87.

[304] Q. Jiang, D. Liu, Y. Gong, Y. Wang, S. Sun, Y. Gui, H. Song, yap is required for the development of brain, eyes, and neural crest in zebrafish, Biochem Biophys Res Commun 384 (2009) 114-119.

[305] W.M. Mahoney, Jr., J.H. Hong, M.B. Yaffe, I.K. Farrance, The transcriptional co-activator TAZ interacts differentially with transcriptional enhancer factor-1 (TEF-1) family members, Biochem J 388 (2005) 217-225.

[306] M. Kitagawa, A Sveinsson's chorioretinal atrophy-associated missense mutation in mouse Tead1 affects its interaction with the co-factors YAP and TAZ, Biochem Biophys Res Commun 361 (2007) 1022-1026.

[307] A. Vassilev, K.J. Kaneko, H. Shu, Y. Zhao, M.L. DePamphilis, TEAD/TEF transcription factors utilize the activation domain of YAP65, a Src/Yes-associated protein localized in the cytoplasm, Genes Dev 15 (2001) 1229-1241.

[308] Y. Goulev, J.D. Fauny, B. Gonzalez-Marti, D. Flagiello, J. Silber, A. Zider, SCALLOPED interacts with YORKIE, the nuclear effector of the hippo tumor-suppressor pathway in Drosophila, Curr Biol 18 (2008) 435-441.

[309] B. Zhao, X. Ye, J. Yu, L. Li, W. Li, S. Li, J.D. Lin, C.Y. Wang, A.M. Chinnaiyan, Z.C. Lai, K.L. Guan, TEAD mediates YAP-dependent gene induction and growth control, Genes Dev 22 (2008) 1962-1971.

[310] Z. Li, B. Zhao, P. Wang, F. Chen, Z. Dong, H. Yang, K.L. Guan, Y. Xu, Structural insights into the YAP and TEAD complex, Genes Dev 24 (2010) 235-240.

[311] L. Chen, S.W. Chan, X. Zhang, M. Walsh, C.J. Lim, W. Hong, H. Song, Structural basis of YAP recognition by TEAD4 in the hippo pathway, Genes Dev 24 (2010) 290-300.

[312] W. Tian, J. Yu, D.R. Tomchick, D. Pan, X. Luo, Structural and functional analysis of the YAP-binding domain of human TEAD2, Proc Natl Acad Sci U S A 107 (2010) 7293-7298.

[313] X. Cao, S.L. Pfaff, F.H. Gage, YAP regulates neural progenitor cell number via the TEA domain transcription factor, Genes Dev 22 (2008) 3320-3334.

[314] S.T. Gee, S.L. Milgram, K.L. Kramer, F.L. Conlon, S.A. Moody, Yes-associated protein 65 (YAP) expands neural progenitors and regulates Pax3 expression in the neural plate border zone, PLoS One 6 (2011) e20309.

[315] B. Zhao, J. Kim, X. Ye, Z.C. Lai, K.L. Guan, Both TEAD-binding and WW domains are required for the growth stimulation and oncogenic transformation activity of yes-associated protein, Cancer Res 69 (2009) 1089-1098.

[316] M. Yasunami, K. Suzuki, H. Ohkubo, A novel family of TEA domain-containing transcription factors with distinct spatiotemporal expression patterns, Biochem Biophys Res Commun 228 (1996) 365-370.

[317] K.J. Kaneko, M.L. DePamphilis, Regulation of gene expression at the beginning of mammalian development and the TEAD family of transcription factors, Dev Genet 22 (1998) 43-55.

[318] S.W. Jiang, D. Desai, S. Khan, N.L. Eberhardt, Cooperative binding of TEF-1 to repeated GGAATG-related consensus elements with restricted spatial separation and orientation, DNA Cell Biol 19 (2000) 507-514.

[319] L. Zhang, F. Ren, Q. Zhang, Y. Chen, B. Wang, J. Jiang, The TEAD/TEF family of transcription factor Scalloped mediates Hippo signaling in organ size control, Dev Cell 14 (2008) 377-387.

[320] S. Wu, Y. Liu, Y. Zheng, J. Dong, D. Pan, The TEAD/TEF family protein Scalloped mediates transcriptional output of the Hippo growth-regulatory pathway, Dev Cell 14 (2008) 388-398.

[321] M. Ota, H. Sasaki, Mammalian Tead proteins regulate cell proliferation and contact inhibition as transcriptional mediators of Hippo signaling, Development 135 (2008) 4059-4069.

[322] S. Campbell, M. Inamdar, V. Rodrigues, V. Raghavan, M. Palazzolo, A. Chovnick, The scalloped gene encodes a novel, evolutionarily conserved transcription factor required for sensory organ differentiation in Drosophila, Genes Dev 6 (1992) 367-379.

[323] T. Ishiji, M.J. Lace, S. Parkkinen, R.D. Anderson, T.H. Haugen, T.P. Cripe, J.H. Xiao, I. Davidson, P. Chambon, L.P. Turek, Transcriptional enhancer factor (TEF)-1 and its cell-specific co-activator activate human papillomavirus-16 E6 and E7 oncogene transcription in keratinocytes and cervical carcinoma cells, EMBO J 11 (1992) 2271-2281.

[324] S. Sun, E.S. Stoflet, J.G. Cogan, A.R. Strauch, M.J. Getz, Negative regulation of the vascular smooth muscle alpha-actin gene in fibroblasts and myoblasts: disruption of enhancer function by sequence-specific single-stranded-DNA-binding proteins, Mol Cell Biol 15 (1995) 2429-2436.

[325] J.G. Cogan, S. Sun, E.S. Stoflet, L.J. Schmidt, M.J. Getz, A.R. Strauch, Plasticity of vascular smooth muscle alpha-actin gene transcription. Characterization of multiple, single-, and double-strand specific DNA-binding proteins in myoblasts and fibroblasts, J Biol Chem 270 (1995) 11310-11321.

[326] L.R. Karns, K. Kariya, P.C. Simpson, M-CAT, CArG, and Sp1 elements are required for alpha 1-adrenergic induction of the skeletal alpha-actin promoter during cardiac

myocyte hypertrophy. Transcriptional enhancer factor-1 and protein kinase C as conserved transducers of the fetal program in cardiac growth, J Biol Chem 270 (1995) 410-417.

[327] D.K. Hsu, Y. Guo, G.F. Alberts, N.G. Copeland, D.J. Gilbert, N.A. Jenkins, K.A. Peifley, J.A. Winkles, Identification of a murine TEF-1-related gene expressed after mitogenic stimulation of quiescent fibroblasts and during myogenic differentiation, J Biol Chem 271 (1996) 13786-13795.

[328] Z. Chen, G.A. Friedrich, P. Soriano, Transcriptional enhancer factor 1 disruption by a retroviral gene trap leads to heart defects and embryonic lethality in mice, Genes Dev 8 (1994) 2293-2301.

[329] K. Kariya, I.K. Farrance, P.C. Simpson, Transcriptional enhancer factor-1 in cardiac myocytes interacts with an alpha 1-adrenergic- and beta-protein kinase C-inducible element in the rat beta-myosin heavy chain promoter, J Biol Chem 268 (1993) 26658-26662.

[330] C. Ambrosino, T. Iwata, C. Scafoglio, M. Mallardo, R. Klein, A.R. Nebreda, TEF-1 and C/EBPbeta are major p38alpha MAPK-regulated transcription factors in proliferating cardiomyocytes, Biochem J 396 (2006) 163-172.

[331] M. Yasunami, K. Suzuki, T. Houtani, T. Sugimoto, H. Ohkubo, Molecular characterization of cDNA encoding a novel protein related to transcriptional enhancer factor-1 from neural precursor cells, J Biol Chem 270 (1995) 18649-18654.

[332] P. Jacquemin, J.J. Hwang, J.A. Martial, P. Dolle, I. Davidson, A novel family of developmentally regulated mammalian transcription factors containing the TEA/ATTS DNA binding domain, J Biol Chem 271 (1996) 21775-21785.

[333] P. Jacquemin, J.A. Martial, I. Davidson, Human TEF-5 is preferentially expressed in placenta and binds to multiple functional elements of the human chorionic somatomammotropin-B gene enhancer, J Biol Chem 272 (1997) 12928-12937.

[334] P. Jacquemin, V. Sapin, E. Alsat, D. Evain-Brion, P. Dolle, I. Davidson, Differential expression of the TEF family of transcription factors in the murine placenta and during differentiation of primary human trophoblasts in vitro, Dev Dyn 212 (1998) 423-436.

[335] T. Maeda, J.R. Mazzulli, I.K. Farrance, A.F. Stewart, Mouse DTEF-1 (ETFR-1, TEF-5) is a transcriptional activator in alpha 1-adrenergic agonist-stimulated cardiac myocytes, J Biol Chem 277 (2002) 24346-24352.

[336] A. Azakie, L. Lamont, J.R. Fineman, Y. He, Divergent transcriptional enhancer factor-1 regulates the cardiac troponin T promoter, Am J Physiol Cell Physiol 289 (2005) C1522-1534.

[337] R. Yagi, M.J. Kohn, I. Karavanova, K.J. Kaneko, D. Vullhorst, M.L. DePamphilis, A. Buonanno, Transcription factor TEAD4 specifies the trophectoderm lineage at the beginning of mammalian development, Development 134 (2007) 3827-3836.

[338] N. Nishioka, S. Yamamoto, H. Kiyonari, H. Sato, A. Sawada, M. Ota, K. Nakao, H. Sasaki, Tead4 is required for specification of trophectoderm in pre-implantation mouse embryos, Mech Dev 125 (2008) 270-283.

[339] C.E. Yockey, G. Smith, S. Izumo, N. Shimizu, cDNA cloning and characterization of murine transcriptional enhancer factor-1-related protein 1, a transcription factor that binds to the M-CAT motif, J Biol Chem 271 (1996) 3727-3736.

[340] A.F. Stewart, C.W. Richard, 3rd, J. Suzow, D. Stephan, S. Weremowicz, C.C. Morton, C.N. Adra, Cloning of human RTEF-1, a transcriptional enhancer factor-1-related gene

preferentially expressed in skeletal muscle: evidence for an ancient multigene family, Genomics 37 (1996) 68-76.

[341] A.F. Stewart, J. Suzow, T. Kubota, T. Ueyama, H.H. Chen, Transcription factor RTEF-1 mediates alpha1-adrenergic reactivation of the fetal gene program in cardiac myocytes, Circ Res 83 (1998) 43-49.

[342] A.E. Bonner, W.J. Lemon, T.R. Devereux, R.A. Lubet, M. You, Molecular profiling of mouse lung tumors: association with tumor progression, lung development, and human lung adenocarcinomas, Oncogene 23 (2004) 1166-1176.

[343] J.L. Shie, G. Wu, J. Wu, F.F. Liu, R.J. Laham, P. Oettgen, J. Li, RTEF-1, a novel transcriptional stimulator of vascular endothelial growth factor in hypoxic endothelial cells, J Biol Chem 279 (2004) 25010-25016.

[344] Y. Jin, J. Wu, X. Song, Q. Song, B.L. Cully, A. Messmer-Blust, M. Xu, S.Y. Foo, A. Rosenzweig, J. Li, RTEF-1, an upstream gene of hypoxia-inducible factor-1alpha, accelerates recovery from ischemia, J Biol Chem 286 (2011) 22699-22705.

[345] H. Zhang, C.Y. Liu, Z.Y. Zha, B. Zhao, J. Yao, S. Zhao, Y. Xiong, Q.Y. Lei, K.L. Guan, TEAD transcription factors mediate the function of TAZ in cell growth and epithelial-mesenchymal transition, J Biol Chem 284 (2009) 13355-13362.

[346] Y. Liu, Y. Xin, F. Ye, W. Wang, Q. Lu, H.J. Kaplan, D.C. Dean, Taz-tead1 links cell-cell contact to zeb1 expression, proliferation, and dedifferentiation in retinal pigment epithelial cells, Invest Ophthalmol Vis Sci 51 (2010) 3372-3378.

[347] R. Kalluri, R.A. Weinberg, The basics of epithelial-mesenchymal transition, J Clin Invest 119 (2009) 1420-1428.

[348] Y. Kang, J. Massague, Epithelial-mesenchymal transitions: twist in development and metastasis, Cell 118 (2004) 277-279.

[349] J.M. Lee, S. Dedhar, R. Kalluri, E.W. Thompson, The epithelial-mesenchymal transition: new insights in signaling, development, and disease, J Cell Biol 172 (2006) 973-981.

[350] R. Levayer, T. Lecuit, Breaking down EMT, Nat Cell Biol 10 (2008) 757-759.

[351] J.P. Thiery, Epithelial-mesenchymal transitions in tumour progression, Nat Rev Cancer 2 (2002) 442-454.

[352] J. Yang, R.A. Weinberg, Epithelial-mesenchymal transition: at the crossroads of development and tumor metastasis, Dev Cell 14 (2008) 818-829.

[353] S.A. Mani, W. Guo, M.J. Liao, E.N. Eaton, A. Ayyanan, A.Y. Zhou, M. Brooks, F. Reinhard, C.C. Zhang, M. Shipitsin, L.L. Campbell, K. Polyak, C. Brisken, J. Yang, R.A. Weinberg, The epithelial-mesenchymal transition generates cells with properties of stem cells, Cell 133 (2008) 704-715.

[354] G. Berx, A.M. Cleton-Jansen, F. Nollet, W.J. de Leeuw, M. van de Vijver, C. Cornelisse, F. van Roy, E-cadherin is a tumour/invasion suppressor gene mutated in human lobular breast cancers, EMBO J 14 (1995) 6107-6115.

[355] K. Yoshiura, Y. Kanai, A. Ochiai, Y. Shimoyama, T. Sugimura, S. Hirohashi, Silencing of the E-cadherin invasion-suppressor gene by CpG methylation in human carcinomas, Proc Natl Acad Sci U S A 92 (1995) 7416-7419.

[356] G. Hennig, J. Behrens, M. Truss, S. Frisch, E. Reichmann, W. Birchmeier, Progression of carcinoma cells is associated with alterations in chromatin structure and factor binding at the E-cadherin promoter in vivo, Oncogene 11 (1995) 475-484.

[357] G. Hennig, O. Lowrick, W. Birchmeier, J. Behrens, Mechanisms identified in the transcriptional control of epithelial gene expression, J Biol Chem 271 (1996) 595-602.

[358] K.M. Hajra, X. Ji, E.R. Fearon, Extinction of E-cadherin expression in breast cancer via a dominant repression pathway acting on proximal promoter elements, Oncogene 18 (1999) 7274-7279.

[359] I. Rodrigo, A.C. Cato, A. Cano, Regulation of E-cadherin gene expression during tumor progression: the role of a new Ets-binding site and the E-pal element, Exp Cell Res 248 (1999) 358-371.

[360] G. Tamura, J. Yin, S. Wang, A.S. Fleisher, T. Zou, J.M. Abraham, D. Kong, K.N. Smolinski, K.T. Wilson, S.P. James, S.G. Silverberg, S. Nishizuka, M. Terashima, T. Motoyama, S.J. Meltzer, E-Cadherin gene promoter hypermethylation in primary human gastric carcinomas, J Natl Cancer Inst 92 (2000) 569-573.

[361] J.I. Risinger, A. Berchuck, M.F. Kohler, J. Boyd, Mutations of the E-cadherin gene in human gynecologic cancers, Nat Genet 7 (1994) 98-102.

[362] S.M. Park, A.B. Gaur, E. Lengyel, M.E. Peter, The miR-200 family determines the epithelial phenotype of cancer cells by targeting the E-cadherin repressors ZEB1 and ZEB2, Genes Dev 22 (2008) 894-907.

[363] P.A. Gregory, A.G. Bert, E.L. Paterson, S.C. Barry, A. Tsykin, G. Farshid, M.A. Vadas, Y. Khew-Goodall, G.J. Goodall, The miR-200 family and miR-205 regulate epithelial to mesenchymal transition by targeting ZEB1 and SIP1, Nat Cell Biol 10 (2008) 593-601.

[364] G. Christofori, Changing neighbours, changing behaviour: cell adhesion molecule-mediated signalling during tumour progression, EMBO J 22 (2003) 2318-2323.

[365] T.T. Onder, P.B. Gupta, S.A. Mani, J. Yang, E.S. Lander, R.A. Weinberg, Loss of E-cadherin promotes metastasis via multiple downstream transcriptional pathways, Cancer Res 68 (2008) 3645-3654.

[366] J. Massague, TGFbeta in Cancer, Cell 134 (2008) 215-230.

[367] E. Vincan, N. Barker, The upstream components of the Wnt signalling pathway in the dynamic EMT and MET associated with colorectal cancer progression, Clin Exp Metastasis 25 (2008) 657-663.

[368] J.M. Bailey, P.K. Singh, M.A. Hollingsworth, Cancer metastasis facilitated by developmental pathways: Sonic hedgehog, Notch, and bone morphogenic proteins, J Cell Biochem 102 (2007) 829-839.

[369] Z. Wang, S. Banerjee, Y. Li, K.M. Rahman, Y. Zhang, F.H. Sarkar, Down-regulation of notch-1 inhibits invasion by inactivation of nuclear factor-kappaB, vascular endothelial growth factor, and matrix metalloproteinase-9 in pancreatic cancer cells, Cancer Res 66 (2006) 2778-2784.

[370] B. Baum, J. Settleman, M.P. Quinlan, Transitions between epithelial and mesenchymal states in development and disease, Semin Cell Dev Biol 19 (2008) 294-308.

[371] H. Hugo, M.L. Ackland, T. Blick, M.G. Lawrence, J.A. Clements, E.D. Williams, E.W. Thompson, Epithelial--mesenchymal and mesenchymal--epithelial transitions in carcinoma progression, J Cell Physiol 213 (2007) 374-383.

[372] J.P. Thiery, J.P. Sleeman, Complex networks orchestrate epithelial-mesenchymal transitions, Nat Rev Mol Cell Biol 7 (2006) 131-142.

[373] M.A. Nieto, The snail superfamily of zinc-finger transcription factors, Nat Rev Mol Cell Biol 3 (2002) 155-166.

[374] C. Kudo-Saito, H. Shirako, T. Takeuchi, Y. Kawakami, Cancer metastasis is accelerated through immunosuppression during Snail-induced EMT of cancer cells, Cancer Cell 15 (2009) 195-206.

[375] I. Ota, X.Y. Li, Y. Hu, S.J. Weiss, Induction of a MT1-MMP and MT2-MMP-dependent basement membrane transmigration program in cancer cells by Snail1, Proc Natl Acad Sci U S A 106 (2009) 20318-20323.

[376] R.G. Rowe, X.Y. Li, Y. Hu, T.L. Saunders, I. Virtanen, A. Garcia de Herreros, K.F. Becker, S. Ingvarsen, L.H. Engelholm, G.T. Bommer, E.R. Fearon, S.J. Weiss, Mesenchymal cells reactivate Snail1 expression to drive three-dimensional invasion programs, J Cell Biol 184 (2009) 399-408.

[377] Z. Hou, H. Peng, D.E. White, P. Wang, P.M. Lieberman, T. Halazonetis, F.J. Rauscher, 3rd, 14-3-3 binding sites in the snail protein are essential for snail-mediated transcriptional repression and epithelial-mesenchymal differentiation, Cancer Res 70 (2010) 4385-4393.

[378] T.A. Martin, A. Goyal, G. Watkins, W.G. Jiang, Expression of the transcription factors snail, slug, and twist and their clinical significance in human breast cancer, Ann Surg Oncol 12 (2005) 488-496.

[379] C. Come, F. Magnino, F. Bibeau, P. De Santa Barbara, K.F. Becker, C. Theillet, P. Savagner, Snail and slug play distinct roles during breast carcinoma progression, Clin Cancer Res 12 (2006) 5395-5402.

[380] J. Yang, S.A. Mani, J.L. Donaher, S. Ramaswamy, R.A. Itzykson, C. Come, P. Savagner, I. Gitelman, A. Richardson, R.A. Weinberg, Twist, a master regulator of morphogenesis, plays an essential role in tumor metastasis, Cell 117 (2004) 927-939.

[381] S. Ansieau, J. Bastid, A. Doreau, A.P. Morel, B.P. Bouchet, C. Thomas, F. Fauvet, I. Puisieux, C. Doglioni, S. Piccinin, R. Maestro, T. Voeltzel, A. Selmi, S. Valsesia-Wittmann, C. Caron de Fromentel, A. Puisieux, Induction of EMT by twist proteins as a

collateral effect of tumor-promoting inactivation of premature senescence, Cancer Cell 14 (2008) 79-89.

[382] M. Beltran, I. Puig, C. Pena, J.M. Garcia, A.B. Alvarez, R. Pena, F. Bonilla, A.G. de Herreros, A natural antisense transcript regulates Zeb2/Sip1 gene expression during Snail1-induced epithelial-mesenchymal transition, Genes Dev 22 (2008) 756-769.

[383] J. Comijn, G. Berx, P. Vermassen, K. Verschueren, L. van Grunsven, E. Bruyneel, M. Mareel, D. Huylebroeck, F. van Roy, The two-handed E box binding zinc finger protein SIP1 downregulates E-cadherin and induces invasion, Mol Cell 7 (2001) 1267-1278.

[384] S.A. Mani, J. Yang, M. Brooks, G. Schwaninger, A. Zhou, N. Miura, J.L. Kutok, K. Hartwell, A.L. Richardson, R.A. Weinberg, Mesenchyme Forkhead 1 (FOXC2) plays a key role in metastasis and is associated with aggressive basal-like breast cancers, Proc Natl Acad Sci U S A 104 (2007) 10069-10074.

[385] C. Hader, A. Marlier, L. Cantley, Mesenchymal-epithelial transition in epithelial response to injury: the role of Foxc2, Oncogene 29 (2010) 1031-1040.

[386] M.A. Smit, D.S. Peeper, Deregulating EMT and senescence: double impact by a single twist, Cancer Cell 14 (2008) 5-7.

[387] E.H. Gort, A.J. Groot, E. van der Wall, P.J. van Diest, M.A. Vooijs, Hypoxic regulation of metastasis via hypoxia-inducible factors, Curr Mol Med 8 (2008) 60-67.

[388] M.Z. Wu, Y.P. Tsai, M.H. Yang, C.H. Huang, S.Y. Chang, C.C. Chang, S.C. Teng, K.J. Wu, Interplay between HDAC3 and WDR5 is essential for hypoxia-induced epithelial-mesenchymal transition, Mol Cell 43 (2011) 811-822.

[389] I.M. Shapiro, A.W. Cheng, N.C. Flytzanis, M. Balsamo, J.S. Condeelis, M.H. Oktay, C.B. Burge, F.B. Gertler, An EMT-driven alternative splicing program occurs in human breast cancer and modulates cellular phenotype, PLoS Genet 7 (2011) e1002218.

[390] K. Gumireddy, A. Li, P.A. Gimotty, A.J. Klein-Szanto, L.C. Showe, D. Katsaros, G. Coukos, L. Zhang, Q. Huang, KLF17 is a negative regulator of epithelial-mesenchymal transition and metastasis in breast cancer, Nat Cell Biol 11 (2009) 1297-1304.

[391] A.E. Lenferink, C. Cantin, A. Nantel, E. Wang, Y. Durocher, M. Banville, B. Paul-Roc, A. Marcil, M.R. Wilson, M.D. O'Connor-McCourt, Transcriptome profiling of a TGF-beta-induced epithelial-to-mesenchymal transition reveals extracellular clusterin as a target for therapeutic antibodies, Oncogene 29 (2010) 831-844.

[392] L. Wyatt, C. Wadham, L.A. Crocker, M. Lardelli, Y. Khew-Goodall, The protein tyrosine phosphatase Pez regulates TGFbeta, epithelial-mesenchymal transition, and organ development, J Cell Biol 178 (2007) 1223-1235.

[393] H. Wang, S.Y. Quah, J.M. Dong, E. Manser, J.P. Tang, Q. Zeng, PRL-3 down-regulates PTEN expression and signals through PI3K to promote epithelial-mesenchymal transition, Cancer Res 67 (2007) 2922-2926.

[394] F. Liang, J. Liang, W.Q. Wang, J.P. Sun, E. Udho, Z.Y. Zhang, PRL3 promotes cell invasion and proliferation by down-regulation of Csk leading to Src activation, J Biol Chem 282 (2007) 5413-5419.

[395] X.B. Wan, Z.J. Long, M. Yan, J. Xu, L.P. Xia, L. Liu, Y. Zhao, X.F. Huang, X.R. Wang, X.F. Zhu, M.H. Hong, Q. Liu, Inhibition of Aurora-A suppresses epithelial-mesenchymal transition and invasion by downregulating MAPK in nasopharyngeal carcinoma cells, Carcinogenesis 29 (2008) 1930-1937.

[396] E. Martin-Villar, D. Megias, S. Castel, M.M. Yurrita, S. Vilaro, M. Quintanilla, Podoplanin binds ERM proteins to activate RhoA and promote epithelial-mesenchymal transition, J Cell Sci 119 (2006) 4541-4553.

[397] A. Wicki, F. Lehembre, N. Wick, B. Hantusch, D. Kerjaschki, G. Christofori, Tumor invasion in the absence of epithelial-mesenchymal transition: podoplanin-mediated remodeling of the actin cytoskeleton, Cancer Cell 9 (2006) 261-272.

[398] M. Shtutman, E. Levina, P. Ohouo, M. Baig, I.B. Roninson, Cell adhesion molecule L1 disrupts E-cadherin-containing adherens junctions and increases scattering and motility of MCF7 breast carcinoma cells, Cancer Res 66 (2006) 11370-11380.

[399] T. Waerner, M. Alacakaptan, I. Tamir, R. Oberauer, A. Gal, T. Brabletz, M. Schreiber, M. Jechlinger, H. Beug, ILEI: a cytokine essential for EMT, tumor formation, and late events in metastasis in epithelial cells, Cancer Cell 10 (2006) 227-239.

[400] J.G. Lyons, V. Patel, N.C. Roue, S.Y. Fok, L.L. Soon, G.M. Halliday, J.S. Gutkind, Snail up-regulates proinflammatory mediators and inhibits differentiation in oral keratinocytes, Cancer Res 68 (2008) 4525-4530.

[401] N.J. Sullivan, A.K. Sasser, A.E. Axel, F. Vesuna, V. Raman, N. Ramirez, T.M. Oberyszyn, B.M. Hall, Interleukin-6 induces an epithelial-mesenchymal transition phenotype in human breast cancer cells, Oncogene 28 (2009) 2940-2947.

[402] H.C. Huang, C.H. Hu, M.C. Tang, W.S. Wang, P.M. Chen, Y. Su, Thymosin beta4 triggers an epithelial-mesenchymal transition in colorectal carcinoma by upregulating integrin-linked kinase, Oncogene 26 (2007) 2781-2790.

[403] S. Orsulic, An RCAS-TVA-based approach to designer mouse models, Mamm Genome 13 (2002) 543-547.

[404] A.H. Shih, C. Dai, X. Hu, M.K. Rosenblum, J.A. Koutcher, E.C. Holland, Dose-dependent effects of platelet-derived growth factor-B on glial tumorigenesis, Cancer Res 64 (2004) 4783-4789.

[405] S. Lal, M. Lacroix, P. Tofilon, G.N. Fuller, R. Sawaya, F.F. Lang, An implantable guide-screw system for brain tumor studies in small animals, J Neurosurg 92 (2000) 326-333.

[406] L. Uhrbom, E.C. Holland, Modeling gliomagenesis with somatic cell gene transfer using retroviral vectors, J Neurooncol 53 (2001) 297-305.

[407] M. Begemann, G.N. Fuller, E.C. Holland, Genetic modeling of glioma formation in mice, Brain Pathol 12 (2002) 117-132.

[408] A.A. Margolin, I. Nemenman, K. Basso, C. Wiggins, G. Stolovitzky, R. Dalla Favera, A. Califano, ARACNE: an algorithm for the reconstruction of gene regulatory networks in a mammalian cellular context, BMC Bioinformatics 7 Suppl 1 (2006) S7.

[409] G. Dennis, Jr., B.T. Sherman, D.A. Hosack, J. Yang, W. Gao, H.C. Lane, R.A. Lempicki, DAVID: Database for Annotation, Visualization, and Integrated Discovery, Genome Biol 4 (2003) P3.

[410] W. Huang da, B.T. Sherman, R.A. Lempicki, Systematic and integrative analysis of large gene lists using DAVID bioinformatics resources, Nat Protoc 4 (2009) 44-57.

[411] A.P. Bird, CpG-rich islands and the function of DNA methylation, Nature 321 (1986) 209-213.

[412] K.P. Bhat, K.L. Salazar, V. Balasubramaniyan, K. Wani, L. Heathcock, F. Hollingsworth, J.D. James, J. Gumin, K.L. Diefes, S.H. Kim, A. Turski, Y. Azodi, Y. Yang, T. Doucette, H. Colman, E.P. Sulman, F.F. Lang, G. Rao, S. Copray, B.D. Vaillant, K.D. Aldape, The transcriptional coactivator TAZ regulates mesenchymal differentiation in malignant glioma, Genes Dev 25 (2011) 2594-2609.

[413] A. Li, J. Walling, S. Ahn, Y. Kotliarov, Q. Su, M. Quezado, J.C. Oberholtzer, J. Park, J.C. Zenklusen, H.A. Fine, Unsupervised analysis of transcriptomic profiles reveals six glioma subtypes, Cancer Res 69 (2009) 2091-2099.

[414] L.A. Cooper, D.A. Gutman, Q. Long, B.A. Johnson, S.R. Cholleti, T. Kurc, J.H. Saltz, D.J. Brat, C.S. Moreno, The proneural molecular signature is enriched in oligodendrogliomas and predicts improved survival among diffuse gliomas, PLoS One 5 (2010) e12548.

[415] J. Martinez, D.G. Chalupowicz, R.K. Roush, A. Sheth, C. Barsigian, Transglutaminase-mediated processing of fibronectin by endothelial cell monolayers, Biochemistry 33 (1994) 2538-2545.

[416] J.R. Masters, Human cancer cell lines: fact and fantasy, Nat Rev Mol Cell Biol 1 (2000) 233-236.

[417] S.W. Chan, C.J. Lim, L.S. Loo, Y.F. Chong, C. Huang, W. Hong, TEADs mediate nuclear retention of TAZ to promote oncogenic transformation, J Biol Chem 284 (2009) 14347-14358.

[418] Lindy E. Barrett, Z. Granot, C. Coker, A. Iavarone, D. Hambardzumyan, Eric C. Holland, H.-s. Nam, R. Benezra, Self-Renewal Does Not Predict Tumor Growth Potential in Mouse Models of High-Grade Glioma, Cancer Cell 21 (2012) 11-24.

[419] D. Hambardzumyan, N.M. Amankulor, K.Y. Helmy, O.J. Becher, E.C. Holland, Modeling Adult Gliomas Using RCAS/t-va Technology, Transl Oncol 2 (2009) 89-95.

[420] T. Doucette, G. Rao, Y. Yang, J. Gumin, N. Shinojima, B.N. Bekele, W. Qiao, W. Zhang, F.F. Lang, Mesenchymal stem cells display tumor-specific tropism in an RCAS/Ntv-a glioma model, Neoplasia 13 (2011) 716-725.

[421] J.P. Robinson, M.W. VanBrocklin, A.R. Guilbeault, D.L. Signorelli, S. Brandner, S.L. Holmen, Activated BRAF induces gliomas in mice when combined with Ink4a/Arf loss or Akt activation, Oncogene 29 (2010) 335-344.

[422] L.M. Moore, K.M. Holmes, G.N. Fuller, W. Zhang, Oncogene interactions are required for glioma development and progression as revealed by a tissue specific transgenic mouse model, Chin J Cancer 30 (2011) 163-172.

[423] S.S. Palii, K.D. Robertson, Epigenetic control of tumor suppression, Crit Rev Eukaryot Gene Expr 17 (2007) 295-316.

[424] A.M. Deaton, A. Bird, CpG islands and the regulation of transcription, Genes Dev 25 (2011) 1010-1022.

[425] K.B. Choo, Epigenetics in disease and cancer, Malays J Pathol 33 (2011) 61-70.

[426] H. Noushmehr, D.J. Weisenberger, K. Diefes, H.S. Phillips, K. Pujara, B.P. Berman, F. Pan, C.E. Pelloski, E.P. Sulman, K.P. Bhat, R.G. Verhaak, K.A. Hoadley, D.N. Hayes, C.M. Perou, H.K. Schmidt, L. Ding, R.K. Wilson, D. Van Den Berg, H. Shen, H. Bengtsson, P. Neuvial, L.M. Cope, J. Buckley, J.G. Herman, S.B. Baylin, P.W. Laird, K. Aldape, Identification of a CpG island methylator phenotype that defines a distinct subgroup of glioma, Cancer Cell 17 (2010) 510-522.

[427] M. Toyota, N. Ahuja, M. Ohe-Toyota, J.G. Herman, S.B. Baylin, J.P. Issa, CpG island methylator phenotype in colorectal cancer, Proc Natl Acad Sci U S A 96 (1999) 8681-8686.

[428] M. Toyota, N. Ahuja, H. Suzuki, F. Itoh, M. Ohe-Toyota, K. Imai, S.B. Baylin, J.P. Issa, Aberrant methylation in gastric cancer associated with the CpG island methylator phenotype, Cancer Res 59 (1999) 5438-5442.

[429] T. Ueki, M. Toyota, T. Sohn, C.J. Yeo, J.P. Issa, R.H. Hruban, M. Goggins, Hypermethylation of multiple genes in pancreatic adenocarcinoma, Cancer Res 60 (2000) 1835-1839.

[430] G. Strathdee, K. Appleton, M. Illand, D.W. Millan, J. Sargent, J. Paul, R. Brown, Primary ovarian carcinomas display multiple methylator phenotypes involving known tumor suppressor genes, Am J Pathol 158 (2001) 1121-1127.

[431] C.A. Eads, R.V. Lord, K. Wickramasinghe, T.I. Long, S.K. Kurumboor, L. Bernstein, J.H. Peters, S.R. DeMeester, T.R. DeMeester, K.A. Skinner, P.W. Laird, Epigenetic patterns in the progression of esophageal adenocarcinoma, Cancer Res 61 (2001) 3410-3418.

[432] L. Shen, N. Ahuja, Y. Shen, N.A. Habib, M. Toyota, A. Rashid, J.P. Issa, DNA methylation and environmental exposures in human hepatocellular carcinoma, J Natl Cancer Inst 94 (2002) 755-761.

[433] M. Abe, M. Ohira, A. Kaneda, Y. Yagi, S. Yamamoto, Y. Kitano, T. Takato, A. Nakagawara, T. Ushijima, CpG island methylator phenotype is a strong determinant of poor prognosis in neuroblastomas, Cancer Res 65 (2005) 828-834.

[434] A.J. Hunter, Have animal models of disease helped or hindered the drug discovery process?, Ann N Y Acad Sci 1245 (2011) 1-2.

[435] H.W. Shen, X.L. Jiang, F.J. Gonzalez, A.M. Yu, Humanized transgenic mouse models for drug metabolism and pharmacokinetic research, Curr Drug Metab 12 (2011) 997-1006.

[436] F.M. Goodsaid, D.L. Mendrick, Translational medicine and the value of biomarker qualification, Sci Transl Med 2 (2010) 47ps44.

[437] K. Wang, C. Degerny, M. Xu, X.J. Yang, YAP, TAZ, and Yorkie: a conserved family of signal-responsive transcriptional coregulators in animal development and human disease, Biochem Cell Biol 87 (2009) 77-91.

[438] S. Akiyoshi, M. Ishii, N. Nemoto, M. Kawabata, H. Aburatani, K. Miyazono, Targets of transcriptional regulation by transforming growth factor-beta: expression profile analysis using oligonucleotide arrays, Jpn J Cancer Res 92 (2001) 257-268.

[439] M.F. Cole, S.E. Johnstone, J.J. Newman, M.H. Kagey, R.A. Young, Tcf3 is an integral component of the core regulatory circuitry of embryonic stem cells, Genes Dev 22 (2008) 746-755.

[440] J. Lee, S. Kotliarova, Y. Kotliarov, A. Li, Q. Su, N.M. Donin, S. Pastorino, B.W. Purow, N. Christopher, W. Zhang, J.K. Park, H.A. Fine, Tumor stem cells derived from glioblastomas cultured in bFGF and EGF more closely mirror the phenotype and genotype of primary tumors than do serum-cultured cell lines, Cancer Cell 9 (2006) 391-403.

[441] P.K. Purbey, S. Singh, P.P. Kumar, S. Mehta, K.N. Ganesh, D. Mitra, S. Galande, PDZ domain-mediated dimerization and homeodomain-directed specificity are required for high-affinity DNA binding by SATB1, Nucleic Acids Res 36 (2008) 2107-2122.

[442] A.B. Gyorgy, M. Szemes, C. de Juan Romero, V. Tarabykin, D.V. Agoston, SATB2 interacts with chromatin-remodeling molecules in differentiating cortical neurons, Eur J Neurosci 27 (2008) 865-873.

VITA

Katrina Lumen Salazar was born in Houston, Texas, the Daughter of Sonia Lumen Salazar and Oscar Atayza Salazar. After completing her work at the Texas Academy of Math and Sciences High School, Denton, Texas, she entered Carnegie Mellon University in Pittsburgh, Pennsylvania. She received the degree of Bachelor of Sciences with a major in biological sciences and minor in ethics from Carnegie Mellon University. For the next two years, she worked as a Post-baccalaureate Intramural Training Award Fellow at the National Cancer Institute, Bethesda, Maryland. After her time at the National Institutes of Health, she entered the joint M.D./Ph.D. program at The University of Texas Health Science Center at Houston Medical School and Graduate School of Biomedical Sciences.

Permanent address:

8318 Seagull Lane

Pearland, Texas 77584